

# Physiological and Metabolic Flux Screening of *Saccharomyces cerevisiae* Single Knockout Mutants on Different Carbon Sources

Dissertation

Zur Erlangung des akademischen Grades

*Doktor der Naturwissenschaften (Dr.rer.nat.)*

Der naturwissenschaftlich-technischen Fakultät III,  
Chemie, Pharmazie, Bio-und Werkstoffwissenschaften  
der Universität des Saarlandes



von

Vidya R. Velagapudi, *M.Sc., PGDiploma*

Saarbrücken, Germany

2009



Tag des kolloquiums: September 21<sup>st</sup>, 2009

Dekan: Prof. Stefan Diebels

Berichterstatter: Prof. Wilhelm F. Maier  
Prof. Elmar Heinzle,  
Prof. Manfred Schmitt  
Dr. Frank Hannemann

# ACKNOWLEDGEMENTS

It is my pleasure to thank the people who made this thesis possible. First of all, I express my deeply felt thanks to my thesis advisor, Prof. Elmar Heinzle, for providing me an opportunity to work in his group, for his continuous support and constant guidance during the tenure of my Ph.D program. It is difficult to overstate my gratitude to Prof. Heinzle, who with his enthusiasm, inspiration, and his great efforts to explain things clearly made this thesis possible. He is responsible for involving me in the Yeast project in the first place. Throughout my thesis-writing period, he provided encouragement, sound advice, good teaching and reviews, and lots of novel ideas and constructive criticism.

I wish to thank my second official thesis reviewer, Prof. Manfred Schmitt and academic reviewer Dr. Frank Hannemann for reviewing this dissertation and also extend my thanks to the thesis chairman, Prof. Wilhelm F. Maier. I wish to thank Prof. Christoph Wittmann for his support during the initial phase of this project and for providing me valuable background on metabolic flux analysis. I wish to thank Prof. Thomas Lengauer, Max-Planck Institute for Informatics (MPI), Saarbrücken for coordinating our regular project meetings and for providing me good insight on the computational aspects. I also thank Dr. Priti Talwar, MPI, who completed her Ph.D thesis by developing computational methods using the data generated from this thesis work, for her collaboration.

I extend my sincere thanks to Dr. Klaus Hollemeyer for his help with the MALDI-ToF-MS measurements. I thank Dr. Tae Hoon Yang for his invaluable support with the MATLAB programming. I also thank Mr. Konstantin Schneider for his timely help. I wish to thank my very good friend, Mr. Gopalacharyulu Peddinti for his timely help and support in the programming part. I also thank Dr. Jing Tang for his help in the modelling aspects. My special thanks to Mr. Michel Fritz for his invaluable help with the HPLC and GC-MS measurements. I extend my thanks to Mrs. Veronika Witte for her help and support with the yeast mutant strains during the initial phase and Mr. Robert Schmidt for his help in ordering the required chemicals in the laboratory. I express my sincere thanks to Dr. Susanne Kohring for her timely help. This thesis is based on three years of research funded by the DFG through the Center for Bioinformatics, University of Saarland and I express my sincere thanks for the financial support.

I also like to thank my good friends Dr. Rahul Deshpande, Dr. Masoud Zabet-Moghaddam, Mrs. Lucia & Dr. Uenal Coskun, Mr. Sathish Kumar and Dr. Maria Lasosa for their good company. I express my gratitude to Mrs. Anna Heinzle for her great hospitality and Ms. Catherine Heinzle for her good company during my initial days at their home in Germany.

I express my sincere thanks to our Vice President R&D Biotechnology, Prof. Anu Kaukovirta-Norja and Technology Manager, Dr. Richard Fagerstrom at VTT Technical Research Center of Finland, who relieved me from the present work to finish my thesis and for constant encouragement and support. Financial support from the VTT Management is greatly acknowledged during the thesis-writing and research papers-writing period and for covering the printing costs of this thesis and also for covering my travelling costs for the Ph.D defense. I express my deep gratitude to Prof. Matej Oresic, Quantitative Biology and Bioinformatics (QBIX) Group, VTT for offering me Post-doc position even before the completion of my thesis work and for his constant support and encouragement at every stage.

I wish to thank all my colleagues at VTT, who shared my present work during this period. Special thanks to Dr. Tuulikki Seppanen-Laakso for her great help and support and I extend my thanks to Mrs. Ulla Lahtinen and Mrs. Anna-Liisa Ruskeepaa. I also would like to thank each and everybody at QBIX group and all my professional collaborators for their good wishes and support. I thank Mrs. Paivi vahala for her support in formatting this thesis. I wish to thank Mrs. Sirpa Nygren for her help in printing this thesis.

I would like to take this opportunity to thank my family. I thank my parents, Mr. Prabhakar Rao & Mrs. Padmavathi for their love and affection. A special thanks to my loving husband Dr. Ramakrishna Velagapudi for his ever lasting love, constant support, patience and for taking care of the family during this period. I would also like to mention about our little daughter Hansika, whose presence has brought a precious change into our lives. I wish to thank my in-laws, Mr. Shiva Nageswara Rao & Mrs. Usha for their constant encouragement, good words and blessings. I also thank my sister's family Mr. Shuan & Mrs. Jaya and my lovely nephews Vickran and Raj for their love and affection. I thank my brother Mr. Rajesh, for his wit and humour that helped me lift my spirits. I also thank my brother-in-law, Mr. Vamsikrishna for always wishing me good success and happiness.

# PUBLICATIONS

This Ph.D thesis work was carried out in Prof. Elmar Heinzle's Applied Biochemistry-Biochemical Engineering group, University of Saarland, Saarbrücken, Germany during January 2003 - December 2005. The following original research articles were published based on this thesis work or are in preparation.

1. **Velagapudi, V.R.**, Wittmann, C., Lengauer, T., Talwar, P., Heinzle, E., 2006. Metabolic Screening of *Saccharomyces cerevisiae* Single Knock-out Strains Reveals Unexpected Mobilization of Metabolic Potential. **Process Biochemistry**. 41, 2170-2179.
2. Hollemeyer, K., **Velagapudi, V.R.**, Wittmann, C., Heinzle, E., 2007. Matrix-assisted laser desorption/ionization time-of-flight mass spectrometry for metabolic flux analyses using isotope-labeled ethanol. **Rapid Communications in Mass Spectrometry**. 21, 336-342.
3. **Velagapudi, V.R.**, Wittmann, C., Schneider, K., Heinzle, E., 2007. Metabolic Flux Screening of *Saccharomyces cerevisiae* Single Knock-out Strains on Glucose and Galactose Supports Elucidation of Gene Function. **Journal of Biotechnology**. 132, 395-404.
4. **Velagapudi, V.R.**, Heinzle, E., 2009. Physiological and metabolic flux profiling of *S. cerevisiae* hexose transporter deletion mutants. (To be submitted)
5. **Velagapudi, V.R.**, Heinzle, E., 2009. Comparative physiological profiling of *S. cerevisiae* single knockouts on different carbon sources – Fructose, Glucose and galactose. (To be submitted)
6. **Velagapudi, V.R.**, Peddinti, G., Tang, J., Lengauer, T., Heinzle, E., 2009. Functional genomics of *S. cerevisiae* by utilising phenotypic and metabolic flux profiling data by using bioinformatics tools (To be submitted)
7. **Velagapudi, V.R.**, Heinzle, E., 2009. Summed fractional labelling analysis of yeast mutants on different carbon sources (To be submitted)
8. Talwar, P., Rahnenführer, J., Heinzle, E., Wittmann, C., **Velagapudi, V.R.**, Lengauer, T., 2009. Computational analysis of metabolite screening data (To be submitted)



# CONTENTS

<b>ACKNOWLEDGEMENTS.....</b>	<b>I</b>
<b>PUBLICATIONS.....</b>	<b>III</b>
<b>1. ABSTRACT .....</b>	<b>1</b>
<b>2. ZUSAMMENFASSUNG.....</b>	<b>2</b>
<b>3. INTRODUCTION.....</b>	<b>3</b>
3.1    MOTIVATION.....	3
3.2    OBJECTIVES .....	4
3.3    THEORETICAL BACKGROUND ON YEAST METABOLISM.....	7
<b>4. MATERIALS AND METHODS .....</b>	<b>21</b>
4.1    YEAST STRAINS .....	21
4.2    MEDIA COMPOSITION.....	21
4.3    DEFINED MEDIUM OPTIMIZATION.....	22
4.4    CULTIVATION.....	23
4.5    ANALYTICS .....	25
4.6    SIMULATIONS.....	28
4.7    ETHANOL LABELING ANALYSIS AND QUANTIFICATION USING MALDI-TOF-MS.....	32
4.8    LABELLING ANALYSIS OF PROTEINOGENIC AMINO ACIDS .....	39
4.9    METABOLIC NETWORK MODEL AND FLUX ANALYSIS.....	40
4.10   STATISTICAL ANALYSES .....	43
<b>5. RESULTS AND DISCUSSION.....</b>	<b>48</b>
5.1    METABOLIC SCREENING OF <i>S. CEREVISIAE</i> SINGLE KNOCKOUT STRAINS ON GLUCOSE AND GALACTOSE.....	49
5.1.1 <i>Background</i> .....	49
5.1.2 <i>Microtiter plate cultivation of S. cerevisiae</i> .....	49
5.1.3 <i>Comparative growth analysis in MTP and SFC</i> .....	50
5.1.4 <i>Effect of shaking rate on oxygen limitation</i> .....	52
5.1.5 <i>Method Validation</i> .....	54
5.1.6 <i>Comparative physiological analysis</i> .....	55
5.1.7 <i>Conclusions</i> .....	67
5.2    MALDI-TOF-MS FOR METABOLIC FLUX ANALYSES USING ISOTOPE LABELED ETHANOL ....	68
5.2.1 <i>Background</i> .....	68

## Contents

---

5.2.2	<i>Ethanol quantification and validation</i> .....	69
5.2.3	<i>Estimation and validation of flux split ratio</i> .....	69
5.2.4	<i>Conclusions</i> .....	70
5.3	METABOLIC FLUX SCREENING OF <i>S. CEREVISIAE</i> KNOCKOUT STRAINS ON GLUCOSE AND GALACTOSE AT MINIATURIZED SCALE .....	72
5.3.1	<i>Background</i> .....	72
5.3.2	<i>Flux through Pentose Phosphate Pathway (PPP)</i> .....	73
5.3.4	<i>Flux through Anaplerotic pathway</i> .....	78
5.3.6	<i>Comparative flux analysis on glucose and galactose</i> .....	79
5.3.7	<i>Conclusions</i> .....	82
5.4	STOICHIOMETRIC AND METABOLIC FLUX SCREENING OF <i>S. CEREVISIAE</i> HEXOSE TRANSPORTER (HXTS) SINGLE KNOCKOUT STRAINS ON GLUCOSE AND GALACTOSE.....	84
5.4.1	<i>Background</i> .....	84
5.4.2	<i>Stoichiometric profiling of HXT knockout strains</i> .....	85
5.4.3	<i>Comparative physiological profiling of HXT mutants</i> .....	93
5.4.3.1	<i>Hexose sensors: rgt2<math>\Delta</math> and snf3<math>\Delta</math></i> .....	93
5.4.3.2	<i>Low affinity HXT mutant strains: hxt1<math>\Delta</math>, hxt3<math>\Delta</math> and hxt4<math>\Delta</math></i> .....	93
5.4.3.3	<i>HXTs with limited known functions</i> .....	94
5.4.3.4	<i>Regulators</i> .....	95
5.4.4	<i>Comparative metabolic flux profiling of HXT mutants</i> .....	96
5.4.4.1	<i>Glycolysis and Pentose phosphate pathway (PPP)</i> .....	96
5.4.4.2	<i>TCA cycle and Fermentative pathway</i> .....	99
5.4.4.3	<i>Anaplerotic pathway</i> .....	100
5.4.5	<i>Conclusions</i> .....	102
5.5	METABOLIC SCREENING OF <i>S. CEREVISIAE</i> SINGLE KNOCKOUT STRAINS ON FRUCTOSE SUGAR AND A COMPARATIVE STUDY ON DIFFERENT CARBON SOURCES.....	104
5.5.1	<i>Background</i> .....	104
5.5.2	<i>Physiological profiling of mutants on fructose</i> .....	107
5.5.3	<i>Comparative physiological profiling of mutants – fructose data with glucose and galactose data</i> .....	114
5.5.4	<i>Physiologically interesting strains</i> .....	120
5.5.5	<i>Conclusions</i> .....	123
5.6	FUNCTIONAL GENOMICS OF <i>S. CEREVISIAE</i> BY UTILISING PHENOTYPIC AND METABOLIC FLUX PROFILING DATA BY USING BIOINFORMATICS TOOLS .....	125
5.6.1	<i>Background</i> .....	125
5.6.2	<i>Statistical analysis of the data</i> .....	125

## Contents

---

5.6.2.1 Hierarchical clustering analysis.....	126
5.6.2.2 Data visualisation as clustered heat maps.....	130
5.6.2.3 Biological significance of mutant pairs.....	133
5.6.3 Functional prediction of hypothetical genes.....	134
5.6.3.1 Euclidean distance approach.....	134
5.6.3.2 Graphical Gaussian Models (GGMs) approach.....	137
5.6.4 Conclusions.....	140
<b>6. SUMMARY &amp; CONCLUSIONS.....</b>	<b>141</b>
<b>7. OUTLOOK.....</b>	<b>144</b>
<b>8. REFERENCES.....</b>	<b>146</b>
<b>9. APPENDICES.....</b>	<b>156</b>
9.1 SYMBOLS AND ABBREVIATIONS.....	156
9.2 BERKELEY MADONNA PROGRAM FOR $K_{LA}$ DETERMINATION.....	157
9.3 BERKELEY MADONNA PROGRAM FOR $Y_{X/O}$ DETERMINATION.....	157
9.4 PROGRAM FOR ETHANOL CORRECTION.....	158
9.5 MATLAB PROGRAMS FOR SOLVING CARBON MASS ISOTOPOMER DISTRIBUTIONS AND CORRECTING NATURAL ISOTOPIE EFFECTS FOR ETHANOL.....	159
9.6 MATLAB PROGRAM FOR FLUX CALCULATIONS.....	165
9.7 PROGRAM FOR QP-GRAPH ANALYSIS.....	166
9.8 STOICHIOMETRIC MATRICES USED FOR METABOLIC FLUX CALCULATIONS.....	168
9.9 GROWTH PROFILES ON GLUCOSE.....	169
9.10 GROWTH PROFILES ON GALACTOSE.....	172
9.11 GROWTH PROFILES ON FRUCTOSE.....	174
9.12 DISSOLVED OXYGEN PROFILES ON GLUCOSE.....	177
9.13 DISSOLVED OXYGEN PROFILES ON GALACTOSE.....	181
<b>10. CURRICULUM VITAE.....</b>	<b>184</b>



## 1. ABSTRACT

A novel method for high-throughput stoichiometric and metabolic flux profiling was developed and a set of deletion mutants of *S. cerevisiae*, which are known to be involved in central carbon metabolism were selected and investigated on glucose, galactose and fructose. On glucose and fructose, the growth was predominantly fermentative and on galactose, respiration was more active. *mae1* $\Delta$  strain did not show any significant growth phenotype on glucose, however, it had highest PPP flux on galactose, which could be due to redirection of NADPH production to the PPP. On fructose, *mae1* $\Delta$  strain had highest oxygen uptake rate with very low ethanol yield, which could be due to reduced PPP flux and to maintain NADPH levels either via NADPH specific -isocitrate dehydrogenase or -aldehyde dehydrogenase. *imp2*' $\Delta$  strain had lowest PPP flux and very high respiratory activity on galactose; and *pck1* $\Delta$  strain had lowest PPP flux on glucose, which might also point to a possible activation of malic enzyme. On fructose, *hxt17* $\Delta$  strain had highest sugar consumption and ethanol production rates and *imp2*' $\Delta$  strain had highest ethanol yield. The functional prediction of hypothetical genes by utilising this quantitative data using computational analyses suggested a possible role in glycolysis or pyruvate metabolism for *YBR184W* and low affinity transporter role for *YIL170W*.

## 2. ZUSAMMENFASSUNG

Es wurde eine neue Hochdurchsatzmethode für die Charakterisierung der Stöchiometrie und der metabolischen Flüsse entwickelt und auf ausgewählte Deletionsmutanten des Zentralstoffwechsels von *S. cerevisiae* angewendet, wobei Glucose, Galactose und Fructose als Substrate eingesetzt wurden. Während auf Glucose und Fructose das Wachstum vorwiegend fermentativ war, war es auf Galactose mehr respirativ. Der *mae1Δ* Stamm zeigte keinen Phänotyp auf Glucose, hatte aber auf Galactose einen sehr hohen Fluss in den Pentosephosphatweg (PPP) mit entsprechend hoher Bereitstellung von NADPH und auf Fructose die höchste Sauerstoffaufnahme mit zugleich sehr niedriger Ethanolausbeute, was auf einen reduzierten Fluss in den PPP und verstärkte Bildung von NADPH über die Isocitratdehydrogenase oder die Aldehyddehydrogenase hindeutet. Der *imp2'Δ* Stamm hatte einen sehr niedrigen PPP-Fluss und starke Respiration auf Galactose. Der *pck1Δ* Stamm hatte die niedrigsten PPP Fluss auf Glucose, was auf eine Aktivierung des Malatenzyms hindeutet. Auf Fructose zeigte der *hxt17Δ* Stamm höchste Zuckerverbrauchs- und Ethanolproduktionsraten und *imp2'Δ* hatte die höchste Ethanolausbeute. Numerische Analysen erlaubten eine erste Vorhersage möglicher Funktionen zweier hypothetischer Gene, in der Glykolyse oder im Pyruvatmetabolismus für *YBR184W* und als niedrig affinen Transporter für *YIL170W*.

## 3. INTRODUCTION

### 3.1 MOTIVATION

*S. cerevisiae* is one of the most thoroughly studied microorganisms. Along with its industrial importance, *S. cerevisiae* serves as a model organism for understanding and engineering eukaryotic cell function. *S. cerevisiae* was the first eukaryotic organism whose genome was fully sequenced (Fig 3.1-1) (Goffeau et al., 1996, 1997). Understanding gene functions in metabolic and regulatory processes in yeast is of central importance for engineering of new production strains and also for the study of these processes with relevance to human metabolism and drug discovery (Barr, 2003; Que and Winzeler, 2002). There have been many studies aiming to unravel the function of orphan genes in the genome, and various functional genomics techniques were first implemented in *S. cerevisiae* (Förster et al., 2003). The phenotype of an organism is the manifestation of its expressed genome and phenotypic screens are frequently the first important steps to the functional characterization of genes (Carpenter et al., 2004). A promising strategy for the elucidation of gene functions combines well-defined, systematic genetic modifications with characterization of the resulting phenotypic analysis for example, growth rate (or fitness) of mutants missing the gene of interest (Baganz et al., 1997; Winzeler et al., 1999; Que et al., 2002).

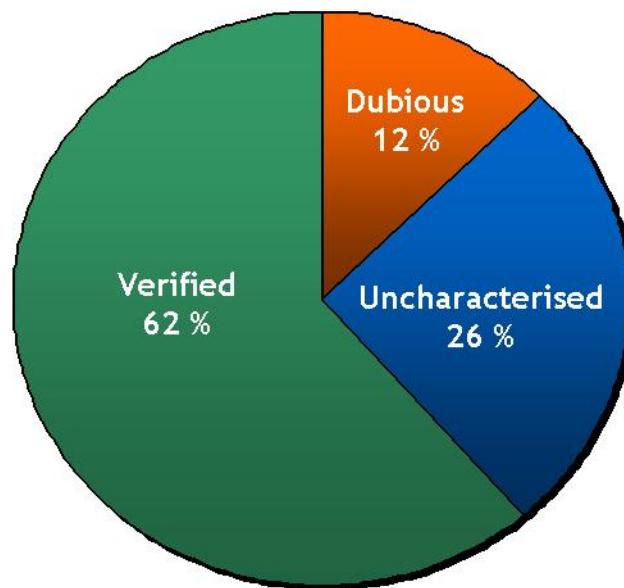


**Figure 3.1-1** Snapshot of *S. cerevisiae* genome. Graphical view of protein coding genes (as of August 2003). Source: Saccharomyces Genome Database ([www.yeastgenome.org](http://www.yeastgenome.org))

In this context, an international consortium established a complete yeast strain collection with the deletion of each single gene (Giaever et al., 2002). The availability of the complete set of deletion mutants of *S. cerevisiae* provides a unique resource for systematic analysis of the functional role of individual genes. Moreover, it is a quantitative tool for systematically measuring the contribution to survival and reproduction (fitness) of most genes in the yeast genome. In many of these analyses, the aim has been to determine how the different genes (both the ones with known function and those open reading frames that have no assigned function) interact with each other, enabling the cells to take up nutrients, grow, divide, regulate their metabolism, release products to the environment, and respond to different stimuli. Exposition of such strains to a suitable environment, e.g. substrate mixture or stress condition, and subsequent measurement of fitness or gene expression supports discovery of gene function.

### **3.2 OBJECTIVES**

To exploit this unique resource of complete set of yeast single gene knockouts, high-throughput assays are needed to provide a phenotypic profile of the functional role of individual genes. Currently many high-throughput techniques are available for large scale screening of yeast mutant library based on fitness (Giaever et al., 2002). Although, these techniques are useful for massive screening of mutant strains to find gene-environment interactions during several stress responses (Gasch et al., 2002), e.g. oxidative stress (Weiss et al., 2004), saline response (Warringer et al., 2003), weak organic acid (Mollapur et al., 2004) quantitative information on the actual metabolic changes induced is limited to growth rate which serves as an overall indicator of so called fitness.

In the field of functional genomics, several comprehensive methods have been developed for the analysis of different ‘Omic’ data i.e. genome, transcriptome, proteome and metabolome depending on the type of compounds measured, i.e., transcripts, proteins, or metabolites (Andreas et al., 2001), respectively. The primary approaches of functional genomics, until recently, have been expression arrays and proteomics. Although these are powerful approaches, they do not necessarily elucidate gene function (Trethewey et al., 2001). Since mRNA molecules are not functional entities within the cell, gene expression profiles alone cannot directly identify the functions of genes. On the other hand, proteins and metabolites constitute func-

tional entities within the cell (Delneri et al., 2001). However, at the proteomic level, changes in protein abundance do not necessarily indicate increases in activity within the cell associated with this protein (Trethewey et al., 2001). Measuring changes in metabolite concentrations (metabolic profiling) is another powerful approach for assessing gene function and relationships to different phenotypes (Phelps et al., 2002).

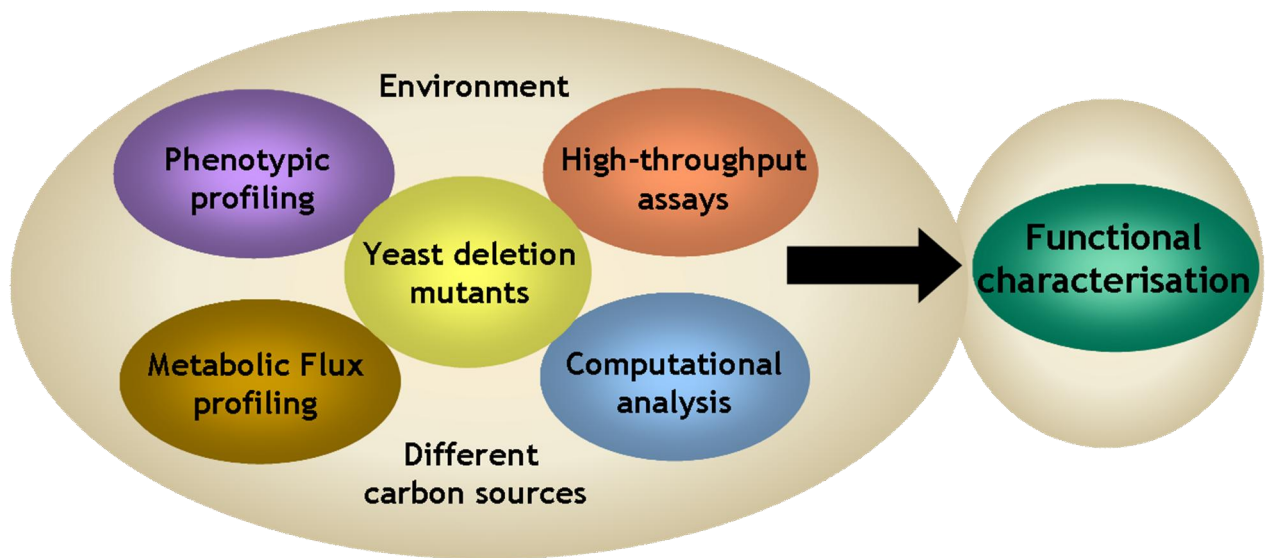


**Figure 3.2-1** Overall picture of the central idea of the project

Generally, the determination of basic physiological parameter as rates of growth, substrate consumption, product formation and respiration and further of metabolic pathway activities is of central importance for the characterization of strains. Thus it would be most desirable to get a more detailed picture of metabolic activities of such mutants (Figure 3.2-1). Allen et al. (2003) analyzed the supernatant of cultivated yeast deletion mutants using HPLC-MS, which served as indicator for metabolic activities. Traditionally, this is only possible by controlled cultivation of strains in fermenters. This is, however, hardly affordable for a large number of strains. Therefore, controlled cultivation of microorganisms in microtiter plates has received increased attention in recent years (John et al., 2003; Kumar et al., 2004; Sauer, 2004). Oxygen supply has a major influence on the physiology of *S. cerevisiae* as has been shown in continuous culture (Furukawa et al., 1983). Oxygen supply is, however, limited in microtiter plates (Kumar et al., 2004). Recently, microtiter plates with integrated optical sensing of dissolved oxygen became available (John et al., 2003) and allow the measurement of dissolved oxygen profiles of microbial cultures, which can serve as a basis for the estimation of oxygen

uptake rate (Dunn et al., 2003). In batch culture the maximum range of exponential growth is limited to a maximal critical cell concentration above which oxygenation is insufficient.

The main objectives of the thesis are

- to develop and optimise a methodology for high-throughput kinetic and stoichiometric analysis of yeast mutant libraries at miniaturized scale
- to investigate the quantitative physiological profiling of the selected mutant strains on different carbon sources for e.g., glucose, galactose and fructose substrates
- to develop a methodology for high-throughput calculation of simplified metabolic fluxes
- to analyse and compare the physiological and metabolic flux profiling of selected mutant strains on different carbon sources
- to investigate the quantitative physiological and metabolic flux profiling of mutant strains with deletion of hexose transporters and regulators on different carbon sources
- to predict the functional role of deleted genes by using statistical analyses and computational tools

### **3.3 THEORETICAL BACKGROUND ON YEAST METABOLISM**

*S. cerevisiae* is one of the most important species for biotechnological production and a most relevant eukaryotic model organism. Yeast metabolism and growth are adapted to the availability of carbon source, in particular, to the type of carbon source for e.g., glucose, galactose or fructose. Metabolism refers to the biochemical assimilation and dissimilation of nutrients by the cells. Assimilatory, anabolic pathways are energy consuming, reductive processes which lead to the biosynthesis of new cellular material. Whereas, dissimilatory, catabolic pathways are oxidative processes, which remove electrons from intermediates and use these to generate energy (Berg et al., 2002).

#### **3.3.1 Glucose metabolism**

The major energy source in yeast is glucose and metabolises to produce energy in the form of adenosine triphosphate (ATP). When ATP is hydrolysed to yield adenosine diphosphate (ADP) and inorganic phosphate ( $P_i$ ), the energy released is used by the cell for various reactions and transformations.

##### **3.3.1.1 Glycolysis**

Glucose is metabolized in a series of steps known as Emben-Meyerhof-Parnas (EMP) pathway or glycolysis in cytosol. Glycolysis provides yeast with energy, together with precursor molecules and reducing power for biosynthetic pathways. Through a set of biochemical reactions, metabolism of glucose eventually yields two pyruvate molecules. In the first stage glucose is converted into fructose 1,6-bisphosphate by phosphorylation and isomerisation reactions. Two ATP molecules are consumed per glucose molecule in these reactions. In the second stage, fructose 1,6-bisphosphate is cleaved by aldolase into interconvertible dihydroxyacetone phosphate and glyceraldehyde 3-phosphate. In the third stage, ATP is generated when glyceraldehyde 3-phosphate is converted to 3-phosphoglycerate. A phosphoryl shift and a dehydration form phosphoenolpyruvate. Another molecule of ATP is formed when phosphoenolpyruvate is converted into pyruvate. There is a net gain of two molecules of ATP, and NADH in the formation of two molecules of pyruvate from one molecule of glucose. The glycolytic pathway is controlled by the regulation of the three irreversible reactions catalysed

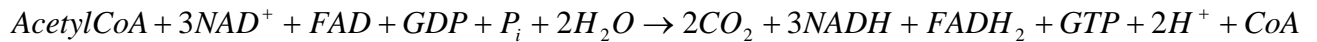
by hexokinase, phosphofructokinase and pyruvate kinase. The overall reaction of glycolysis is (Berg et al., 2002)



### 3.3.1.2 TCA cycle

The pyruvate can enter either the Krebs cycle or tri carboxylic acid (TCA) cycle for complete oxidation and production of carbon dioxide and adenosine triphosphate (ATP) under aerobic conditions or it can be converted to fermentation products i.e., ethanol. The TCA cycle occurs in the mitochondria of eukaryotic cells. The TCA cycle is responsible for the production of reducing equivalents, required for ATP formation, and also for supplying biosynthetic precursors. The reducing equivalents are produced during the oxidation of carbon compounds. The pyruvate produced by the glycolytic pathway from glucose easily enters the matrix of the mitochondria. The pyruvate is then converted to a two-carbon fragment with the loss of the carboxyl group as CO<sub>2</sub> and this two carbon fragment attaches to a coenzyme known as coenzyme-A (CoA) forming acetyl-CoA. This reaction is catalyzed by pyruvate dehydrogenase.

Oxaloacetate reacts with acetyl-CoA and H<sub>2</sub>O to yield citrate and CoA by aldol condensation followed by hydrolysis and is catalysed by citrate synthase. Citrate is isomerised to isocitrate, catalysed by aconitase, accomplished by dehydration and hydration steps. Isocitrate is oxidised and decarboxylated to  $\alpha$ -ketoglutarate by isocitrate dehydrogenase and this reaction generates the first high-transfer-potential electron carrier, NADH.  $\alpha$ -ketoglutarate is oxidative decarboxylated to yield succinyl CoA by  $\alpha$ -ketoglutarate dehydrogenase complex and generates the second NADH. Succinyl CoA synthase catalyses the formation of succinate from the energy-rich thioester compound, succinyl CoA and generates guanine triphosphate (GTP), a compound with high-phosphoryl transfer capacity. Succinate is oxidised to fumarate by succinate dehydrogenase and generates FADH<sub>2</sub>. Fumarate is hydrated to malate by fumarase. Finally, malate is oxidised to form oxaloacetate by malate dehydrogenase and generate the third NADH. A complete turn of the cycle results in the oxidation of the two carbon fragment and formation of reducing equivalents. The TCA cycle is regulated by the activities of the enzymes pyruvate dehydrogenase, citrate synthase, isocitrate dehydrogenase,  $\alpha$ -ketoglutarate dehydrogenase and malate dehydrogenase (Berg et al., 2002). The net reaction of the citric acid cycle is



### 3.3.1.3 Oxidative phosphorylation

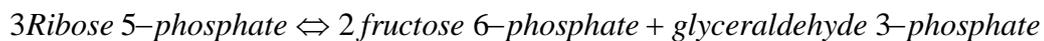
The NADH and FADH<sub>2</sub> produced from glycolysis and TCA cycle are reoxidised to form NAD<sup>+</sup> and FAD through a complicated series of reactions known as oxidative phosphorylation and generate energy in the form of ATP for the cellular requirements. In eukaryotes oxidative phosphorylation occurs in the mitochondrial compartment via the electron transport assembly. The electron transport assembly is comprised of a series of protein complexes that catalyze sequential oxidation reduction reactions. This process is facilitated by a proton carrier in the inner mitochondrial membrane known as ATP synthase. These reactions involve the transfer of electrons through cytochromes with the ultimate electron acceptor being oxygen to form water. Because of the need of oxygen, these reactions are active only under aerobic conditions. ATP will be produced from these reactions by a membrane-bound enzyme ATPase at a rate of maximum 3 ATP molecules per a molecule of NADH oxidized (maximum 2 ATP molecules per a molecule of FADH<sub>2</sub> oxidised). The oxidative phosphorylation is controlled by the availability of ADP. Higher amount of ADP drives the process faster, as the cells require more ATP (Berg et al., 2002).

### 3.3.1.4 Pentose phosphate pathway (PPP)

The PPP generates necessary reducing equivalents, NADPH, pentose and erythrose carbon units for the biosynthetic requirements of the cell. This pathway consists of two phases: the oxidative generation of NADPH and non-oxidative interconversion of three-, four-, five-, six- and seven-carbon molecules and results in the synthesis of five carbon sugars and connecting the PPP with glycolysis. The first reaction in the oxidative phase is the dehydrogenation of glucose 6-phosphate to 6-phosphoglucono- $\delta$ -lactone by glucose 6-phosphate dehydrogenase. The next step is the conversion of 6-phosphoglucono- $\delta$ -lactone to 6-phosphogluconate by lactonase. This six-carbon sugar is then oxidatively decarboxylated by 6-phosphogluconate dehydrogenase to yield ribulose 5-phosphate. Two molecules of NADPH are generated from these biochemical reactions. The net reaction of oxidative phase is (Berg et al., 2002)

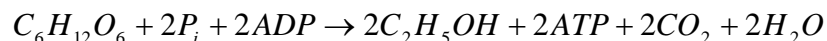


In non-oxidative phase, phosphopentose isomerase isomerizes ribulose 5-phosphate to ribose 5-phosphate and phosphopentose epimerase converts to xylulose 5-phosphate. Glyceraldehyde 3-phosphate and sedoheptulose 7-phosphate are generated by the transketolase and then react to form fructose 6-phosphate and erythrose 4-phosphate by transaldolase. In the next reaction, transketolase catalyses the synthesis of fructose 6-phosphate and glyceraldehyde 3-phosphate from erythrose 4-phosphate and xylulose 5-phosphate. The first step of the oxidative branch by the enzyme glucose 6-phosphate dehydrogenase, which is irreversible acts as the main regulatory control for the pathway. The activity of this enzyme is determined by the ratio of  $\text{NADP}^+/\text{NADPH}$ . The net reaction of non-oxidative phase is (Berg et al., 2002).



### 3.3.1.5 Fermentation

Several biotechnologically important yeasts are fermentative i.e., organisms which use organic substrates anaerobically as electron donor, electron acceptor and carbon source. When oxygen is not available, the ability of the cell to reoxidise the reduced coenzymes ( $\text{NADH}$  and  $\text{FADH}_2$ ) is greatly diminished. To compensate, the biochemistry of the cell is altered such that pyruvate is decarboxylated by pyruvate decarboxylase to acetaldehyde and then to ethanol by alcohol dehydrogenase in the fermentation process, which requires  $\text{NADH}$ . Thus, the formation of ethanol allows the cell to reoxidise the  $\text{NADH}$  that was produced in earlier steps of glycolysis (Eberhardt et al., 1999).



Central carbon metabolic network model is depicted in figure 3-1, representing major pathways, i.e., glycolysis, TCA cycle, pentose phosphate pathway, anaplerotic pathway and fermentation pathway.

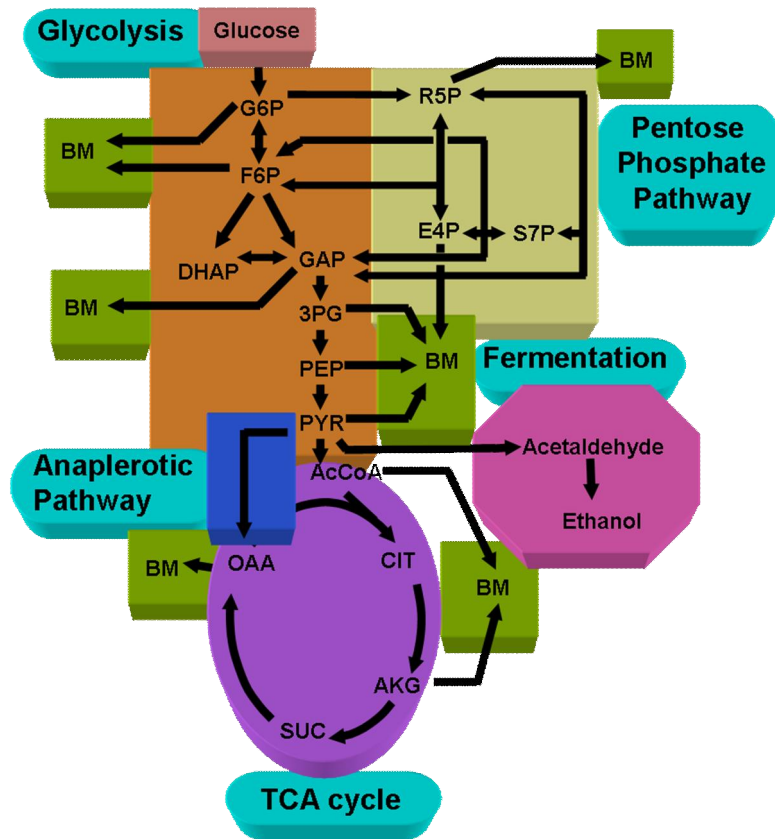


**Figure 3-1** Metabolic network model in *S. cerevisiae* representing the major pathways in central carbon metabolism; glycolysis, TCA cycle, pentose phosphate pathway, anaplerotic pathway and fermentation pathway G6P - Glucose 6-phosphate, R5P - Ribose 5-phosphate, F6P - Fructose 6-phosphate, E4P - Erythrose 4-phosphate, DHAP - Dihydroxyacetone phosphate, GAP - Glyceraldehyde 3-phosphate, S7P - Sedoheptulose 7-phosphate, 3PG - 3-phosphoglycerate, PEP - Phosphoenol pyruvate, PYR - Pyruvate, AcCoA - Acetyl CoA, CIT - Citrate, AKG -  $\alpha$ -ketoglutarate, SUC - Succinate, OAA - Oxaloacetate, BM - Bio-mass

### 3.3.1.6 Crabtree effect

The Crabtree effect is a phenomenon, where at high glucose concentrations (>9 g/L) fermentative metabolism and ethanol production continue to occur even in the presence of oxygen. Here, NADH generated from the glycolysis is reoxidised by producing ethanol rather than the combined pathways of respiration i.e., glycolysis, TCA cycle and oxidative phosphorylation. The Crabtree effect may be due to a saturation of the limited respiratory capacity of yeast cells. Thus glucose sensitive yeasts like *S. cerevisiae* i.e., Crabtree-positive yeast, may possess a limited oxidative capacity when grown on glucose which leads to an overflow reaction at the pyruvate branch (Figure 3-2). This respiratory bottleneck in yeast indicates overflow metabolism of glucose to ethanol when the respiratory capacity is saturated either due to glu-

cose overload, the Crabtree Effect or to anaerobic conditions, the Pasteur Effect (Barwald and Fischer, 1996).

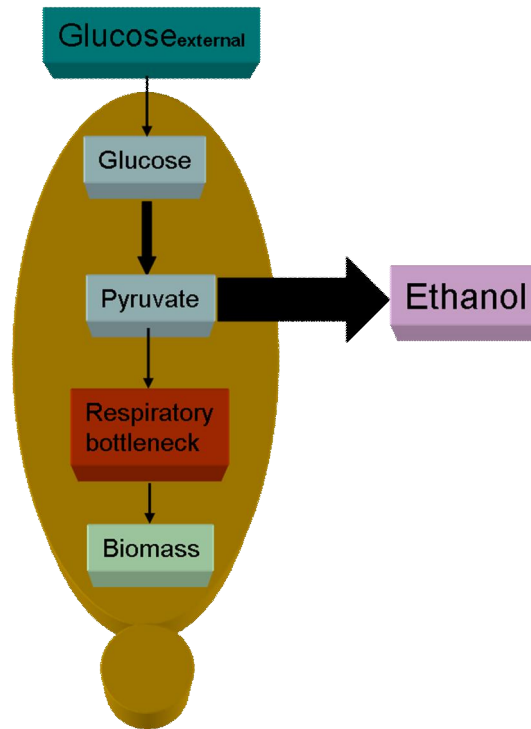


**Figure 3-2** Schematic representation of overflow metabolism at pyruvate branch in *S. cerevisiae*

### 3.3.1.7 Carbon catabolite repression

Glucose and fructose are the most preferred carbon substrates for yeast. When one of these sugars is present, the enzymes required for the utilization of alternative carbon sources are synthesized at low rates or not at all. This phenomenon is called “carbon catabolite repression” or most commonly “glucose repression”. Glucose may affect enzyme levels by causing a decrease in the concentration of corresponding mRNAs, a decrease in their translation rate, or an increase in the degradation rate of the protein. The main effect of glucose takes place at the transcriptional level as the control of mRNA translation rate is not common in yeast (Gancedo, 1998). Glucose and other repressing sugars can affect the rate of transcription by two basic mechanisms; they interfere with activators of transcription, or they facilitate the action of proteins with a negative effect on transcription (Gancedo, 1998).

### 3.3.2 Galactose metabolism

The galactose metabolic pathway is commonly known as Leloir pathway. *S. cerevisiae* contains genes, which code for regulatory proteins for a number of metabolic pathways (Sellik et al., 2008). This group of regulatory proteins acts as both positive as well as negative regulatory proteins. Galactose utilization consists of a biochemical pathway that converts galactose into glucose-6-phosphate and a regulatory mechanism that controls whether the pathway is on (in the presence of galactose) or off (in the absence of galactose). Several regulatory genes are present, which code for these enzymes devoted to convert galactose to glucose phosphate. The four enzymes are, galactokinase (coded by the gene, *GAL1*), uridylyltransferase (coded by the gene, *GAL7*), epimerase (coded by a gene, *GAL10*), and phosphoglucomutase (coded by the gene, *GAL5/PGM2*). These four genes are located on chromosome II of yeast cells. A transporter gene (coded by the gene, *GAL2*) encodes a permease that transports galactose into the cell. This gene is located on chromosome XII. Galactose acts as inducer in expressing all the genes by a modulator called Gal4p. All the genes are never expressed unless Gal4p is present in a cell. Hence, it's a key player in gene regulation and plays a significant role in the utilization of galactose. The Gal4p acts as positive regulator. It acts by binding to a specific DNA sequence upstream from the site of initiation and transcription of the *GAL1*, *GAL7* and *GAL10* genes (Platt and Reece, 1998) (Figure 3-3).

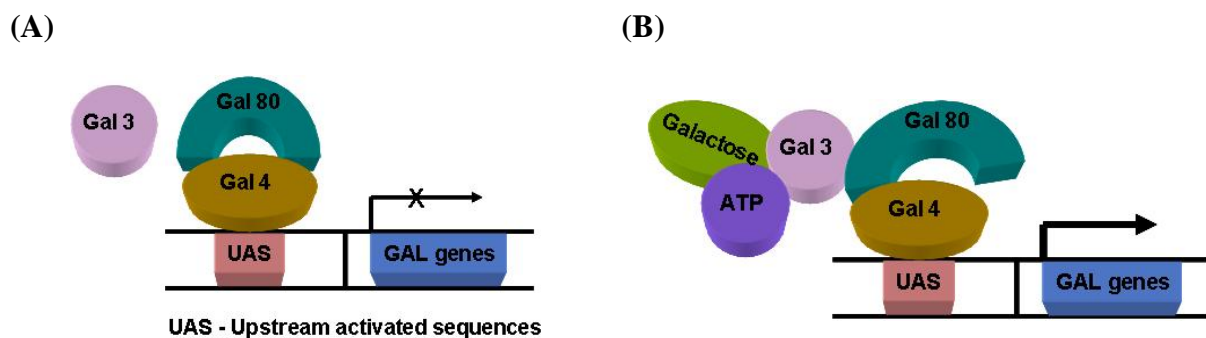


**Figure 3-3** Regulation of galactose metabolism. (A) When there is no galactose, the transcription of *GAL* genes is repressed by Gal80p by binding to the active site on Gal4p (B) In the presence of galactose, the repression on Gal4p by Gal80p is relieved by inducers, Gal3p, ATP and galactose

The regulatory genes *GAL3*, *GAL4*, and *GAL80* exert tight transcriptional control over the transporter, the enzymes, and to a certain extent, each other. Gal4p is a DNA-binding factor that can strongly activate transcription, but in the absence of galactose, Gal80p binds Gal4p

and inhibits its activity. When galactose is present in the cell, it causes Gal3p to associate with Gal80p. This association causes Gal80p to release its repression of Gal4p, so that the transporter and enzymes are expressed at a high level (Figure 3-3). In the presence of galactose, genes for galactose utilizing enzymes are turned on and transcription is switched off when galactose is absent (Ostergaard et al., 2001) (Figure 3-4). Although these genes and interactions form the core of the GAL pathway, the complete regulatory mechanism is more complex and involves genes whose roles in galactose utilization are not entirely clear. For instance, the gene *GAL6* (*LAP3*) functions predominantly in a drug-resistance pathway, but can suppress transcription of the GAL transporter and enzymes under certain conditions and may itself be transcriptionally controlled by *GAL4*.

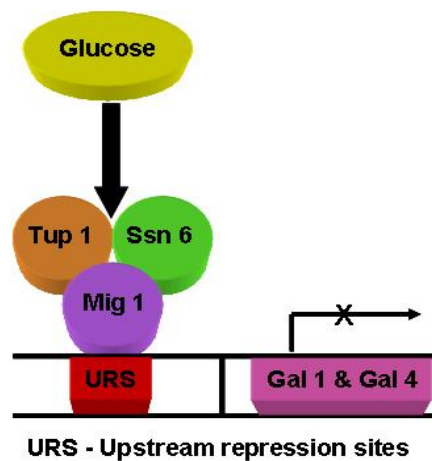


**Figure 3-4** In the presence of glucose, the transcription of *GAL* genes is repressed by a repressor complex involving Tup1p, Ssn6p and Mig1p

In this galactose-glucose interconversion pathway, galactose is phosphorylated to galactose 1-phosphate by galactokinase. Galactose 1-phosphate acquires an uridyl group from UDP-glucose, an intermediate in the synthesis of glycosidic linkages, and produces UDP-galactose and glucose 1-phosphate by galactose 1-phosphate uridyl transferase. The galactose moiety of UDP-galactose is then epimerized to glucose by UDP-galactose 4-epimerase (Schulz et al., 2004). Glucose 1-phosphate is isomerized to glucose 6-phosphate by phosphoglucomutase and later on funnelled to glycolytic pathway (Figure 3-5). In many yeast species, growth on certain sugars (such as galactose, raffinose, and maltose) occurs only under respiratory conditions (Goffrini et al., 2002). That means yeast species can grow on these sugars aerobically, but they cannot grow anaerobically or in the absence of respiration (Entian et al., 1983; Goffrini et al., 1989, 1996; Sims et al., 1978). Assimilation of these sugars occur only under respiring conditions i.e., growth does not take place if inhibitors, mutation, or anaerobiosis

blocks respiration. This apparent dependence on respiration for the utilization of certain sugars has often been suspected to be associated with the mechanism of the sugar uptake step. The phenomenon has been known by the classical name of the “Kluyver effect”. The kind of sugars involved varies depending on the species and sometimes on the strains within a species. Although the reason for this apparent dependence on respiration for the assimilation of certain sugars is not clear, the phenomenon does appear to be brought about by the interplay of several factors involving lowered rate of transport and metabolism of certain sugars. *S. cerevisiae* generally does not show this phenomenon (Kluyver effect negative), although *K. lactis* and *S. cerevisiae* seem to use similar pathways to metabolize galactose, raffinose, and maltose.

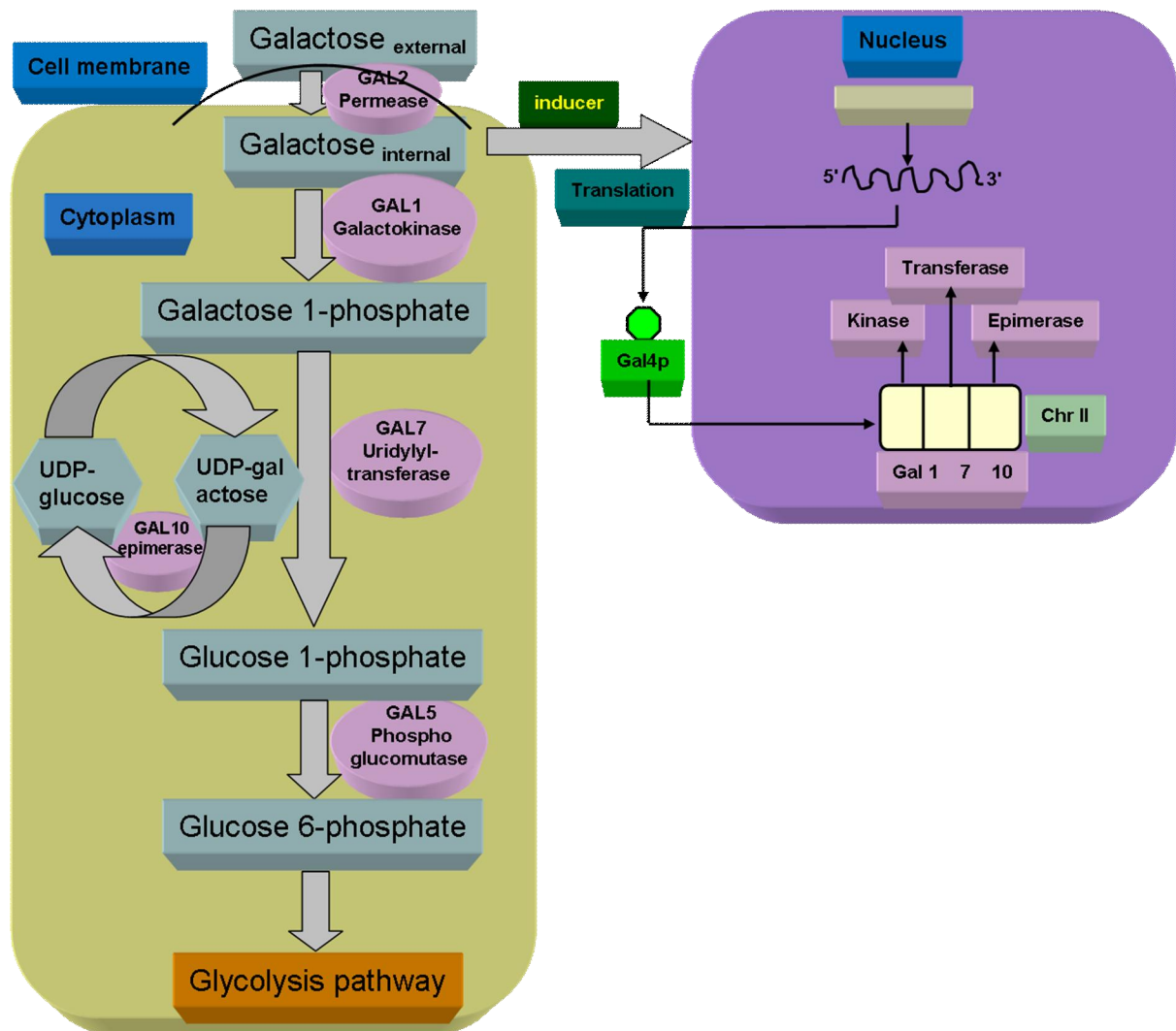


**Figure 3-5** Galactose metabolism in yeast. Schematic representation of interconversion of galactose to glucose 6-phosphate, a glycolytic intermediate and regulation of galactose metabolism by Gal4p

### 3.3.3 Fructose metabolism

In yeast, fructose is metabolized by the fructose 6-phosphate pathway. Fructose is phosphorylated to fructose 6-phosphate by hexokinase (*HXK1* gene) enzyme and then converted to fructose 1, 6-bisphosphate by 6-phosphofructokinase (*PFK1* gene) enzyme. A specific fructose bisphosphate aldolase (*FBA1* gene) enzyme converts fructose 1, 6-bisphosphate to glyceraldehyde 3-phosphate and DHAP. Glyceraldehyde 3-phosphate is funnelled into glycolytic pathway and further metabolized (Berg et al., 2002) (Figure 3-6).

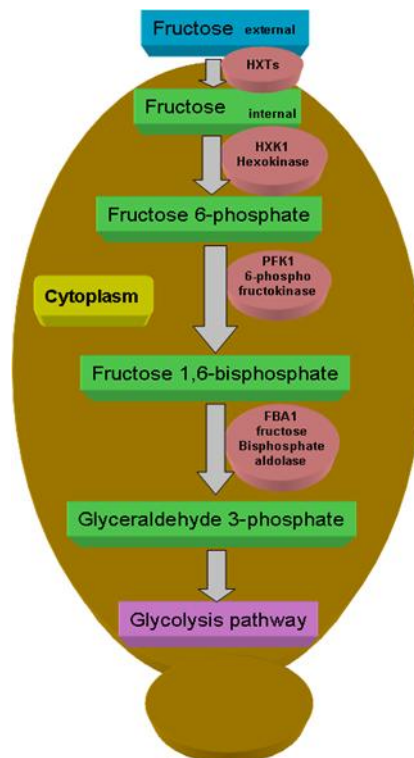


**Figure 3-6** Fructose metabolism in yeast. Schematic representation of interconversion of fructose to glyceraldehyde 3-phosphate, a glycolytic intermediate

### 3.3.4 Hexose transporters (HXTs)

The most preferred hexose carbon sources of yeast are glucose, fructose and mannose. At very high concentrations of these sugars, glycolytic flux rates can attain very high levels leading to alcohol production even in the presence of oxygen. Yeast has a broad range of hexose concentration tolerance, ranging from 1.5 M to micro-molar concentrations and exhibits characteristic responses to changes in the environmental sugar concentrations. Among hexoses, glucose is the most preferred carbon and energy source and its transport into the cells exerts a high control on the glycolytic flux. Glucose can also act as a “growth hormone” to regulate

several aspects of cell growth, metabolism and development and it triggers regulatory mechanisms that are responsible for rapid changes in the activity of proteins and for slower changes in the expression level of specific proteins. But how a cell senses glucose and signal transduction, how this signal affects cellular processes and how optimal utilization of the sugar is achieved are still unknown mechanisms. Defects in glucose sensing, signalling and metabolism cause the severe metabolic disorders in mammals known as diabetes. Thus, it is of major interest to understand these processes.

The first and essential step in hexose utilization is the transport of sugar molecules across the plasma membrane into the cells. Hexose transport is mediated by two different mechanisms, carrier mediated facilitated diffusion, which is energy independent and transports its substrates down a concentration gradient and active proton-sugar symport systems, which is energy dependent and couples the uptake of glucose molecules to the uptake of protons. Yeast has 20 different genes related to hexose sensors and transporters, which belong to major facilitator super family (MFS) of transporters (Ko et al., 1993). This includes

- Hexose sensors - Snf3p and Rgt2p;
- Galactose transporter - Gal2p;
- Low affinity transporters - Hxt1p, Hxt3p;
- Moderate affinity transporter – Hxt5p
- High affinity transporters – Hxt2p, Hxt4p, Hxt6p, Hxt7p;
- Pleiotropic drug resistance (PDR) process - Hxt9p and Hxt11p;
- Unknown transporters – Hxt8p, Hxt10p, Hxt12p to Hxt17p;

### 3.3.4.1 Hexose sensors

*SNF3* and *RGT2* have only limited sequence similarities to the other hexose transporters. Snf3p serves as a regulatory signal (Liang et al., 1996) rather than nutritional uptake and Snf3p functions as a sensor for low concentrations of glucose. *RGT2* is 60 % identical to *SNF3* and is located 100 kb downstream of *SNF3* on chromosome IV and functions as a sensor for high concentrations of glucose (Moriya and Johnston, 2003).

### 3.3.4.2 Galactose transporter

The deletion of *GAL2*, the gene coding for the transporter of galactose, which is located on chromosome XII, causes poor growth on galactose medium (Tscopp et al., 1986; Nehlin et al., 1989). *HXT6* and *HXT7* are 71.8% identical to *GAL2*.

### 3.3.4.3 Low affinity hexose transporters

*HXT1* is located on chromosome VIII. Hxt1p has extremely low-affinity for glucose, fructose and mannose ( $K_m$  (glucose) = 100 mM;  $K_m$  (fructose) > 300 mM). *HXT3* is located on chromosome IV and 86.4% identical to *HXT1*. Hxt3p is also a low-affinity hexose transporter with a very high  $K_m$  for glucose (60 mM). Induction of *HXT3* is independent of sugar concentration and is expressed only on glucose medium. *HXT4* is located on chromosome VIII, just downstream of *HXT1* and 83.4% identical to *HXT6* and *HXT7*. Hxt4p has a moderately low affinity for glucose ( $K_m$  about 9 mM) and a low affinity for fructose ( $K_m$  about 50 mM).

### 3.3.4.4 High affinity hexose transporters

*HXT6* and *HXT7* are highly similar and located on chromosome IV, downstream of *HXT3*. These are high-affinity glucose transporters ( $K_m$  about 1-2 mM). Hxt9p, Hxt11p and Hxt12p are very closely related proteins with similar regulatory signals and located on chromosomes X, XV and IX respectively. *HXT9* and *HXT11* are weakly expressed and are not regulated by the carbon source. These have been found to be involved in the pleiotropic drug resistance (PDR) process. Hxt5p and Hxt8p do not contribute significantly to catabolite glucose transport. *HXT5* is located on chromosome VIII, just upstream of *HXT1* and *HXT4*. *HXT8* is located on chromosome X. *HXT13*, *HXT15*, *HXT16* and *HXT17*, which are located on chromosomes V, IV, X and XIV respectively are closely related hexose transporter proteins and distantly related to the other members of the Hxtp family. Actual function of these transporters is not known yet. Deletion of these genes did not cause any obvious growth phenotype.

### 3.3.4.5 Glucose sensing mechanisms in yeast

In yeast, glucose is not only the most preferred carbon and energy source but also an important primary messenger molecule, a global regulator of metabolism and signalling optimal growth conditions to the cellular machinery (Rolland et al., 2002). Moreover, the major transporters are also regulated at transcriptional level by the extracellular glucose concentration

(Özcan et al., 1999). There are three different glucose sensing systems in yeast. Each system senses the extracellular glucose and transmits the signal to the appropriate effectors differently.

- 1) Main glucose repression pathway.** When glucose concentration is high, Snf1p protein kinase represses the expression of many genes involved in utilization of alternative carbon sources via Snf1-Mig1 glucose repression pathway (Gancedo et al., 1998; Carlson et al., 1999; Kuchin et al., 2000, 2002).
  
- 2) Snf3/Rgt2 pathway.** Snf3 and Rgt2 sensors induce expression of genes encoding hexose transporters in the presence of glucose via Snf3-Rgt2-Rgt1 glucose induction pathway (Johnston et al., 1999). Rgt1, a zinc-finger-containing DNA binding transcriptional factor, is an ultimate target of this pathway. In the absence of glucose, Rgt1p recruits the Ssn6p repressor complex to the promoters of specific genes (Ozcan et al., 1996) and binds and represses the expression of both intermediate and low affinity *HXT* genes with the help of two paralogous proteins, Mth1p and Std1p (Schmidt et al., 1999; Lafuente et al., 2000). Even low amounts of glucose inhibits the repressor function of Rgt1p in the presence of Grr1p protein (Ozcan et al., 1995), resulting in derepression of expression of *HXT* genes. In order to act as an activator, removal of Mth1p and Std1p as well as phosphorylation of Rgt1p is required. The glucose signal mediated by Snf3p and Rgt2p sensors inhibits Rgt1-mediated repression by stimulating the degradation of Mth1p and Std1p (Flick et al., 2003; Li et al., 1997).
  
- 3) Gpr1/Gpa2 pathway.** The glucose signal mediated by G-protein-coupled receptor Gpr1 and cyclic AMP as a second messenger (Thevelein et al., 1998; Rolland et al., 2002) leads to activation of protein kinase A, which phosphorylates Rgt1p and releases the repression of *HXT* genes (Kaniak et al., 2004; Ozcan et al., 1996).

Figure 3-7 representing the hexose sensors and transporters and their regulation according to the glucose levels (Ozcan and Johnston, 1995).

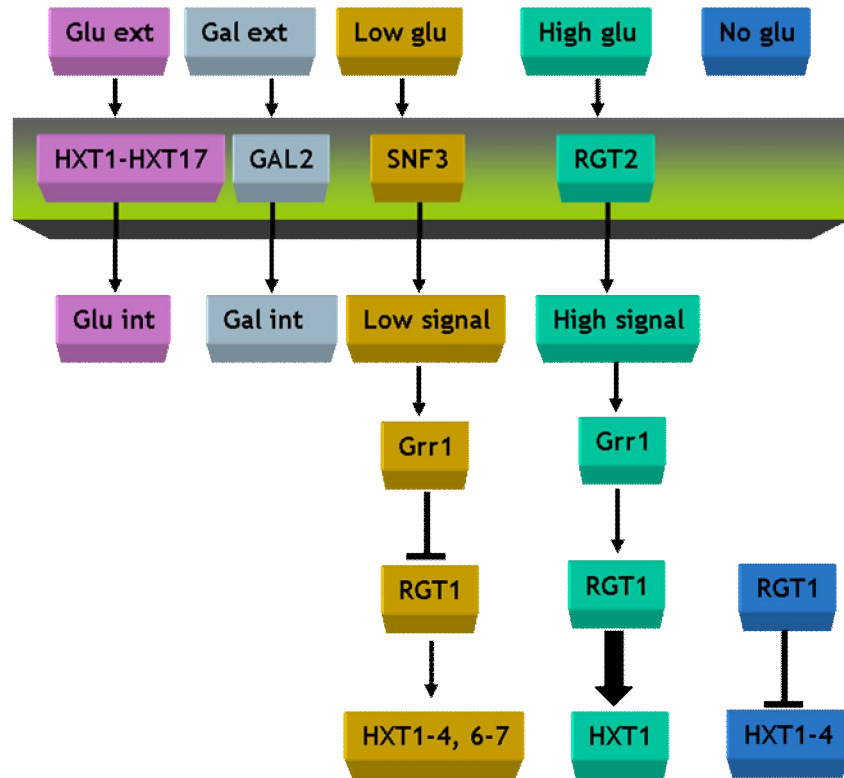


**Figure 3-7** Hexose sensors and transporters and their regulation.

## 4. MATERIALS AND METHODS

### 4.1 YEAST STRAINS

*S. cerevisiae* deletion mutants with parental genotype of BY4742 *Mat $\alpha$  his3 $\Delta$ 1 leu2 $\Delta$ 0 lys2 $\Delta$ 0 ura3 $\Delta$ 0* were obtained from Open Biosystems (Heidelberg, Germany). These strains exhibit auxotrophy for lysine, leucine, histidine, and uracil, and are resistant to the antibiotic geneticin. From this collection, the parental strain, which was used as the reference strain, and a set of deletion mutants, where genes are known to be involved in central carbon metabolism, amino acid biosynthesis and a few strains with unknown function were chosen.

### 4.2 MEDIA COMPOSITION

Freeze cultures were revived on YPD agar plates with 200 mg L<sup>-1</sup> geneticin. First precultivations were carried out in complex medium. Second precultivations and main cultivations were carried out in defined medium. The media compositions are as follows. Vitamin and trace element stock solutions, and stock solutions for lysine, leucine, histidine, and uracil, respectively, were sterilized by filtration. All other solutions were sterilized by autoclaving (15 min, 121 °C).

**Table 4-1.** YPD agar medium composition

Component	Concentration (g/L)
Yeast extract	10
Peptone	20
Glucose	20
Agar	20

**Table 4-2.** Complex medium composition

Component	Concentration (g/L)
Glucose monohydrate	11
Yeast extract	3
Peptone	5
Malt extract	3

**Table 4-3.** Defined medium composition

Component	Concentration (g/L)
(NH <sub>4</sub> ) <sub>2</sub> HPO <sub>4</sub>	1.0
(NH <sub>4</sub> ) <sub>2</sub> SO <sub>4</sub>	8.75
MgSO <sub>4</sub> ·7H <sub>2</sub> O	1.0
Citric acid	0.025
KCl	1.1
CaCl <sub>2</sub> ·2H <sub>2</sub> O	0.15
Glucose monohydrate	22.0
Lysine	0.12
Leucine	0.12
Histidine	0.08
Uracil	0.08
Component	Concentration (ml/L)
0.5 M Na-phosphate buffer (pH 6)	100
100x Trace element solution	10
100x Vitamin solution	10

**Table 4-4.** 100x Trace element solution (pH <2)

Component	Concentration (mg/50ml)
FeCl <sub>3</sub> ·6H <sub>2</sub> O	75
MnSO <sub>4</sub> ·H <sub>2</sub> O	53
ZnSO <sub>4</sub> ·7H <sub>2</sub> O	45
CuSO <sub>4</sub> ·5H <sub>2</sub> O	12

**Table 4-5.** 100x Vitamin solution

Component	Concentration (mg/50ml)
myo-inositol	301.5
Ca-pantothenic acid	150
Thiamin hydrochloride	30
Pyridoxine hydrochloride	7.5
Biotin	0.15

### 4.3 DEFINED MEDIUM OPTIMIZATION

In order to obtain quantitative data for phenotypic profiling, reproducible and defined cultivation of the examined deletion mutants of *S. cerevisiae* was required. For this purpose a defined medium was developed. Mutants exhibit auxotrophy for the amino acids lysine, leucine and histidine and for uracil. To investigate the optimum amino acid concentrations required for good growth of deletion mutants, growth experiments were carried out with YML054C strain with different amino acid concentrations in the medium as follows, one fold concentra-

tion of lysine, leucine (each 30 mg/L) & histidine, uracil (each 20 mg/L), two fold, four fold, six fold and eight fold concentrations. Figure 4-1 shows that four-fold concentration of lysine, leucine (each 120 mg/L) & histidine, uracil (each 80 mg/L) was optimal for good growth. Defined medium with this composition was used for cultivation in all experiments.

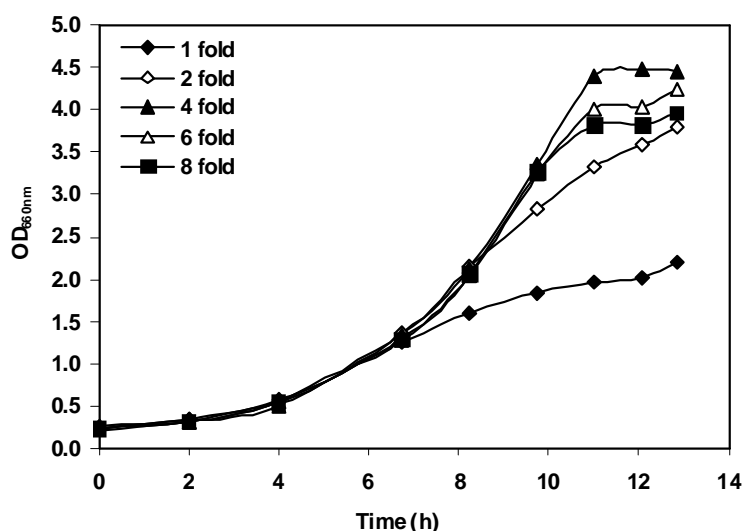


**Figure 4-1** Medium optimization. Strain YML054C was grown in 96-well microtiter plate with different amino acid concentrations in the defined medium. Cultivation profile with one, two, four, six and eight fold concentrations of lysine, leucine, histidine and uracil.

## 4.4 CULTIVATION

Cultivations were carried out either in shake flasks (SFC) or in microtiter plates (MTP).

### 4.4.1 Shake flask cultures

Initially revived cells from YPD agar plates were inoculated into 5 ml complex medium and grown in 50 ml baffled shake flask at 30° C, 250 rpm (INFORS AG, Bottmingen-Basel, Switzerland) for 12 h. Subsequently, cells were harvested by centrifugation (Labofuge 400 R, Functionline, Heraeus Instruments, Bensheim, Germany) at 4° C, 3000 x g for 15 min in Falcon tubes with rotor 8172, and washed two times with sterile 0.9 % (w/v) NaCl. Hundred microliters of the obtained cell suspension was then inoculated into 5 ml defined preculture medium and grown as described above. Prior to main cultivation the inoculum was harvested by centrifugation and washed as described above. Resulting pellet was resuspended in 1 ml defined medium. Main cultivations were carried out in 100 ml baffled shake flasks with 10 ml defined medium and cultivated as described above.

#### 4.4.2 Cross contamination check in MTP

Parallel handling of large number of strains in microtiter plate could lead to cross contamination risk. To check this, a cultivation experiment was carried out with the reference strain at both high (1020 rpm) and low (540 rpm) shaking rates for 24 h. The microtiter plate layout was, only the center four wells were inoculated and the surrounding wells were filled with medium (Figure 4-2A). Only the inoculated wells showed increased optical density, which confirmed that there was no cross contamination at both the shaking rates (Figure 4-2B).

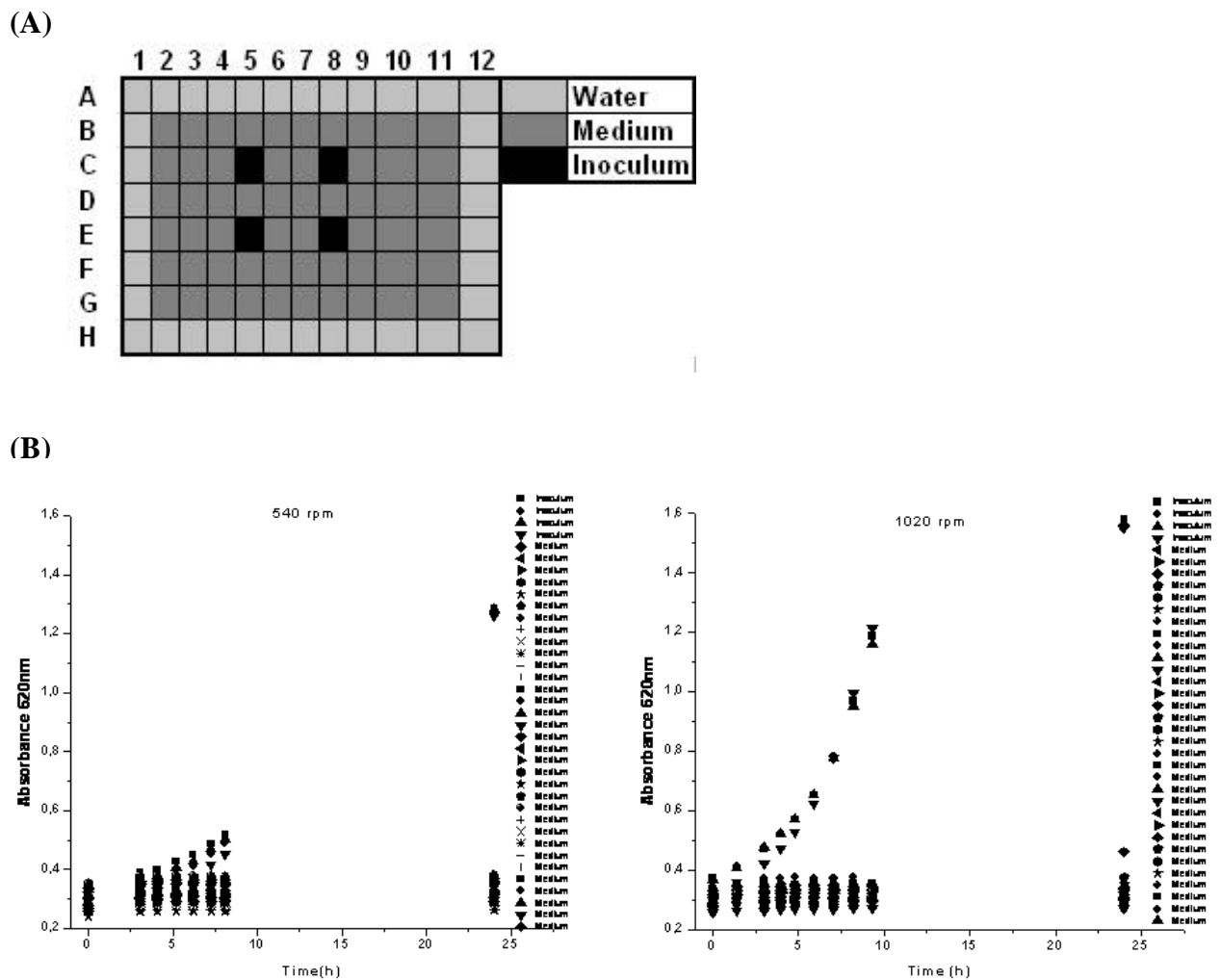


**Figure 4-2** Cross contamination check. (A) Microtiter plate layout. (B) The reference strain was cultivated at low, 540 rpm (left panel) and high, 1020 rpm (right panel) shaking rates for 24 h.

### **4.4.3 Microtiter plate cultures**

For microtiter plate cultivations, precultivations were carried out in 96 well microtiter plates (Greiner bio-one, Frickenhausen, Germany) with 250  $\mu$ l per well. The outermost wells of the plate were not used for cultivation because of higher evaporation in these wells (John et al., 2003). All wells not used for cultivation were filled with water. The microtiter plate was additionally covered with a lid. Cells were incubated for 12 h in a fluorescence reader (Fluoroskan Ascent, Thermo Labsystems, Helsinki, Finland) at 30° C and 1020 rpm (orbital) with a shaking diameter of 1 mm. Cells were harvested by centrifugation (Labofuge 400 R, Functionline, Heraeus Instruments, Bensheim, Germany) at 4° C, 1660 x g for 10 min directly in MTP with rotor 8177, and washed two times with sterile 0.9 % (w/v) NaCl. Ten micro liters of the obtained cell suspension was then inoculated into 250  $\mu$ l defined preculture medium and grown as described above. Prior to main cultivation the inoculum was harvested by centrifugation and washed as described above. The resulting pellet was re-suspended in 200  $\mu$ l defined medium. Main cultivations were carried out in 96 well microtiter plates with immobilized oxygen sensors (Oxoplate F96, PreSens GmbH, Regensburg, Germany) with 150  $\mu$ l defined medium per well.

## **4.5 ANALYTICS**

The following analytical methods were employed to calculate the sugar concentrations, optical density and dissolved oxygen measurements.

### **4.5.1 Sugars and ethanol measurements**

Enzyme assays were applied for the determination of glucose, fructose and ethanol (Boehringer–Mannheim, R-Biopharm GmbH, and Germany). Galactose was quantified by HPLC (Bio-Tek, Neufahrn, Germany) with an Aminex HPX 87-H column (300 x 7.8 mm; Bio-Rad, Hercules, California) and 0.05 N H<sub>2</sub>SO<sub>4</sub> as an eluent with a flow rate of 0.8 ml/min at 45° C and UV detection at 210 nm.

### **4.5.2 Optical density measurements**

Growth was monitored via optical density either at 660 nm (OD<sub>660</sub>) with a spectrophotometer (Novaspec II, Pharmacia Biotech, Cambridge, England) or at 620 nm (OD<sub>620</sub>) with an ab-

sorbance reader (iEMS Ascent, Thermo Labsystems, Helsinki, Finland) directly in the Oxoplate. The obtained correlation between the absorbance reader signals and spectrophotometer measurements is not linear. For calibration, a growth experiment was carried out with strain YML054C in a 96-well Oxoplate as described above for 16 h. Parallel OD measurements were taken for every 1 h directly in the Oxoplate in the absorbance reader ( $OD_{620}$ ) and in the spectrophotometer ( $OD_{660}$ ). A calibration curve was obtained between undiluted reader signals and diluted spectrophotometer measurements (Figure 4-3). Thus OD values measured in an absorbance reader can be directly converted to the corresponding diluted  $OD_{660}$  values by using this calibration curve and equation 4-1.

$$OD_{660corrected} = 0.62 - 4.71 \cdot (OD_{620}) + 6.78 \cdot (OD_{620})^2 + 16.05 \cdot (OD_{620})^3 - 31.76 \cdot (OD_{620})^4 + 15.53(OD_{620})^5$$

(Eq 4-1)

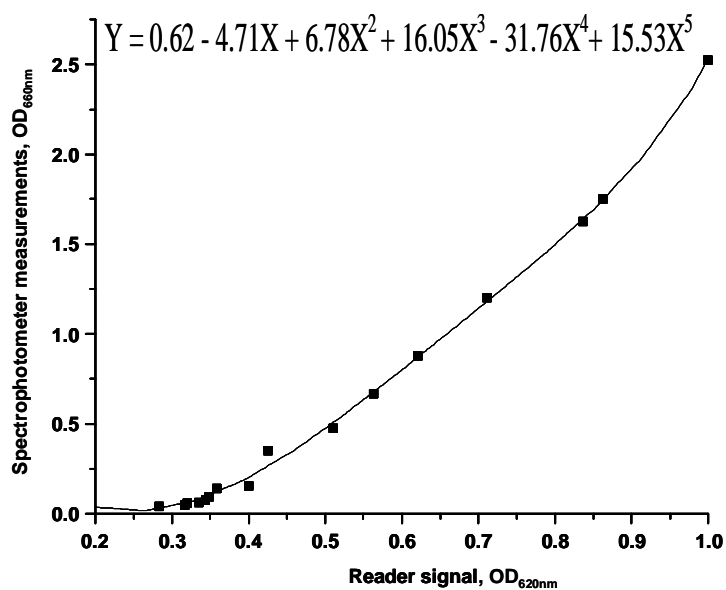


**Figure 4-3** Calibration curve for on-line measurement of OD. Strain YML054C was grown in 96-well microtiter plate and parallel OD measurements were taken in the absorbance reader ( $OD_{620}$ ) and in the spectrophotometer ( $OD_{660}$ ).

Biomass dry weight (BDW) was determined from corrected  $OD_{660}$  after calibration. For this purpose, the reference strain was cultivated in a shake flask and dry cell weight was determined gravimetrically. For this purpose, 10 ml of culture was centrifuged at 4 ° C for 10 min at 10,000 rpm, washed twice with 0.9 % NaCl and then with water and centrifuged again. Washed cells were dried at 80 ° C to constant weight (Kiefer et al., 2002).

The correlation factor (g biomass/OD<sub>660</sub>) between dry cell weight and OD<sub>660</sub> was 0.498. Biomass dry weight can be obtained by using the equation 4-2,

$$BDW = 0.498 \cdot OD_{660corrected} \quad (\text{Eq 4-2})$$

### 4.5.3 Dissolved oxygen measurements

The use of microtiter plates with immobilized oxygen sensors allows on-line monitoring of dissolved oxygen concentrations during cultivation. The OxoPlate F96 is a sterile polystyrene microplate (PRESENS, Germany) with 96 integrated sensors and is calibration-free (Figure 4-4).



**Figure 4-4** OxoPlate F96, 96-well round bottom microtiter plate with an immobilized oxygen sensor.

High accuracy is assured using two different dyes to get an internal referenced signal. Because these two dyes are immobilized in a thin hydrophilic matrix (10 µm thickness) of the OxoPlate, response times are very low. The fluorescent intensities were measured with the fluorescence filter combinations 544/644 nm and 544/590 nm. The first one was depending on oxygen concentration; the latter was a reference signal, which was independent of oxygen concentration. The relationship between fluorescence intensity and dissolved oxygen concentration is nonlinear and described by the Stern – Volmer equation for collision quenching (Equation 4-3) (John et al., 2003),

$$\frac{I_r}{I_{r,o}} = \frac{1}{1 + K_{sv}(O)} \quad (\text{Eq 4-3})$$

$O$  - Dissolved oxygen concentration

$I_{r,o}$  - Fluorescence intensity in the absence of  $O$ ;

$I_r$  - Fluorescence intensity at  $O$

$K_{sv}$  - Stern-Volmer constant

#### 4.5.4 Malic enzyme activity

Preparation of cell extracts and determination of malic enzyme activity was carried out as described by Boles et al. (1998) with slight modifications. Extracts were not dialysed. Cells were disrupted by sonication with 0.5-mm-diameter glass beads at 0° C for 3 min (15-s intervals with 15-s resting time), using an MSE sonicator (Soniprep 150 with 150-W output, 10µm peak-to-peak amplitude).

### 4.6 SIMULATIONS

The following simulations were carried out to estimate oxygen mass transfer coefficient and to correct ethanol and water evaporation during the cultivation.

#### 4.6.1 Dynamic oxygen mass transfer coefficient ( $k_{La}$ )

Oxygen uptake rate can be determined from a stationary liquid phase oxygen balance,

$$\frac{dO}{dt} = k_{La}(O^* - O) - OUR \quad (\text{Eq 4-4})$$

where  $O^*$  and  $O$  are the dissolved oxygen concentrations in the liquid phase and in equilibrium with the gas phase respectively,  $k_{La}$  is the volumetric liquid phase mass transfer coefficient and OUR is the oxygen uptake rate.

The volumetric liquid phase mass transfer coefficient,  $k_{La}$  was determined experimentally in Oxoplates in 200 µL at 540 rpm by using sodium dithionite method as described previously (John et al., 2003). In brief, dissolved oxygen was initially depleted by addition of 2 % (w/w) sodium dithionite solution in 0.1 M sodium carbonate solution. Due to fast chemical reaction, oxygen reaction rate was much greater than the air–liquid oxygen transfer. After consumption of dithionite, oxygen reaction rate became zero and oxygen started to accumulate in the medium. In this phase,  $k_{La}$  was estimated from the slope of the curve  $\ln(O^* - O)$  versus time.

Alternatively, the equation 4-4 was programmed and the simulations were done using BERKELEY MADONNA software 8.0.2 (Dunn et al., 2003). Corresponding program is supplied in the Appendix.

Figure 4-5 depicts the typical profile for the dynamic estimation of  $k_{LA}$ . Due to the oxidation of dithionite, dissolved oxygen concentration was dropped to zero and after the consumption, dissolved oxygen concentration again started to rise due to oxygen transfer from air eventually reaching the saturation concentration. The rise of oxygen is first order and the  $k_{LA}$  was estimated from liquid phase oxygen balance using the simulation program. The estimated  $k_{LA}$  was  $1.46 \text{ h}^{-1}$ .

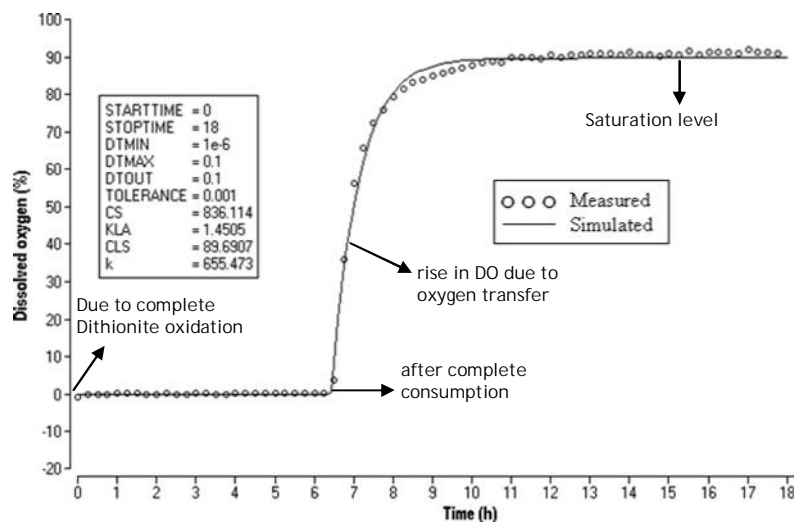


**Figure 4-5** Dynamic estimation of  $k_{LA}$  using dithionite method in Oxoplate at 540 rpm, orbital shaking, 1 mm shaking diameter,  $T = 30^\circ \text{ C}$  in  $200 \mu\text{L}$  volume. Symbols indicate experimental data and solid line represents simulations.

#### 4.6.2 Dynamic model for yields and specific growth rates

Specific growth rate was determined using a simple dynamic growth model suitable for balanced growth comprising balances for biomass,  $X$ , substrate glucose,  $S$ , product ethanol,  $P$ , and dissolved oxygen,  $O$ . This model was also used to determine biomass yield on oxygen and to correct for evaporation losses of ethanol and water. The model assumes constant yield of biomass and ethanol on glucose and oxygen. The variable volume mass balance equations were as follows

$$\frac{d(XV)}{dt} = r_X V = \mu XV \quad (\text{Eq 4-5})$$

$$\frac{d(SV)}{dt} = -\frac{r_X V}{Y_{XG}} \quad (\text{Eq 4-6})$$

$$\frac{d(PV)}{dt} = r_X Y_{PX} V - r_{P, \text{evap}} = r_X Y_{PX} V - k_{P, \text{evap}} P \quad (\text{Eq 4-7})$$

$$\frac{d(OV)}{dt} = k_L a (O^* - O) - \frac{r_X V}{Y_{XO}} \quad (\text{Eq 4-8})$$

$$\frac{d(V)}{dt} = -\frac{r_{H_2O, \text{evap}} + r_{P, \text{evap}}}{\rho} \quad (\text{Eq 4-9})$$

Growth kinetics were described with Monod-type kinetics (Dunn et al., 2003)

$$r_X = \mu_{\max} \frac{S}{K_S + S} \frac{O}{K_O + O} \quad (\text{Eq 4-10})$$

Simulations were carried out using BERKELEY MADONNA software and corresponding program is supplied in the Appendix. The meaning of the symbols is

V – Volume [L];

X – Biomass concentration [g L<sup>-1</sup>];

S – Glucose concentration [mol L<sup>-1</sup>];

P – Ethanol concentration [mol L<sup>-1</sup>];

O – Dissolved oxygen concentration [mol L<sup>-1</sup>];

O\* – Gas-liquid equilibrium dissolved oxygen concentration [mol L<sup>-1</sup>];

t – Time [h];

r<sub>X</sub> – Biomass formation rate [g L<sup>-1</sup> h<sup>-1</sup>];

μ - Specific growth rate [h<sup>-1</sup>];

Y<sub>XG</sub> – Biomass yield on glucose [g mol<sup>-1</sup>];

Y<sub>PX</sub> – Ethanol yield with reference to biomass production [mol g<sup>-1</sup>];

Y<sub>XO</sub> – Biomass yield on oxygen [g mol<sup>-1</sup>];

r<sub>P, evap</sub> – Rate of ethanol evaporation [mol h<sup>-1</sup>];

k<sub>P, evap</sub> – First order rate constant for ethanol evaporation [h<sup>-1</sup>];

k<sub>L</sub>a – Oxygen mass transfer coefficient [h<sup>-1</sup>];

k<sub>H2O, evap</sub> – Rate of evaporation of water [g h<sup>-1</sup>];

K<sub>S</sub>, K<sub>O</sub> – Substrate and oxygen affinity constant [mol L<sup>-1</sup>]

### 4.6.3 Dynamic model for correcting ethanol and water

To estimate the loss of ethanol and water during cultivation, experiments were carried out with different initial ethanol concentrations of 2.5, 4 and 6 g L<sup>-1</sup> at the same operating conditions as the main cultivations. Ethanol concentrations were determined for every 2 h and rate of ethanol evaporation was calculated. The estimated first order evaporation rate constant,  $k_{P, \text{evap}}$ , was 0.052 h<sup>-1</sup>. There was no influence of shaking rate on the ethanol evaporation rate constant, which agrees with previous work (Oeggerli et al., 1994). Since water was also evaporating, the culture volume was checked at the end of the cultivation to find the rate constant. The difference in culture volume was 5 µl after 12.5 h of cultivation. Thus the evaporation constant for water was estimated as  $0.4 \times 10^{-3}$  g h<sup>-1</sup>. Kinetic parameters  $K_O$  (= 2.2 mmol L<sup>-1</sup>) and  $K_S$  (= 0.5 mmol L<sup>-1</sup>) were taken from the literature (Furukawa et al., 1983). The saturation concentration of oxygen,  $O^*$ , under the applied conditions was 7.53 mg L<sup>-1</sup>. By using this simulation model with determined ethanol and water evaporation rates, a hypothetical ethanol concentration can be calculated which would have been observed in the absence of evaporation (Figure 4-6).

$$\frac{d(P_h V)}{dt} = r_X Y_{PX} V \quad (\text{Eq 4-11})$$

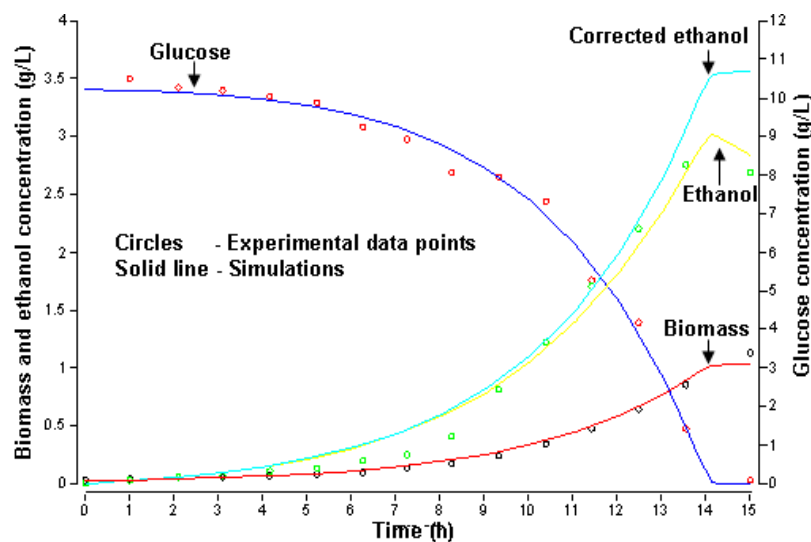


**Figure 4-6** Dynamic model for ethanol correction using BERKELY MADONNA program. Strain 56 was grown in an Oxoplate at 1020 rpm, orbital shaking, 1mm shaking diameter, T = 30 C in 200 µL volume.

This simplified growth model was only used for growth phases exhibiting balanced growth, i.e. as long as there wasn't any limitation of glucose or oxygen. Oxygen uptake rates were only estimated at dissolved oxygen concentrations between 40 % and 90 % air saturation. If oxygen mass transfer is very high, dissolved oxygen concentration is near saturation and because of experimental errors it is not possible to get reliable estimates of oxygen uptake rate. Therefore, in cases of low oxygen uptake rates additional cultures at lower shaking rate were carried out. In cases with oxygen limitation, ethanol evaporation and specific growth rate were estimated with a reduced model lacking oxygen balance (Equation 4-8) and the oxygen term of Equation 4-10.

Specific growth rates were directly estimated from estimated biomass concentrations during true exponential growth phase. From the increase in biomass concentration and glucose consumption, biomass yield on hexoses was directly determined. Ethanol yield on hexoses was estimated using the model and high shaking rate experimental data. Biomass yield on oxygen was determined from low shaking rate experiments during declining dissolved oxygen concentration above 20 % air saturation using the model (Equations 4-5 and 4-6). The dissolved oxygen profiles for all the strains are given in the Appendix.

## **4.7 ETHANOL LABELING ANALYSIS AND QUANTIFICATION USING MALDI-TOF-MS**

A new method was developed for the quantitative estimation of isotope-labeled ethanol produced from labelled substrate during cultivation. Subsequently metabolic split ratio between glycolysis and PP pathway was estimated based on the ethanol labelling using matrix-assisted laser desorption/ionization time-of-flight mass spectrometry (MALDI-ToF-MS).

### **4.7.1 Principle**

The working principle is an alcohol dehydrogenase (ADH) enzymatic oxidation of labelled ethanol to acetaldehyde (AC) with subsequent formation of the barely volatile acetaldehyde-2,4-dinitrophenylhydrazone (Ac-DNPH) in a separate vial after diffusion through the gas headspace. Derivatization with 2, 4-dinitrophenylhydrazine (DNPH) has been shown to be very efficient for trapping trace amounts of carbonyl compounds (Dong et al., 2004). After extraction with ethyl acetate and evaporation of the organic phase, the solid Ac-DNPH is

dissolved in  $\alpha$ -cyano-4-hydroxycinnamic acid (CCA) matrix solution and analyzed by MALDI-ToF-MS. Schematic representation of the work flow is given in figure 4-7.

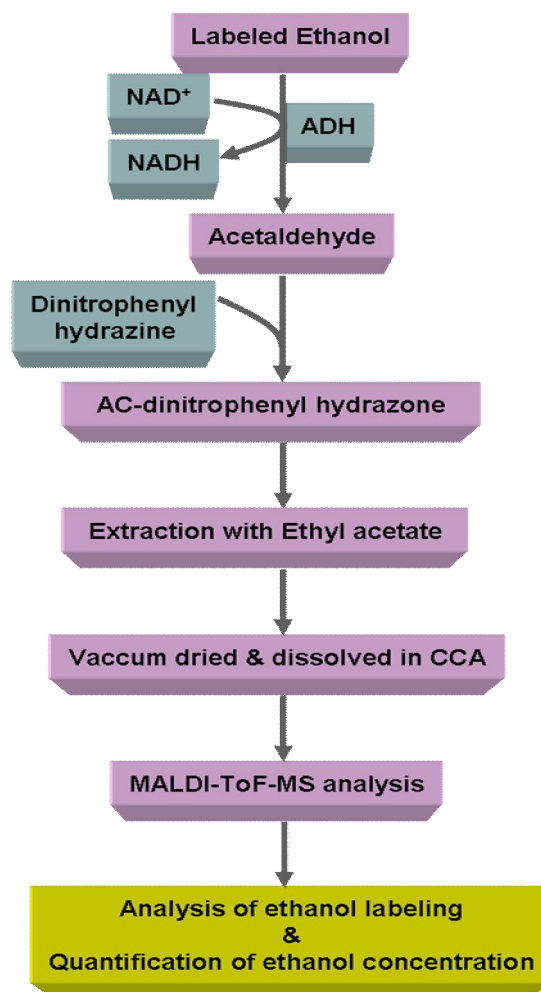


**Figure 4-7** Schematic representation of analysis of ethanol labelling using MALDI-ToF-MS.

## 4.7.2 Sample preparation

Seventy-five microliter of centrifuged and diluted culture supernatant was put into a 2 ml glass vial sealable with rubber septum and alumina crimp seal. To this solution, 25  $\mu$ l of 0.7 % [ $^{13}\text{C}_2$ ]-ethanol in 400 mM Tris/HCl (pH 8.8) was added. For unlabeled ethanol quantification 14 samples from 1 to 50  $\mu$ l of 0.7 % (w/w) ethanol in 100 mM Tris/HCl (pH 8.8), topped up with 100 mM Tris/HCl buffer to 100  $\mu$ l were used. For quantification of [ $1\text{-}^{13}\text{C}$ ]-ethanol, 14 samples from 1 to 25  $\mu$ l unlabeled ethanol plus the equal volumes of [ $1\text{-}^{13}\text{C}$ ]-ethanol were topped with buffer and 25  $\mu$ l of [ $^{13}\text{C}_2$ ]-ethanol as described above. All three ethanol types were 0.7 % (w/w) in 100 mM Tris/HCl buffer (pH 8.8). The enzymatic reaction was started by adding 50  $\mu$ l of 1 mg /ml ADH (corresponding to 30 U) followed by 50  $\mu$ l of 70 mg/ml  $\text{NAD}^+$ , both in 100 mM Tris/HCl buffer (pH 8.8). A 0.3 ml micro insert tube containing 75  $\mu$ l

of supernatant of centrifuged saturated DNPH solution in 10 % phosphoric acid was placed inside this 2 ml tube. The 2 ml vial was tightly closed immediately and incubated at 25° C for 16 h.

This set up (Figure 4-8) consists of an inner compartment of acidified DNPH solution, which is separated from the culture supernatant. Volatile compounds can freely diffuse into this inner compartment via the gas phase. After incubation, the insert tube was removed and 150 µl of ethyl acetate was added and intensively mixed several times by pipetting. Organic and aqueous phases were separated by short centrifugation. Hundred microliters of the upper organic phase was transferred into a PCR tube and dried in a vacuum centrifuge (Speed-Vac, Juan, RC 10.22, Saint-Nazaire, France) for 30 min. The residue was dissolved in 15 µl of CCA- matrix solution (saturated α-cyano-4-hydroxycinnamic acid in 50 % acetonitrile and 1 % trifluoroacetic acid). Then 2 µl of this solution was pipetted onto the 384 MALDI-TOF steel target plate and air-dried.

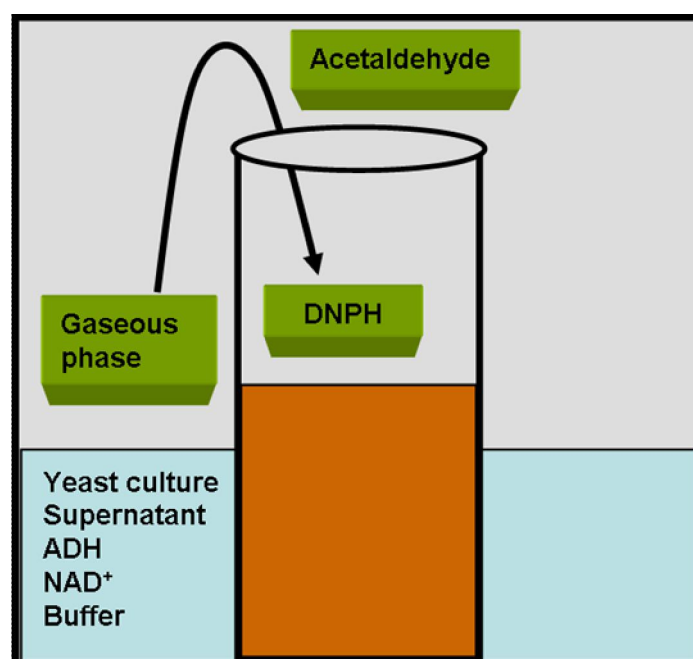


**Figure 4-8** Design of the reaction vials. The outer tightly closed 2 ml vial contains 200 µl liquid consisting of sample, ADH from *S. cerevisiae*, NAD<sup>+</sup> and [<sup>13</sup>C<sub>2</sub>]-ethanol as internal standard. The insert was filled with 75 µl supernatant of saturated DNPH solution in diluted phosphoric acid.

### 4.7.3 Acquisition of MS spectra and peak selection

Analyses were performed on a Bruker Reflex III<sup>TM</sup> time of flight mass spectrometer (Bruker-Daltonics, Bremen, Germany) equipped with the SCOUT 384<sup>TM</sup> probe ion source. The system used a pulsed nitrogen laser (337 nm, Model VSL-337ND, Laser Science Inc., Boston, MA) with energy of 400 $\mu$ J/pulse. The ions were accelerated under delayed extraction conditions in the positive mode with an acceleration voltage of 20 kV and a reflector voltage of 22.5 kV. A 6.7 kV potential difference between target and the extraction lens was applied with a time delay of 200 ns. A Lecroy Signalyst LS 10, 2GS/s, 1 GHz digital storage oscilloscope was used for data acquisition (Lecroy Corp., Chestnut Ridge, NY, USA). The detector signals were amplified in two stages, digitized and transferred to the XACQ program on a NT 4 work-station (Microsoft, USA). Autoexecute mode was chosen for automated measurements with 26-32 % laser power, a resolution better than 1400, a signal to noise-ratio (S/N) better than 4 and a noise range of 100 leading to optimal intensity. Spectra with saturated peaks were not used. For each spectrum, 12 sub spectra from more than 6 spots consisting of 25 successful laser shots were added. The data were further processed with the program XMASS 5.15 (Bruker Daltonics, Bremen, Germany) using the APEX-algorithm for the detection of all peaks within 215-237 Da with a threshold of 250 a.i. Each sample was measured in four replicates.

All  $m/z$  values were rounded to integers and used with their absolute intensities. Carbon mass isotopomer fractions of ethanol were calculated from the measured distribution of the derivatized analyte mass distribution using the method developed by Yang et al. (2006 and 2009), which is based on earlier work of Wiechert et al. (2001). The peak with  $m/z$  225 represents the mono isotopic mass of the Ac-DNPH product formed with unlabeled acetaldehyde [ $m_i$ ] (Figure 4-9A). The peak with  $m/z$  226 represents the mono isotopic mass of the single labeled [ $1-^{13}\text{C}$ ]-Ac-DNPH [ $m_i+1$ ] as well as the mass of the unlabeled Ac-DNPH (Fig 4-9B). The peak with  $m/z$  227 comprises the mono isotopic peak mass of the double-labeled [ $^{13}\text{C}_2$ ]-Ac-DNPH as well as the [ $m_i+2$ ] mass for the unlabeled Ac-DNPH and the [ $m_i+1$ ] mass of the single labeled [ $1-^{13}\text{C}$ ]-Ac-DNPH. The measured signal intensities of  $m/z$  225, 226 and 227 were used for the calculation for the carbon mass isotopomer fractions.

#### 4.7.4 Quantification of natural isotope ethanol

Ethanol concentrations from 30 to 720 mM in the enzymatic assay were used to determine the maximum linear range for unlabeled ethanol quantification. Volumes of 5–115  $\mu\text{L}$  of 1.9 M ethanol were topped with 100mM Tris/HCl buffer to 165  $\mu\text{L}$ . To this solution 3.3 % (w/w) [ $^{13}\text{C}_2$ ]-ethanol (25  $\mu\text{L}$ ) was added as internal standard (45 mM in the enzymatic assay) followed by 100  $\mu\text{L}$  100 mM  $\text{NAD}^+$  and 10  $\mu\text{L}$  1 mg/mL ADH, both in 100mM Tris/HCl buffer. After incubation, ethyl acetate (150  $\mu\text{L}$ ) was added to separate the Ac-DNPH formed without adding any additional acetaldehyde.

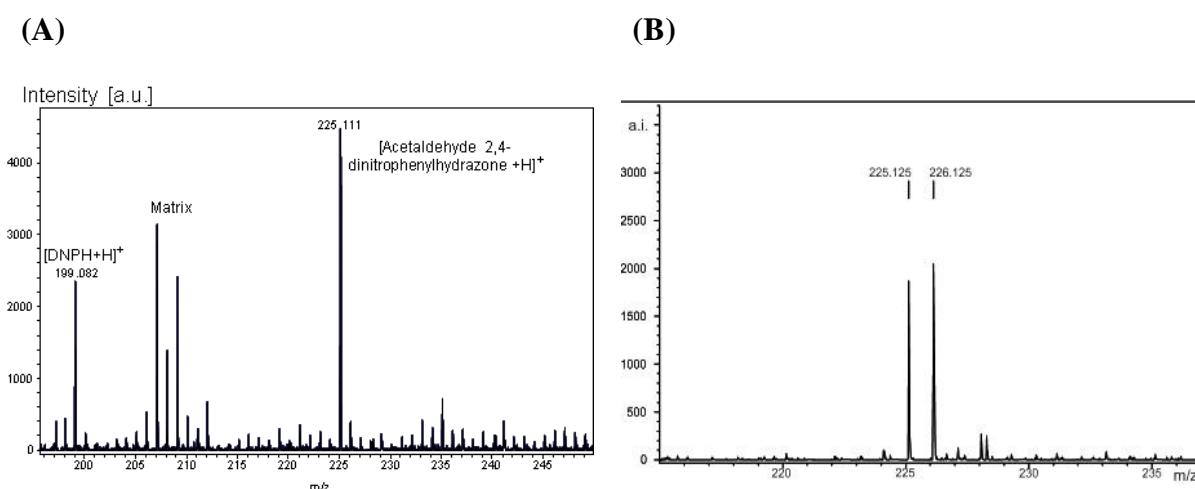


**Figure 4-9** (A) Mass spectrum showing the peaks of reagent, protonated DNPH ( $m/z$  199.0); matrix, CCA and mono isotopic mass of unlabeled Ac-DNPH ( $m/z$  225.1) [ $m_i$ ] and (B) Mass spectrum showing the peaks of mono isotopic mass of the single labeled [ $1-^{13}\text{C}$ ]-Ac-DNPH ( $m/z$  226.1) [ $m_i+1$ ]

#### 4.7.5 Quantification of unlabeled and [ $1-^{13}\text{C}$ ]-ethanol

Parallel quantification of both ethanol types was performed in the range 1–50 mM, representing the expected ethanol concentrations of the culture supernatant experiments. For quantification of both ethanol isotopes, equal volumes were taken from 1 to 80  $\mu\text{L}$  each. The resulting volumes were made up to 165  $\mu\text{L}$  with 100 mM Tris/HCl buffer and 1.1 % (w/w) [ $^{13}\text{C}_2$ ]-ethanol (25  $\mu\text{L}$ ) as internal standard was added.  $\text{NAD}^+$  and ADH were added as described above. The incubation time was 16 h. The other steps of sample preparation were identical to those described above. In the present experiment, the signal intensities of  $m/z$  226 and 227 are influenced by the intensities of unlabeled Ac-DNPH and [ $1-^{13}\text{C}$ ]-Ac-DNPH, respectively.

To obtain a standard curve for the quantification of natural isotope ethanol, different mixtures of unlabeled and [ $^{13}\text{C}_2$ ]-ethanol were applied and analyzed. Also in this case a correction for natural isotopes was not necessary. The relative intensity of the peak  $m/z$  225 ( $I_{rel, 225, mi}$ ) was calculated using the absolute peak intensities of  $m/z$  225 ( $I_{225, mi}$ ) and of  $m/z$  227 ( $I_{227, mi+2}$ ) according to equation 4-12

$$I_{rel, 225} = \frac{I_{225, mi}}{I_{227}} \quad (\text{Eq 4-12})$$

Linear regression analysis was performed using these relative intensities in relation to the unlabeled ethanol concentrations (Figure 4-10). The slope of the straight line was 1.194, the intercept 0.119 and the correlation  $r^2 = 0.9948$ .

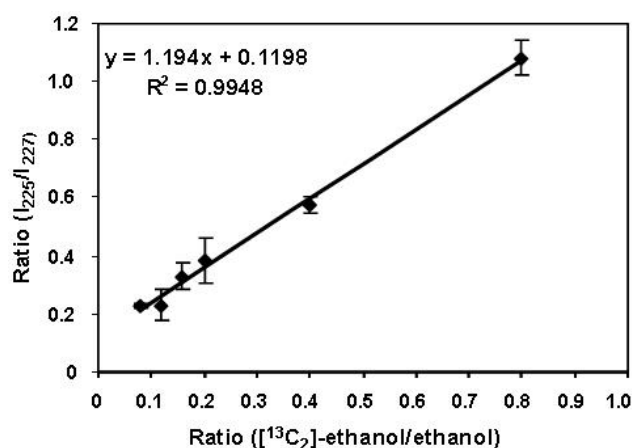


**Figure 4-10** Standard curve for the quantification of natural isotope ethanol. Linear regression analysis was performed between relative intensities [ $I_{225}/I_{227}$ ] and unlabeled ethanol concentrations.

#### 4.7.6 Estimation of the flux split ratio between pentose-phosphate pathway (PPP) and glycolysis ( $\Phi_{PPP}$ )

The flux split ratio ( $\Phi_{PPP}$ ) between pentose-phosphate pathway and glycolysis can be estimated simply from metabolite labeling of compounds directly derived from pyruvate, e.g. alanine or ethanol as described by Wittmann et al. (2004) and the principle involved in the calculation of  $\Phi_{PPP}$  is shown in figure 4-11.

$$\Phi_{PPP} = \frac{1 - I_{226, corr} / I_{225, mi}}{1 + 2/3 * I_{226, corr} / I_{225, mi}} \quad (\text{Eq 4-13})$$

This simplified calculation provides a minimal value for the flux ratio between PPP and glycolysis as has been shown for *Corynebacterium glutamicum*, but gives reasonable results especially for low values of  $\Phi_{PPP}$  (Wittmann et al., 2004). For screening comparison of a large collection of mutants or effective compounds, calculations using equation 4-13 are clearly sufficient since the reversibility of the glucose 6-phosphate isomerase would be very similar. Once a mutant is identified showing a different PPP flux split ratio, it must be characterized more thoroughly using a more detailed method using isotopomer models which require, however, much more detailed data involving analysis of labeling of metabolites using, e.g., GC/MS or HPLC/MS. For such screening experiments, the incomplete labeling of [1- $^{13}\text{C}$ ]-glucose introduces only a marginal error and it was therefore neglected.

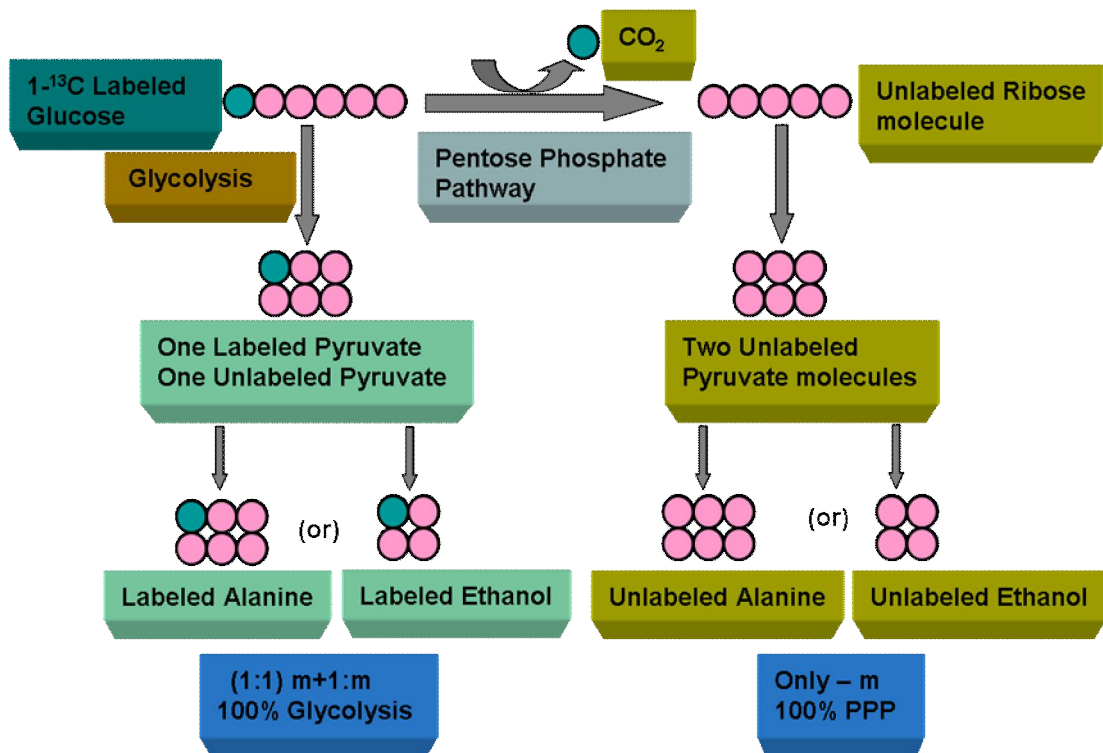


**Figure 4-11** The principle involved in the flux split ratio ( $\Phi_{PPP}$ ) between pentose-phosphate pathway and glycolysis calculation.

## 4.8 LABELLING ANALYSIS OF PROTEINOGENIC AMINO ACIDS

Labelling patterns of proteinogenic amino acids were analysed from biomass hydrolysates using gas chromatography mass spectrometry (GC-MS).

### 4.8.1 Biomass hydrolysate sample preparation

Aliquots of batch cultures were harvested at  $OD_{660nm}$  of 1.5-2.5, and centrifuged at 3000 g at room temperature for 15 min. Pellets were washed twice with 1 ml 0.9 % (w/v) NaCl and hydrolysed in 100  $\mu$ L of 6 M HCl at 105° C for 24 h. The hydrolysate was filtered and freeze dried and subsequently derivatised at 80° C in 20  $\mu$ L of Dimethylformamide (DMF) with 0.1 % pyridine and 20  $\mu$ L of MBDSTFA (N-methyl-tert.-butyldimethylsilyl-trifluoroacetamide, Macherey-Nagel, Düren, Germany) for 1 h. Protic sites of amino acids (OH-, NH-, and SH-groups) were blocked by silylation to reduce dipole-dipole interactions and to increase volatility for GC separation. The use of MBDSTFA had the advantage that mostly neutral and volatile byproducts are formed that did not react with the column, hence enabling direct GC-MS analysis.

### 4.8.2 Gas Chromatography Mass Spectrometry

GC-MS was carried out using a HP 6890 GC-System equipped with HP5MS (95 % dimethyl-5 % diphenylpolysiloxane; 30 m  $\times$  0.25 mm  $\times$  250  $\mu$ m, Restek, Bellefonte, PA, USA) that was directly connected to a Quadrupole Mass Selective Detector 5973 Network (Agilent Technologies, Waldbronn, Germany) with electron ionization at 70 eV. The injection volume was 0.5  $\mu$ L at a carrier gas flow rate of 1.5ml/min helium and column head pressure was 70 kPa. The temperature gradient for the separation of complex amino acid mixtures was 120 °C for 5min, 4 °C/min up to 270 °C and 20 °C/min to 320 °C. Further operation temperatures were 300 °C (inlet), 280 °C at the interface and 320 °C (quadrupole). In order to increase the sensitivity, the mass isotopomer fractions  $[m_i]$ ,  $[m_{i+1}]$ , and  $[m_{i+2}]$  were quantified with selected ion monitoring (SIM) of the corresponding ion clusters. Figure 4-12 demonstrating the TIC chromatogram obtained using SIM method and about 14 amino acids were detected and the names of the amino acids were given in the table 4-6.

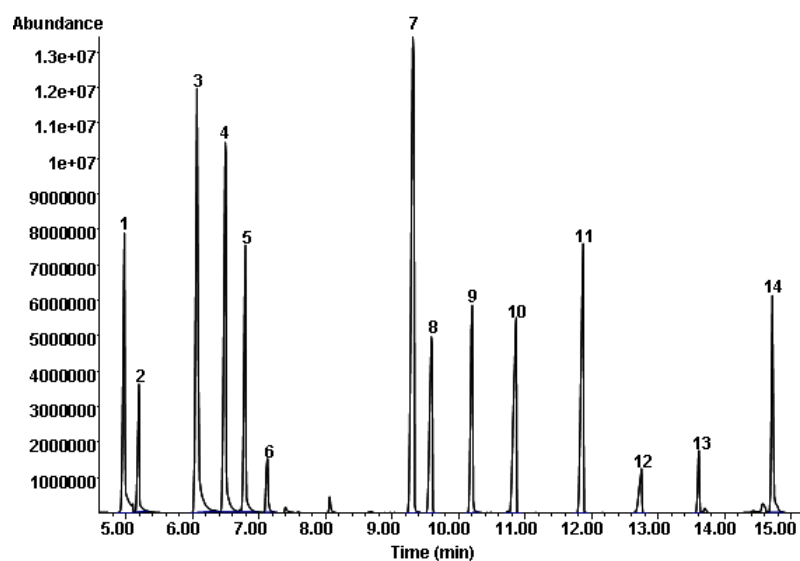


**Figure 4-12** GC-MS chromatogram showing all the detected amino acids. Numbers on top of each peak represents serial number of detected peaks.

**Table 4-6** Peak table showing the peak number in the chromatogram (Fig 4-12) and its corresponding amino acid

Peak number	Amino acid	Peak number	Amino acid
1	Alanine	8	Threonine
2	Glycine	9	Phenyl alanine
3	Valine	10	Aspartic acid
4	Leucine	11	Glutamic acid
5	Isoleucine	12	Lysine
6	Proline	13	Arginine
7	Serine	14	Tyrosine

## 4.9 METABOLIC NETWORK MODEL AND FLUX ANALYSIS

A system of connected chemical reactions that determine the physiological and biochemical properties of a cell is called a metabolic network. These inter-connected metabolic networks comprise a regulatory mechanism with the involvement of numerous enzymes. Metabolic flux analysis (MFA) is a constraint based methodology for identifying metabolic flux distributions using the stoichiometry based approach. The main advantage of MFA is a detailed quantification of intracellular fluxes in the central metabolic pathways, which results in a flux map that shows the distribution of anabolic and catabolic fluxes over the metabolic network (Wiechert et al., 2001).

### 4.9.1 Metabolite balancing

Metabolite balancing applies the principle of material conservation for each and every metabolite pool in the metabolic network. At steady state, metabolite pools are constant; hence the total of all metabolic fluxes entering a specific pool must equal the total of fluxes leaving that same pool. This yields, for every metabolite pool, one linear equation relating all fluxes connecting with that pool. Available measurement data on fluxes e.g. substrate uptake rates ( $q_s$ ) and product production rates ( $q_p$ ) provide additional equations. Setting up the equations for every pool in the network then yields a high-dimensional system of linear equations, with the fluxes as unknowns that can be solved mathematically using matrix procedures, provided the system is (over)determined i.e., there are more independent equations than the unknowns (De Graaf et al., 1996; Varma and Palsson, 1994).

$$S \cdot v = b \quad (\text{Eq 4-14})$$

where  $S$  is the stoichiometric matrix,  $v$  is the vector of fluxes and  $b$  is the net specific excretion rate vector (in the case of substrate uptake rate, the elements of  $b$  will be negative). The stoichiometric matrices are given in the Appendix section. Fluxes were estimated using the inverse of the stoichiometric matrix using standard methods implemented in MATLAB (Stephanopoulos et al., 1998). The program for calculation of fluxes is given in the Appendix.

### 4.9.2 Yeast metabolic network model

A simplified yeast biochemical reaction network was used for the calculation of metabolic fluxes. The specific substrate i.e., glucose or galactose ( $q_s$ ) consumption rate; specific product, ethanol ( $q_p$ ) production rate; specific growth rate ( $\mu$ ) and the flux split ratio between glycolysis and pentose phosphate pathway ( $\Phi_{PPP}$ ) were used in the model for flux calculations. The mass balance equations around each node are as follows (Figure 4-13),

$$G6P : v_1 - v_2 - v_3 - vb_1 = 0 \quad (\text{Eq 4-15})$$

$$F6P : v_3 + v_{13} + v_{12} - v_4 = 0 \quad (\text{Eq 4-16})$$

$$GAP : v_4 + v_{13} + v_{11} - v_{12} - v_{15} - vb_3 = 0 \quad (\text{Eq 4-17})$$

$$PYR : v_5 - v_6 - v_7 - v_{14} - vb_4 = 0 \quad (\text{Eq 4-18})$$

$$AcCoA : v_7 - v_8 - vb_7 = 0 \quad (\text{Eq 4-19})$$

$$AKG : v_8 - v_9 - vb_5 = 0 \quad (\text{Eq 4-20})$$

$$SUC : v_9 - v_{10} = 0 \quad (\text{Eq 4-21})$$

$$OAA : v_{14} + v_{10} - v_8 - vb_6 = 0 \quad (\text{Eq 4-22})$$

$$P5P : v_2 - v_{11} - v_{13} - vb_2 = 0 \quad (\text{Eq 4-23})$$

$$E4P : v_{12} - v_{13} - vb_8 = 0 \quad (\text{Eq 4-24})$$

$$S7P : v_{11} - v_{12} = 0 \quad (\text{Eq 4-25})$$

$v$  is a reaction rate or flux as specified in figure 4-13. This stoichiometric network has 15 metabolic reactions,  $v_1$  to  $v_{15}$ , and 8 anabolic reactions,  $v_1$  to  $v_8$ , representing biomass formation. The anabolic demand reactions were calculated as function of the specific growth rate as described by Frick et al. (2004). The specific substrate, i.e., glucose or galactose consumption rate ( $q_{\text{Hexose}} = v_1$ ), specific ethanol production rate ( $q_p = v_6$ ) are two external fluxes.

This system would be underdetermined unless there was an additional measurement. The flux split ratio between glycolysis and pentose phosphate pathway,  $\Phi_{\text{PPP}}$ , provided an additional measured variable and therefore the system was fully determined. The  $\Phi_{\text{PPP}}$  can be estimated simply from metabolite labeling of compounds directly derived from pyruvate, e.g. alanine or ethanol as described by Wittmann et al. (2002). The net  $\Phi_{\text{PPP}}$  flux split ratio is defined as

$$\phi_{\text{PPP}} = \frac{v_2}{v_2 + v_3} \quad (\text{Eq 4-26})$$

The net anaplerotic flux split ratio was calculated from the fluxes already calculated,  $\Phi_{\text{Anaplerotic}}$

$$\phi_{\text{Anaplerotic}} = \frac{v_{14}}{v_6 + v_7 + v_{14}} \quad (\text{Eq 4-27})$$

This value does not take into account any reversibility of anaplerotic reactions. The estimation of these would require a much more in-depth analysis (Frick et al., 2004; Blank et al., 2005; Gombert et al., 2001; van Winden et al., 2005).

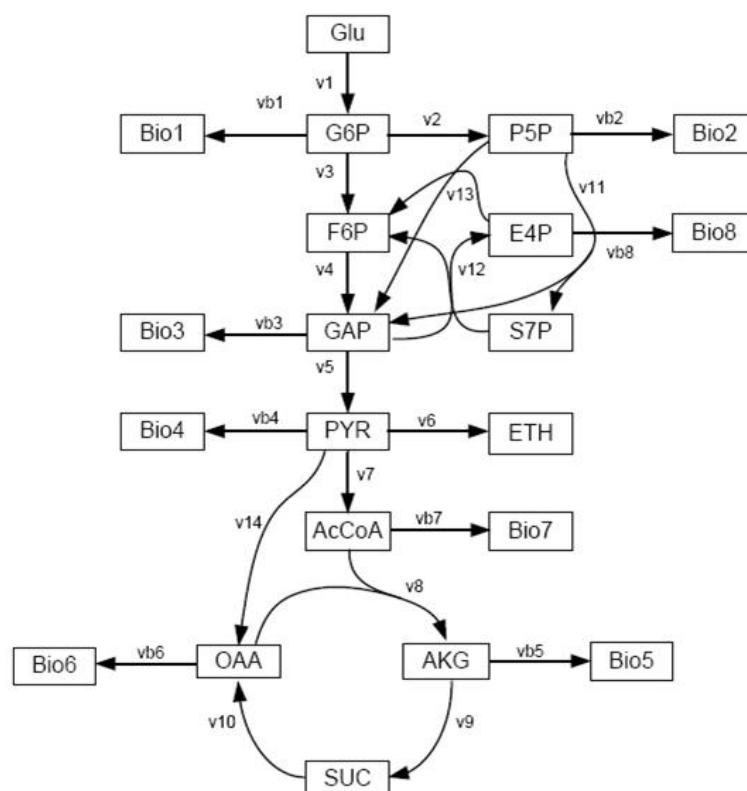


**Figure 4-13** Schematic diagram of the simplified central yeast metabolic network.

Glu, Glucose; G6P, Glucose-6-phosphate; F6P, Fructose-6-phosphate; P5P, Pentose-5-phosphate; E4P, Erythrose-4-phosphate; S7P, Sedoheptulose-7-phosphate; GAP, Glyceraldehyde-3-phosphate; Pyr, Pyruvate; ETH, Ethanol; AcCoA, Acetyl Co-A; AKG, Alpha-keto glutarate; SUC, Succinate; OAA, Oxaloacetate, Bio-Biomass

## 4.10 STATISTICAL ANALYSES

Mean errors of hexoses i.e., glucose, galactose and ethanol determination were derived from all pair wise measurements carried out for each well. For the specific growth rate the 90 % confidence interval was estimated according to Massart et al. (1997). 90 % confidence intervals for yields and flux partitioning to the pentose phosphate pathway were estimated by calculating Gaussian error propagation. Errors of metabolic fluxes were estimated using Monte Carlo simulation (MATLAB, Mathworks) assuming Gaussian distribution of errors. The error of biomass yield on oxygen was estimated from a sensitivity analysis and visual inspection using the software BERKELEY MADONNA. To distinguish different mutant strains from each other and different mutant strains from the reference strain, strains were compared pair wise using a t-test with 90 % confidence interval. Strains with overlapping confidence intervals were considered equal. These comparisons were made for all four individual parameters specified above for both sugar substrates.

### 4.10.1 Confidence intervals in regression analysis

The rate of cell growth is proportional to cell concentration during exponential phase of cultivation. Thus a plot of natural logarithm of biomass concentration ( $X$ ) against time ( $t$ ) yields a straight line and the slope of this is the specific growth rate ( $\mu$ ).

$$\frac{dx}{dt} = \mu X \quad (\text{Eq 4-28})$$

The regression coefficient,  $\mu$  is the specific growth rate. Confidence intervals were set for specific growth rates by calculating the critical value for regression coefficient as follows (Kreyszig et al., 1993).

1. A confidence level  $\gamma$  of 90 % was chosen.
2. The solution for  $p$  of the equation was determined from the table of the t-distribution with  $n-2$  degrees of freedom ( $n$  = sample size).

$$F(p) = \frac{1}{2(1 + \gamma)} \quad (\text{Eq 4-29})$$

3. For a sample of size  $(x_1, y_1)$  to  $(x_n, y_n)$ , variances  $S_1$  and  $S_2$  were calculated for  $x$  and  $y$ , respectively.

Critical value  $K$  for regression coefficient  $\mu$  was computed as follows

$$K = p \sqrt{\left( S_2 - \mu^2 \cdot \frac{S_1}{n-2} \cdot S_1 \right)} \quad (\text{Eq 4-30})$$

The confidence interval is

$$CONF \{ \mu - K < \mu < \mu + K \} \quad (\text{Eq 4-31})$$

### 4.10.2 Standard deviations for yield calculations

Yield coefficients were estimated as quantity of cell dry weight or ethanol produced per quantity of carbon substrate utilized. Thus yield coefficients were coming from two independent measurements i.e. the amount of glucose consumed, the amount of biomass or ethanol produced. When the final result is obtained from more than one independent measurement, or when it is influenced by two or more independent sources of error, these errors can accumulate or compensate. Thus standard deviations were calculated according to the law of

propagation of errors (Massart et al., 1997). Random errors accumulate according to the law of propagation of errors is given by:

$$z = \frac{x}{y} \quad (\text{Eq 4-32})$$

$$\sigma^2_z = \left(\frac{dz}{dx}\right)^2 \cdot \sigma^2_x + \left(\frac{dz}{dy}\right)^2 \cdot \sigma^2_y \quad (\text{Eq 4-33})$$

$$\text{Where } z = f(x, y) \quad (\text{Eq 4-34})$$

and  $x$ ,  $y$  must be independent variables and  $\sigma^2_x$ ,  $\sigma^2_y$ , and  $\sigma^2_z$  are variances of  $x$ ,  $y$  and  $z$ , respectively. Standard deviation of  $z$  can be calculated by taking the partial derivative for the above equation,

$$\sigma_z = \left[ \left(\frac{1}{y}\right)^2 \cdot \sigma^2_x + \left(\frac{x}{y^2}\right)^2 \cdot \sigma^2_y \right]^{\frac{1}{2}} \quad (\text{Eq 4-35})$$

### 4.10.3 Mutant comparison

Mutant-mutant and mutant-reference separations were done in the following way; two strains were checked, if the confidence intervals of specific growth rates and standard deviations of all yields of one strain were overlapping the confidence intervals and standard deviations of another strain or not. Strains, which were common in all four dimensions i.e. specific growth rates, biomass yields, ethanol yields and biomass yields on oxygen were considered as ‘not distinguishable’ strains i.e., strains with overlapping confidence intervals were considered equal and strains that were not overlapping in at least one dimension were considered as ‘distinguishable’ strains.

### 4.10.4 Hierarchical clustering

Hierarchical clustering was based on complete linkage method with Euclidean metric by using *hclust* function of *stats* package of R statistical language software (<http://www.r-project.org/>). The log2 transformed fold changes of metabolic flux values of mutant strains vs. reference strain were visualized using the *heatmap.2* function of the *gplots* package of R.

### 4.10.5 Euclidean distance approach

Mutant strains were compared using relative Euclidean distance,  $d$ , between two strains using all the available biological parameters i.e., specific growth rate, biomass yield on substrate, ethanol yield on substrate and biomass yield on oxygen, using the equation 4-36,

$$d(x, y) = \sqrt{\sum_1^{npar} \left( \frac{(x_i - y_i)}{\bar{y}_i} \right)^2} \quad (\text{Eq 4-36})$$

where  $x$  and  $y$  are the parameter values for the two selected strains.  $y_i$  is the mean value of parameter  $i$  for all strains.

### 4.10.6 Graphical Gaussian Modelling (GGM) approach

Graphical Gaussian Modelling (GGM) or Covariance selection model or Concentration graph is useful for learning undirected graphical Gaussian Markov models from data sets, where the number of random variables ‘ $p$ ’ exceeds the available sample size ‘ $n$ ’ (Waddell and Kishino, 2000). GGM is used to infer the network of linear dependencies among a set of mutant strains based on partial correlations as a measure of independence of any two strains by computing all pair-wise correlations and subsequently the corresponding graph (To and Horimoto, 2002). If there is a missing edge between any two mutant strains i.e., partial correlation is close to zero, that would mean that there is no direct dependency between those two strains. If the partial correlation is close to one that would mean that there is a strong direct dependency between those two strains. The corresponding program was written in ‘R’ is given in the Appendix.

## Materials and methods

The total work flow, starting from the selection of mutants strains from the yeast knockout library till calculation of metabolic fluxes was illustrated in figure 4-14.

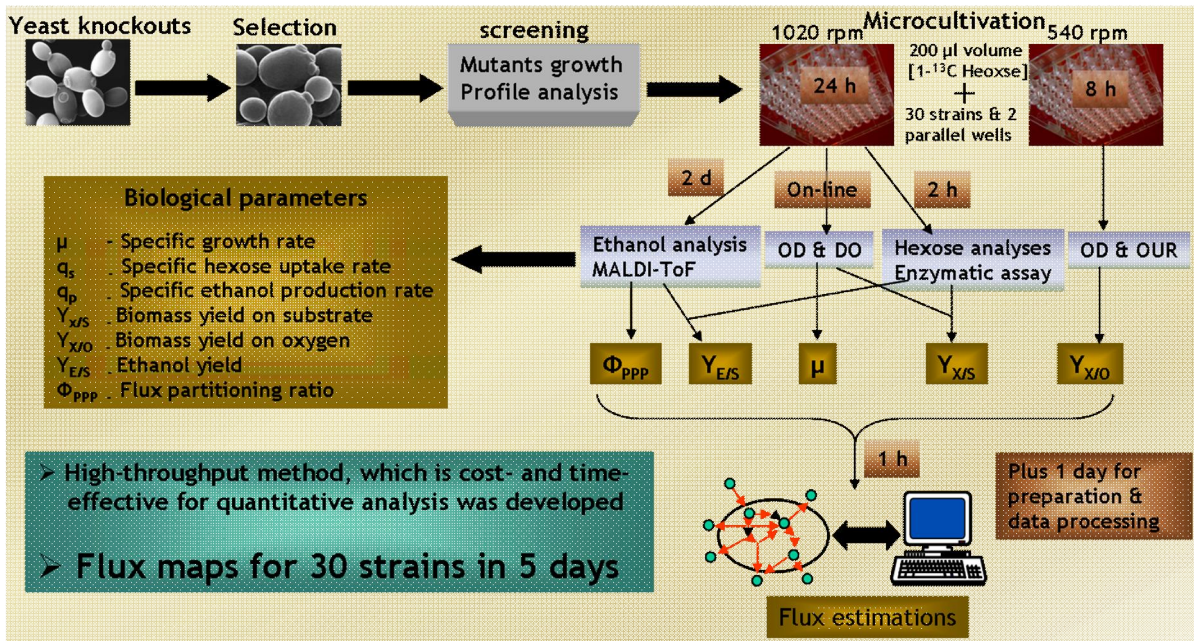


**Figure 4-14** Schematic illustration of the total work flow

## 5. RESULTS AND DISCUSSION

Results and discussion chapter is organised in the following manner. This chapter is divided in to six sub-chapters (sub-chapters: 5.1 to 5.6).

- The first sub-chapter, 5.1 deals with the high-throughput stoichiometric and metabolic screening of a set of selected *S. cerevisiae* single deletion mutants, which are known to be involved in central carbon metabolism using 96-well microtiter plates with integrated optical sensors for dissolved oxygen monitoring on glucose and galactose sugars.
- The 5.2 sub-chapter deals with the new method that was developed for the high-throughput quantification of unlabeled and mono-<sup>13</sup>C-labeled ethanol, which also permits the calculation of the flux split ratio between glycolysis and the pentose-phosphate pathway (PPP).
- The sub-chapter 5.3 deals with the comparative quantitative metabolic flux profiling of the selected set of mutants on glucose and galactose sugars at miniaturised scale.
- The sub-chapter 5.4 deals with the comparative stoichiometric and quantitative metabolic flux profiling of hexose transporter deletion mutant strains on glucose and galactose.
- The sub-chapter 5.5 deals with the stoichiometric and quantitative metabolic profiling of a set of selected mutants on fructose sugar and comparison with the other carbon sources i.e., glucose and galactose.
- In the final overview sub-chapter 5.6, all the strains discussed so far are combined together and analysed statistically by employing several techniques i.e., hierarchical clustering, mutant comparison using Euclidean distance approach and data visualisation using clustered heat maps etc. Based on the available quantitative information on different carbon sources for different strains, the functions of hypothetical genes are predicted using Graphical Gaussian modelling approach.

## 5.1 METABOLIC SCREENING OF *S. CEREVISIAE* SINGLE KNOCKOUT STRAINS ON GLUCOSE AND GALACTOSE

Most of the results presented in this chapter are contained in the following publication.

**Velagapudi, V.R.**, Wittmann, C., Lengauer, T., Talwar, P., Heinzle, E., 2006. Metabolic screening of *Saccharomyces cerevisiae* single knockout strains reveals unexpected mobilization of metabolic potential. **Process Biochem.** 41, 2170–2179.

### 5.1.1 Background

The determination of basic physiological parameters as rates of growth, substrate consumption, product formation and respiration and further of metabolic pathway activities is of central importance for the characterization of strains. To this end, a methodology for high-throughput kinetic and stoichiometric analysis of yeast mutant libraries in 96 well microtiter plates with on-line sensing of dissolved oxygen at miniaturized scale was developed and optimized. From this method, reliable data for specific growth rate, biomass and ethanol yields on glucose and biomass yield on oxygen, which also allows mutant characterization, was calculated. This method was applied to a selected set of mutants that were cultured on glucose and galactose. A set of 27 deletion mutants were selected, which are proposed to be involved in central carbon metabolism. The detailed information i.e., known or putative molecular, biological and cellular localization, about the mutants is described in Table 5.1-1.

### 5.1.2 Microtiter plate cultivation of *S. cerevisiae*

The growth profile of the wild type *S. cerevisiae* ATCC 32167 in a 96 well microtiter plate is shown in Figure 5.1-1. Cells grew exponentially with a specific growth rate of  $\mu = 0.46 \text{ h}^{-1}$  and eventually reached an OD of 3.7 after 8 h of cultivation. Glucose was completely consumed during first 5 h of cultivation, which was accompanied by an increase in ethanol concentration (Figure 5.1-1A). The cells thus revealed the typical profile of yeast, where high levels of readily metabolizable sugars repress the ability of the cell to carry out full aerobic respiration (Postma et al., 1989).

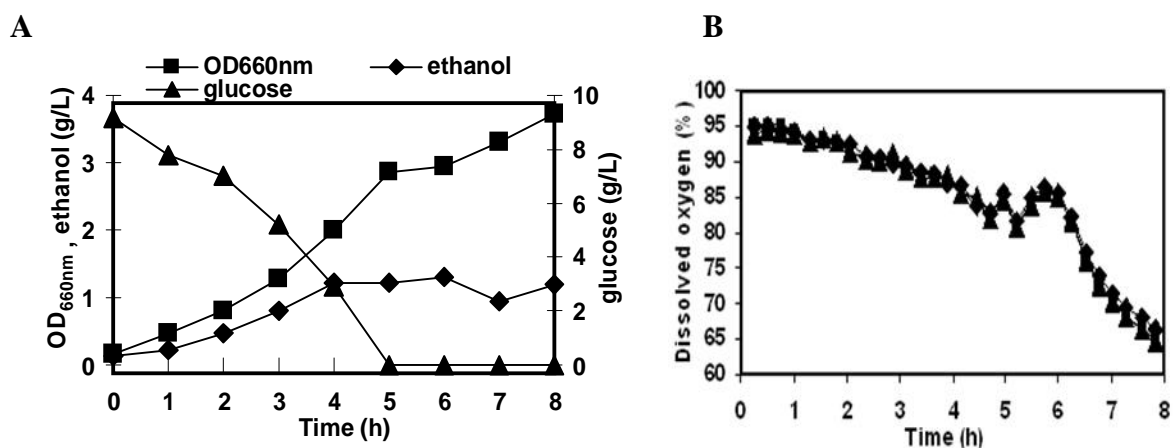


**Figure 5.1-1** Cultivation profile of *S. cerevisiae* ATCC 32167. Wild-type yeast *S. cerevisiae* was grown in 96-well microtiter plate (A), dissolved oxygen concentration was measured during cultivation in three parallel wells (B). Microtiter plate reader operating conditions: orbital shaking, 1080 rpm,  $r = 1$  mm,  $T = 30$  °C for 8 h.

It was observed that there was no limitation of oxygen throughout the cultivation. This assures that ethanol production during cultivation was exclusively due to the “Crabtree Effect” but not anaerobic fermentation. Furthermore, the oxygen profile revealed distinct events of the cultivation. A gradual decrease in DO concentration was observed during initial cultivation. At about 5 h a significant increase in the DO level was observed, which coincided with the depletion of glucose. This transient increase in DO concentration obviously results from a short lag phase of decreased metabolic activity. Cells of *S. cerevisiae* have to synthesize the enzymes necessary for the aerobic metabolism of ethanol. In addition, three parallel wells showed almost identical oxygen profiles (Figure 5.1-1B). This underlines the high precision of the DO measurements and the high reproducibility of cultivation in parallel wells.

### 5.1.3 Comparative growth analysis in MTP and SFC

In order to check the validity of the methodology developed for the cultivation in microtiter plates, parallel growth experiments were carried out for *S. cerevisiae* ATCC 32167 in conventional shake flasks and microtiter plates. Identical growth profiles were observed with both cultivation tools (Figure 5.1-2). This showed that the developed approach is appropriate for cultivation of *S. cerevisiae*. Thus the use of microtiter plate with online oxygen sensing is a suitable approach for the subsequent physiological studies of yeast deletion mutants or other mutant libraries.

**Table 5.1-1** Information about the selected yeast deletion mutant strains

ORF	Gene Name	Biological process	Molecular function
YMR280C	<i>CAT8</i>	Regulation of transcription from Pol II promoter	Specific RNA pol II transcription factor activity
YML054C	<i>CYB2</i>	Electron transport	L-lactate dehydrogenase
YDL174C	<i>DLD2</i>	Aerobic respiration	D-lactate dehydrogenase (cytochrome) activity
YLR377C	<i>FBP1</i>	Gluconeogenesis	Fructose-bisphosphatase activity
YJL155C	<i>FBP26</i>	Gluconeogenesis	Fructose-2,6-bisphosphate 2-phosphatase activity
YMR250W	<i>GAD1</i>	Response to oxidative stress	Glutamate decarboxylase activity
YBR019C	<i>GAL10</i>	Galactose metabolism	Unknown
YPL248C	<i>GAL4</i>	Regulation of transcription	DNA-dependent transcriptional activator activity
YBR018C	<i>GAL7</i>	Galactose metabolism	UTP-hexose-1-phosphate uridylyltransferase activity
YCL040W	<i>GLK1</i>	Carbohydrate metabolism	Glucokinase activity
YML004C	<i>GLO1</i>	Glutathione metabolism	Lactoylglutathione lyase activity
YIL154C	<i>IMP2</i>	DNA repair	Transcription co-activator activity
YNL104C	<i>LEU4</i>	Leucine biosynthesis	2-isopropylmalate synthase activity
YKL029C	<i>MAE1</i>	Pyruvate metabolism	Malate dehydrogenase (oxaloacetate decarboxylating) activity
YBR297W	<i>MAL33</i>	Regulation of transcription	DNA-dependent transcription factor activity
YGL209W	<i>MIG2</i>	Regulation of transcription from Pol II promoter	RNA pol II transcription factor activity
YKL062W	<i>MSN4</i>	Response to stress	Transcription factor activity
YKR097W	<i>PCK1</i>	Gluconeogenesis	Phosphoenolpyruvate carboxykinase (ATP) activity
YIL107C	<i>PFK26</i>	Fructose-2,6-bisphosphate metabolism	6-phosphofructo-2-kinase activity
YOL136C	<i>PFK27</i>	Fructose-2,6-bisphosphate metabolism	6-phosphofructo-2-kinase activity
YDL168W	<i>SFA1</i>	Formaldehyde assimilation	Formaldehyde dehydrogenase (glutathione) activity
YNL257C	<i>SIP3</i>	Transcription initiation from pol II promotor	Transcription cofactor activity
YDR073W	<i>SNF11</i>	Chromatin modeling	RNA pol II transcription factor activity
YOR344C	<i>TYE7</i>	Transcription	Transcription factor activity
YBR006W	<i>UGA5</i>	Response to oxidative stress	Succinate-semialdehyde dehydrogenase (NAD(P)+) activity
YGR194C	<i>XKS1</i>	Xylulose catabolism	Xylulokinase activity
YBR184W	<i>YBR184W</i>	Unknown	Unknown

(Sources: *Saccharomyces* genome deletion project)

SGD ([http://www.sequence.stanford.edu/group/yeast\\_deletion\\_project/references.html](http://www.sequence.stanford.edu/group/yeast_deletion_project/references.html)),

MIPS (<http://mips.gsf.de/genre/proj/yeast/>)

SGD (<http://www.yeastgenome.org/>) databases

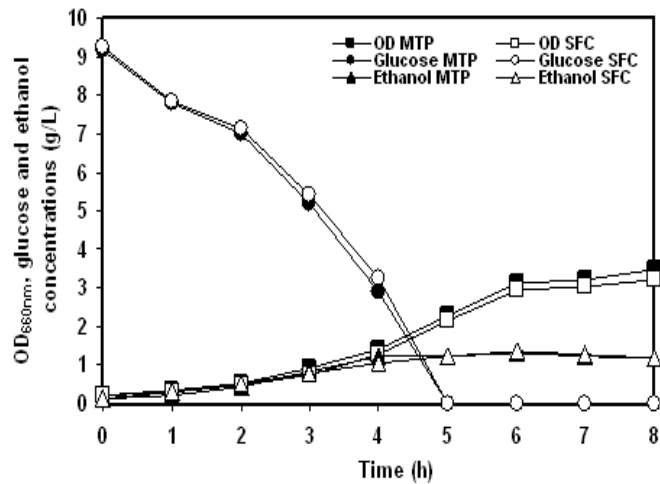


**Figure 5.1-2** Comparative growth profile analysis of Wild-type yeast *S. cerevisiae* in microtiter plate (MTP) and shake flask (SFC). Culture volumes were 10 ml in 100 ml shake flask,  $T = 30\text{ }^{\circ}\text{C}$ , 250 rpm for 8 h and 150  $\mu\text{l}$  in microtiter plate. Microtiter plate operating conditions were same as in Fig 5.1-1. (Open symbols: shake flask and closed symbols: microtiter plate)

#### 5.1.4 Effect of shaking rate on oxygen limitation

To investigate the effect of shaking rate on oxygen limitation, two cultivation experiments were carried out with *suc2A* strain with an initial  $\text{OD} \sim 0.05$  at low shaking rate (540 rpm) and at high shaking rate (1020 rpm). During cultivation at low shaking rate (540 rpm), cells grew slowly and produced  $0.55\text{ g L}^{-1}$  of biomass at 14.6 h of cultivation. There was still residual glucose even after 14 h of cultivation. Figure 5.1-3A shows a fit between experimental and simulated data of biomass, glucose and ethanol concentrations. Using equations (Eq 4-5 – 4-11) overall specific growth rate that was calculated by the model was  $0.17\text{ h}^{-1}$ . Experimentally determined ethanol concentration at 13.6 h was  $1.85\text{ g L}^{-1}$ , whereas the corrected ethanol concentration by the model was  $1.98\text{ g L}^{-1}$  corresponding to a difference of about 6%. This difference is larger than the estimation error. In other cultivations differences were significantly larger. At 13.6 h of cultivation, estimated yield of biomass on glucose,  $Y_{\text{XS}}$ , was  $0.086\text{ g g}^{-1}$ , of ethanol on glucose,  $Y_{\text{PS}}$ , it was  $0.35\text{ g g}^{-1}$ , and  $Y_{\text{PX}}$ , the stoichiometric ratio of ethanol to biomass production, was  $4.0\text{ g g}^{-1}$ . Figure 5.1-3B depicts the oxygen profile together with optical density, which shows oxygen limitation after 8 h of cultivation. The measured DO concentration at 15 h was 3%. Simulations were made using the full model but only for the first 8 h of cultivation, where there was no oxygen limitation. From this, the biomass yield on oxygen,  $Y_{\text{XO}}$ , and specific growth rate,  $\mu$ , were calculated. The calculated  $Y_{\text{XO}}$  for this time period was  $10.1\text{ g g}^{-1}$ . This is clearly higher than typical yields at aerobic conditions with

purely respiratory growth without any ethanol production. Furukawa et al. (1983) reported a value of  $1.1 \text{ g g}^{-1}$  for a specific growth rate of  $0.25 \text{ h}^{-1}$  in continuous culture of *S. cerevisiae*, where growth is almost entirely respiratory. The calculated specific growth rate for this time period was  $0.25 \text{ h}^{-1}$ , which was significantly different from the overall average growth rate determined from growth until depletion of glucose, which was  $0.17 \text{ h}^{-1}$ .

Careful investigation of experimental and simulated growth curves of figure 5.1-3A shows systematic deviations also indicating biphasic growth on glucose. This also shows that the strain revealed two different growth phases during the cultivation on glucose based on the oxygen availability. When there was enough oxygen, the strain grew with high growth rate, whereas it showed slow growth during oxygen limitation, which finally resulted in low biomass production. This shows that oxygen limitation is not always very clearly seen solely from growth profiles, whereas the measurement of dissolved oxygen provides a clear indication of oxygen limitation. During cultivation at a high shaking rate of 1020 rpm  $0.89 \text{ g L}^{-1}$  of biomass was produced at 15 h of cultivation. During this process, it consumed all the glucose, which was accompanied with an increase in ethanol concentration. Figure 5.1-3C shows a fit between experimental and simulated data of biomass, glucose and ethanol concentrations. Specific growth rate that was calculated by the model was  $0.27 \text{ h}^{-1}$ . Experimentally determined ethanol concentration at 13.5 h was  $2.75 \text{ g L}^{-1}$ , where as the corrected ethanol concentration by the model was  $3.06 \text{ g L}^{-1}$  corresponding to about 10 % difference. Estimated yields at 13.5 h were:  $Y_{XS} = 0.091 \text{ g g}^{-1}$ ;  $Y_{PS} = 0.34 \text{ g g}^{-1}$  and  $Y_{PX} = 3.7 \text{ g g}^{-1}$ .  $Y_{XS}$  is slightly larger than in the oxygen limited case with a shaking rate of 540 rpm and  $Y_{PS}$  is slightly lower. The deviations are, however not really significant since the error of estimation of these yields is in the order of 5 to 10 %. Figure 5.1-3D shows the oxygen profile during the cultivation. The measured DO concentration at 15 h was 95 %, which clearly shows that there wasn't any oxygen limitation throughout the cultivation. The specific growth rate for the first 8 h of cultivation calculated by the model was  $0.29 \text{ h}^{-1}$ , which was about 15 % higher than the above reported growth rate. It was not possible to get any reliable estimate of the oxygen uptake rate and therefore of  $Y_{XO}$  because of the very small difference of the measured dissolved oxygen concentration from the saturation value. Determination of oxygen uptake rate and  $Y_{XO}$  using the method proposed here requires cultivation at an appropriate oxygen transfer rate.

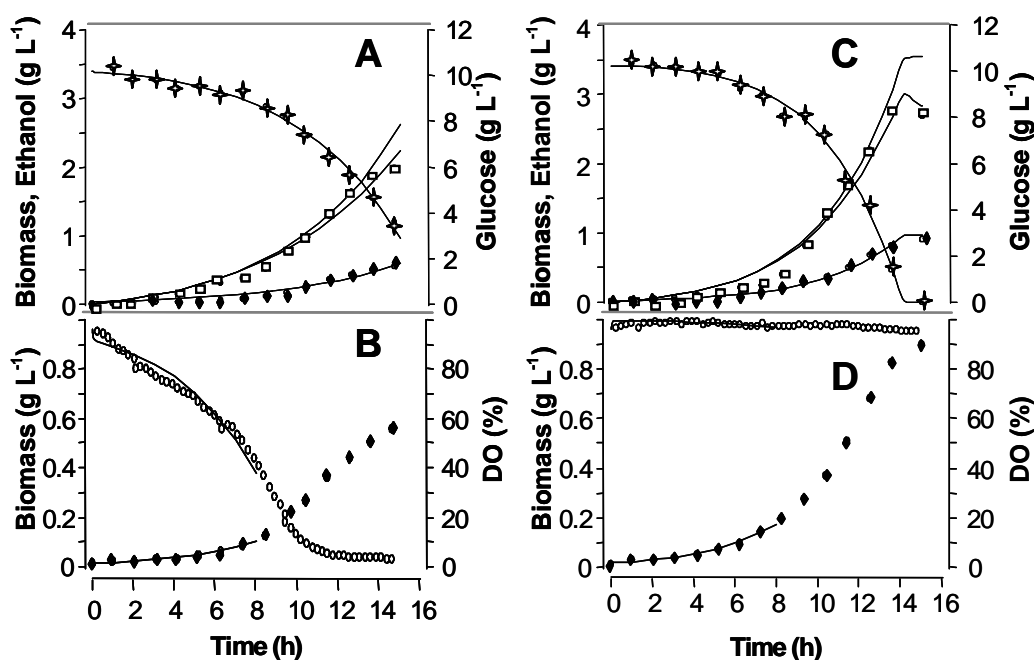


**Figure 5.1-3** Effect of shaking rate on oxygen limitation. *suc2Δ* strain was grown in 96-well microtiter plate at two different shaking rates and correction for evaporation loss of ethanol was made by using dynamic model. A fit was shown between these experimental data and simulated data. At low shaking rate of 540 rpm, Biomass ( $\diamond$ ), glucose consumption ( $\blackplus$ ) and ethanol production profiles ( $\square$ ) and corrected ethanol concentration (line) (A), Oxygen profile ( $\circ$ ) (B). At high shaking rate of 1020 rpm, Biomass ( $\diamond$ ), glucose consumption ( $\blackplus$ ) and ethanol production profiles ( $\square$ ) and corrected ethanol concentration (line) (C), oxygen profile ( $\circ$ ) (D).

This clearly indicates that at these operation conditions balanced growth prevailed throughout the cultivation without oxygen limitation. The data of this strain were compared with that of the reference strain (Table 5.1-2). The observed specific growth rate and the biomass yield on glucose were significantly lower compared to the reference strain, whereas biomass yield on oxygen and ethanol yield on glucose were not significantly different. The biological meaning of these differences is not really clear since deletion of *SUC2* should not have any effect, provided the exclusive function of *SUC2* was its known fructofuranosidase activity.

### 5.1.5 Method Validation

To experimentally further proof the developed method, growth characteristics of mutants with similar knocked out ORF functions were compared. We selected gene deletions for two isoenzymes of 6-phosphofructose-2-kinase, *pfk26Δ* and *pfk27Δ*. It has been reported that these two genes have almost identical function and identical kinetic behaviour in susceptibility to activation by cAMP-dependent protein kinase (Aragon et al., 1987). The second selected pair

is *nrg1Δ* and *nrg2Δ*. These two regulatory proteins involved in glucose repression, are two very similar proteins, which have closely related functions in the regulation of glucose-repressed genes (Vyas et al., 2001; Berkey et al., 2004). However, these genes are themselves differently regulated in response to carbon source. Growing on glucose as sole carbon source, one would expect similar physiological behaviour of these strains. Experiments showed significant decreases in growth rate and biomass yield on glucose of all four mutants compared to the reference strain. At the same time biomass yield on oxygen increased significantly which indicates a reduction in respiratory activities compared to the reference strain. Higher biomass yield is consistent with increased respiratory activity with higher ATP-yields. Changes in ethanol yield on glucose were not significant. This indicates that there must be other fermentation products apart from ethanol since the same fraction of glucose was transformed into ethanol in all experiments (Table 5.1-2).

**Table 5.1-2** Stoichiometric data of the examined strains originating from the reference strain *S. cerevisiae* BY4742 *Mata* *his3Δ1 leu2Δ0 lys2Δ0 ura3Δ0*. (Relative errors were calculated from each duplicate measurement for specific growth rates and yields. The average relative error of each parameter was applied for the calculation of the errors.)

Strain name	Silenced gene	Specific growth rate $\mu$ (h <sup>-1</sup> )	Biomass yield on glucose $Y_{xs}$ (g g <sup>-1</sup> )	Biomass yield on oxygen $Y_{xo}$ (g g <sup>-1</sup> )	Corrected ethanol yield on glucose $Y_{ps}$ (g g <sup>-1</sup> )
Reference	-	0.306 ± 0.006	0.128 ± 0.008	12.8 ± 1.3	0.35 ± 0.03
YIL107C	<i>PFK26</i>	0.231 ± 0.004	0.085 ± 0.006	32.7 ± 3.2	0.36 ± 0.03
YOL136C	<i>PFK27</i>	0.243 ± 0.005	0.082 ± 0.006	28.8 ± 2.8	0.36 ± 0.03
YDR043C	<i>NRG1</i>	0.228 ± 0.004	0.098 ± 0.006	30.1 ± 3.0	0.30 ± 0.03
YBR066C	<i>NRG2</i>	0.224 ± 0.004	0.087 ± 0.006	30.0 ± 3.0	0.30 ± 0.03
YIL162W	<i>SUC2</i>	0.270 ± 0.005	0.091 ± 0.006	10.1 ± 1.0	0.34 ± 0.03

### 5.1.6 Comparative physiological analysis

After an initial selection, mutants were first cultivated on glucose at high shaking rate of 1020 rpm. Then mutants were classified into three groups. Some mutants grew only slowly with  $\mu_{max} < 0.17$  h<sup>-1</sup>. These were not further quantitatively investigated with the method developed here because of too high evaporation of ethanol and water during long term cultivation. Strains growing with specific growth rates of 0.17 to 0.26 h<sup>-1</sup> were classified as slow growers and were later cultivated together to allow a reasonable common harvest time point. The rest of the strains with growth rates higher than 0.26 h<sup>-1</sup> were classified as fast growers, which were also cultivated as a group for more detailed studies. From these group-wise cultivations

maximum specific growth rates,  $\mu_{\max}$ , and yield coefficients of biomass and ethanol on glucose were determined. All strains that did not show a significant decrease of dissolved oxygen concentration were then cultivated at a shaking rate of 540 rpm to determine oxygen uptake rates. In cases, where only a few biomass data points were measured within the period of dissolved oxygen concentration higher than 20 % air saturation, the specific growth rate of the fully aerated culture was applied. The resulting data set is listed in Table 5.1-3 for glucose and in Table 5.1-4 for galactose. The errors for the estimation of growth rates, biomass and ethanol yields were typically between 5 and 10 %, whereas the error for biomass yield on oxygen was typically between 10 and 20 %. These allow various ways of comparison of the mutants. First, specific rates calculated from specific growth rate and yield coefficients are compared. Next, growth parameters of all strains on both sugars are compared. Then, every single mutant is compared with the reference strain. Later, binary comparisons of all mutants with respect to the 4 parameters determined for glucose and galactose as carbon substrates follow.

#### **5.1.6.1 Comparison of specific rates and yields of mutant set**

In Figure 5.1-4 specific hexose consumption rates,  $q_{\text{Hexose}}$ , specific rates of ethanol production,  $q_{\text{Ethanol}}$ , and specific oxygen consumption rates are plotted versus the maximum specific growth rate of each mutant,  $\mu_{\max}$ . From a first inspection it is evident that growth on galactose is clearly different from growth on glucose. On glucose substrate consumption and ethanol production are typically higher and respiration is clearly repressed. The parental reference strain, indicated by the arrows, has about average characteristics for all specific rates. As mentioned earlier, strains growing with slower rates than  $0.17 \text{ h}^{-1}$  were excluded from this analysis. As expected, the strains *gal4Δ*, *gal7Δ* and *gal10Δ* did not grow on galactose at all. Generally, the specific hexose uptake rate,  $q_{\text{Hexose}}$ , and the specific rate of ethanol production,  $q_{\text{Ethanol}}$ , were about proportional to the specific growth rate,  $\mu_{\max}$ , whereby the increase of  $q_{\text{Ethanol}}$  with  $\mu_{\max}$  was slightly higher on glucose than on galactose. The specific oxygen uptake rate,  $q_{\text{O}_2}$ , was generally low on glucose because of the Crabtree-effect but  $q_{\text{O}_2}$  increased with increasing  $\mu_{\max}$ . Oxygen uptake varied much more on galactose with some highly respiring strains and a few almost complete lacking of respiration.

**Table 5.1-3** Growth data on glucose for all strains used together with corresponding 90 % confidence intervals.

Gene name	$\mu_{\text{Glu}} \text{ h}^{-1}$	$Y_{\text{X/S,Glu}} \text{ g g}^{-1}$	$Y_{\text{E/S,Glu}} \text{ g g}^{-1}$	$Y_{\text{X/O,Glu}} \text{ g g}^{-1}$
Reference	0.320 ± 0.014	0.128 ± 0.009	0.336 ± 0.018	4.3 ± 0.8
<i>CAT8</i>	0.350 ± 0.026	0.083 ± 0.004	0.305 ± 0.006	6.0 ± 1.0
<i>CYB2</i>	0.279 ± 0.025	0.099 ± 0.023	0.399 ± 0.011	6.8 ± 1.2
<i>DLD2</i>	0.303 ± 0.029	0.093 ± 0.005	0.430 ± 0.031	9.3 ± 1.4
<i>FBP1</i>	0.225 ± 0.014	0.101 ± 0.011	0.429 ± 0.036	10.0 ± 1.2
<i>FBP26</i>	0.288 ± 0.014	0.101 ± 0.007	0.423 ± 0.024	8.4 ± 1.4
<i>GAD1</i>	0.312 ± 0.012	0.083 ± 0.005	0.320 ± 0.006	6.8 ± 1.2
<i>GAL10</i>	0.338 ± 0.037	0.085 ± 0.004	0.412 ± 0.007	3.6 ± 1.0
<i>GAL4</i>	0.280 ± 0.027	0.092 ± 0.005	0.411 ± 0.026	4.0 ± 0.8
<i>GAL7</i>	0.306 ± 0.015	0.085 ± 0.004	0.251 ± 0.009	8.6 ± 1.4
<i>GLK1</i>	0.320 ± 0.016	0.083 ± 0.005	0.276 ± 0.005	8.1 ± 1.0
<i>GLO1</i>	0.342 ± 0.019	0.089 ± 0.005	0.320 ± 0.011	4.8 ± 0.6
<i>IMP2</i>	0.296 ± 0.046	0.100 ± 0.006	0.305 ± 0.010	9.9 ± 1.2
<i>LEU4</i>	0.314 ± 0.026	0.110 ± 0.007	0.361 ± 0.012	7.7 ± 1.0
<i>MAE1</i>	0.282 ± 0.038	0.098 ± 0.010	0.446 ± 0.016	8.6 ± 1.1
<i>MAL33</i>	0.306 ± 0.019	0.083 ± 0.004	0.423 ± 0.023	7.7 ± 1.2
<i>MIG2</i>	0.288 ± 0.027	0.118 ± 0.014	0.420 ± 0.033	10.3 ± 1.8
<i>MSN4</i>	0.294 ± 0.038	0.102 ± 0.009	0.381 ± 0.010	10.2 ± 1.6
<i>PCK1</i>	0.338 ± 0.023	0.082 ± 0.005	0.334 ± 0.017	5.0 ± 0.8
<i>PFK26</i>	0.243 ± 0.046	0.085 ± 0.012	0.358 ± 0.043	9.6 ± 1.5
<i>PFK27</i>	0.286 ± 0.038	0.082 ± 0.007	0.357 ± 0.013	9.9 ± 1.2
<i>SFA1</i>	0.351 ± 0.016	0.090 ± 0.006	0.333 ± 0.020	3.3 ± 0.5
<i>SIP3</i>	0.329 ± 0.023	0.095 ± 0.006	0.400 ± 0.022	6.5 ± 0.9
<i>SNF11</i>	0.400 ± 0.029	0.097 ± 0.013	0.436 ± 0.038	5.1 ± 1.0
<i>TYE7</i>	0.333 ± 0.022	0.085 ± 0.005	0.356 ± 0.028	8.0 ± 1.0
<i>UGA2</i>	0.237 ± 0.004	0.096 ± 0.019	0.311 ± 0.009	10.8 ± 1.8
<i>XKS1</i>	0.396 ± 0.026	0.097 ± 0.004	0.380 ± 0.012	6.7 ± 1.2
<i>YBR184W</i>	0.292 ± 0.028	0.101 ± 0.008	0.445 ± 0.015	9.0 ± 1.5

**Table 5.1-4** Growth data on galactose for all strains used together with corresponding 90 % confidence intervals.

Gene name	$\mu_{\text{Glu}} \text{ h}^{-1}$	$Y_{\text{X/S,Gal}} \text{ g g}^{-1}$	$Y_{\text{E/S,Gal}} \text{ g g}^{-1}$	$Y_{\text{X/O,Gal}} \text{ g g}^{-1}$
Reference	0.223 ± 0.012	0.190 ± 0.014	0.325 ± 0.019	1.3 ± 0.3
<i>CAT8</i>	0.276 ± 0.008	0.148 ± 0.006	0.380 ± 0.014	25.0 ± 5.0
<i>CYB2</i>	0.307 ± 0.069	0.119 ± 0.015	0.209 ± 0.006	1.7 ± 0.2
<i>DLD2</i>	0.199 ± 0.005	0.189 ± 0.012	0.187 ± 0.028	1.3 ± 0.2
<i>FBP1</i>	0.335 ± 0.019	0.214 ± 0.011	0.186 ± 0.022	1.1 ± 0.3
<i>FBP26</i>	0.236 ± 0.021	0.132 ± 0.011	0.251 ± 0.013	2.0 ± 0.2
<i>GAD1</i>	0.316 ± 0.021	0.166 ± 0.010	0.402 ± 0.018	1.8 ± 0.3
<i>GAL10</i>	0.005 ± 0.001	- ± -	- ± -	- ± -
<i>GAL4</i>	0.005 ± 0.001	- ± -	- ± -	- ± -
<i>GAL7</i>	0.005 ± 0.001	- ± -	- ± -	- ± -
<i>GLK1</i>	0.243 ± 0.023	0.122 ± 0.002	0.236 ± 0.004	1.5 ± 0.2
<i>GLO1</i>	0.316 ± 0.023	0.131 ± 0.007	0.237 ± 0.013	2.4 ± 0.3
<i>IMP2</i>	0.293 ± 0.017	0.164 ± 0.004	0.211 ± 0.012	1.6 ± 0.3
<i>LEU4</i>	0.220 ± 0.011	0.239 ± 0.013	0.294 ± 0.005	1.2 ± 0.2
<i>MAE1</i>	0.260 ± 0.015	0.181 ± 0.011	0.367 ± 0.033	1.4 ± 0.2
<i>MAL33</i>	0.196 ± 0.013	0.183 ± 0.010	0.159 ± 0.026	1.9 ± 0.2
<i>MIG2</i>	0.340 ± 0.028	0.140 ± 0.009	0.366 ± 0.030	4.5 ± 1.0
<i>MSN4</i>	0.261 ± 0.018	0.123 ± 0.007	0.356 ± 0.033	1.9 ± 0.2
<i>PCK1</i>	0.181 ± 0.012	0.158 ± 0.009	0.131 ± 0.014	1.7 ± 0.4
<i>PFK26</i>	0.234 ± 0.013	0.235 ± 0.008	0.312 ± 0.012	1.3 ± 0.3
<i>PFK27</i>	0.268 ± 0.028	0.145 ± 0.007	0.158 ± 0.017	5.6 ± 0.6
<i>SFA1</i>	0.253 ± 0.021	0.147 ± 0.014	0.409 ± 0.027	1.2 ± 0.3
<i>SIP3</i>	0.272 ± 0.014	0.134 ± 0.007	0.328 ± 0.014	1.9 ± 0.3
<i>SNF11</i>	0.207 ± 0.011	0.154 ± 0.005	0.406 ± 0.020	22.0 ± 4.0
<i>TYE7</i>	0.216 ± 0.018	0.136 ± 0.010	0.286 ± 0.026	1.7 ± 0.2
<i>UGA2</i>	0.221 ± 0.015	0.156 ± 0.007	0.143 ± 0.013	1.3 ± 0.3
<i>XKS1</i>	0.297 ± 0.020	0.084 ± 0.003	0.225 ± 0.007	1.7 ± 0.2
<i>YBR184W</i>	0.259 ± 0.011	0.119 ± 0.008	0.275 ± 0.028	3.3 ± 0.4

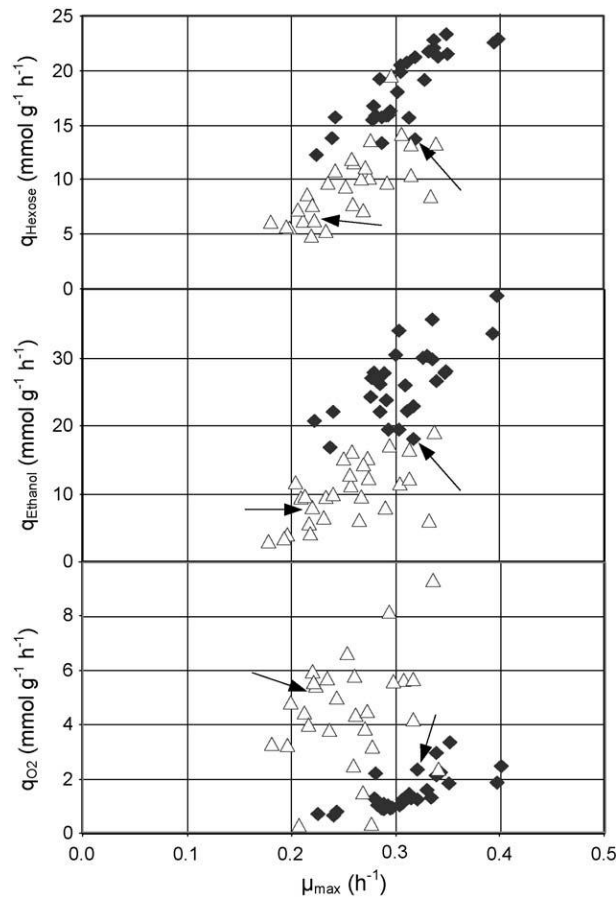


**Figure 5.1-4** Specific conversion rates of carbon substrate, ethanol and oxygen as function of the specific growth rate,  $\mu_{\max}$ , for selected deletion mutants during growth on glucose and galactose (Tables 5.1-3 and 5.1-4).  $\blacklozenge$  -glucose;  $\triangle$  - galactose. Arrows indicate the reference strain BY4742 *Mat $\alpha$  his3 $\Delta$ 1 leu2 $\Delta$ 0 lys2 $\Delta$ 0 ura3 $\Delta$ 0*.

The maximum sugar uptake was close to  $25 \text{ mmol g}^{-1} \text{ h}^{-1}$ . On glucose, 11 strains consumed glucose at rates higher than  $20 \text{ mmol g}^{-1} \text{ h}^{-1}$ : *cat8 $\Delta$*  – 23.3; *gad1 $\Delta$*  – 20.8; *gal10 $\Delta$*  – 22.1; *gkl1 $\Delta$*  – 21.3; *mal33 $\Delta$*  – 20.5; *pck1 $\Delta$*  – 22.8; *sfa1 $\Delta$*  – 21.6; *glo1 $\Delta$*  – 21.3; *snf11 $\Delta$*  – 22.9; *tye7 $\Delta$*  – 21.8; *xks1 $\Delta$*  – 22.6  $\text{mmol g}^{-1} \text{ h}^{-1}$ , whereas a single mutant consumed galactose at such high rate: *xks1 $\Delta$*  - 19.6  $\text{mmol g}^{-1} \text{ h}^{-1}$ . Rodriguez-Pena et al. (1998) assigned this gene xylulokinase activity. Most of the high glucose consumers had specific oxygen consumption rates below  $2 \text{ mmol g}^{-1} \text{ h}^{-1}$ , but on galactose *xks1 $\Delta$*  consumed oxygen at about  $5.6 \text{ mmol g}^{-1} \text{ h}^{-1}$ . At the same time it had a relatively low specific maximum ethanol production rate of  $17.3 \text{ mmol g}^{-1} \text{ h}^{-1}$  on galactose. On glucose, all high rate glucose consumers had values of  $q_{\text{Ethanol}}$  between 20 and  $40 \text{ mmol g}^{-1} \text{ h}^{-1}$  (Figure 5.1-5).

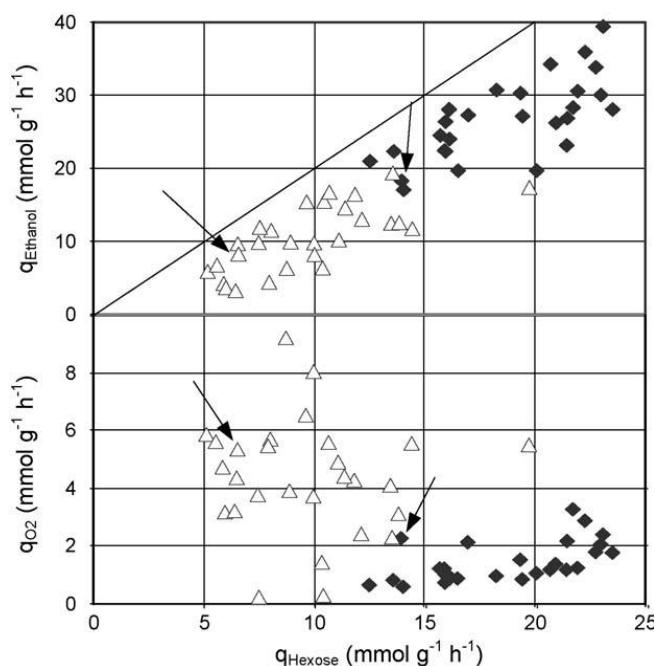


**Figure 5.1-5** Specific conversion rates of ethanol and oxygen as function of the specific hexose consumption rate,  $q_{\text{Hexose}}$ , for selected deletion mutants during growth on glucose and galactose (Tables 5.1-3 and 5.1-4).  $\blacklozenge$  -glucose;  $\triangle$  - galactose. Arrows indicate the reference strain BY4742 *Mat $\alpha$  his3 $\Delta$  leu2 $\Delta$ 0 lys2 $\Delta$ 0 ura3 $\Delta$ 0*. Straight line indicates the maximum possible ethanol yield of 2 mol mol<sup>-1</sup>

Some of the strains growing on galactose showed very high respiratory capacities with the following  $q_{\text{O}_2}$  values (mmol g<sup>-1</sup> h<sup>-1</sup>): *fbp1 $\Delta$*  - 9.3; *imp2 $\Delta$*  - 8.1; *sfa1 $\Delta$*  - 6.6. The two almost respiratory deficient mutants were *cat8 $\Delta$*  and *snf11 $\Delta$*  that are both involved in RNA pol II transcription factor activity. There isn't any report so far reporting similar effects. Overall, this part of the analysis shows that a significant number of strains show activities, which are quite different from the reference strain. Some of them show entirely unanticipated improvements of biotechnological interest. A number of strains grow clearly faster than the reference strain. A significant number had higher specific substrate uptake rates and also high ethanol production rates. The *mig2 $\Delta$*  mutant, involved in the regulation of transcription from the pol II promoter, showed  $q_{\text{Ethanol}}$  on galactose even higher than the corresponding value of the reference strain growing on glucose.

Figure 5.1-6 shows the missing carbon balance from these strains on glucose and galactose. Most of the strains had less than 30 % of missing carbon balance, whereas few strains had about 35 - 45 % of missing carbon balance, especially on galactose, which could be due to the production of other metabolites, e.g. glycerol.

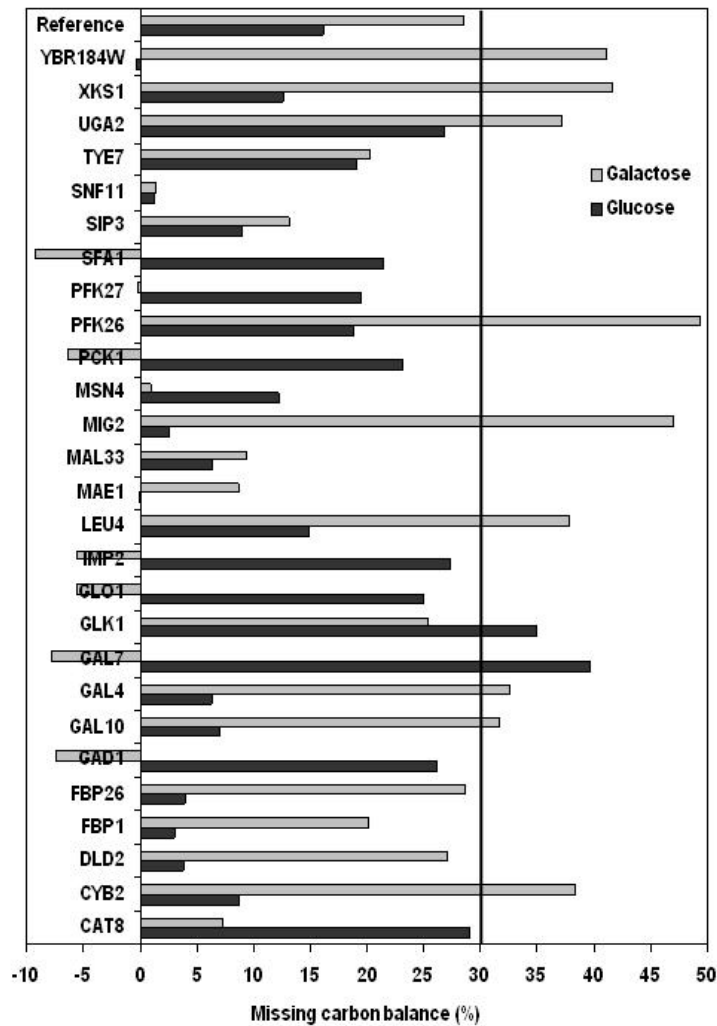
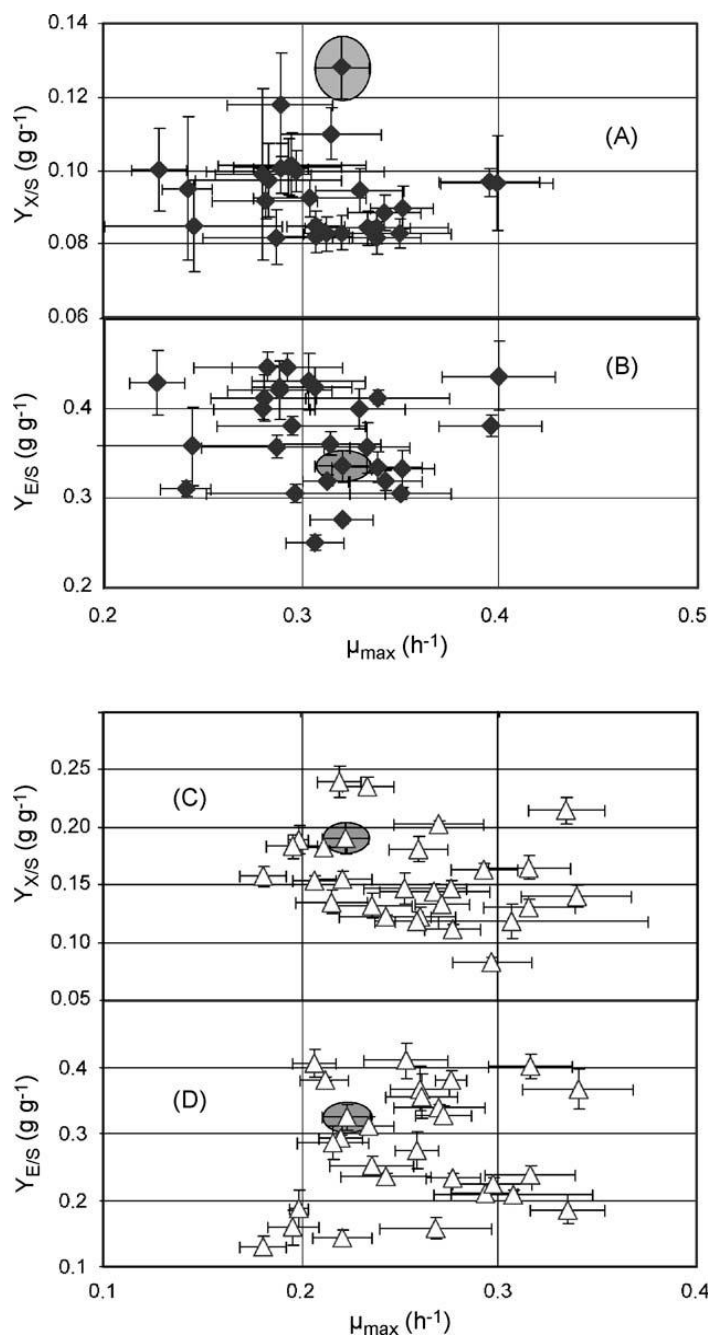


Figure 5.1-6 Missing carbon balance (%) on glucose and galactose for the selected strains.

### 5.1.6.2 Comparison with reference strain

The reference strain was quite close to an average value with respect to  $\mu_{\max}$ ,  $q_{O_2}$ ,  $q_{\text{Ethanol}}$  on galactose and  $q_{\text{Galactose}}$ , where  $q_{\text{Glucose}}$  and  $q_{\text{Ethanol}}$  on glucose were at the lower boundary of the observed values (figures 5.1-4, 5.1-5 and 5.1-7 and Table 5.1-3).  $\mu_{\max}$  on glucose of the reference strain was identical with *dld2Δ*, *gad1Δ*, *gal10Δ*, *glk1Δ*, *imp2Δ*, *leu4Δ*, *sip3Δ* and *tye7Δ*; on galactose with *fbp26Δ*, *leu4Δ*, *tye7Δ* and *uga2Δ*. Therefore, for *leu4Δ* and *tye7Δ*,  $\mu_{\max}$  was indistinguishable from the reference strain on glucose and on galactose. *dld2Δ*, *fbp1Δ*, *fbp26Δ*, *gal4Δ*, *leu4Δ*, *mig2Δ*, *pfk26Δ*, *sip3Δ*, *snf11Δ* and *ybr184wΔ* had the same biomass yield on glucose; *dld2Δ*, *mae1Δ* and *mal33Δ* on galactose and therefore no strain had the same  $Y_{X/S}$  on both sugars. *gad1Δ*, *glo1Δ*, *leu4Δ*, *pck1Δ*, *pfk26Δ*, *pfk27Δ*, *sfa1Δ* and *tye7Δ* showed the same ethanol yield on glucose,  $Y_{E/S}$ , as the reference strain, *mae1Δ*, *mig2Δ*, *msn4Δ*, *pfk26Δ* and *sip3Δ* on galactose and *pfk26Δ* on both sugars. Biomass yields on oxygen,

$Y_{X/O}$ , of the reference strain were identical with *gal10Δ*, *gal4Δ* and *glo1Δ* during growth on glucose, with *dld2Δ*, *fbp1Δ*, *glk1Δ*, *imp2Δ*, *leu4Δ*, *mae1Δ*, *pck1Δ*, *pfk26Δ*, *sfa1Δ* and *uga2Δ* on galactose and no single strain had identical  $Y_{X/O}$  on both sugars.



**Figure 5.1-7** Stoichiometric profiling of selected yeast deletion mutants. Correlation between specific growth rate,  $\mu_{\max}$ , and biomass yields,  $Y_{X/S}$ , on glucose (A) and galactose (C) as well as with ethanol yield,  $Y_{E/S}$ , on glucose (B) and galactose (D). Circled points indicate the reference strain BY4742 *Mat $\alpha$  his3Δ1 leu2Δ0 lys2Δ0 ura3Δ0*.

Another interesting comparison relates physiological parameters on both sugars for each single mutant (Figure 5.1-7).  $Y_{E/S}$  was only identical for the reference strain on glucose ( $0.336 \pm 0.018 \text{ g g}^{-1}$ ) and galactose ( $0.325 \pm 0.019 \text{ g g}^{-1}$ ). The specific growth rate,  $\mu_{\max}$ , was identical on both sugars for *cyb2Δ*, *gad1Δ*, *imp2Δ*, *mae1Δ*, *pfk26Δ* and *pfk27Δ*, respectively. Two strains grew slower on glucose than on galactose, *fbp1Δ*: glucose -  $0.225 \text{ h}^{-1}$  and galactose -  $0.335 \text{ h}^{-1}$  and *mig2Δ*: glucose -  $0.288 \text{ h}^{-1}$  and galactose -  $0.340 \text{ h}^{-1}$ . *fbp1Δ*, fructose-bisphosphatase, is usually required for gluconeogenesis and is therefore considered of minor importance for growth on glucose and galactose, which joins glycolysis at the level of glucose 6-phosphate. *mig2Δ* has RNA pol II transcription factor activity and it remains unclear, why the deletion of this gene has such a pronounced effect on the growth on galactose.

### 5.1.6.3 Comparison of mutants against mutants

All the examined mutants were compared against each other in all eight dimensions. We searched for the indistinguishable strain combinations. Depending on the parameter investigated and on the substrate the discrimination between strains varied (Table 5.1-5).

**Table 5.1-5** Strains not distinguishable based on maximum specific growth rate,  $\mu_{\max}$ , biomass yield on carbon substrate,  $Y_{X/S}$ , ethanol yield on carbon substrate,  $Y_{E/S}$ , and on biomass yield on oxygen,  $Y_{X/O}$ , and growth on glucose and/or galactose as limiting substrate.

	$\mu_{\max}$	$Y_{X/S}$	$Y_{E/S}$	$Y_{X/O}$	all
Glucose	109	337	114	85	13
Galactose	44	65	52	109	1
Glucose and galactose	44	58	17	28	0

Generally, with this set of strains the discrimination was stronger with galactose except on the basis of  $Y_{X/O}$  where growth on glucose was more discriminative. Experiments on galactose alone would only lead to one indistinguishable mutant pair, *msn4Δ* - *sip3Δ*. Both genes have transcription factor activity, *MSN4* upon stress and *SIP3* in connection with transcription initiation from pol II. On glucose alone, the 13 indistinguishable pairs were: *dld2Δ* - *fbp26Δ*, *dld2Δ* - *mae1Δ*, *dld2Δ* - *mig2Δ*, *dld2Δ* - *ybr184wΔ*, *fbp26Δ* - *mae1Δ*, *fbp26Δ* - *ybr184wΔ*, *glo1Δ* - *pck1Δ*, *leu4Δ* - *tye7Δ*, *mae1Δ* - *mal33Δ*, *mae1Δ* - *ybr184wΔ*, *mig2Δ* - *msn4Δ* and *mig2Δ* - *ybr184wΔ*.

### 5.1.6.4 Hierarchical clustering

In order to identify mutant pairs with similar physiological profiling, hierarchical clustering was done using stoichiometric data on glucose, galactose, and combined data on glucose and galactose i.e.,  $\mu_{\max}$ ,  $Y_{X/S}$ ,  $Y_{E/S}$  and  $Y_{X/O}$  using Euclidian distance as a distance metric. The relative Euclidian distances were calculated between mutant pairs and also between mutant and the reference strain.

#### • Glucose

The top five most closely related mutant pairs were *mae1Δ -ybr184wΔ* (0.07); *fbp26Δ -mae1Δ* (0.077); *glo1Δ -pck1Δ* (0.088); *fbp26Δ -ybr184wΔ* (0.101); *gal7Δ -glk1Δ* (0.108). The top three most closely related mutants with the reference strain were *glo1Δ* (0.427); *sfa1Δ* (0.436) and *gal4Δ* (0.453) and one mutant, *uga2Δ* (0.975) was distantly related to the reference strain indicating that this strain had a clear phenotype when grown on glucose. The measured Euclidean distances were visualised as dendrogram and the data revealed 3 main clusters, highlighted with colours in Figure 5.1-8.

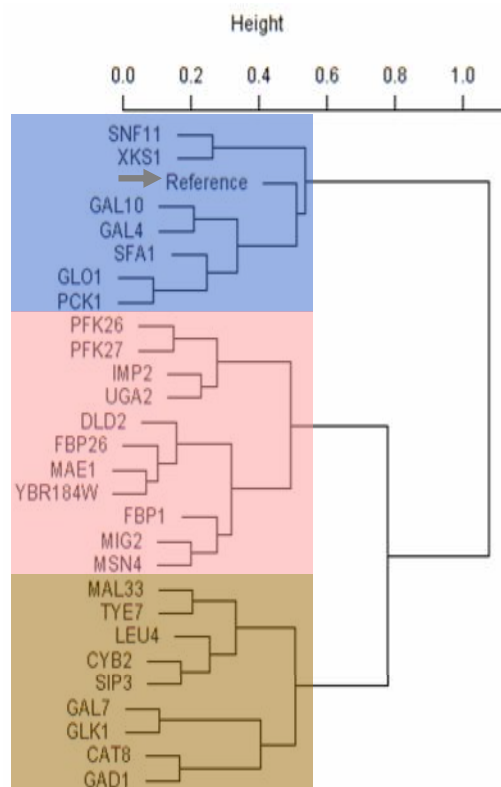


**Figure 5.1-8** Dendrogram on glucose. Hierarchical clustering was done using stoichiometric data by using Euclidean distances as a metric.

In the first cluster (top to bottom), few strains that are involved in galactose metabolism were clustered close to the reference strain for e.g., *gal10Δ* and *gal4Δ* suggesting no clear pheno-

type on glucose. In the second cluster, isoenzymes *pfk26Δ* and *pfk27Δ* (phosphofructokinase activity) were clustered together suggesting an identical phenotype and *mae1Δ*, *fbp26Δ* and *dld2Δ* that are involved in pyruvate metabolism and glucose metabolic process were clustered together and also close to the hypothetical gene *ybr184wΔ*.

### • Galactose

Similarly hierarchical clustering was done using stoichiometric data on galactose as well and the relative Euclidian distances were calculated between mutant pairs and also between mutant and the reference strain. The top five most closely related mutant pairs were *leu4Δ* - *pfk26Δ* (0.097); *msn4Δ* - *sip3Δ* (0.133); *fbp26Δ* - *glk1Δ* (0.162); *fbp26Δ* - *tye7Δ* (0.177); *dld2Δ* - *mal33Δ* (0.196). The top three most closely related mutants with the reference strain were *mae1Δ* (0.231); *pfk26Δ* (0.296) and *leu4Δ* (0.335). The measured Euclidean distances were visualised as dendrogram and the data revealed 4 main clusters, highlighted with colours in Figure 5.1-9.

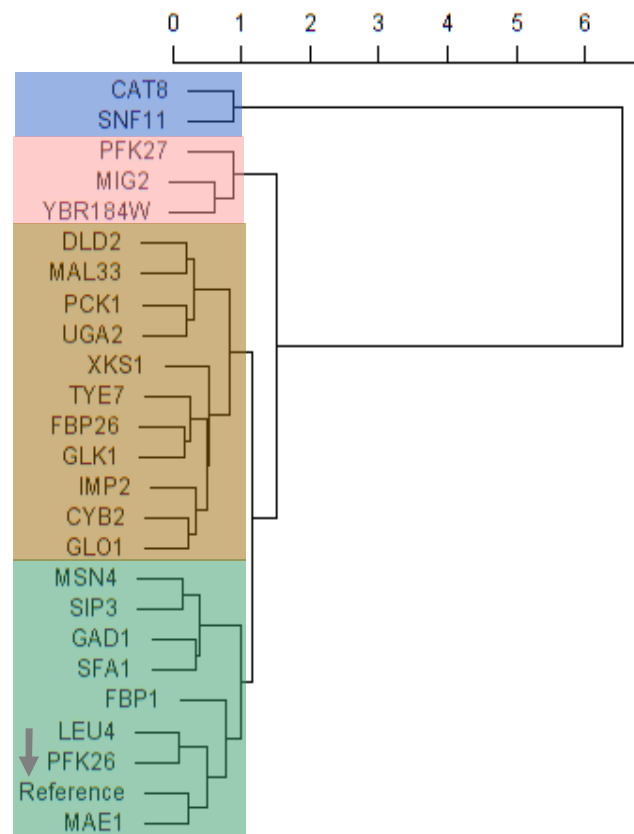


**Figure 5.1-9** Dendrogram on galactose. Hierarchical clustering was done using stoichiometric data by using Euclidean distances as a metric.

The clustering results were different on glucose and galactose suggesting substrate specific phenotypes of the mutant strains. The distance between the mutant pairs is smaller on glucose than on galactose, representing strong phenotype of deletion mutants on galactose when compared to glucose grown conditions. Furthermore, two mutants, *snf11Δ* (5.62) and *cat8Δ* (6.43) were very distantly related to the reference strain. Whereas these strains were ten times closer to the reference strain when grown on glucose (*snf11Δ* -0.51 and *cat8Δ* -0.54) indicating that these strains had clearer phenotypes when grown on galactose than on glucose.

• **Combined analysis – Glucose and Galactose**

Hierarchical clustering was done using combined stoichiometric data on glucose and galactose and the relative Euclidian distances were calculated in the similar fashion. The top five most closely related mutant pairs were *dld2Δ –mal33Δ* (0.31); *glk1Δ –tye7Δ* (0.328); *sip3Δ –tye7Δ* (0.39); *fbp26Δ – ybr184wΔ* (0.398); *leu4Δ –pfk26Δ* (0.444). The top three most closely related mutants with the reference strain were *leu4Δ* (0.601); *sfa1Δ* (0.615) and *sip3Δ* (0.663). The measured Euclidean distances were visualised as dendrogram and the data revealed 4 main clusters, highlighted with colours in Figure 5.1-10.

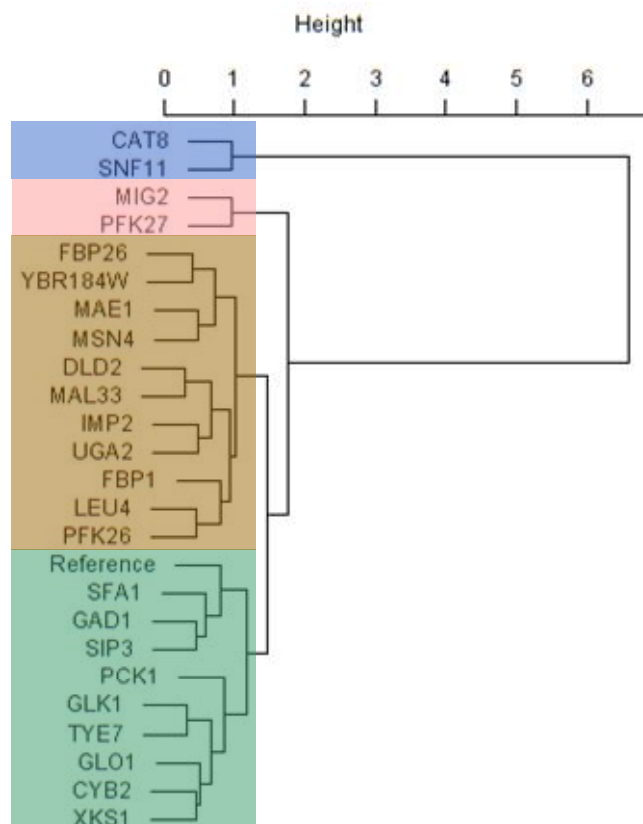


**Figure 5.1-10** Dendrogram for glucose and galactose data. Hierarchical clustering was done using stoichiometric data by using Euclidean distances as a metric.

### 5.1.7 Conclusions

Twenty-seven deletion mutants of *S. cerevisiae* were investigated using a novel method for high-content stoichiometric and kinetic metabolic profiling. From high-throughput quantitative stoichiometric profiling of yeast mutants at miniaturized scale, quantitative information was obtained about the metabolism of all tested mutants. Cultivation on glucose and galactose in 96-well microtiter plates with on-line optical sensing of dissolved oxygen was reproducible and identical to shake flask cultivation. At high shaking rate (1020 rpm) there was no oxygen limitation throughout all cultivations whereas at low shaking rate (540 rpm) oxygen uptake rate could be measured during declining dissolved oxygen concentration.

First one could detect, whether oxygen limitation is occurring during cultivation using the oxygen sensing microtiter plate. Secondly, dissolved oxygen profiles indicate most substrate limitations and diauxic behaviour (Figures 5.1-1 and 5.1-3). The application of a simple balanced growth model allows correction for ethanol and water evaporation. From this new method, reliable data for specific growth rate, biomass and ethanol yields on carbon substrate and biomass yield on oxygen were calculated. Using the two substrates glucose and galactose, overall 8 parameters were obtained which could successfully discriminate between the 27 strains described here. Maximum specific growth rates were in the same range for both sugars. On glucose the growth was predominantly fermentative with high yield of ethanol, low yield of biomass and low oxygen consumption rate. Clustering analysis on glucose revealed that knockout strains with similar function were clustered together. On galactose, respiration was more active with correspondingly lower ethanol yields, higher biomass yields and higher rates of oxygen consumption. The clustering results were different on galactose than on glucose with large distance between the mutant strains and to the reference strain suggesting strong phenotypes on galactose. Some strains showed unexpectedly high or low growth rates and rates of ethanol production and respiration. Overall the four parameters determined for each mutant on two different carbon sources (Figure 5.1-10) allowed statistically significant discrimination of all mutants studied.

## 5.2 MALDI-TOF-MS FOR METABOLIC FLUX ANALYSES USING ISOTOPE LABELED ETHANOL

Most of the results presented in this chapter are contained in the following publication.

Hollemeier, K., **Velagapudi, V.R.**, Wittmann, C., Heinzle, E., 2007. Matrix-assisted laser desorption/ionization time-of-flight mass spectrometry for metabolic flux analyses using isotope-labeled ethanol. **Rapid Commun Mass Spectrom.** 21, 336-342.

### 5.2.1 Background

Unknown gene function can be determined by phenotypic analysis of mutants missing the gene of interest (Winzeler et al., 1999; Que et al., 2002). Complete libraries of gene deletion mutants of *S. cerevisiae* have been established (Giaever et al., 2002; Brachmann et al., 1998). Gene function analysis would be greatly supported by additional analysis of metabolic flux distributions of mutants of this library. This requires the analysis of substrate consumption as well as of biomass and product formation. Flux distribution can be determined by feeding  $^{13}\text{C}$ -labeled substrate with subsequent precise analysis of metabolites or products by using mass spectrometry (MS). This is also possible at a microliter scale using, e.g., 96-well microplates. Usually, ethanol is derivatized prior to GC/MS analysis (Knapp, 1979) and most derivatizations have to be carried out in a water-free organic solvent. Derivatization of highly diluted ethanol on the microtiter plate scale is therefore difficult because of the small amounts produced, the high volatility of ethanol and the presence of the aqueous matrix.

A new method was developed for the quantification of isotope-labeled ethanol (A detailed description of the method was given in the Materials and Methods section). The new method is now routinely used for the determination of unlabeled and mono- $^{13}\text{C}$ -labeled ethanol as products of 1- $^{13}\text{C}$ -labeled hexose substrates in yeast fermentation experiments. This permits the calculation of the flux split ratio between glycolysis and the pentose-phosphate pathway (PPP). Compared with standard GC/MS analysis the new application works with much higher throughput, with an average MALDI-TOF measuring time of less than 30 s per sample with the instrument applied here, and less than 2 s with a high-frequency laser instrument. For high throughput purposes, all steps of the method can be automated. Furthermore, no hazardous chemicals such as diazomethane or trimethylchlorosilane are required.

## 5.2.2 Ethanol quantification and validation

The selected three *S. cerevisiae* deletion strains were cultivated in a 96-well microtiter plate using [1-<sup>13</sup>C]-glucose as carbon source. Ethanol produced from the culture supernatant was quantified using MALDI-ToF-MS (Figure 5.2-1) as described in the materials and methods section. To validate these results, ethanol concentrations were also quantified enzymatically using a spectrophotometer. The results from both methods were similar and the differences were about 3.3 % on average (Table 5.2-1). This makes the new Ac-DNPH method suitable for measurements of singly labeled <sup>13</sup>C-ethanol in fermentation experiments.

## 5.2.3 Estimation and validation of flux split ratio

The flux split ratio between the PPP and glycolysis,  $\Phi_{ppp}$  was estimated (Eq 4-13), based on ethanol labeling, by MALDI-ToF-MS and the obtained values were compared with those obtained from GC/MS which were based on alanine labeling. The differences between both methods were about 4.3 % (Table 5.2-1).

**Table 5.2-1** Determination of ethanol concentration and flux partitioning ratio between glycolysis and PP pathway,  $\Phi_{ppp}$  (Eq 4-13) in yeast cultures using MALDI-TOF MS and comparison with established reference methods, enzymatic conversion and spectroscopic detection and GC-MS analysis of alanine

Yeast deletion strains	Ethanol concentration [g/l]			$\Phi_{ppp}$ value		
	Spectroscopic	MALDI-TOF	Difference (%)	MALDI-TOF	GC-MS	Difference (%)
<i>fbp26Δ</i>	2.63 ± 0.02	2.55 ± 0.18	3.13	0.068	0.07	2.9
<i>tye7Δ</i>	3.09 ± 0.26	3.16 ± 0.16	2.22	0.074	0.07	5.7
<i>pck1Δ</i>	3.36 ± 0.19	3.52 ± 0.05	4.55	0.067	0.07	4.3

This difference is very small considering the amplification of errors. Additionally, in the GC/MS measurements, all three carbon atoms of alanine can be labeled because of anaplerotic reactions but only two carbon atoms in ethanol. Clearly, other methods based on the GC/MS analysis of amino acids from cell proteins and isotopomer modelling provide more accurate data on the flux partitioning between the PPP and glycolysis. These approaches, however, are linked to a higher experimental effort, which hampers their application to large-scale screening of fluxes.

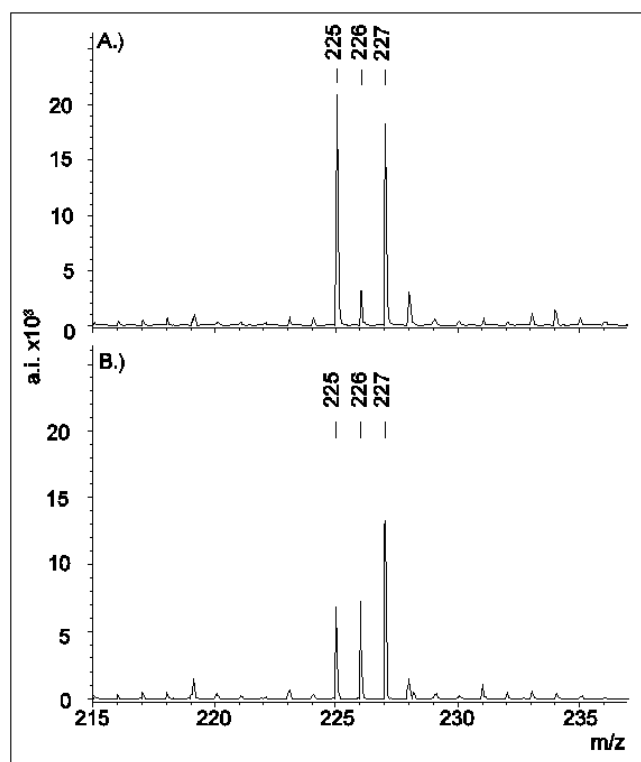


**Figure 5.2-1** (A) Blank value solely using [ $^{13}\text{C}_2$ ]-labeled acetaldehyde-DNPH. (B) Mass spectrum of naturally and [ $1\text{-}^{13}\text{C}$ ]-labeled acetaldehyde-DNPH in equimolar ratio (50mM) each together with [ $^{13}\text{C}_2$ ]-labeled acetaldehyde-DNPH (15 mM) as internal standard.

## 5.2.4 Conclusions

A novel method was developed for the determination of the concentration and labeling degree of ethanol originating from  $1\text{-}^{13}\text{C}$ -labeling experiments. This method is suitable for high-throughput metabolic flux analysis because of the possible parallel sample preparation and fast final analysis using MALDI-ToF-MS.

This new application of the hydrazone reaction of 2, 4-dinitrophenylhydrazine with acetaldehyde, formed by an enzymatic reaction, is a sufficiently sensitive method for the quantification of ethanol formed by fermentation. Not only unlabeled ethanol but also mono- $^{13}\text{C}$ -labeled ethanol originating from labeled substrates can be quantified, even at a minimum concentration of 1 mM, using [ $^{13}\text{C}_2$ ]-ethanol as internal standard. Ethanol quantification using this method was compared with enzymatic analysis and exhibited differences of less than 3.3 % on average. Similar results from spectrometric tests for total content of ethanol showed the accuracy of the method. The method is linear up to 500 mM ethanol.

Comparison of flux partitioning ratios between glycolysis and the pentose-phosphate pathway (PPP) based on MALDI-TOFMS and gas chromatography GC/MS methods showed good agreement, with differences for ethanol and alanine labeling of only 4.3 %. The main advantage of the method compared with GC/MS methods is the possibility for high-throughput analysis with parallel sample treatment using MALDI-TOFMS. Using MALDI-TOFMS, large numbers of analyses of isotope-labeled ethanol can be performed almost in parallel with measurement times of only a few seconds each. The sample preparation step of the new method can also be automated using a robotic system. Therefore, this method is suitable for high-throughput metabolic studies, e.g. of mutant libraries of yeast.

## 5.3 METABOLIC FLUX SCREENING OF *S. CEREVISIAE* KNOCKOUT STRAINS ON GLUCOSE AND GALACTOSE AT MINIATURIZED SCALE

Most of the results presented in this chapter are contained in the following publication.

**Velagapudi, V.R.**, Wittmann, C., Schneider, K., Heinzle, E., 2007. Metabolic Flux Screening of *Saccharomyces cerevisiae* Single Knockout Strains on Glucose and Galactose Supports Elucidation of Gene Function. **J Biotechnol.** 132, 395–404.

### 5.3.1 Background

The full understanding of yeast physiology requires quantitative methods. Continuous cultivation allows most thorough studies but requires an enormous amount of labour (von Meyenburg et al., 1969; Furukawa et al., 1983; Postma et al., 1989). Controlled batch cultivation also may provide rich information (Westergaard et al., 2007) but the number of experiments carried out is rather limited because of the high effort. New screening methods based on new cultivation methods in microtiter plates as described in this thesis or by other groups (Fischer and Sauer, 2003; Wittmann et al., 2004; Sauer, 2004) open up new possibilities in this field particularly, when combined with modern analytical methods based on mass spectrometric analysis.

The application of  $^{13}\text{C}$ -labelling techniques using mass spectrometry (Wittmann and Heinzle, 1999; 2001a and 2001b; Wittmann, 2002) shows a potential to carry out such analysis even at a 96-well microtiter plate scale (Sauer, 2004) as was shown for *C. glutamicum* (Wittmann et al., 2004), *B. subtilis* (Zamboni and Sauer, 2004) and *E. coli* (Fischer and Sauer, 2003). Comprehensive flux analysis of yeast is complicated by the compartmentation, particularly mitochondrial activity. Therefore, it requires extensive labelling analysis of amino acids contained in cellular proteins (Frick and Wittmann, 2005; Blank et al., 2005; Gombert et al., 2001) or even of intracellular metabolites (van Winden et al., 2005).

New microtiter plate cultivation techniques with integrated optical sensing of dissolved oxygen (John et al., 2003) allow large-scale determination of specific growth rate, ethanol production rate and glucose and oxygen consumption rates (Velagapudi et al., 2006). This study

showed clear differences between strains cultivated on glucose and galactose. It also discovered unexpected mobilization of metabolic potential and discrimination of all studied strains using the four parameters mentioned above. It would be very interesting to extend the metabolic information obtained by applying metabolic flux analysis. The above described new technique in section 5.2, particularly suited to determine flux split ratios into the pentose phosphate pathway in yeast that is based on MALDI-ToF mass spectrometry (Hollemeyer et al., 2007). Using microtiter plate cultivation with dissolved oxygen measurement combined with the new  $^{13}\text{C}$  flux screening method (for detailed description please refer to Materials and Methods, section 4.10), a set of *S. cerevisiae* deletion mutants cultivated on glucose and galactose were studied to gain information about the function of deleted genes.

### 5.3.2 Flux through Pentose Phosphate Pathway (PPP)

Metabolic flux split ratios at glucose 6-phosphate branch point towards pentose phosphate pathway ( $\Phi_{\text{PPP}}$ ) were obtained based on the ethanol labelling using MALDI-ToF-MS as described in section 5.2.3. Based on the obtained  $\Phi_{\text{PPP}}$  values, mutants were classified into three groups. Strains having  $\Phi_{\text{PPP}}$  of 0.05 to 0.15 were classified as strains with low  $\Phi_{\text{PPP}}$ . On glucose, 17 strains were having low  $\Phi_{\text{PPP}}$ , whereas on galactose only 2 strains had low  $\Phi_{\text{PPP}}$ . Strains having  $\Phi_{\text{PPP}}$  of 0.15 to 0.25 were classified as strains with high  $\Phi_{\text{PPP}}$ . On glucose, 11 strains were having low  $\Phi_{\text{PPP}}$  whereas on galactose, 9 strains had high  $\Phi_{\text{PPP}}$ . Strains with  $\Phi_{\text{PPP}}$  of 0.25 to 0.35 were classified as strains with very high  $\Phi_{\text{PPP}}$ . On galactose, 12 strains had very high  $\Phi_{\text{PPP}}$  whereas none of the strains had very high  $\Phi_{\text{PPP}}$  on glucose. One strain *mae1Δ* had exceptionally very high  $\Phi_{\text{PPP}}$  of 0.455 on galactose, whereas on glucose this strain *mae1Δ* had low  $\Phi_{\text{PPP}}$  of 0.138 (Tables 5.3-1 and 5.3-2).

The flux through the PPP,  $\Phi_{\text{PPP}}$  was correlated to the yield of biomass  $Y_{\text{XS}}$ , suggesting a balanced production and consumption of NADPH. This trend was more certain on galactose rather than on glucose (Figure 5.3-1).

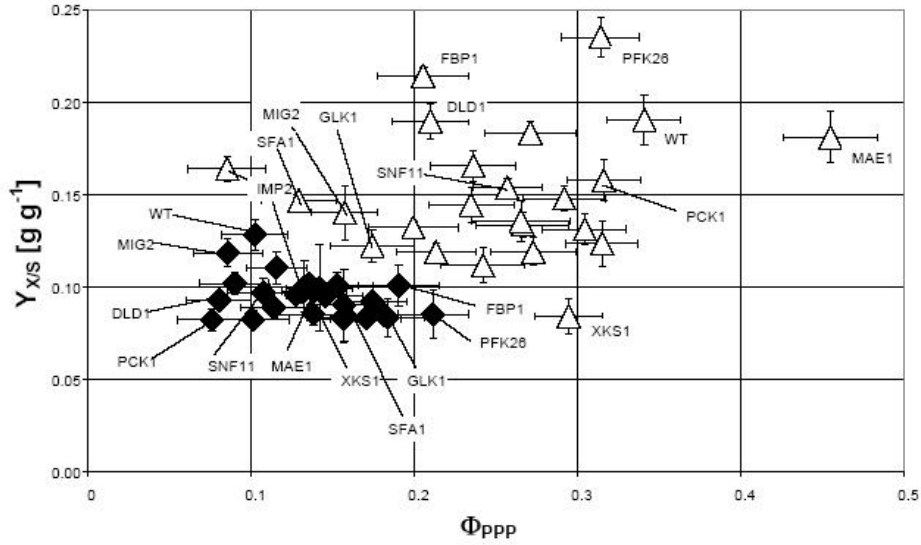


**Figure 5.3-1** Comparison of biomass yield,  $Y_{X/S}$ , and flux partitioning into the pentose phosphate pathway,  $\Phi_{PPP}$ , in galactose and glucose cultures. Error bars indicate 90 % confidence levels.  $\blacklozenge$  - glucose;  $\triangle$  - galactose.

**Table 5.3-1** Growth data on glucose. Specific growth rate,  $\mu_{\text{Glu}}$ , specific uptake rate of glucose,  $q_{\text{Glu}}$ , specific rate of ethanol production,  $q_{\text{ETH}}$ , flux partitioning from glucose 6-phosphate into the pentose phosphate pathway,  $\Phi_{\text{PPP,Glu}}$ ; and from pyruvate/PEP into oxaloacetate/malate,  $\Phi_{\text{Anaplerotic,Glu}}$ , and biomass yield on glucose,  $Y_{\text{X/S,Glu}}$ , all with 90 % confidence levels. The last line shows the average values of all strains (Table 5.1-1) and standard deviation between them.

Gene name	$\mu_{\text{Glu}} \text{ h}^{-1}$	$q_{\text{Glu}} \text{ mmol g}^{-1} \text{ h}^{-1}$	$q_{\text{ETH}} \text{ mmol g}^{-1} \text{ h}^{-1}$	$\Phi_{\text{PPP,Glu}}$	$\Phi_{\text{Anaplerotic,Glu}}$	$Y_{\text{X/S,Glu}} \text{ g g}^{-1}$
Reference	0.320 ± 0.014	13.9 ± 0.9	18.2 ± 1.5	0.102 ± 0.020	0.025 ± 0.004	0.128 ± 0.009
<i>CAT8</i>	0.350 ± 0.026	23.4 ± 1.0	27.9 ± 1.3	0.170 ± 0.022	0.016 ± 0.002	0.083 ± 0.004
<i>CYB2</i>	0.279 ± 0.025	15.6 ± 1.0	24.4 ± 1.7	0.142 ± 0.020	0.018 ± 0.003	0.099 ± 0.023
<i>DLI1</i>	0.303 ± 0.029	18.1 ± 2.7	30.5 ± 5.1	0.081 ± 0.020	0.017 ± 0.003	0.093 ± 0.005
<i>FBP1</i>	0.225 ± 0.014	12.4 ± 1.9	20.9 ± 3.6	0.191 ± 0.025	0.018 ± 0.003	0.101 ± 0.011
<i>FBP26</i>	0.288 ± 0.014	15.8 ± 1.6	26.2 ± 3.1	0.153 ± 0.022	0.019 ± 0.003	0.101 ± 0.007
<i>GAD1</i>	0.312 ± 0.012	20.8 ± 0.7	26.1 ± 1.0	0.156 ± 0.022	0.016 ± 0.002	0.083 ± 0.005
<i>GALI0</i>	0.338 ± 0.037	22.1 ± 1.3	35.7 ± 2.2	0.158 ± 0.020	0.017 ± 0.003	0.085 ± 0.004
<i>GAL4</i>	0.280 ± 0.027	16.9 ± 2.1	27.1 ± 3.8	0.174 ± 0.024	0.017 ± 0.003	0.092 ± 0.005
<i>GAL7</i>	0.306 ± 0.015	20.0 ± 1.0	19.6 ± 1.2	0.138 ± 0.020	0.016 ± 0.002	0.085 ± 0.004
<i>GLK1</i>	0.320 ± 0.016	21.3 ± 0.7	23.0 ± 0.8	0.184 ± 0.022	0.016 ± 0.002	0.083 ± 0.005
<i>GLO1</i>	0.342 ± 0.019	21.3 ± 1.2	26.7 ± 1.8	0.114 ± 0.021	0.017 ± 0.003	0.089 ± 0.005
<i>IMP2</i>	0.296 ± 0.046	16.4 ± 1.3	19.6 ± 1.7	0.133 ± 0.022	0.019 ± 0.003	0.100 ± 0.006
<i>LEU4</i>	0.314 ± 0.026	15.8 ± 0.9	22.3 ± 1.5	0.116 ± 0.021	0.021 ± 0.003	0.110 ± 0.007
<i>MAE1</i>	0.282 ± 0.038	16.0 ± 1.5	27.9 ± 2.7	0.139 ± 0.022	0.018 ± 0.003	0.098 ± 0.010
<i>MAL33</i>	0.306 ± 0.019	20.6 ± 2.5	34.1 ± 4.5	0.157 ± 0.021	0.016 ± 0.003	0.083 ± 0.004
<i>MIG2</i>	0.288 ± 0.027	13.5 ± 1.7	22.2 ± 3.3	0.086 ± 0.021	0.022 ± 0.004	0.118 ± 0.014
<i>MSN4</i>	0.294 ± 0.038	16.0 ± 1.1	23.9 ± 1.8	0.090 ± 0.019	0.019 ± 0.003	0.102 ± 0.009
<i>PCK1</i>	0.338 ± 0.023	22.9 ± 2.1	29.9 ± 3.1	0.076 ± 0.020	0.016 ± 0.002	0.082 ± 0.005
<i>PFK26</i>	0.243 ± 0.046	15.8 ± 3.7	22.2 ± 5.8	0.212 ± 0.021	0.015 ± 0.002	0.085 ± 0.012
<i>PFK27</i>	0.286 ± 0.038	19.3 ± 1.7	27.0 ± 2.5	0.101 ± 0.021	0.015 ± 0.002	0.082 ± 0.007
<i>SFA1</i>	0.351 ± 0.016	21.6 ± 2.1	28.1 ± 3.2	0.157 ± 0.021	0.018 ± 0.003	0.090 ± 0.006
<i>SIP3</i>	0.329 ± 0.023	19.2 ± 2.0	30.1 ± 3.6	0.145 ± 0.021	0.018 ± 0.003	0.095 ± 0.006
<i>SNF11</i>	0.400 ± 0.029	22.9 ± 3.9	39.2 ± 7.5	0.108 ± 0.022	0.020 ± 0.004	0.097 ± 0.013
<i>TYE7</i>	0.333 ± 0.022	21.8 ± 3.1	30.4 ± 4.9	0.181 ± 0.022	0.017 ± 0.003	0.085 ± 0.005
<i>UGA5</i>	0.240 ± 0.004	14.0 ± 0.6	17.0 ± 0.9	0.128 ± 0.020	0.017 ± 0.003	0.096 ± 0.019
<i>XKS1</i>	0.396 ± 0.026	22.6 ± 1.3	33.6 ± 2.3	0.132 ± 0.023	0.020 ± 0.003	0.097 ± 0.004
<i>YBR184W</i>	0.292 ± 0.028	16.0 ± 1.2	27.9 ± 2.3	0.136 ± 0.022	0.019 ± 0.003	0.101 ± 0.008
Average	0.309 ± 0.010	18.4 ± 0.9	26.5 ± 1.6	0.138 ± 0.001	0.018 ± 0.000	0.094 ± 0.005

**Table 5.3-2** Growth data on galactose. Specific growth rate,  $\mu_{Gal}$ , specific uptake rate of galactose,  $q_{Gal}$ , specific rate of ethanol production,  $q_{ETH}$ , flux partitioning from glucose 6-phosphate into the pentose phosphate pathway,  $\Phi_{PPP,Gal}$ ; and from pyruvate/PEP into oxaloacetate/malate,  $\Phi_{Anaplerotic,Gal}$ , and biomass yield on glucose,  $Y_{X/S,Gal}$ , all with 90 % confidence levels. The last line shows the average values of all strains and standard deviation between them.

Gene name	$\mu_{Gal} \text{ h}^{-1}$	$q_{Gal} \text{ mmol g}^{-1} \text{ h}^{-1}$	$q_{ETH} \text{ mmol g}^{-1} \text{ h}^{-1}$	$\Phi_{PPP,Gal}$	$\Phi_{Anaplerotic,Gal}$	$Y_{X/S,Gal} \text{ g g}^{-1}$
Reference	0.223 ± 0.012	6.5 ± 0.2	8.3 ± 0.6	0.341 ± 0.029	0.037 ± 0.006	0.190 ± 0.014
<i>CAT8</i>	0.276 ± 0.008	10.4 ± 0.2	15.4 ± 0.7	0.292 ± 0.028	0.029 ± 0.005	0.148 ± 0.006
<i>CYB2</i>	0.307 ± 0.069	14.3 ± 1.1	11.7 ± 0.9	0.213 ± 0.021	0.023 ± 0.003	0.119 ± 0.015
<i>DLD1</i>	0.199 ± 0.005	5.8 ± 0.2	4.3 ± 0.6	0.210 ± 0.022	0.035 ± 0.005	0.189 ± 0.012
<i>FBP1</i>	0.335 ± 0.019	8.7 ± 0.3	6.3 ± 0.8	0.206 ± 0.023	0.045 ± 0.006	0.214 ± 0.011
<i>FBP26</i>	0.236 ± 0.021	9.9 ± 0.5	9.7 ± 0.7	0.200 ± 0.024	0.024 ± 0.004	0.132 ± 0.011
<i>GAD1</i>	0.316 ± 0.021	10.6 ± 0.4	16.7 ± 1.0	0.236 ± 0.026	0.034 ± 0.006	0.166 ± 0.010
<i>GAL10</i>	0.000					
<i>GAL4</i>	0.000					
<i>GAL7</i>	0.000					
<i>GLK1</i>	0.243 ± 0.023	11.0 ± 0.5	10.2 ± 0.5	0.174 ± 0.023	0.022 ± 0.003	0.122 ± 0.002
<i>GLO1</i>	0.316 ± 0.023	13.4 ± 0.5	12.4 ± 0.8	0.305 ± 0.028	0.026 ± 0.004	0.131 ± 0.007
<i>IMP2</i>	0.293 ± 0.017	9.9 ± 0.3	8.2 ± 0.5	0.086 ± 0.021	0.032 ± 0.005	0.164 ± 0.004
<i>LEU4</i>	0.220 ± 0.011	5.1 ± 0.2	5.9 ± 0.2			0.239 ± 0.013
<i>MAE1</i>	0.260 ± 0.015	8.0 ± 0.3	11.5 ± 1.1	0.455 ± 0.030	0.037 ± 0.006	0.181 ± 0.011
<i>MAL33</i>	0.196 ± 0.013	5.9 ± 0.2	3.7 ± 0.6	0.271 ± 0.026	0.034 ± 0.005	0.183 ± 0.010
<i>MIG2</i>	0.340 ± 0.028	13.5 ± 0.6	19.3 ± 1.8	0.157 ± 0.021	0.028 ± 0.005	0.140 ± 0.009
<i>MSN4</i>	0.261 ± 0.018	11.8 ± 0.5	16.4 ± 1.6	0.315 ± 0.026	0.024 ± 0.004	0.123 ± 0.007
<i>PCK1</i>	0.181 ± 0.012	6.4 ± 0.2	3.3 ± 0.4	0.316 ± 0.026	0.029 ± 0.004	0.158 ± 0.009
<i>PFK26</i>	0.234 ± 0.013	5.5 ± 0.2	6.8 ± 0.3	0.314 ± 0.026	0.047 ± 0.007	0.235 ± 0.008
<i>PFK27</i>	0.268 ± 0.028	10.3 ± 0.5	6.4 ± 0.7	0.235 ± 0.024	0.028 ± 0.004	0.145 ± 0.007
<i>SFA1</i>	0.253 ± 0.021	9.6 ± 0.5	15.3 ± 1.3	0.130 ± 0.023	0.027 ± 0.005	0.147 ± 0.014
<i>SIP3</i>	0.272 ± 0.014	11.3 ± 0.4	14.5 ± 0.8	0.267 ± 0.025	0.026 ± 0.004	0.134 ± 0.007
<i>SNF11</i>	0.207 ± 0.011	7.5 ± 0.2	11.9 ± 0.7	0.257 ± 0.024	0.028 ± 0.004	0.154 ± 0.005
<i>TYE7</i>	0.216 ± 0.018	8.8 ± 0.4	9.9 ± 1.0	0.266 ± 0.024	0.025 ± 0.004	0.136 ± 0.010
<i>UGA5</i>	0.277 ± 0.015	13.8 ± 0.4	12.5 ± 0.5	0.242 ± 0.028	0.021 ± 0.003	0.112 ± 0.004
<i>XKS1</i>	0.297 ± 0.020	19.6 ± 0.6	17.3 ± 0.8	0.295 ± 0.027	0.016 ± 0.002	0.084 ± 0.003
<i>YBR184W</i>	0.259 ± 0.011	12.1 ± 0.4	13.0 ± 1.4	0.273 ± 0.026	0.023 ± 0.003	0.119 ± 0.008
Average	0.232 ± 0.012	10.0 ± 0.2	10.8 ± 0.4	0.252 ± 0.003	0.029 ± 0.001	0.155 ± 0.003

The correlation of  $\Phi_{\text{PPP}}$  between glucose and galactose showed  $\Phi_{\text{PPP}}$  values are quite high on galactose than on glucose. The reference strain itself showed three times higher PPP flux on galactose than on glucose. Only 2 strains, *glk1Δ* and *fbp1Δ* had comparable  $\Phi_{\text{PPP}}$  on both the sugars. Mutant strains, *pfk27Δ*, *sip3Δ*, *snf11Δ*, *xks1Δ* and *ybr184wΔ* had double  $\Phi_{\text{PPP}}$  values on galactose than on glucose; deletion strains, *glo1Δ*, *msn4Δ* and *pck1Δ* had three times higher  $\Phi_{\text{PPP}}$  values on galactose than on glucose. One strain, *mae1Δ* showed extremely high about 3.5 times higher  $\Phi_{\text{PPP}}$  values on galactose than on glucose. Interestingly two strains had higher  $\Phi_{\text{PPP}}$  values on glucose than on galactose, *imp2'Δ* (about tow times) and *sfa1Δ* (slightly higher) (Figure 5.3-2; Tables 5.3-1 and 5.3-2).

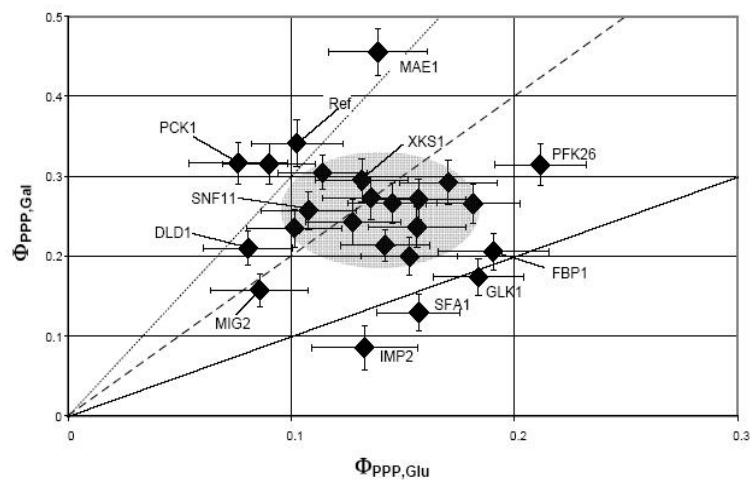


**Figure 5.3-2** Comparison of flux partitioning into the pentose phosphate pathway,  $\Phi_{\text{PPP}}$ , in galactose and glucose cultures. Error bars indicate 90 % confidence levels. The full straight line indicates identical values on glucose and galactose, the dashed one double  $\Phi_{\text{PPP}}$  on galactose compared to glucose, and dotted line triple values.

An increasing hexose uptake rate was observed with increasing specific growth rate (Figure 5.3-3 upper part). An inverse correlation was observed between the maximum growth rate and  $\Phi_{\text{PPP}}$  on both the sugars (Figure 5.3-3 lower part).

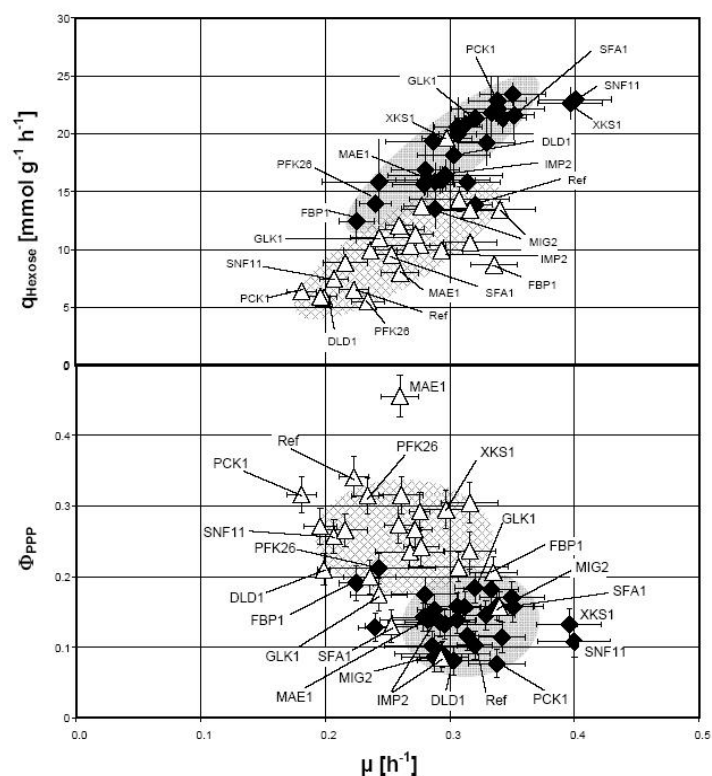


**Figure 5.3-3** Specific growth rate,  $\mu$ , specific hexose uptake rates,  $q_{\text{Hexose}}$  (upper part), and flux partitioning into the pentose phosphate pathway,  $\Phi_{\text{PPP}}$  (lower part). Gene names are specified in Table 5.1-1. Error bars indicate 90 % confidence regions (Tables 5.3-1 and 5.3-2).  $\blacklozenge$  - glucose;  $\triangle$  - galactose.

### 5.3.3 Flux through Anaplerotic pathway

Strains having  $\Phi_{\text{Anaplerotic}}$  of 0.005 to 0.015 were classified as strains with low  $\Phi_{\text{Anaplerotic}}$ . On glucose, 17 strains were having low  $\Phi_{\text{Anaplerotic}}$  whereas on galactose only 1 strain had low  $\Phi_{\text{Anaplerotic}}$ . Strains having  $\Phi_{\text{Anaplerotic}}$  of 0.015 to 0.025 were classified as strains with high  $\Phi_{\text{Anaplerotic}}$ . On glucose, 11 strains were having low  $\Phi_{\text{Anaplerotic}}$  whereas on galactose 13 strains had high  $\Phi_{\text{Anaplerotic}}$ . Strains with  $\Phi_{\text{Anaplerotic}}$  of 0.025 to 0.035 were classified as strains with very high  $\Phi_{\text{Anaplerotic}}$ . On galactose, 8 strains had very high  $\Phi_{\text{Anaplerotic}}$  whereas none of the strains had very high  $\Phi_{\text{Anaplerotic}}$  on glucose. Two strains *fbp1Δ* and *pfk26Δ* had exceptionally high  $\Phi_{\text{Anaplerotic}}$  0.0366 and 0.041 respectively on galactose (Figure 5.3-4; Tables 5.3-1 and 5.3-2).

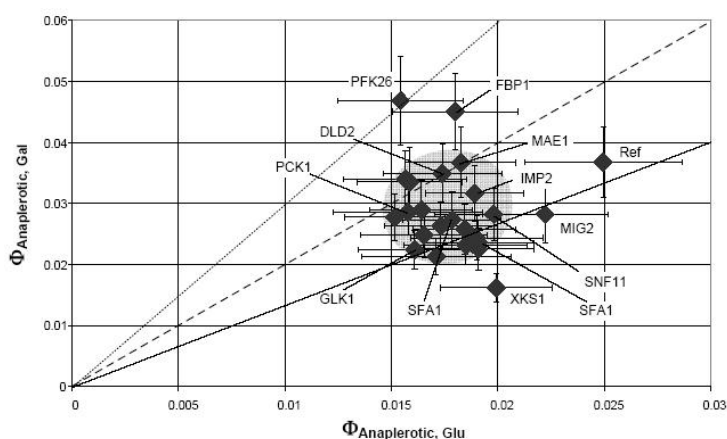


**Figure 5.3-4** Comparison of flux partitioning into the anaplerotic pathways,  $\Phi_{\text{Anaplerotic}}$ , in galactose and glucose cultures. Error bars indicate 90 % confidence regions. The full straight line indicates identical values on glucose and galactose, the dashed one double  $\Phi_{\text{Anaplerotic}}$  on galactose compared to glucose, and dotted line triple values.

### 5.3.4 Comparative flux analysis on glucose and galactose

The available metabolic flux profiling data on glucose and galactose for the examined strains were utilised to make a comparative metabolic flux profiling analysis. The following interesting and metabolically significant results were obtained.

#### 5.3.4.1 *MAE1* is important for NADPH supply on galactose

Significant differences were seen in the lower part of figure 5.3-3 where the flux partitioning ratio,  $\Phi_{\text{PPP}}$ , was plotted versus specific growth rate. Again cultivation on glucose was clearly separated from cultivation on galactose for most strains with higher values for growth on galactose. The most significant outlier here is *mae1Δ* strain. *MAE1* codes for the mitochondrial malic enzyme, which is known to have a preference to NADPH (Boles et al., 1998).

The effect of deletion of *MAE1* is even clearer when plotting  $\Phi_{\text{PPP,gal}}$  versus  $\Phi_{\text{PPP,Glu}}$  (Figure 5.3-2). A significant group of strains, representing the majority of the selected strains showed  $\Phi_{\text{PPP,gal}}$  values between 0.2 and 0.4, a few below and only *mae1Δ* showed a value above 0.4. This high upregulation of the PPP activity can be explained by modifications in the NADPH supply. During growth of the wild type and other strains, part of NADPH is likely produced via *Mae1p* and deletion of *MAE1* redirects NADPH formation to the PPP. During growth on glucose no clear phenotype could be observed similar to the findings of Boles et al. (1998).

Obviously, sufficient NADPH is supplied during highly fermentative growth and correspondingly lower biomass yield by reactions other than catalyzed by Mae1p. No significant difference was observed when comparing the net anaplerotic flux split on glucose,  $\Phi_{\text{Anaplerotic,Glu}}$ , with that on galactose,  $\Phi_{\text{Anaplerotic,Gal}}$ , (Figure 5.3-4) again agreeing with earlier observations of no clear phenotype (Boles et al., 1998). This metabolic split ratio only considers net fluxes. The plot of the biomass yield on glucose,  $Y_{X/S}$ , versus  $\Phi_{\text{PPP}}$  does not show any clear difference of the *mae1Δ* strain compared to the others during growth on glucose (Figure 5.3-1). On the other hand *mae1Δ* has by far the highest value of  $\Phi_{\text{PPP}}$  on galactose but only high value of  $Y_{X/S}$ . Earlier a clear phenotype of this enzyme was only found during growth on ethanol when *PYK1* and *MAE1* were both deleted (Boles et al., 1998). Either of the corresponding proteins Pyk1p or Mae1p is required and permits biosynthesis of amino acids of the pyruvate family. Disruption of *MAE1* alone, however, did not show a clear phenotype during growth on ethanol. Mae1p was not directly related to the supply of NADPH in that study.

#### 5.3.4.2 *xks1Δ* and *snf11Δ* are fastest growing on glucose

The two strains *xks1Δ* and *snf11Δ* exhibited the highest growth rates on glucose and also very high glucose consumption rates.

- ***xks1Δ***: Xks1p is xylulokinase (Rodriguez-Pena et al., 1998) and is therefore important for pentose metabolism, particularly for fermentation of D-xylose and D-xylulose (Toivari et al., 2001; van Maris et al., 2006). Deletion of *XKSI* also resulted in the strain with the highest galactose consumption rate.  $\Phi_{\text{PPP}}$  was in an average range growing on glucose and galactose (Figures 5.3-3 and 5.3-2). However,  $\Phi_{\text{Anaplerotic,Gal}}$  was exceptionally low in this strain (Figure 5.3-4). Biomass yield on galactose was lowest observed in this set of mutants (Figure 5.3-1). Specific ethanol production was also very high both on glucose and galactose (Tables 5.3-1 and 5.3-2). It is hard to imagine that Xks1p would be catalytically active in the other strains since the phosphorylation of D-xylulose is an exergonic reaction consuming ATP. The yield of ethanol on glucose is not higher than with several other strains (Vela-gapudi et al., 2006). It might be that Xks1p has unknown enzymatic activities producing a compound limiting the growth rate.
- ***snf11Δ***: Snf11p is part of the SWI/SNF complex, which is a very large, 2000-KDa protein complex that appears to be highly conserved in all eukaryotes. In yeast it is composed of 11 different polypeptide subunits, and it is required *in vivo* for the transcriptional induction

of a subset of yeast genes and for the functioning of a variety of sequence-specific transcriptional activators. Conde et al. (2003) found affects in mannosylphosphorylation of cell wall mannoproteins in *snf11Δ* strains when screening the strain from the same library as here. *SNF11* deletion did only influence maximal specific growth rate on glucose. No other significant effect could be observed.

#### 5.3.4.3 *pfk26Δ* shows highest biomass yield

The deletion of *PFK26* that is involved in the regulation of carbohydrate metabolism gave the highest biomass yield on galactose with a high  $\Phi_{\text{PPP,Gal}}$  and on glucose a low growth rate and the highest  $\Phi_{\text{PPP,Glu}}$  but no increase in yield. Pfk26p produces fructose 2,6-bisphosphate that usually stimulates phosphofructokinase-1 and inhibits fructose 1,6-bisphosphatase. Muller et al. (1997) demonstrated that Pfk26p is not needed in *S. cerevisiae* to sustain an adequate glycolytic flux under fermentative conditions, but rather is concerned with the homeostasis of metabolite concentrations. No physiological significance found for inhibition of fructose 1,6-bisphosphatase by Pfk26p (Muller et al., 1997).

#### 5.3.4.4 *fbp1Δ* had different growth rates on glucose and galactose

Fbp1p, fructose 1,6-bisphosphatase, is essential for growth on ethanol when gluconeogenesis is required. It seems, therefore, unnecessary during growth on glucose or galactose, and it is even degraded in the proteasome when readily degradable sugars as glucose are available for the cells (Hammerle et al., 1998). In this study, showing quantitative physiological data going beyond published work, a lower growth rate on glucose and a higher one on galactose (Figure 5.3-3) and a higher biomass yield on galactose were observed (Figure 5.3-1).  $\Phi_{\text{PPP,Glu}}$  is relatively high but close to the majority of mutants (Figure 5.3-2). The increase in yield on galactose is certainly not caused by an increased PPP activity.

#### 5.3.4.5 Other strains exhibiting significant differences

There are several other strains that are exhibiting interesting and significant metabolic flux profiles on glucose and galactose.

- ***glk1Δ* strain:** Deletion of glucokinase, *GLK1*, converting glucose to glucose 6-phosphate does not show a very clear phenotype. It is however remarkable that  $\Phi_{\text{PPP}}$  and  $\Phi_{\text{Anaplerotic}}$  were the same on both sugars. The glucose uptake and ethanol production rates

were about half on galactose compared to glucose (Tables 5.3-1 and 5.3-2). In *Penicillium chrysogenum* the deletion of *GLK1* resulted in stimulation of beta-galactosidase and penicillin biosynthesis (Barredo et al., 1988).

- ***mig2Δ* strain:** *MIG2* together with *MIG1* is involved in glucose repression (Westergaard et al., 2007). Disruption of *MIG2* resulted in similar behaviour of yeast on both sugars concerning most growth parameters. Only  $\Phi_{\text{PPP,Gal}}$  was about 1.5 fold higher than  $\Phi_{\text{PPP,Glu}}$  both exhibiting relatively low values. Much clearer effects would be expected when feeding mixed substrates.
- ***pck1Δ* strain:** Pck1p, an ATP dependent phosphoenolpyruvate carboxykinase is important for gluconeogenesis (Valdes-Hevia et al., 1989) and possibly for cyclic fluxes between the PEP/pyruvate and oxaloacetate/malate pools that are frequently observed in many organisms. Its deletion does not show a very drastic phenotype. The very low  $\Phi_{\text{PPP,Glu}}$  might point to a possible activation of Mae1p for the generation of NADPH. However, the determined specific malic enzyme activity, referred to total protein was very similar,  $9.68 \pm 0.13$  nmol/min/mg protein for the reference strain and  $9.38 \pm 0.17$  nmol/min/mg protein for the *pck1Δ* mutant.
- ***sfa1Δ* strain:** Sfa1p is a long-chain alcohol dehydrogenase also capable of reducing formaldehyde (Wehner et al., 1993). In this study *sfa1Δ* was only exceptional having lower  $\Phi_{\text{PPP,Gal}}$  than  $\Phi_{\text{PPP,Glu}}$ , a characteristic it shares with *imp2'Δ*.
- ***dld1Δ* and *imp2'Δ* strains:** Deletion of *DLD1*, a D-lactate dehydrogenase, showed low  $\Phi_{\text{PPP,Glu}}$  but no other very significant differences. The deletion of *IMP2* resulted in the lowest  $\Phi_{\text{PPP,Gal}}$  value of all strains studied but biomass yield similar to other strains. Imp2'p is a sugar regulatory protein. Again it seems that the requirement of NADPH needed for anabolic purposes may be supplied by Mae1p.

### 5.3.5 Conclusions

New methods for an extended physiological characterization of yeast at a microtiter plate scale were applied to twenty-seven deletion mutants of *S. cerevisiae* cultivated on glucose and galactose as sole carbon sources. In this way specific growth rates, specific rates of glucose consumption and ethanol production were determined. Flux distribution, particularly concerning branching into the pentose phosphate pathway was determined using a new <sup>13</sup>C-labelling method using MALDI-ToF mass spectrometry showed some new phenotypes that

are useful for the elucidation of the function of the corresponding genes and other important flux distributions at branching points were determined using metabolic network model.

On glucose the growth was predominantly fermentative whereas on galactose respiration was more active with correspondingly lower ethanol production. Some deletion strains showed unexpected behaviour providing very informative data about the function of the corresponding gene. Deletion of *MAE1* did not show any significant phenotype when grown on glucose but a drastically increased branching from glucose 6-phosphate into the pentose phosphate pathway on galactose. This allows the conclusion that Mae1p is important for the supply of NADPH during aerobic growth on galactose. In *pfk1Δ* the pentose phosphate pathway flux decreased significantly pointing to a replacement of Pfk1p catalyzed gluconeogenic flux by Mae1p activity.

## 5.4 STOICHIOMETRIC AND METABOLIC FLUX SCREENING OF *S. CEREVISIAE* HEXOSE TRANSPORTER (HXTS) SINGLE KNOCKOUT STRAINS ON GLUCOSE AND GALACTOSE

Velagapudi, V.R., Heinzle, E., 2009. Physiological and metabolic flux profiling of *S. cerevisiae* hexose transporter deletion mutants (In preparation)

### 5.4.1 Background

The first step in the sugar metabolism is the transport of external sugar inside the cell. *S. cerevisiae* comprises a family encoding 20 different hexose transporter (HXTs) related proteins (Hxtp), which are involved in sugar transport and regulation. They represent a major facilitator superfamily (Reifenberger, 1997; Kruckeberg, 1996; Ciriacy and Reifenberger, 1997). The reason for having 20 genes for hexose transport (18 genes encoding transporters, *HXT1-HXT17* and *GAL2*; and two genes encoding sensors, *SNF3* and *RGT2*) may be due to constantly changing nutrient availability in the environment. Yeast is exposed to an extremely broad range of sugar concentrations under natural conditions. Yeast might have evolved to meet these environmental challenges by developing an unusual diversity of hexose transporter genes.

Hxtp transporters have been classified based on their affinities as low affinity transporters (Hxt1p and Hxt3p) with  $K_m$  values between 50 and 100 mM, moderately low affinity transporters (Hxt2p and Hxt4p) with  $K_m$  values of about 10 mM and high affinity transporters (Hxt6p and Hxt7p) with  $K_m$  values of 1-2 mM. Gal2p is a galactose transporter but also able to transport glucose with high affinity with the same  $K_m$  values as Hxt6p and Hxt7p but *GAL2* gene express only in the presence of galactose (Reifenberger, 1997; Platt et al., 1998). Only the *hxtA* null mutant (*hxt1-17A* disruption mutant), with the deletion of all the 17 *HXT* transporter genes and *GAL2* gene, is unable to grow on glucose or fructose or mannose and overexpression of any one of these genes, except *HXT12*, in the null mutant restores growth on one of these hexoses (Wieczorke, 1999). There have been studies related to kinetic characterization of individual transporters by expressing only one transporter in an *hxtA* null mutant (Reifenberger et al., 1997), transcriptional profiling of *HXT* genes at different oxygen concentrations (Rintala et al., 2008) or at different glucose concentrations (Klockow et al., 2008),

but quantitative physiological information is lacking in strains with missing single *HXT* genes. In order to address this issue, we have selected a set of available hexose transporter deletion strains from the mutant library (Table 5.4-1) and studied each deletion mutant strain on glucose and galactose and obtained quantitative stoichiometric and metabolic flux data using previously developed platforms (Velagapudi et al., 2006; Hollemeyer et al., 2007).

**Table 5.4-1** Information about the selected yeast deletion mutant strains

ORF	Gene name	Metabolic function	Activity
YHR094C	<i>HXT1</i>	Cellular sugar import	Low affinity transmembrane hexose transport activity
YDR345C	<i>HXT3</i>	Cellular sugar import	Low affinity transmembrane hexose transport activity
YHR092C	<i>HXT4</i>	Cellular sugar import	High affinity transmembrane hexose transport activity
YJL214W	<i>HXT8</i>	Cellular sugar import	Unknown
YFL011W	<i>HXT10</i>	Cellular sugar import	Unknown
YIL170W	<i>HXT12</i>	Unknown	Unknown
YNL318C	<i>HXT14</i>	Cellular sugar import	Transmembrane galactose transport activity
YNR072W	<i>HXT17</i>	Cellular sugar import	Unknown
YDL194W	<i>SNF3</i>	Sugar binding	High affinity glucose sensor
YDL138W	<i>RGT2</i>	Sugar binding	Low affinity glucose sensor
YKL038W	<i>RGT1</i>	Regulation of carbohydrate metabolism	Transcription factor activity
YLR081W	<i>GAL2</i>	Galactose metabolism	Galactose permease activity
YDR277C	<i>MTH1</i>	Regulation of carbohydrate metabolism	Repressor of hexose transport genes
YDR043C	<i>NRG1</i>	Regulation of carbohydrate metabolism	Transcriptional repressor activity
YBR066C	<i>NRG2</i>	Regulation of carbohydrate metabolism	Transcriptional repressor activity

## 5.4.2 Stoichiometric profiling of HXT knockout strains

A recently developed novel method for high-content stoichiometric and kinetic metabolic profiling was used to obtain quantitative information on physiological parameters i.e., specific growth rate, biomass yield, ethanol yield, specific substrate uptake rate and specific ethanol production rate, of selected HXTs deletion mutants on glucose and galactose substrates at miniaturized scale using 96-well microtiter plates with on-line optical sensing of dissolved oxygen (Velagapudi et al., 2006). The results are presented in the tables 5.4-2 and 5.4-3.

#### 5.4.2.1 Specific growth rate ( $\mu_{\max}$ )

Strains growing with specific growth rates of  $0.17 \text{ h}^{-1}$  to  $0.26 \text{ h}^{-1}$  were classified as slow growers and the rest of the strains with growth rates higher than  $0.26 \text{ h}^{-1}$  were classified as fast growers. Growth on galactose is clearly distinct from that on glucose. The specific growth rate of mutants on glucose was higher than on galactose. On glucose, mutants showed varied growth patterns with specific growth rates ranging from  $0.232 \text{ h}^{-1}$  to  $0.334 \text{ h}^{-1}$ , whilst on galactose, specific growth rates ranged from  $0.198 \text{ h}^{-1}$  to  $0.294 \text{ h}^{-1}$ . On glucose, 2 strains, *nrg1Δ* and *nrg2Δ*, were slow growers with maximum specific growth rates,  $\mu_{\max}$ , of  $0.232 \text{ h}^{-1}$  and  $0.237 \text{ h}^{-1}$ , respectively, and the rest of the 14 strains were fast growers. On galactose, 11 strains were slow growers having maximum specific growth rates,  $\mu_{\max}$ , less than  $0.26 \text{ h}^{-1}$  and only 4 strains are fast growers. As expected, the strain with deletion of *GAL2*, a galactose transporter with galactose permease activity, did not grow on galactose at all.

#### 5.4.2.2 Specific hexose uptake rate ( $q_{\text{hexose}}$ )

Substrate consumption rates of transporter mutants were always higher on glucose than on galactose. On glucose, specific consumption rates,  $q_{\text{glucose}}$ , are ranging from  $12 \text{ mmol/g/h}$  –  $27 \text{ mmol/g/h}$ , whereas on galactose, specific consumption rates,  $q_{\text{galactose}}$ , are ranging from  $3 \text{ mmol/g/h}$  -  $10 \text{ mmol/g/h}$ . A single mutant, *hxt8Δ*, consumed glucose at a very high rate of  $26.6 \text{ mmol/g/h}$ , whereas on galactose, *hxt8Δ* had  $q_{\text{galactose}}$  of  $7.6 \text{ mmol/g/h}$ . One strain, *hxt4Δ*, had highest galactose consumption rate of  $9.5 \text{ mmol/g/h}$ , which is still less than the minimum consumption rate on glucose and the same strain, *hxt4Δ* had  $q_{\text{glucose}}$  of  $23.3 \text{ mmol/g/h}$  on glucose.

#### 5.4.2.3 Specific ethanol production rate ( $q_{\text{ethanol}}$ )

Specific ethanol production rate,  $q_{\text{ethanol}}$ , on glucose ranges from  $14 \text{ mmol/g/h}$  -  $42 \text{ mmol/g/h}$ . Except *hxt8Δ* strain, all other high rate glucose consumers with  $q_{\text{glucose}}$  above  $20 \text{ mmol/g/h}$ , had specific ethanol production rates,  $q_{\text{ethanol}}$ , between  $20$  and  $40 \text{ mmol/g/h}$ . Two strains, *hxt3Δ* and *snf3Δ* with  $q_{\text{glucose}}$   $16.4 \text{ mmol/g/h}$  and  $18.8 \text{ mmol/g/h}$ , respectively, had  $q_{\text{ethanol}}$  above  $20 \text{ mmol/g/h}$  (*hxt3Δ* -  $22.5 \text{ mmol/g/h}$  and *snf3Δ* -  $32.4 \text{ mmol/g/h}$ ). The deletion strain *hxt8Δ*, which had the maximum glucose consumption rate,  $26.6 \text{ mmol/g/h}$  had a  $q_{\text{ethanol}}$  of only  $17.8 \text{ mmol/g/h}$ . Maximum  $q_{\text{ethanol}}$  value was observed for *hxt4Δ* strain -  $41.2 \text{ mmol/g/h}$ . On galactose, specific ethanol production rates,  $q_{\text{ethanol}}$ , were ranging from  $2$  -  $13 \text{ mmol/g/h}$ . Maximum  $q_{\text{ethanol}}$  value was observed for *rgt1Δ* strain -  $12.5 \text{ mmol/g/h}$ .

**Table 5.4-2** Growth data on glucose. Specific growth rate,  $\mu_{\text{Glu}}$ , biomass yield,  $Y_{\text{X/S,Glu}}$ , ethanol yield,  $Y_{\text{E/S,Glu}}$ , specific uptake rate,  $q_{\text{Glu}}$ , specific rate of ethanol production,  $q_{\text{ETH}}$ . The last line shows the average values of all strains and standard deviation between them.

Gene	$\mu_{\text{Glu}}$ $\text{h}^{-1}$	$Y_{\text{X/S,Glu}}$ $\text{g g}^{-1}$	$Y_{\text{E/S,Glu}}$ $\text{g g}^{-1}$	$q_{\text{glucose}}$ $\text{mmol g}^{-1} \text{h}^{-1}$	$q_{\text{ethanol}}$ $\text{mmol g}^{-1} \text{h}^{-1}$
<i>Reference</i>	0.320 ± 0.014	0.128 ± 0.009	0.336 ± 0.018	13.9	18.2
<i>HXT1</i>	0.304 ± 0.047	0.080 ± 0.003	0.313 ± 0.005	21.1	25.8
<i>HXT3</i>	0.305 ± 0.035	0.103 ± 0.002	0.350 ± 0.054	16.4	22.5
<i>HXT4</i>	0.319 ± 0.040	0.076 ± 0.006	0.451 ± 0.031	23.4	41.2
<i>HXT8</i>	0.334 ± 0.051	0.070 ± 0.004	0.171 ± 0.020	26.6	17.8
<i>HXT10</i>	0.295 ± 0.047	0.082 ± 0.002	0.353 ± 0.010	20.1	27.8
<i>HXT12</i>	0.329 ± 0.043	0.076 ± 0.002	0.343 ± 0.016	24.2	32.4
<i>HXT14</i>	0.330 ± 0.035	0.121 ± 0.021	0.426 ± 0.064	15.1	25.2
<i>HXT17</i>	0.272 ± 0.058	0.061 ± 0.003	0.394 ± 0.014	24.9	38.3
<i>SNF3</i>	0.301 ± 0.035	0.089 ± 0.003	0.439 ± 0.013	18.9	32.5
<i>RGT2</i>	0.292 ± 0.052	0.129 ± 0.007	0.304 ± 0.026	12.6	15.0
<i>RGT1</i>	0.293 ± 0.037	0.070 ± 0.002	0.272 ± 0.016	23.2	29.4
<i>GAL2</i>	0.285 ± 0.043	0.089 ± 0.003	0.214 ± 0.010	17.9	14.9
<i>MTH1</i>	0.274 ± 0.039	0.083 ± 0.003	0.204 ± 0.010	18.2	14.6
<i>NRG1</i>	0.232 ± 0.014	0.098 ± 0.013	0.245 ± 0.012	13.1	15.2
<i>NRG2</i>	0.237 ± 0.016	0.087 ± 0.007	0.251 ± 0.031	15.1	17.5
Average	0.295 ± 0.038	0.090 ± 0.006	0.317 ± 0.022	19.0	24.3

**Table 5.4-3** Growth data on galactose. Specific growth rate,  $\mu_{\text{Gal}}$ , biomass yield,  $Y_{\text{X/S,Gal}}$ , ethanol yield,  $Y_{\text{E/S,Gal}}$ , specific uptake rate,  $q_{\text{Gal}}$ , specific rate of ethanol production,  $q_{\text{ETH}}$ . The last line shows the average values of all strains and standard deviations.

Gene	$\mu_{\text{Gal}}$ $\text{h}^{-1}$	$Y_{\text{X/S,Gal}}$ $\text{g g}^{-1}$	$Y_{\text{E/S,Gal}}$ $\text{g g}^{-1}$	$q_{\text{gal}}$ $\text{mmol g}^{-1} \text{h}^{-1}$	$q_{\text{ethanol}}$ $\text{mmol g}^{-1} \text{h}^{-1}$
<i>Reference</i>	0.223 ± 0.012	0.190 ± 0.014	0.325 ± 0.019	6.5	8.3
<i>HXT1</i>	0.236 ± 0.017	0.265 ± 0.018	0.141 ± 0.025	4.9	2.7
<i>HXT3</i>	0.203 ± 0.009	0.340 ± 0.032	0.249 ± 0.018	3.3	3.2
<i>HXT4</i>	0.261 ± 0.031	0.152 ± 0.002	0.207 ± 0.012	9.5	7.7
<i>HXT8</i>	0.264 ± 0.030	0.193 ± 0.018	0.342 ± 0.012	7.6	10.2
<i>HXT10</i>	0.247 ± 0.022	0.172 ± 0.002	0.217 ± 0.003	7.9	6.8
<i>HXT12</i>	0.198 ± 0.009	0.219 ± 0.005	0.369 ± 0.020	5.0	7.21
<i>HXT14</i>	0.255 ± 0.021	0.371 ± 0.014	0.273 ± 0.007	3.8	4.1
<i>HXT17</i>	0.262 ± 0.025	0.208 ± 0.006	0.322 ± 0.010	7.0	8.8
<i>SNF3</i>	0.253 ± 0.022	0.211 ± 0.004	0.207 ± 0.009	6.6	5.4
<i>RGT2</i>	0.235 ± 0.015	0.162 ± 0.001	0.259 ± 0.007	8.1	8.2
<i>RGT1</i>	0.258 ± 0.018	0.171 ± 0.001	0.382 ± 0.009	8.4	12.5
<i>GAL2</i>					
<i>MTH1</i>	0.230 ± 0.021	0.232 ± 0.014	0.306 ± 0.015	5.5	6.6
<i>NRG1</i>	0.235 ± 0.017	0.311 ± 0.019	0.124 ± 0.036	4.2	2.0
<i>NRG2</i>	0.294 ± 0.024	0.258 ± 0.015	0.343 ± 0.069	6.3	8.5
Average	0.244 ± 0.020	0.231 ± 0.011	0.271 ± 0.018	6.3	6.8

### 5.4.2.4 Comparison of specific rates and yields of mutant set

Specific uptake rate of hexose,  $q_{\text{hexose}}$  and specific ethanol production rate,  $q_{\text{ethanol}}$ , were plotted versus the maximum specific growth rate of each mutant,  $\mu_{\text{max}}$  (Figure 5.4-1A). Increasing specific hexose consumption and ethanol production rates were observed with increasing specific growth rate. However, the increase of  $q_{\text{ethanol}}$  with  $\mu_{\text{max}}$  was higher on glucose than on galactose. On glucose, 7 strains consumed glucose at rates higher than 20  $\text{mmol g}^{-1} \text{h}^{-1}$ : *hxt10Δ* – 20.1; *hxt1Δ* – 21.1; *rgt1Δ* – 23.2; *hxt4Δ* – 23.3; *hxt12Δ* – 24.1; *hxt17Δ* – 24.8; *hxt8Δ* – 26.6  $\text{mmol g}^{-1} \text{h}^{-1}$ .

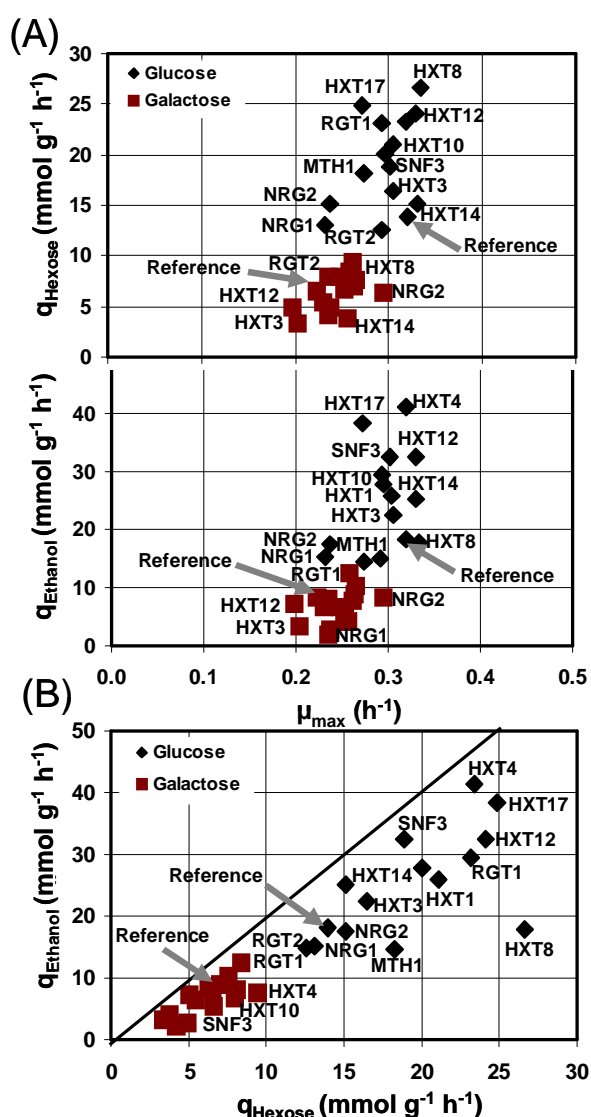


**Figure 5.4-1** (A) Specific hexose uptake rate and specific ethanol production rates as function of the specific growth rate,  $\mu_{\text{max}}$ , during growth on glucose and galactose (B) Specific rate of ethanol production as a function of the specific hexose consumption rate,  $q_{\text{Hexose}}$ , during growth on glucose and galactose (Tables 5.4-2 and 5.4-3). The solid line indicates the maximum theoretical  $q_{\text{ethanol}}$ . Arrows indicate the reference strain BY4742 *Mata his3Δ1 leu2Δ0 lys2Δ0 ura3Δ0*.

On glucose, reference strain had  $q_{\text{glucose}}$  of  $13.9 \text{ mmol g}^{-1} \text{ h}^{-1}$  and  $q_{\text{ethanol}}$  of  $18.2 \text{ mmol g}^{-1} \text{ h}^{-1}$ , values that are below the average values of all the other examined strains ( $q_{\text{glucose}} - 19.0 \text{ mmol g}^{-1} \text{ h}^{-1}$  and  $q_{\text{ethanol}} - 24.3 \text{ mmol g}^{-1} \text{ h}^{-1}$ ). In contrast, the specific uptake rate of galactose and specific ethanol production rate on galactose were very small compare to glucose and ranging from  $3 - 10 \text{ mmol g}^{-1} \text{ h}^{-1}$  and  $2 - 10 \text{ mmol g}^{-1} \text{ h}^{-1}$ , respectively. On galactose, the reference strain had  $q_{\text{galactose}}$  of  $6.5 \text{ mmol g}^{-1} \text{ h}^{-1}$  and  $q_{\text{ethanol}}$  of  $8.3 \text{ mmol g}^{-1} \text{ h}^{-1}$ , the values which are about average values of all the other examined strains ( $q_{\text{galactose}} - 6.3 \text{ mmol g}^{-1} \text{ h}^{-1}$  and  $q_{\text{ethanol}} - 6.8 \text{ mmol g}^{-1} \text{ h}^{-1}$ ).

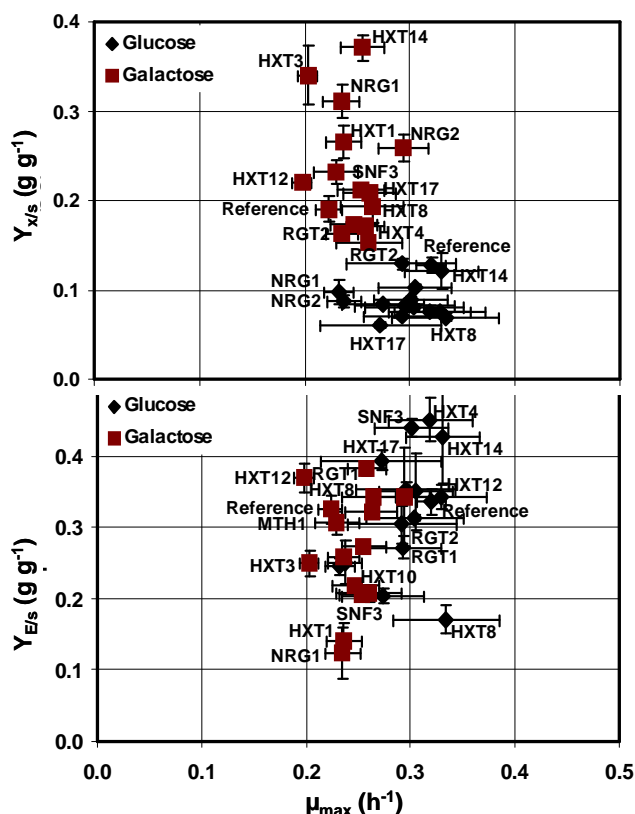
A clear trend was observed when specific uptake rate of hexose,  $q_{\text{hexose}}$ , was plotted against specific ethanol production rate,  $q_{\text{ethanol}}$ , of each mutant (Figure 5.4-1B). An increasing specific ethanol production rate was observed with increasing specific uptake rate both in glucose and galactose. On glucose, all high rate glucose consumers had values of  $q_{\text{Ethanol}}$  between 20 and  $40 \text{ mmol g}^{-1} \text{ h}^{-1}$  except *hxt8Δ*, the strain with maximum glucose consumption rate of  $26.6 \text{ mmol g}^{-1} \text{ h}^{-1}$  had  $q_{\text{Ethanol}}$  of only  $17.8 \text{ mmol g}^{-1} \text{ h}^{-1}$ , which is very close to the reference strain (Figure 5.4-1B). One strain, *rgt1Δ* with high specific uptake rate of galactose ( $8.4 \text{ mmol g}^{-1} \text{ h}^{-1}$ ), also had highest specific ethanol production rate,  $q_{\text{ethanol}}$  ( $12.5 \text{ mmol g}^{-1} \text{ h}^{-1}$ ).

Figure 5.4-2 represents the correlation between specific growth rate,  $\mu_{\text{max}}$ , and biomass yields,  $Y_{\text{X/S}}$ , as well as with ethanol yield,  $Y_{\text{E/S}}$  on glucose and galactose. The deletion mutants had much higher biomass yield on galactose ( $0.15 - 0.35 \text{ g/g}$ ) than on glucose ( $0.06 - 0.13 \text{ g/g}$ ). One strain, *hxt14Δ*, had a very high biomass yield on both the sugars ( $0.121 \text{ g/g}$  on glucose and  $0.371 \text{ g/g}$  on galactose). The strains had higher ethanol yields on glucose ( $0.17 - 0.45 \text{ g/g}$ ) than on galactose ( $0.12 - 0.39 \text{ g/g}$ ). This represents that the strains showed higher respiratory activity on galactose and fermentative activity on glucose.

#### 5.4.2.5 Comparison of growth and yields with the reference strain

The maximum specific growth rate,  $\mu_{\text{max}}$  on glucose of the reference strain was identical with *hxt1Δ*, *hxt3Δ*, *hxt4Δ*, *hxt8Δ*, *hxt10Δ*, *hxt12Δ*, *hxt14Δ*, *hxt17Δ*, *snf3Δ*, *rgt2Δ*, *rgt1Δ*, *gal2Δ*, *grr1Δ*, *mth1Δ*; on galactose with *hxt1Δ*, *hxt3Δ*, *hxt4Δ*, *hxt8Δ*, *hxt10Δ*, *hxt14Δ*, *snf3Δ*, *rgt2Δ*, *nrg1Δ*, *grr1Δ*, *mth1Δ*. Therefore, for *hxt1Δ*, *hxt3Δ*, *hxt4Δ*, *hxt8Δ*, *hxt10Δ*, *hxt14Δ*, *snf3Δ*, *rgt2Δ*, *grr1Δ* and *mth1Δ* strains,  $\mu_{\text{max}}$  was indistinguishable from the reference strain on glucose and on galactose. *hxt14Δ* and *rgt2Δ* strains had the same biomass yield as the reference

on glucose; *hxt8Δ* and *hxt17Δ* on galactose and therefore no strain had the same  $Y_{X/S}$  on both sugars. *hxt1Δ*, *hxt3Δ*, *hxt10Δ*, *hxt12Δ* and *rgt2Δ* showed the same ethanol yield on glucose,  $Y_{E/S}$ , as the reference strain, *hxt8Δ*, *hxt17Δ*, *grr1Δ*, *mth1Δ* and *nrg2Δ* on galactose and therefore no strain had the same  $Y_{E/S}$  on both sugars.



**Figure 5.4-2** Stoichiometric profiling of HXTs yeast deletion mutants. Correlation between specific growth rate,  $\mu_{\max}$ , and biomass yields,  $Y_{X/S}$ , as well as with ethanol yield,  $Y_{E/S}$ , on glucose and galactose.

#### 5.4.2.6 Comparison of mutants against mutants

All the examined 14 mutants were compared against each other in all six dimensions i.e., three parameters on each carbon source and searched for the indistinguishable strain combinations from the total of 91 possible unique binary combinations on glucose and galactose. Depending on the parameter investigated and on the substrate the discrimination between strains varied (Table 5.4-4). The discrimination of mutants against mutants was stronger on galactose than on glucose. Experiments on galactose alone would only lead to one indistinguishable mutant pair, *hxt8Δ* – *hxt17Δ*. On glucose alone, 2 indistinguishable pairs were detected: *hxt3Δ* – *hxt14Δ* and *nrg1Δ* – *nrg2Δ*. None of the mutant pairs was common in all the biological parameters on both the sugars.

**Table 5.4-4** Strains not distinguishable based on maximum specific growth rate,  $\mu_{\max}$ , biomass yield on carbon substrate,  $Y_{X/S}$ , ethanol yield on carbon substrate,  $Y_{E/S}$ , and growth on glucose and/or galactose as limiting substrate.

Carbon source	$\mu_{\max}$	$Y_{X/S}$	$Y_{E/S}$	all
Glucose	74	25	19	2
Galactose	63	11	17	1
Glucose and galactose	51	4	5	0

### 5.4.2.7 Hierarchical clustering

Hierarchical clustering was done using stoichiometric data of glucose and galactose separately using Euclidian distance as a distance metric. The relative Euclidian distances were calculated between mutant pairs and also between mutant and the reference strain. The number of biological parameters is in total six, three on glucose and three on galactose. Seven deletion mutant pairs, *hxt4Δ* – *snf3Δ* (0.033); *hxt10Δ* – *snf3Δ* (0.044); *hxt1Δ* – *nrg1Δ* (0.062); *hxt4Δ* – *hxt10Δ* (0.068); *hxt8Δ* – *hxt17Δ* (0.073); *hxt14Δ* – *rgt2Δ* (0.097) on galactose; and *nrg1Δ* – *nrg2Δ* (0.126) on glucose were most closely related to each other. The measured Euclidean distances were visualised as dendrograms. Dendrogram of glucose and galactose data revealed 4 clusters on each substrate, highlighted with colours in Figure 5.4-3.

On glucose, in the first cluster (bottom to top), *snf3Δ* and *hxt4Δ* were clustered together. Details of protein interactions and complexes using MIPS MPact Protein Interactions and Complex DB (Guldener et al., 2006) ([www.mips.gsf.de/genre/proj/impact](http://www.mips.gsf.de/genre/proj/impact)) revealed that *snf3Δ* has genetic interaction with *hxt4Δ* (Ko et al., 1993). In the second cluster, low affinity transporters *hxt1Δ* and *hxt3Δ* and transporters with limited known function *hxt10Δ* and pseudogene *hxt12Δ* were clustered together. *hxt8Δ* strain is only distantly related to all other strains.

On galactose, members of the first cluster (bottom to top) comprise transporters with limited known function, *hxt8Δ*, *hxt12Δ* and *hxt17Δ*. In the second cluster, hexose sensors, *rgt2Δ* and *snf3Δ* were grouped. Protein-protein interaction studies revealed that *snf3Δ* has direct genetic interactions with *rgt2Δ* (Yang and Bisson, 1996); low affinity transporters *hxt1Δ* and *hxt3Δ* were clustered together. On glucose, *hxt8Δ* strain is distantly related to all other strains whereas on galactose *hxt8Δ* is closely related to *hxt17Δ*.

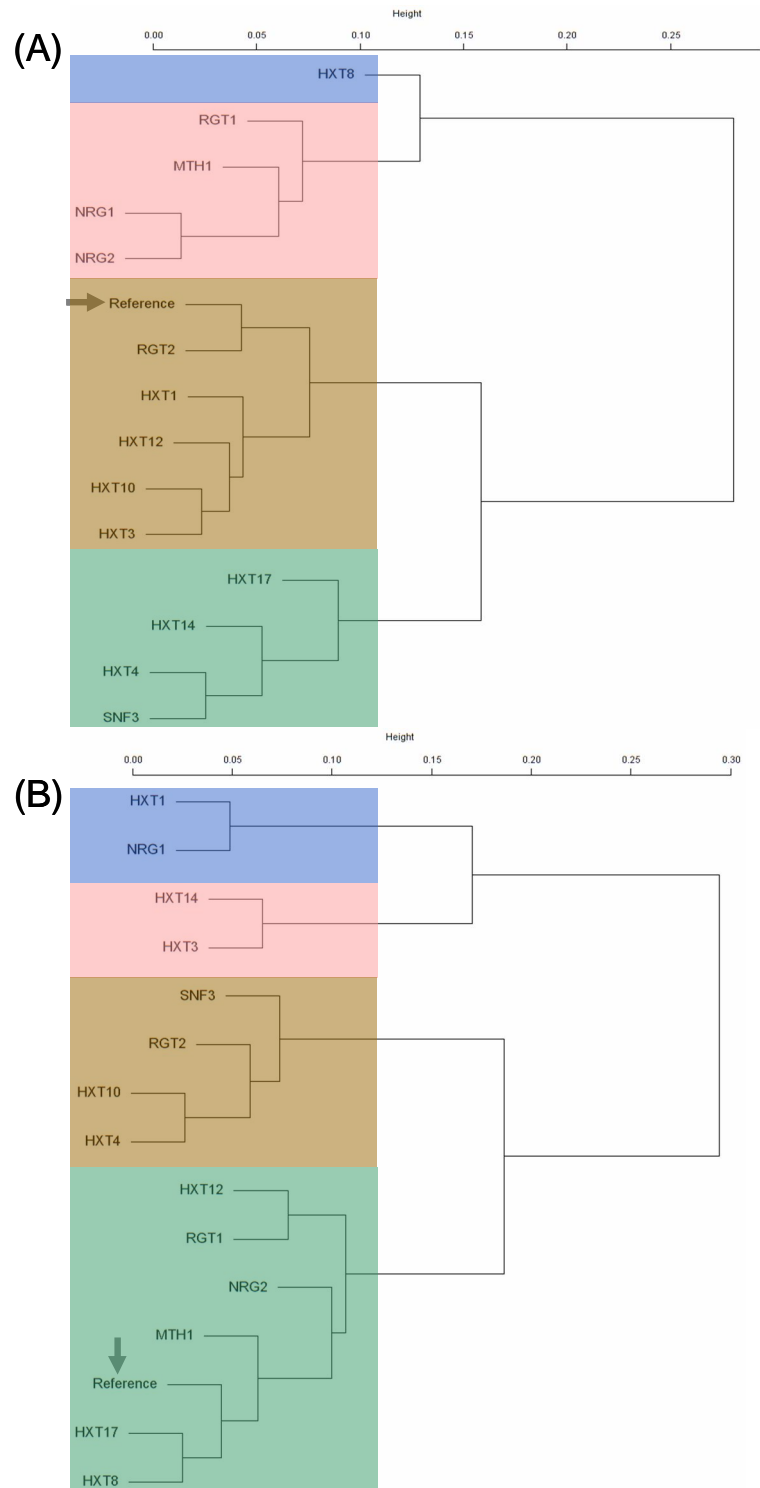


**Figure 5.4-3** Dendrograms on (A) glucose and (B) galactose. Hierarchical clustering was done using stoichiometric data by using Euclidean distances as a metric. Arrows indicate the reference strain BY4742 *Mat $\alpha$  his3 $\Delta$ 1 leu2 $\Delta$ 0 lys2 $\Delta$ 0 ura3 $\Delta$ 0*.

### 5.4.3 Comparative physiological profiling of HXT mutants

Another interesting comparison relates physiological parameters on both sugars for each single mutant. The specific growth rate,  $\mu_{\max}$ , was indistinguishable on both the sugars for *hxt4Δ*, *hxt8Δ*, *hxt10Δ*, *hxt17Δ*, *snf3Δ*, *rgt2Δ*, *rgt1Δ*, and *mth1Δ* and *nrg1Δ* mutant strains. One strain, *nrg2Δ*, grew slower on glucose ( $0.237 \text{ h}^{-1}$ ) than on galactose ( $0.294 \text{ h}^{-1}$ ). None of the mutants had similar biomass yield on glucose and galactose. Ethanol yield,  $Y_{E/S}$ , was identical on both the sugars for *hxt12Δ* and *nrg2Δ*. Interestingly, five mutant strains, *hxt8Δ*, *hxt12Δ*, *rgt1Δ*, *mth1Δ* and *nrg2Δ*, showed higher ethanol yields on galactose than on glucose.

#### 5.4.3.1 Hexose sensors: *rgt2Δ* and *snf3Δ*

On glucose, *rgt2Δ* strain grew slowly ( $\mu_{\max} = 0.292 \text{ h}^{-1}$ ) and had lowest specific glucose uptake rate ( $q_{\text{hexose}} = 12.6 \text{ mmol g}^{-1} \text{ h}^{-1}$ ) and specific ethanol production rate ( $q_{\text{ethanol}} = 14.9 \text{ mmol g}^{-1} \text{ h}^{-1}$ ) as expected. This low affinity hexose sensor, Rgt2p, a glucose receptor that binds glucose outside the cell and is induced only at high glucose concentrations. In *rgt2Δ* strain, no signal can be generated inside the cell for induction of expression of *HXT* genes (Ozcan and Johnston, 1999). The high affinity hexose sensor, *snf3Δ* is induced only at low concentration of sugar. Thus the deletion of *snf3Δ* didn't cause any physiological effect on glucose under the examined experimental conditions of high glucose concentrations. Since these hexose sensors are more specific to glucose and fructose, the deletion mutants didn't show any specific phenotype on galactose (Ozcan and Johnston, 1995).

#### 5.4.3.2 Low affinity transporters: *hxt1Δ*, *hxt3Δ* and *hxt4Δ*

Low affinity transporters *hxt1Δ* and *hxt3Δ* (share 80 % homology) and *hxt4Δ* are induced at high levels of glucose. Since the selected deletion mutants are single knockouts, deletion of one transporter can be compensated by another transporter and vice versa (Ko et al., 1993). Hence phenotype was not observed on glucose and the strains were close to the reference strain in all the biological parameters, especially *hxt3Δ* (Euclidean distance  $d$ : 0.288). Moreover, these strains are indistinguishable from each other in most of the biological parameters. *hxt1Δ* and *hxt3Δ* are quite close to each other (Euclidean distance  $d$ : 0.282), whereas *hxt4Δ* is far and equally distant from both *hxt1Δ* and *hxt3Δ* (Euclidean distance  $d$ : 0.435) in all the biological parameters. On glucose, *hxt1Δ* and *hxt3Δ* had similar maximum specific growth rate,  $\mu_{\max}$  (*hxt1Δ* –  $0.304 \text{ h}^{-1}$ ; *hxt3Δ* –  $0.305 \text{ h}^{-1}$ ), specific uptake rate,  $q_{\text{hexose}}$  (*hxt1Δ* –  $21.1$

mmol g<sup>-1</sup> h<sup>-1</sup>; *hxt3Δ* – 16.4 mmol g<sup>-1</sup> h<sup>-1</sup>) and specific ethanol production rate,  $q_{\text{ethanol}}$  (*hxt1Δ* – 25.8 mmol g<sup>-1</sup> h<sup>-1</sup>; *hxt3Δ* – 22.5 mmol g<sup>-1</sup> h<sup>-1</sup>).

### 5.4.3.3 HXTs with limited known functions

Except *HXT12*, which is a pseudo gene and not related to the hexose transporter family, the function of the hexose transporters Hxt8p-Hxt17p is still not known completely. *HXT8*-*HXT17* transcript levels were very low in glucose-limited chemostat cultivation (Diderich et al., 1999).

- ***hxt8Δ***: In a most recent global gene expression analysis study at different glucose concentrations, it has been shown that *HXT8* is active during starvation and at low glucose concentrations (Klockow et al., 2008). On glucose substrate, the *hxt8Δ* strain showed a clear phenotype with the highest specific growth rate ( $\mu_{\text{max}} = 0.334 \text{ h}^{-1}$ ), highest specific glucose consumption rate ( $q_{\text{hexose}} = 26.6 \text{ mmol g}^{-1} \text{ h}^{-1}$ ) but low specific ethanol production rate ( $q_{\text{ethanol}} = 17.8 \text{ mmol g}^{-1} \text{ h}^{-1}$ ) with only 0.171 g/g ethanol yield. This phenotype might suggest a possible role of Hxt8p on glucose fermentation capacity. *hxt8Δ* strain had the maximum Euclidean distance ( $d$ , Eq 4-36) from the reference strain among all the other strains,  $d = 0.829$ . In order to obtain first insight on the function of this unknown transporter activity, *hxt8Δ* strain was compared with all the other strains in all the biological parameters and the Euclidean distances were calculated. On glucose, *hxt8Δ* strain was close to *meth1Δ* and *gal2Δ* strains with  $d = 0.27$  and  $d = 0.3$ , respectively. On galactose, it showed no specific phenotype and was indistinguishable from the reference strain in all the parameters with Euclidean distance  $d = 0.181$ . When compared pair-wise against each mutant, the following mutants were close to the *hxt8Δ* strain; *hxt17Δ* ( $d = 0.073$ ), *nrg2Δ* ( $d = 0.124$ ), *rgt1Δ* ( $d = 0.148$ ) and *meth1Δ* ( $d = 0.192$ ). Thus, *meth1Δ* is closely related to the *hxt8Δ* strain on both the sugars with less distance on galactose than on glucose.
- ***hxt10Δ***: On glucose substrate, *hxt10Δ* strain was closely related to *hxt1Δ* ( $d = 0.131$ ) and *hxt12Δ* ( $d = 0.137$ ) in all the biological parameters. Whereas on galactose, *hxt10Δ* strain was closely related to *snf3Δ* ( $d = 0.044$ ) and *rgt2Δ* ( $d = 0.161$ ).
- ***hxt12Δ***: *HXT12*, a pseudogene, is not coding for a hexose transporter. *hxt12Δ* strain was close to *hxt1Δ* strain on glucose ( $d = 0.134$ ) and to *rgt1Δ* on galactose ( $d = 0.253$ ).

- ***hxt14Δ***: *hxt14Δ* strain had the highest biomass yield on both the sugars. The closest strain to *hxt14Δ* on glucose is *hxt3Δ* strain (d = 0.322). On galactose, *rgt2Δ* is the most closely related strain (d = 0.097) followed by *mth1Δ* (d = 0.159) and *hxt17Δ* (d = 0.181).
- ***hxt17Δ***: *hxt17Δ* strain had the lowest biomass yield on glucose and differs from the reference strain (d = 0.788). The closest strain to *hxt17Δ* on glucose is *hxt10Δ* (d = 0.278). On galactose, *mth1Δ* (d = 0.145) and *nrg2Δ* (d = 0.153) are closely related to *hxt17Δ* and are closely related to the reference strain (d = 0.162). An upregulation of *HXT17* promoter activity was observed on media containing galactose and raffinose at pH 7.7 versus pH 4.7 (Greatrix et al., 2006). *HXT17* promoter is a target for Mac1p transcription factor, which regulates high affinity copper uptake genes under copper deficient conditions (Gross et al., 2000; Jungmann et al., 1993).

#### 5.4.3.4 Regulators

- ***mth1Δ***: *MTH1* is also known as *HTR1*. It encodes a component of the glucose induction mechanism that regulates *HXT* gene expression. Mth1p is a negative regulator of the glucose-sensing signal transduction pathway (Schmidt et al., 1999). A mutation in *MTH1* causes defective transcription of probably all *HXT* genes. Thus deletion of *MTH1* causes impaired glucose transport and consequently grows poorly on glucose. As expected, *mth1Δ* deletion strain grew relatively slowly ( $\mu_{\max} = 0.274 \text{ h}^{-1}$ ) when compare to the rest of the studied mutant strains and had relatively low specific glucose consumption rate ( $q_{\text{hexose}} = 18.2 \text{ mmol g}^{-1} \text{ h}^{-1}$ ) and the lowest specific ethanol production rate ( $q_{\text{ethanol}} = 14.5 \text{ mmol g}^{-1} \text{ h}^{-1}$ ) on glucose. On galactose, *mth1Δ* showed no specific phenotype.
- ***nrg1Δ* and *nrg2Δ***: Nrg1p (Negative Regulator of Glucose-repressed genes) and Nrg2p are C<sub>2</sub>H<sub>2</sub> zinc finger proteins that function as transcriptional repressors, regulating glucose repressed genes (Park et al., 1999). These proteins interact with Snf1p (Sucrose Non-Fermenting) protein kinase complex, a key component of glucose signalling pathway and is essential for the transcription of many glucose-repressed genes (Celenza and Carlson, 1986; Vyas et al., 2001; Zhou et al., 2001). Though both the proteins have similar DNA binding domains (87 % identity), they differ in sequence outside the DNA binding domains (27 % identity). Thus they are differentially regulated and functionally distant in response to carbon source (Berkey et al., 2004). *nrg1Δ* and *nrg2Δ* showed substrate specific phenotypes.

Among the selected set of mutants, *nrg1Δ* and *nrg2Δ* were slow growers ( $\mu_{\max} = 0.232 \text{ h}^{-1}$  and  $\mu_{\max} = 0.237 \text{ h}^{-1}$ , respectively) and they showed similar phenotypic profile on glucose ( $q_{\text{hexose}} = 13.1 \text{ mmol g}^{-1} \text{ h}^{-1}$  and  $q_{\text{hexose}} = 15.0 \text{ mmol g}^{-1} \text{ h}^{-1}$ , respectively;  $q_{\text{ethanol}} = 15.1 \text{ mmol g}^{-1} \text{ h}^{-1}$  and  $q_{\text{ethanol}} = 17.5 \text{ mmol g}^{-1} \text{ h}^{-1}$ ). On galactose, *nrg1Δ* and *nrg2Δ* had very different phenotypic profile. The Euclidean distance between *nrg1Δ* and *nrg2Δ* is less on glucose ( $d = 0.126$ ) than on galactose ( $d = 0.834$ ) in all the biological parameters.

#### 5.4.4 Comparative metabolic flux profiling of HXT mutants

Metabolic fluxes were calculated based on mass balances. The fluxes given are relative values normalized to the corresponding specific hexose uptake rates.

##### 5.4.4.1 Glycolysis and Pentose Phosphate Pathway (PPP)

Generally the absolute flux through glycolysis is higher on glucose than on galactose, except for *hxt8Δ* and *hxt17Δ* mutant strains. Based on the  $\Phi_{\text{PPP}}$  values, mutants were classified into three groups. Strains having  $\Phi_{\text{PPP}}$  of 0.1 to 0.15 were classified as strains with low  $\Phi_{\text{PPP}}$ . On glucose, 8 strains had low  $\Phi_{\text{PPP}}$ , whereas on galactose none of the strains had low  $\Phi_{\text{PPP}}$ . Strains having  $\Phi_{\text{PPP}}$  of 0.15 to 0.25 were classified as strains with high  $\Phi_{\text{PPP}}$ . On glucose, 4 strains had high  $\Phi_{\text{PPP}}$  whereas on galactose, 12 strains had high  $\Phi_{\text{PPP}}$ . Strains with  $\Phi_{\text{PPP}}$  of 0.25 to 0.35 were classified as strains with very high  $\Phi_{\text{PPP}}$ . On glucose, 4 strains had very high  $\Phi_{\text{PPP}}$  whereas on galactose, 3 strains had very high  $\Phi_{\text{PPP}}$ . One strain *rgt1Δ* had an exceptionally high  $\Phi_{\text{PPP}}$  of 0.445 on galactose, whereas on glucose this strain *rgt1Δ* had a low  $\Phi_{\text{PPP}}$  of 0.126 (Figure 5.4-4).

A slight inverse correlation was observed between the maximum growth rate and  $\Phi_{\text{PPP}}$  on both the sugars. The correlation of  $\Phi_{\text{PPP}}$  between glucose and galactose showed that only 3 strains, *hxt3Δ*, *hxt1Δ* and *hxt10Δ* had comparable  $\Phi_{\text{PPP}}$  on both the sugars; and two strains, *hxt14Δ* and *nrg2Δ* had double  $\Phi_{\text{PPP}}$  values on galactose than on glucose (Figure 5.4-4).

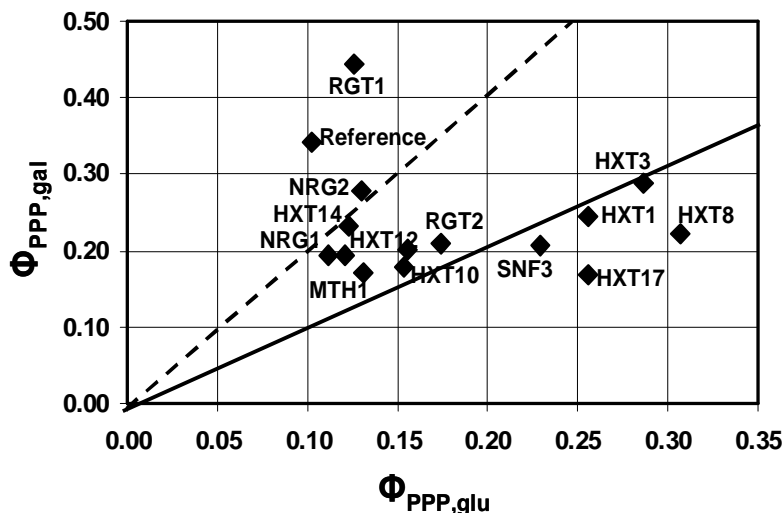


**Figure 5.4-4** Comparison of flux partitioning into the pentose phosphate pathway,  $\Phi_{PPP}$ , on galactose and glucose. The solid line indicates identical values on glucose and galactose and the dashed line indicates double  $\Phi_{PPP}$  values on galactose compared to glucose.

Absolute flux through PP pathway increased with increasing specific hexose uptake rate (Figure 5.4-5) as was also shown in Blank et al. (2005).

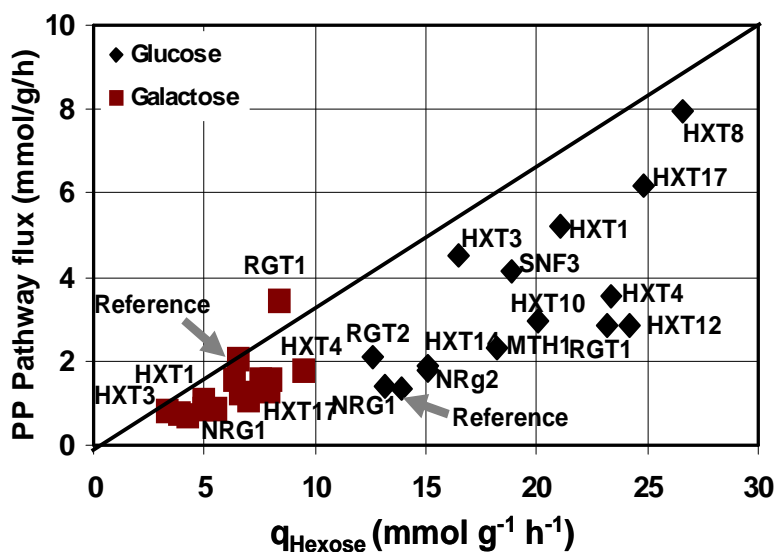


**Figure 5.4-5** Correlation between the specific hexose uptake rates,  $q_{Hexose}$  and flux partitioning into the pentose phosphate pathway in galactose and glucose cultures. Solid line represents  $\Phi_{PPP}$  of 33%. Arrows indicate the reference strain BY4742 *Mat $\alpha$  his3 $\Delta$ 1 leu2 $\Delta$ 0 lys2 $\Delta$ 0 ura3 $\Delta$ 0*.

The ratio between the biomass yields on galactose and glucose,  $Y_{X/S,gal}/Y_{X/S,glu}$ , and between the ethanol yields on galactose and glucose,  $Y_{E/S,gal}/Y_{E/S,glu}$ , were plotted against the ratio between the  $\Phi_{PPP}$  on galactose and glucose,  $\Phi_{PPP,gal}/\Phi_{PPP,glu}$  (Figure 5.4-6).

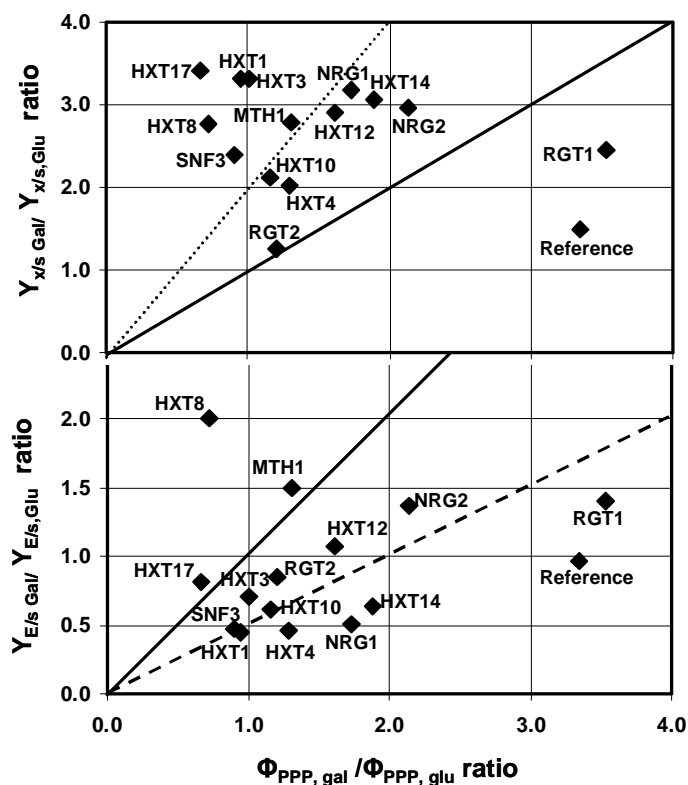


**Figure 5.4-6** Correlation between the ratio of  $\Phi_{PPP}$  on galactose and glucose,  $\Phi_{PPP,gal}/\Phi_{PPP,glu}$  and ratios of biomass yields on galactose and glucose,  $Y_{X/S,gal}/Y_{X/S,glu}$  (upper) and ethanol yields on galactose and glucose,  $Y_{E/S,gal}/Y_{E/S,glu}$  (lower). The solid line indicates identical values on both the axes, dotted line indicates the double the values of  $Y_{X/S,gal}/Y_{X/S,glu}$  and dashed line indicates half the values of  $Y_{E/S,gal}/Y_{E/S,glu}$  compared to,  $\Phi_{PPP,gal}/\Phi_{PPP,glu}$ .

One strain, *rgt2Δ* had similar  $\Phi_{PPP,gal}/\Phi_{PPP,glu}$  and  $Y_{X/S,gal}/Y_{X/S,glu}$  ratios i.e., this strain had 1.21 times higher  $\Phi_{PPP}$  value and 1.26 times higher  $Y_{X/S}$  on galactose than glucose. Two strains, *hxt10Δ* and *mth1Δ* had almost double the values of  $Y_{X/S,gal}/Y_{X/S,glu}$  ratios than  $\Phi_{PPP,gal}/\Phi_{PPP,glu}$  ratios i.e., they had 2-fold higher biomass yields,  $Y_{X/S}$  than their corresponding  $\Phi_{PPP}$  values on galactose than glucose. Two strains, *hxt3Δ* and *hxt1Δ*, which had almost identical  $\Phi_{PPP}$  values both on galactose and glucose ( $\Phi_{PPP,gal}/\Phi_{PPP,glu}$  values about 1) had about 3-fold higher biomass yields on galactose than glucose. The strain with highest  $\Phi_{PPP}$  value on galactose, *rgt1Δ*, had about 3.5-fold higher  $\Phi_{PPP}$  and about 2.5-fold higher biomass yield on galactose than on glucose. Reference strain, which had about 3.3-fold higher  $\Phi_{PPP}$  on galactose had about 1.5-

fold higher biomass yield on galactose than on glucose (Figure 5.4-6 upper part). Two strains, *hxt17Δ* and *mtl1Δ* had about similar  $\Phi_{\text{PPP,gal}}/\Phi_{\text{PPP,glu}}$  and  $Y_{\text{X/S,gal}}/Y_{\text{X/S,glu}}$  ratios (Figure 5.4-6 lower part). This means that biomass yield is not directly related to PPP activity in these mutants.

Two strains, *hxt1Δ* and *snf3Δ* which had almost identical  $\Phi_{\text{PPP}}$  values both on galactose and glucose ( $\Phi_{\text{PPP,gal}}/\Phi_{\text{PPP,glu}}$  values about 1) had about half the ethanol yield on galactose than glucose; one strain, *hxt3Δ* with  $\Phi_{\text{PPP,gal}}/\Phi_{\text{PPP,glu}}$  value equal to 1 had about 75% ethanol yield on galactose compared to glucose. *hxt10Δ* strain had half the values of  $Y_{\text{E/S,gal}}/Y_{\text{E/S,glu}}$  compared to,  $\Phi_{\text{PPP,gal}}/\Phi_{\text{PPP,glu}}$ . *hxt8Δ*, which had lower  $\Phi_{\text{PPP}}$  value on galactose, had 2-fold higher ethanol yields on galactose than glucose. *rgt1Δ* strain, which had about 3.5-fold higher  $\Phi_{\text{PPP}}$  had about 1.5-fold higher ethanol yield on galactose than on glucose. Reference strain, which had about 3.3-fold higher  $\Phi_{\text{PPP}}$  on galactose had almost identical ethanol yield values on both galactose and glucose sugars (Figure 5.4-6 lower part).

#### 5.4.4.2 TCA cycle and Fermentative pathway

On glucose, *hxt4Δ*, *hxt14Δ* and *snf3Δ* strains and on galactose, *hxt12Δ*, *rgt1Δ* and *nrg2Δ* had very low TCA cycle flux and also OAA originating from TCA cycle fluxes, which represents the non-cyclic operation of TCA cycle. These strains showed higher fermentative fluxes i.e., ethanol production on both the sugars. There was a very strong inverse correlation between the TCA cycle flux and fermentative pathway flux on both the sugars. However, the strains *hxt4Δ*, *hxt10Δ* and *snf3Δ* had similar TCA cycle and fermentative pathway fluxes on galactose (Figure 5.4-7).

The strains, *hxt8Δ* and *mtl1Δ* on glucose and *hxt1Δ*, *hxt4Δ* and *nrg1Δ* strains on galactose had very high TCA cycle flux. Interestingly, the strains *hxt4Δ* and *snf3Δ* had extremely low TCA cycle flux on glucose and extremely high TCA cycle flux on galactose. *rgt1Δ* and *nrg2Δ* strains had very low TCA cycle flux on galactose and very high TCA cycle flux on glucose. When compared to the reference strain, *hxt14Δ* strain had low TCA cycle flux on both the sugars and *hxt17Δ* strain had similar TCA cycle fluxes on both the sugars. TCA cycle flux is neither correlated to the maximum specific growth rate nor to the specific hexose uptake rate

on both the sugars and these observations are consistent with previous findings (Blank et al., 2004).

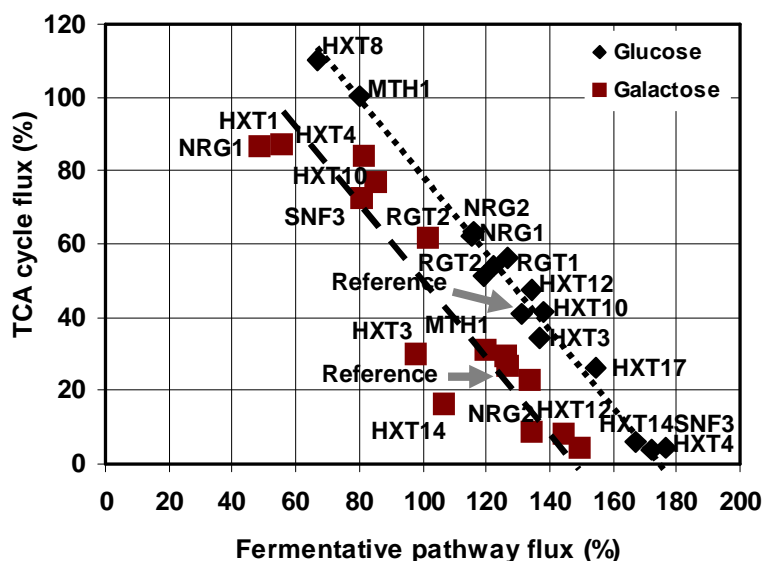


**Figure 5.4-7** Correlation between TCA cycle flux and fermentative pathway (ethanol production) flux on both the sugars. The dotted line represents a linear regression on glucose and the dashed line on galactose.

#### 5.4.4.3 Anaplerotic pathway

Pyruvate carboxylase mediates an anaplerotic reaction, replenishing the oxaloacetate (OAA) pool, which is used to produce many of the biosynthetic intermediates needed for anabolism. Strains having  $\Phi_{\text{anaplerotic}}$  of 0.005 to 0.015 were classified as strains with low  $\Phi_{\text{anaplerotic}}$ . On glucose, 12 strains were having low  $\Phi_{\text{anaplerotic}}$ , whereas none of the strains had low  $\Phi_{\text{anaplerotic}}$  on galactose. Strains having  $\Phi_{\text{anaplerotic}}$  of 0.015 to 0.025 were classified as strains with high  $\Phi_{\text{anaplerotic}}$ . On glucose, 4 strains were having high  $\Phi_{\text{anaplerotic}}$  whereas on galactose one strain had high  $\Phi_{\text{anaplerotic}}$ . Strains with  $\Phi_{\text{anaplerotic}}$  of 0.025 to 0.035 were classified as strains with very high  $\Phi_{\text{anaplerotic}}$ . On galactose, 5 strains had very high  $\Phi_{\text{anaplerotic}}$  whereas none of the strains had very high  $\Phi_{\text{anaplerotic}}$  on glucose. Eight strains had exceptionally high  $\Phi_{\text{anaplerotic}}$  on galactose; *snf3 $\Delta$*  (0.036), *hxt12 $\Delta$*  (0.038), *mth1 $\Delta$*  (0.04), *nrg2 $\Delta$*  (0.046), *hxt1 $\Delta$*  (0.047), *nrg1 $\Delta$*  (0.057), *hxt3 $\Delta$*  (0.065) and *hxt14 $\Delta$*  (0.071) (Figure 5.4-8).

The correlation of  $\Phi_{\text{anaplerotic}}$  between glucose and galactose showed that except *rgt2 $\Delta$*  and reference strains, none of the other strains had comparable  $\Phi_{\text{anaplerotic}}$  on both the sugars.

Most of the strains had three times higher  $\Phi_{\text{anaplerotic}}$  values on galactose than on glucose. *hxt14Δ*, *hxt3Δ* and *nrg1Δ* strains had extremely high  $\Phi_{\text{anaplerotic}}$  values (Figure 5.4-8).

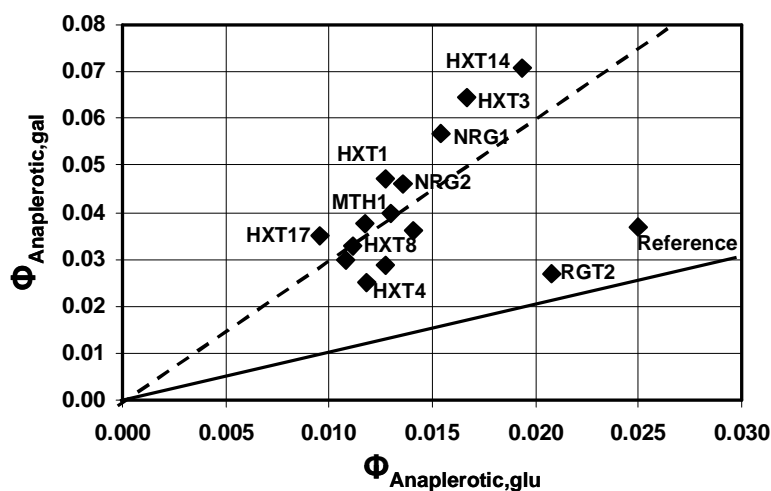


**Figure 5.4-8** Comparison of flux partitioning into the anaplerotic pathways,  $\Phi_{\text{Anaplerotic}}$ , in galactose and glucose cultures. The solid line indicates identical values on glucose and galactose and the dashed line indicates three times higher  $\Phi_{\text{Anaplerotic}}$  values on galactose compared to glucose.

The flux through anaplerotic pathway, which is normalised with the hexose uptake rate is correlated to the maximum specific growth rate on glucose, which is in agreement with the previous findings by Frick and Wittmann (2005) but no correlation was observed on galactose (Figure 5.4-9 A). A strong inverse correlation was observed between the flux through anaplerotic pathway and specific hexose uptake rate and specific ethanol production rate on both the sugars (Figure 5.4-9 B).

*hxt4Δ* strain had lower respiration than other strains on glucose, whereas on galactose it had highest respiratory flux. In contrast, *hxt8Δ* strain showed an opposite effect. Isogenic strains, *nrg1Δ* and *nrg2Δ* had identical fluxes on glucose whereas on galactose they exhibited different profiles. On galactose, *nrg2Δ* strain had higher PPP flux, biosynthesis from AKG in TCA cycle flux and fermentative capacity than *nrg1Δ*.

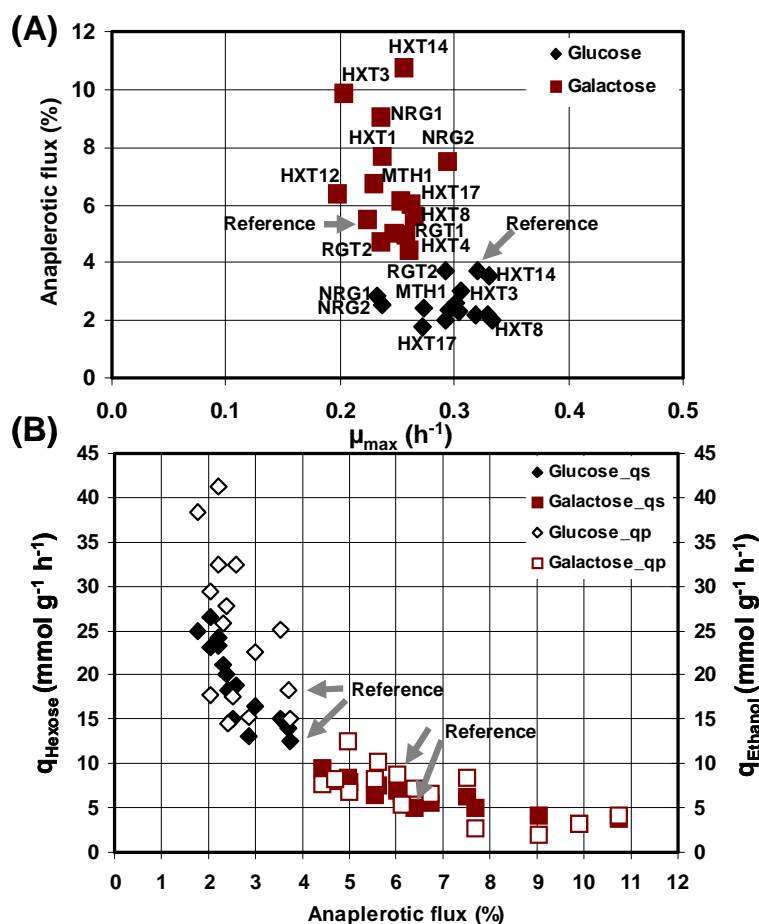


**Figure 5.4-9** Correlation between (A) specific growth rate,  $\mu$ , and flux partitioning into the anaplerotic pathway, which is normalised with the hexose uptake rate (B) flux partitioning into the anaplerotic pathway, which is normalised with the hexose uptake rate and specific hexose uptake rate,  $q_{\text{Hexose}}$ , and specific ethanol production rate  $q_{\text{Ethanol}}$ .

## 5.4.5 Conclusions

A set of hexose transporter deletion mutants were selected and quantitative stoichiometric and metabolic flux data on glucose and galactose as sole carbon sources was obtained using previously developed methodology (Velagapudi et al., 2006; Hollemeyer et al., 2007). Since these are single knockouts and complementary, these strains had no growth defects, except for *gal2Δ* on galactose. This type of quantitative stoichiometric and metabolic flux profiling revealed different phenotypic profiles on different carbon sources. Strains had mainly fermentative activity on glucose and respiratory and biosynthetic activity on galactose.

- On glucose, *hxt4Δ* strain had as low TCA fluxes as anaplerotic fluxes (2-3 %) with highest ethanol yield. On galactose, it had higher respiratory flux.

- On galactose, *rgt1Δ* strain had extremely high PPP flux.
- On glucose, *hxt8Δ* grew with highest specific growth rate and had highest specific glucose uptake rate with lowest ethanol yield. The strain had highest PPP and TCA cycle fluxes, i.e., the *hxt8Δ* strain is highly respiring, thus most of the carbon flux that was channelled to PPP and TCA cycle and released as CO<sub>2</sub>.
- The mutant strain *hxt14Δ* had similar anaplerotic and TCA fluxes on both the sugars.
- The mutant strain *hxt17Δ* had similar TCA and PPP fluxes as well as ethanol yields on both the sugars.

## 5.5 METABOLIC SCREENING OF *S. CEREVISIAE* SINGLE KNOCKOUT STRAINS ON FRUCTOSE SUGAR AND A COMPARATIVE STUDY ON DIFFERENT CARBON SOURCES

**Velagapudi, V.R.,** Heinzle, E., 2009. Comparative physiological profiling of *S. cerevisiae* single knockouts on different carbon sources – Fructose, Glucose and galactose (in preparation)

### 5.5.1 Background

Glucose and fructose are the most preferred carbon sources for *S. cerevisiae* and are metabolised primarily via the glycolytic pathway. Like other hexoses, fructose is also transported via a facilitated diffusion system mediated by hexose transporters. In *S. cerevisiae*, fructose is first converted to fructose 6-phosphate pathway (detailed description was given in section 3.3.3) that is part of glycolysis. *S. cerevisiae* is the preferred species of yeasts for wine-making. Both sugars are present in musts approximately in equal amounts. Since the affinity for glucose is higher than for fructose in *S. cerevisiae*, in the wine alcoholic fermentation process, glucose metabolises first leaving large quantities of fructose (approximately ten times compared to glucose) at the end. As a consequence, maximal rate of fermentation is reduced after most of the glucose is consumed, which leads to sluggish or stuck fermentation. Therefore, fructose consumption by wine-yeast is of great importance for maintenance of high rate of fermentation (Schutz et al., 1995). According to a previous study, it is possible to predict the sluggish or stuck fermentation based on the glucose/fructose ratio (GFR) (Gafner et al., 1996). Thus the studies on metabolic profiling on fructose substrate have significant importance in wine industries. Hence it is of great interest in the point of industrial biotechnology to study the physiological profiling of *S. cerevisiae* mutants with deletions in central carbon metabolism on fructose substrate. This kind of physiological analysis will provide an insight on quantitative metabolic profiling i.e., specific fructose uptake rate and specific ethanol production rate, specific growth rate and yields of mutants on fructose, which might help in identifying an industrially useful strain. In this chapter, about 50 mutant strains were selected (Table 5.5-1) and grown on fructose as a sole carbon source as described in previous chapters. In the first step, all the physiological parameters were calculated on fructose and then compared with the glucose and galactose data, which were described in previous chapters.

## Results and discussion

**Table 5.5-1** Information about the selected yeast deletion mutant strains

<b>ORF</b>	<b>Gene name</b>	<b>Metabolic function</b>	<b>Activity</b>
YML054C	<i>CYB2</i>	Lactate metabolic process	L-lactate dehydrogenase activity
YML051W	<i>GAL80</i>	Positive regulation of transcription by galactose	Specific transcriptional repressor activity
YMR205C	<i>PFK2</i>	Glycolysis	6-phosphofructokinase activity
YMR250W	<i>GAD1</i>	Response to oxidative stress	Glutamate decarboxylase activity
YMR280C	<i>CAT8</i>	Positive regulation of gluconeogenesis	Specific RNA pol II transcription factor activity
YNL257C	<i>SIP3</i>	Transcription initiation from pol II promoter	Transcription cofactor activity
YOR344C	<i>TYE7</i>	Transcription	Transcription factor activity
YPL248C	<i>GAL4</i>	Positive regulation of transcription by galactose	DNA-dependent transcriptional activator activity
YBR184W	<i>YBR184W</i>	Unknown	Unknown
YDR073W	<i>SNF11</i>	Chromatin modelling	RNA pol II transcription factor activity
YGR194C	<i>XKS1</i>	Xylulose catabolism	Xylulokinase activity
YCL040W	<i>GLK1</i>	Glycolysis	Glucokinase activity
YLR131C	<i>ACE2</i>	Transcription during G1 mitotic cell cycle	Transcription factor activity
YKL029C	<i>MAE1</i>	Pyruvate metabolism	Malate dehydrogenase (oxaloacetate decarboxylating) activity
YKL062W	<i>MSN4</i>	Response to stress	Transcription factor activity
YJL155C	<i>FBP26</i>	Gluconeogenesis	Fructose-2,6-bisphosphate 2-phosphatase activity
YDR216W	<i>ADR1</i>	Transcription	Transcription factor activity
YGL209W	<i>MIG2</i>	Regulation of transcription from Pol II promoter	RNA pol II transcription factor activity
YGL253W	<i>HXK2</i>	Carbohydrate metabolic process	Hexokinase activity
YGR019W	<i>UGA1</i>	Gamma-aminobutyric acid catabolic process	4-aminobutyrate transaminase activity
YDR248C	<i>YDR248C</i>	Unknown	Unknown
YKR097W	<i>PCK1</i>	Gluconeogenesis	Phosphoenolpyruvate carboxykinase (ATP) activity
YJR153W	<i>PGU1</i>	Pectin catabolic process	Polygalacturonase activity
YBR297W	<i>MAL33</i>	Regulation of transcription	DNA-dependent transcription factor activity
YCR036W	<i>RBK1</i>	Ribose metabolic process	Ribokinase activity
YDL168W	<i>SFA1</i>	Formaldehyde assimilation	Formaldehyde dehydrogenase (glutathione) activity
YDL174C	<i>DLD2</i>	Aerobic respiration	D-lactate dehydrogenase (cytochrome) activity
YBR006W	<i>UGA5</i>	Response to oxidative stress	Succinate-semialdehyde dehydrogenase (NAD(P)+) activity
YBR018C	<i>GAL7</i>	Galactose metabolism	UDP-hexose-1-phosphate uridylyltransferase activity
YBR019C	<i>GAL10</i>	Galactose metabolism	UDP-glucose-4-epimerase activity
YIL107C	<i>PFK26</i>	Fructose-2,6-bisphosphate metabolism	6-phosphofructo-2-kinase activity

## Results and discussion

YNL071W	<i>LAT1</i>	Pyruvate metabolism	Dihydrolipoyllysine-residue acetyltransferase activity
YNL104C	<i>LEU4</i>	Leucine biosynthesis	2-isopropylmalate synthase activity
YLR377C	<i>FBP1</i>	Gluconeogenesis	Fructose-bisphosphatase activity
YIL154C	<i>IMP2</i>	DNA repair	Transcription co-activator activity
YOR290C	<i>SNF2</i>	Chromatin remodelling	RNA pol II transcription factor activity
YHR094C	<i>HXT1</i>	Cellular sugar import	Low affinity transmembrane hexose transport activity
YDR345C	<i>HXT3</i>	Cellular sugar import	Low affinity transmembrane hexose transport activity
YHR092C	<i>HXT4</i>	Cellular sugar import	High affinity transmembrane hexose transport activity
YJL214W	<i>HXT8</i>	Cellular sugar import	Unknown
YFL011W	<i>HXT10</i>	Cellular sugar import	Unknown
YIL170W	<i>HXT12</i>	Unknown	Unknown
YNL318C	<i>HXT14</i>	Cellular sugar import	Transmembrane galactose transport activity
YNR072W	<i>HXT17</i>	Cellular sugar import	Unknown
YDL194W	<i>SNF3</i>	Sugar binding	High affinity glucose sensor
YDL138W	<i>RGT2</i>	Sugar binding	Low affinity glucose sensor
YKL038W	<i>RGT1</i>	Regulation of carbohydrate metabolism	Transcription factor activity
YLR081W	<i>GAL2</i>	Galactose metabolism	Galactose permease activity
YDR277C	<i>MTH1</i>	Regulation of carbohydrate metabolism	Repressor of hexose transport genes
YDR043C	<i>NRG1</i>	Regulation of carbohydrate metabolism	Transcriptional repressor activity
YBR066C	<i>NRG2</i>	Regulation of carbohydrate metabolism	Transcriptional repressor activity

**Sources:** *Saccharomyces* genome deletion project.

SGD ([http://www.sequence.stanford.edu/group/yeast\\_deletion\\_project/references.html](http://www.sequence.stanford.edu/group/yeast_deletion_project/references.html)),

MIPS (<http://mips.gsf.de/genre/proj/yeast/>)

SGD (<http://www.yeastgenome.org/>) databases

## 5.5.2 Physiological profiling of mutants on fructose

Recently developed novel method for high-content stoichiometric and kinetic metabolic profiling was used to obtain quantitative information of physiological parameters i.e., specific growth rate, biomass yield, ethanol yield, specific substrate uptake rate, specific ethanol production rate and specific oxygen uptake rate of selected deletion mutants on fructose substrate as sole carbon source at miniaturized scale using 96-well microtiter plates with on-line optical sensing of dissolved oxygen (Velagapudi et al., 2006).

### 5.5.2.1 Specific growth rate ( $\mu_{\max}$ )

On fructose carbon source, deletion mutants were growing in a varying range of specific growth rates,  $\mu_{\max}$ , ranging from 0.238 h<sup>-1</sup> to 0.438 h<sup>-1</sup>. Strains with  $\mu_{\max}$  less than 0.26 h<sup>-1</sup> are classified as “slow growers”,  $\mu_{\max}$  from 0.26 h<sup>-1</sup> to 0.4 h<sup>-1</sup> are classified as “fast growers” and  $\mu_{\max}$  above 0.4 h<sup>-1</sup> are classified as “very fast growers”. The reference strain had specific growth rate,  $\mu_{\max}$ , of 0.236 h<sup>-1</sup> and all other mutant strains were growing faster than the reference strain. According to the above classification, 3 strains, *hxt4Δ*, *ace2Δ* and *snf3Δ* were slow growers; 39 strains were fast growers and 12 strains were very fast growers.

### 5.5.2.2 Specific hexose uptake rate ( $q_{\text{hexose}}$ )

On fructose, deletion mutants had a very broad range of specific fructose consumption rates ( $q_{\text{fructose}}$ ) ranging from 12 mmol/g/h - 48 mmol/g/h. Most of the strains had  $q_{\text{fructose}}$  from 12 mmol/g/h - 25 mmol/g/h; 9 strains had high  $q_{\text{fructose}}$  from 25 mmol/g/h - 30 mmol/g/h; 4 strains had very high  $q_{\text{fructose}}$  from 30 mmol/g/h - 40 mmol/g/h; and one strain, *hxt14Δ* had extremely high  $q_{\text{fructose}}$  43.8 mmol/g/h, and one strain, *hxt17Δ* had exceptionally high  $q_{\text{fructose}}$  48 mmol/g/h. Specific uptake rate of fructose,  $q_{\text{fructose}}$ , is plotted versus the maximum specific growth rate of each mutant,  $\mu_{\max}$  (Figure 5.5-1A). In most of the strains, an increasing specific hexose consumption rate was observed with increasing specific growth rate. Interestingly, all the deletion strains with very high and exceptionally high fructose consumption rates are related to hexose transporter family and regulators (Figure 5.5-1A).

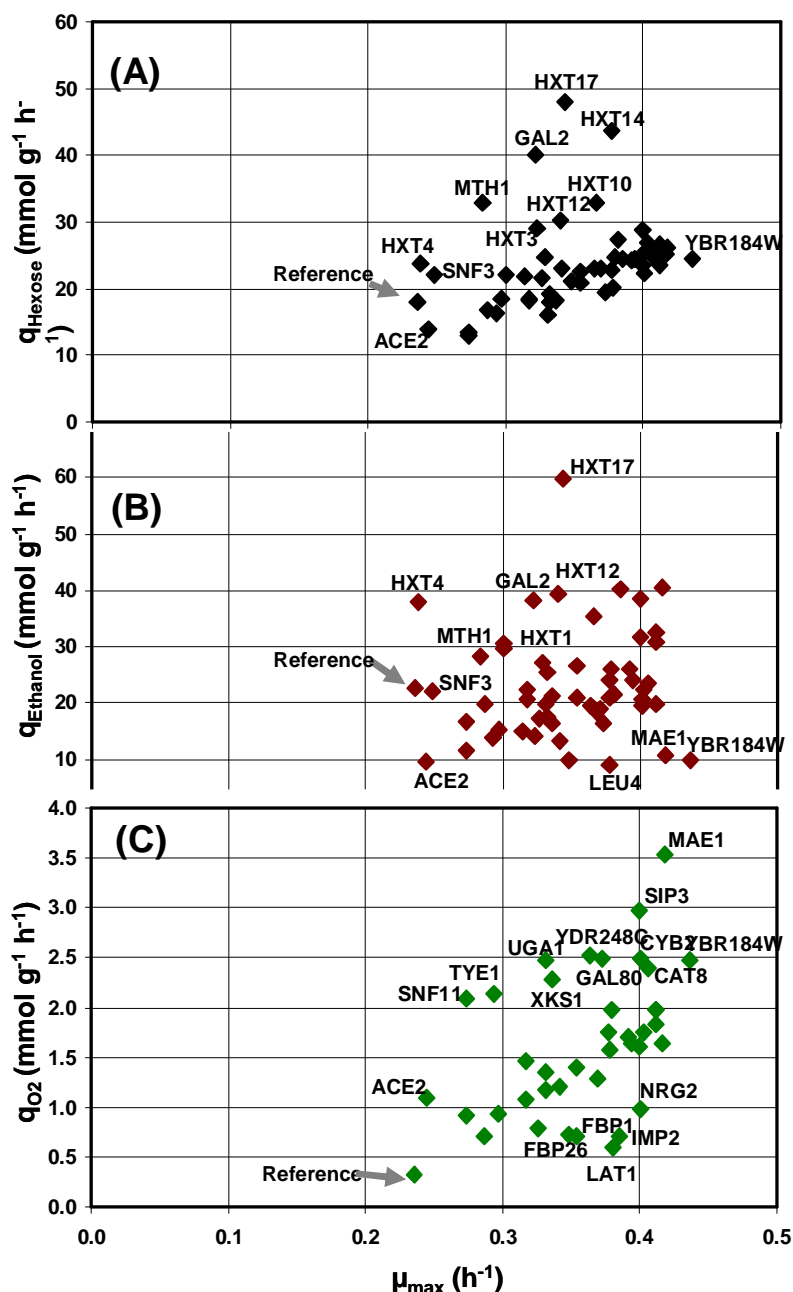


**Figure 5.5-1** (A) Specific fructose uptake rate,  $q_{\text{fructose}}$ , (B) specific ethanol production rate,  $q_{\text{ethanol}}$ , and (C) specific oxygen uptake rate,  $q_{\text{O}_2}$ , as function of the specific growth rate,  $\mu_{\max}$ . Arrows indicate the reference strain BY4742 *Mata his3 $\Delta$ 1 leu2 $\Delta$ 0 lys2 $\Delta$ 0 ura3 $\Delta$ 0*.

### 5.5.2.3 Specific ethanol production rate ( $q_{\text{ethanol}}$ )

Specific ethanol production rate,  $q_{\text{ethanol}}$ , on fructose ranges from 9 mmol/g/h - 60 mmol/g/h. Two strains had very high  $q_{\text{ethanol}}$  above 40 mmol/g/h (*imp2 $\Delta$*  – 40.2 mmol/g/h and *rgt1 $\Delta$*  – 40.5 mmol/g/h) and one strain, *hxt17 $\Delta$* , had exceptionally high  $q_{\text{ethanol}}$  of 59.8 mmol/g/h. An increasing  $q_{\text{ethanol}}$  was observed with increasing specific growth rate. (Figure 5.5-1B).

#### 5.5.2.4 Specific oxygen uptake rate ( $q_{O_2}$ )

Most of the high fructose consumers had low specific oxygen consumption rates,  $q_{O_2}$ , below 2 mmol/g/h. Ten strains had high  $q_{O_2}$  from 2 mmol/g/h - 3 mmol/g/h and these strains had low  $q_{ethanol}$  of less than 20 mmol/g/h. One strain, *mae1Δ*, had very high  $q_{O_2}$  of 3.53 mmol/g/h and had only 10.9 mmol/g/h of  $q_{ethanol}$ . Few almost respiratory deficient mutants with  $q_{O_2}$  less than 1 mmol/g/h were *snf2Δ*, *lat1Δ*, *fbp1Δ*, *fbp26Δ*, *imp2Δ*, *gal7Δ*, *hxx2Δ* and *glk1Δ*. An increasing  $q_{O_2}$  was observed with increasing specific growth rate (Figure 5.5-1C). The reference strain had the lowest oxygen uptake rate of 0.31 mmol/g/h.

#### 5.5.2.5 Comparison of specific rates and yields on fructose

When specific fructose consumption rate,  $q_{fructose}$  was plotted against specific ethanol production rates,  $q_{ethanol}$  (Figure 5.5-2A), most of the strains showed increasing  $q_{ethanol}$  with increasing  $q_{fructose}$ . Except *mae1Δ* and *hxt3Δ* strains, all other high rate fructose consumers with  $q_{fructose}$  above 25 mmol/g/h had specific ethanol production rates,  $q_{ethanol}$ , between 20 and 40 mmol/g/h (Figure 5.5-2A). Specific oxygen uptake rate,  $q_{O_2}$  was plotted against  $q_{fructose}$  (Figure 5.5-2B). *mae1Δ* had highest oxygen uptake rate of 3.53 mmol/g/h. *snf11Δ* with low  $q_{fructose}$  of 13.5 mmol/g/h had  $q_{O_2}$  above 2 mmol/g/h. The deletion strains, *imp2Δ*, *lat1Δ* and *nrg2Δ* with high  $q_{fructose}$  of about 25 mmol/g/h had low  $q_{O_2}$  of less than 1.0 mmol/g/h (Figure 5.5-2B). When  $q_{O_2}$  was plotted against  $q_{ethanol}$ , strains showed varied patterns (Figure 5.5-2C). For instance, the mutant strain *mae1Δ* with low  $q_{ethanol}$  of 10.8 mmol/g/h had maximum  $q_{O_2}$  of 3.5 mmol/g/h; similarly a couple of strains with low  $q_{ethanol}$  had high  $q_{O_2}$  above 2 mmol/g/h. The mutant strain *imp2Δ* with very high  $q_{ethanol}$  of 40.2 mmol/g/h had very low  $q_{O_2}$  of 0.7 mmol/g/h, similarly a couple of strains with high  $q_{ethanol}$  had  $q_{O_2}$  below 2 mmol/g/h. Surprisingly one strain *sip3Δ*, had high  $q_{ethanol}$  of 38.5 mmol/g/h as well as high  $q_{O_2}$  of 3 mmol/g/h.

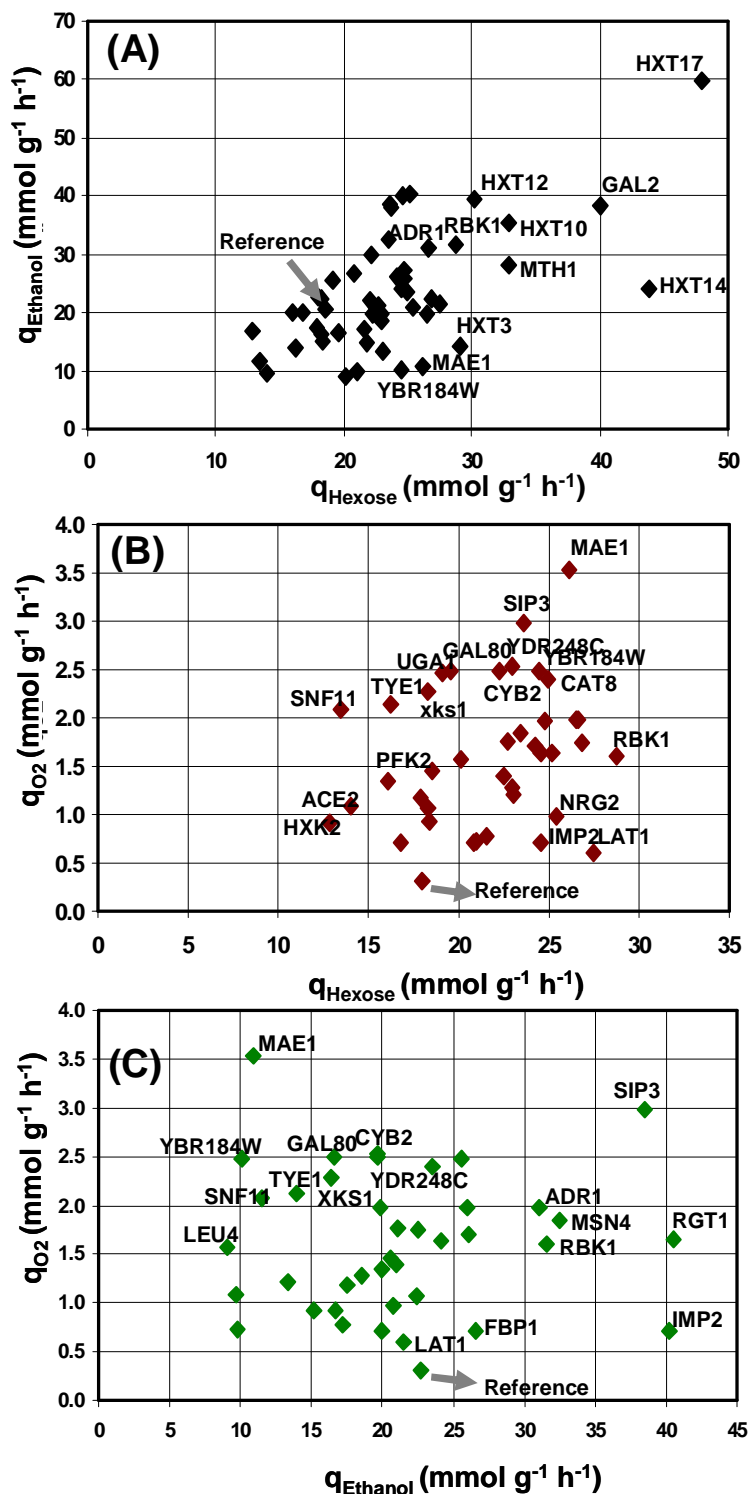


**Figure 5.5-2** (A) Specific rate of ethanol production,  $q_{\text{ethanol}}$ , and (B) specific oxygen uptake rate,  $q_{\text{O}_2}$ , as a function of the specific fructose consumption rate,  $q_{\text{fructose}}$  (C) Specific oxygen uptake rate,  $q_{\text{O}_2}$ , as a function of the specific rate of ethanol production,  $q_{\text{ethanol}}$ , Arrows indicate the reference strain BY4742 *Mat $\alpha$  his3 $\Delta$ 1 leu2 $\Delta$ 0 lys2 $\Delta$ 0 ura3 $\Delta$ 0*.

Figure 5.5-3 represents the correlation between specific growth rate,  $\mu_{\max}$ , and biomass yields,  $Y_{X/S}$ , ethanol yield,  $Y_{E/S}$  as well as with biomass yield on oxygen,  $Y_{X/O}$ . The results were given in the Table 5.5-2. Most of the deletion mutants had biomass yield from 0.06 to 0.12 g/g, few strains, *hxt17Δ*, *hxt4Δ*, *hxt14Δ* and *mth1Δ* had low  $Y_{X/S}$  ranging from 0.04 to 0.06 g/g. Two strains, *hxx2Δ* and *pfk2Δ*, had a very high biomass yield (0.118 and 0.115 g/g, respectively) (Figure 5.5-3A). Most of the strains had ethanol yields ranging from 0.20 – 0.35 g/g, some strains had low ethanol yields ranging from 0.10 – 0.2 g/g, and few strains, *hxt4*, *imp2Δ*, *sip3Δ* and *rgt1Δ* had higher ethanol yields above 0.40 g/g (Figure 5.5-3B). Most of the strains had biomass yield on oxygen,  $Y_{X/O}$ , ranging from 5 – 10 g/g, some strains had low  $Y_{X/O}$  ranging from 3 – 5 g/g, and some strains had higher  $Y_{X/O}$  ranging from 10 – 20 g/g, the reference strain had the highest  $Y_{X/O}$  of 23.5 g/g (Figure 5.5-3C).

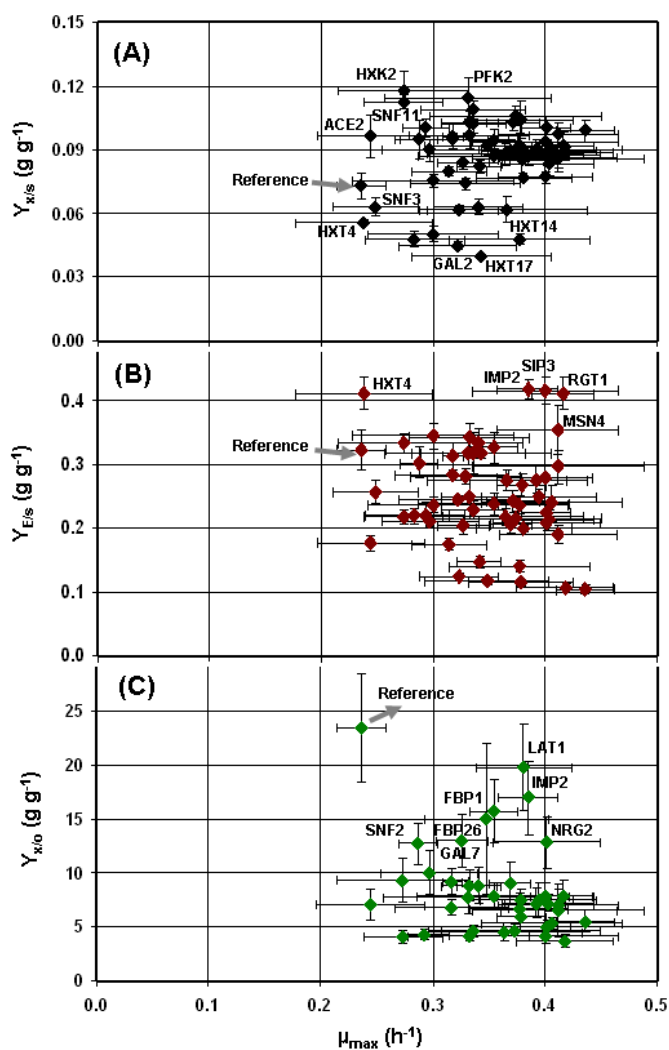


**Figure 5.5-3** Correlation between specific growth rate,  $\mu_{\max}$ , and biomass yield on fructose,  $Y_{X/S}$ , ethanol yield,  $Y_{E/S}$ , as well as with biomass yield on oxygen,  $Y_{X/O}$  (Table 5.5-2) Arrows indicate the reference strain BY4742 *Matα his3Δ1 leu2Δ0 lys2Δ0 ura3Δ0*.

**Table 5.5-2** Growth data on fructose. Specific growth rate,  $\mu_{\max}$ , biomass yield on fructose,  $Y_{X/S,\text{Fru}}$ , biomass yield on oxygen,  $Y_{X/O}$ , and ethanol yield,  $Y_{E/S,\text{Fru}}$ , with corresponding 90 % confidence intervals. (ND – Not Determined)

Gene name	$\mu_{\text{Fru}}$ $\text{h}^{-1}$	$Y_{X/S,\text{Fru}}$ $\text{g g}^{-1}$	$Y_{E/S,\text{Fru}}$ $\text{g g}^{-1}$	$Y_{X/O,\text{Fru}}$ $\text{g g}^{-1}$
<i>Reference</i>	0.236 ± 0.022	0.073 ± 0.007	0.323 ± 0.032	23.5 ± 5.0
<i>CYB2</i>	0.401 ± 0.022	0.100 ± 0.005	0.226 ± 0.012	5.0 ± 0.5
<i>GAL80</i>	0.373 ± 0.077	0.106 ± 0.005	0.217 ± 0.010	4.7 ± 0.5
<i>PFK2</i>	0.331 ± 0.075	0.115 ± 0.010	0.317 ± 0.016	7.7 ± 1.5
<i>GAD1</i>	0.317 ± 0.051	0.095 ± 0.003	0.284 ± 0.008	6.8 ± 0.7
<i>CAT8</i>	0.406 ± 0.063	0.090 ± 0.003	0.241 ± 0.028	5.3 ± 0.5
<i>SIP3</i>	0.400 ± 0.066	0.094 ± 0.006	0.416 ± 0.021	4.2 ± 0.8
<i>TYE7</i>	0.293 ± 0.021	0.100 ± 0.004	0.220 ± 0.020	4.3 ± 0.5
<i>GAL4</i>	0.369 ± 0.019	0.089 ± 0.006	0.206 ± 0.012	9.0 ± 2.0
<i>YBR184W</i>	0.436 ± 0.026	0.099 ± 0.005	0.105 ± 0.007	5.5 ± 1.0
<i>SNF11</i>	0.273 ± 0.035	0.113 ± 0.003	0.219 ± 0.012	4.1 ± 0.6
<i>XKS1</i>	0.336 ± 0.029	0.102 ± 0.004	0.229 ± 0.014	4.6 ± 0.5
<i>GLK1</i>	0.297 ± 0.043	0.090 ± 0.005	0.211 ± 0.010	10.0 ± 2.0
<i>ACE2</i>	0.244 ± 0.048	0.097 ± 0.010	0.176 ± 0.012	7.0 ± 1.4
<i>MAE1</i>	0.418 ± 0.043	0.089 ± 0.002	0.106 ± 0.007	3.7 ± 0.6
<i>MSN4</i>	0.412 ± 0.054	0.098 ± 0.006	0.354 ± 0.039	7.0 ± 1.5
<i>FBP26</i>	0.348 ± 0.056	0.092 ± 0.005	0.119 ± 0.006	15.0 ± 7.0
<i>ADR1</i>	0.412 ± 0.077	0.086 ± 0.006	0.298 ± 0.026	6.5 ± 1.0
<i>MIG2</i>	0.354 ± 0.068	0.087 ± 0.003	0.238 ± 0.018	7.9 ± 1.2
<i>HXK2</i>	0.273 ± 0.058	0.118 ± 0.009	0.333 ± 0.014	9.3 ± 2.0
<i>UGA1</i>	0.332 ± 0.054	0.097 ± 0.006	0.343 ± 0.021	4.2 ± 0.5
<i>YDR248C</i>	0.364 ± 0.070	0.088 ± 0.005	0.219 ± 0.013	4.5 ± 0.8
<i>PCK1</i>	0.412 ± 0.052	0.086 ± 0.005	0.191 ± 0.014	6.5 ± 2.4
<i>PGU1</i>	0.379 ± 0.022	0.085 ± 0.006	0.268 ± 0.018	6.0 ± 1.4
<i>MAL33</i>	0.332 ± 0.025	0.103 ± 0.005	0.250 ± 0.033	8.8 ± 1.4
<i>RBK1</i>	0.400 ± 0.043	0.077 ± 0.003	0.281 ± 0.038	7.8 ± 1.3
<i>SFA1</i>	0.394 ± 0.052	0.089 ± 0.004	0.251 ± 0.011	7.5 ± 1.5
<i>DLD2</i>	0.341 ± 0.020	0.082 ± 0.003	0.148 ± 0.009	8.8 ± 1.7
<i>UGA2</i>	0.377 ± 0.044	0.092 ± 0.006	0.237 ± 0.015	6.7 ± 1.4
<i>GAL7</i>	0.326 ± 0.023	0.084 ± 0.003	0.205 ± 0.014	13.0 ± 2.5
<i>GAL10</i>	0.317 ± 0.009	0.096 ± 0.006	0.313 ± 0.021	9.2 ± 1.2
<i>PFK26</i>	0.392 ± 0.027	0.090 ± 0.005	0.275 ± 0.022	7.2 ± 1.4
<i>LAT1</i>	0.381 ± 0.043	0.077 ± 0.001	0.200 ± 0.004	19.8 ± 4.0
<i>LEU4</i>	0.378 ± 0.047	0.104 ± 0.009	0.115 ± 0.006	7.5 ± 1.0
<i>FBP1</i>	0.354 ± 0.022	0.094 ± 0.006	0.326 ± 0.024	15.7 ± 3.0
<i>IMP2</i>	0.385 ± 0.027	0.087 ± 0.004	0.418 ± 0.016	17.0 ± 3.4
<i>SNF2</i>	0.287 ± 0.017	0.095 ± 0.009	0.303 ± 0.023	12.7 ± 2.0
<i>HXT1</i>	0.300 ± 0.072	0.075 ± 0.003	0.344 ± 0.019	ND
<i>HXT3</i>	0.323 ± 0.036	0.062 ± 0.001	0.124 ± 0.006	ND
<i>HXT4</i>	0.238 ± 0.060	0.056 ± 0.001	0.411 ± 0.025	ND
<i>HXT8</i>	0.314 ± 0.034	0.080 ± 0.002	0.175 ± 0.009	ND
<i>HXT10</i>	0.366 ± 0.072	0.062 ± 0.006	0.275 ± 0.015	ND
<i>HXT12</i>	0.340 ± 0.040	0.063 ± 0.004	0.334 ± 0.023	ND
<i>HXT14</i>	0.377 ± 0.063	0.048 ± 0.003	0.141 ± 0.010	ND
<i>HXT17</i>	0.343 ± 0.062	0.040 ± 0.001	0.318 ± 0.009	ND
<i>SNF3</i>	0.248 ± 0.038	0.063 ± 0.004	0.257 ± 0.018	ND
<i>RGT2</i>	0.329 ± 0.049	0.074 ± 0.003	0.282 ± 0.011	ND
<i>RGT1</i>	0.416 ± 0.028	0.092 ± 0.007	0.411 ± 0.024	7.9 ± 1.4
<i>GAL2</i>	0.322 ± 0.053	0.045 ± 0.002	0.244 ± 0.007	ND
<i>MTH1</i>	0.283 ± 0.044	0.048 ± 0.004	0.220 ± 0.012	ND
<i>NRG1</i>	0.403 ± 0.041	0.083 ± 0.006	0.214 ± 0.015	7.2 ± 0.8
<i>NRG2</i>	0.401 ± 0.048	0.088 ± 0.005	0.209 ± 0.011	12.8 ± 2.4

### 5.5.2.6 Comparison of mutants against mutants and with reference

All the examined mutants were compared against each other in all four dimensions i.e.,  $\mu_{\max}$ ,  $Y_{X/S}$ ,  $Y_{E/S}$  and  $Y_{X/O}$  and searched for the indistinguishable strain combinations and Table 5.5-3 reveals all the 38 indistinguishable strain combinations. The mutant strain *mig2 $\Delta$*  had maximum of 6 indistinguishable mutant pairs (*mig2 $\Delta$ -nrg1 $\Delta$* ; *mig2 $\Delta$ -uga2 $\Delta$* ; *mig2 $\Delta$ -pfk26 $\Delta$* ; *mig2 $\Delta$ -pgu1 $\Delta$* ; *mig2 $\Delta$ -sfa1 $\Delta$* ; *mig2 $\Delta$ -glk1 $\Delta$* ) followed by *adr1 $\Delta$*  with 5 (*adr1 $\Delta$ -gad1 $\Delta$* ; *adr1 $\Delta$ -pfk26 $\Delta$* ; *adr1 $\Delta$ -pgu1 $\Delta$* ; *adr1 $\Delta$ -rbk1 $\Delta$* ; *adr1 $\Delta$ -msn4 $\Delta$* ) and then followed by *pgu1 $\Delta$*  with 4 (*pgu1 $\Delta$ -pfk26 $\Delta$* ; *pgu1 $\Delta$ -rbk1 $\Delta$* ; *pgu1 $\Delta$ -sfa1 $\Delta$* ; *pgu1 $\Delta$ -uga2 $\Delta$* ) indistinguishable mutant pairs.

The reference strain was quite close to an average value with respect to  $Y_{X/S}$  and  $q_{\text{Ethanol}}$  whereas  $\mu_{\max}$  and  $Y_{E/S}$  were at the upper boundary and  $Y_{E/S}$  at the lower boundary of the observed values (Figures 5.5-1 and 5.5-3 and Table 5.5-2).  $\mu_{\max}$  of the reference strain was identical with *ace2 $\Delta$* , *glk1 $\Delta$* , *hxx2 $\Delta$* , *hxt1 $\Delta$* , *hxt4 $\Delta$* , *meth1 $\Delta$* , *pfk2 $\Delta$* , *snf11 $\Delta$*  and *snf3 $\Delta$* . The deletion strains *adr1 $\Delta$* , *dld2 $\Delta$* , *hxt1 $\Delta$* , *hxt10 $\Delta$* , *hxt12 $\Delta$* , *hxt8 $\Delta$* , *lat1 $\Delta$* , *nrg1 $\Delta$* , *pgu1 $\Delta$* , *rbk1 $\Delta$* , *rgt2 $\Delta$*  and *snf3 $\Delta$*  had the same biomass yield as reference strain. Mutant strains *adr1 $\Delta$* , *fbp1 $\Delta$* , *gad1 $\Delta$* , *gal10 $\Delta$* , *hxx2 $\Delta$* , *hxt1 $\Delta$* , *hxt2 $\Delta$* , *hxt12 $\Delta$* , *hxt17 $\Delta$* , *msn4 $\Delta$* , *pfk2 $\Delta$* , *pfk26 $\Delta$* , *rbk1 $\Delta$* , *rgt2 $\Delta$* , *snf2 $\Delta$*  and *uga1 $\Delta$*  showed the same ethanol yield as the reference strain. Knockout strains, *fbp1 $\Delta$* , *fbp26 $\Delta$* , *imp2 $\Delta$*  and *lat1 $\Delta$*  had the same biomass yield on oxygen as reference strain. Therefore, *hxt1 $\Delta$*  strain was indistinguishable from the reference strain in all the three examined biological parameters,  $\mu_{\max}$ ,  $Y_{X/S}$  and  $Y_{E/S}$  indicating that the deletion of *HXT1* gene wouldn't cause any specific phenotype when grown on fructose.

**Table 5.5-3** Strains not distinguishable based on specific growth rate,  $\mu_{\max}$ , biomass yield on carbon substrate,  $Y_{X/S}$ , ethanol yield,  $Y_{E/S}$ , and biomass yield on oxygen,  $Y_{X/O}$ 

Strain name							Number of mutant pair(s)
<i>adr1</i> $\Delta$	<i>gad1</i> $\Delta$	<i>pfk26</i> $\Delta$	<i>pgu1</i> $\Delta$	<i>rbk1</i> $\Delta$	<i>msn4</i> $\Delta$		5
<i>cat8</i> $\Delta$	<i>pgu1</i> $\Delta$	<i>uga2</i> $\Delta$	<i>ydr248c</i> $\Delta$				3
<i>cyb2</i> $\Delta$	<i>gal80</i> $\Delta$	<i>uga2</i> $\Delta$					2
<i>gad1</i> $\Delta$	<i>mal33</i> $\Delta$	<i>pfk26</i> $\Delta$					2
<i>gal4</i> $\Delta$	<i>nrg2</i> $\Delta$	<i>pck1</i> $\Delta$					2
<i>gal80</i> $\Delta$	<i>snf11</i> $\Delta$	<i>tye7</i> $\Delta$	<i>xks1</i> $\Delta$				3
<i>glk1</i> $\Delta$	<i>gal7</i> $\Delta$						2
<i>mig2</i> $\Delta$	<i>nrg1</i> $\Delta$	<i>uga2</i> $\Delta$	<i>pfk26</i> $\Delta$	<i>pgu1</i> $\Delta$	<i>sfa1</i> $\Delta$	<i>glk1</i> $\Delta$	6
<i>msn4</i> $\Delta$	<i>rgt1</i> $\Delta$						1
<i>pck1</i> $\Delta$	<i>nrg1</i> $\Delta$						1
<i>pfk2</i> $\Delta$	<i>hvk2</i> $\Delta$						1
<i>pgu1</i> $\Delta$	<i>pfk26</i> $\Delta$	<i>rbk1</i> $\Delta$	<i>sfa1</i> $\Delta$	<i>uga2</i> $\Delta$			4
<i>leu4</i> $\Delta$	<i>fbp26</i> $\Delta$	<i>ybr184w</i> $\Delta$					2
<i>tye7</i> $\Delta$	<i>xks1</i> $\Delta$						1
<i>uga2</i> $\Delta$	<i>nrg1</i> $\Delta$	<i>mal33</i> $\Delta$					2
<i>sfa1</i> $\Delta$	<i>uga2</i> $\Delta$	<i>pfk26</i> $\Delta$					2

### 5.5.3 Comparative physiological profiling of mutants – fructose data with glucose and galactose data

The deletion mutants grown on glucose and galactose (Velagapudi et al., 2006) and fructose were combined to study the comparative physiological profiling on these three carbon sources.

#### 5.5.3.1 Comparison of specific rates

Specific uptake rates  $q_{\text{Hexose}}$ , specific ethanol production rates,  $q_{\text{ethanol}}$  and specific oxygen uptake rates,  $q_{O_2}$  were plotted against specific growth rates,  $\mu_{\max}$ , of each mutant (Figure 5.5-5). Most of the mutants were growing faster than the reference strain on all the 3 carbon sources. Strains grown on galactose were growing slowly when compared to glucose and fructose. Some fructose grown strains were growing very fast when compared to the rest of the strains on other carbon sources. A clear trend of increasing  $q_{\text{Hexose}}$  was observed with increasing  $\mu_{\max}$  for all most all the mutants on all the three carbon sources. However, there are some outliers on fructose sugar with very high uptake rates and interestingly all of them are hexose transport deletion mutants (Figure 5.5-5A).

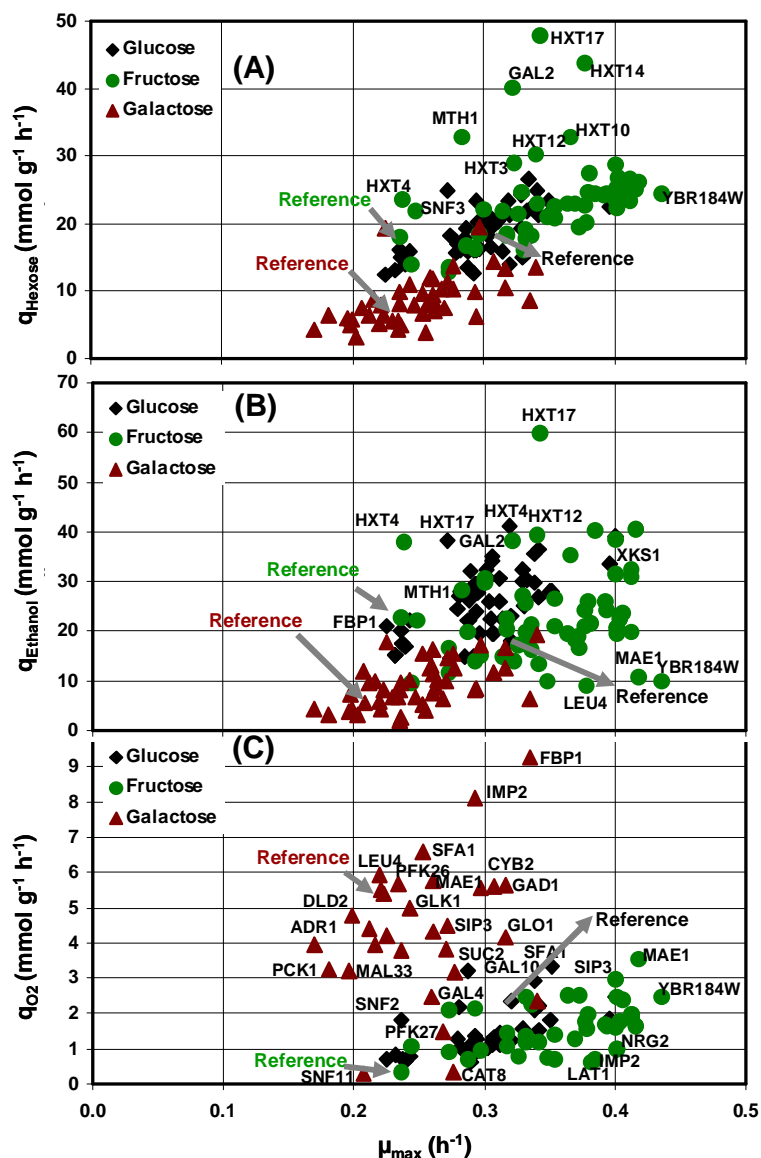


**Figure 5.5-5** Comparative stoichiometric profiling on glucose, galactose and fructose (A) Specific fructose uptake rate,  $q_{\text{hexose}}$ , (B) specific ethanol production rate,  $q_{\text{ethanol}}$ , and (C) specific oxygen uptake rate,  $q_{\text{O}_2}$ , as function of the specific growth rate,  $\mu_{\max}$ . Arrows indicate the reference strain BY4742 *Mata his3 $\Delta$ 1 leu2 $\Delta$ 0 lys2 $\Delta$ 0 ura3 $\Delta$ 0*.

Based on this observation, one could hypothesise a possible involvement of these hexose transporter genes in controlling fructose uptake rate. A general trend of increasing  $q_{\text{ethanol}}$  was observed with increasing  $\mu_{\max}$  for most of the strains on all the carbon sources. Strains grown on galactose had lower  $q_{\text{ethanol}}$ . Strains grown on glucose and some strains grown on fructose had higher  $q_{\text{ethanol}}$  when compared to other carbon sources (Figure 5.5-5B). Strains grown on galactose had very high  $q_{\text{O}_2}$  when compared to glucose and fructose substrates. Few glucose grown strains and a couple of fructose grown strains had higher  $q_{\text{O}_2}$  when compared to the rest of the strains (Figure 5.5-5C). This analysis clearly indicates that strains grown on glu-

cose were most fermentative followed by fructose grown strains, whereas strains grown on galactose had higher respiration rates. A steep increase of  $q_{\text{ethanol}}$  was observed with increasing specific uptake rate when  $q_{\text{Hexose}}$  was plotted against  $q_{\text{ethanol}}$  of each mutant grown on all the three carbon sources. However, some strains grown on fructose didn't follow this trend and had very high uptake rates (Figure 5.5-6A). Strains grown on galactose showed a distinct phenotype with very high  $q_{\text{O}_2}$  representing that the strains had higher respiratory capacity (Figure 5.5-6B) than fermentating capacity and in addition strains with lower  $q_{\text{ethanol}}$  had higher  $q_{\text{O}_2}$  (Figure 5.5-6C).

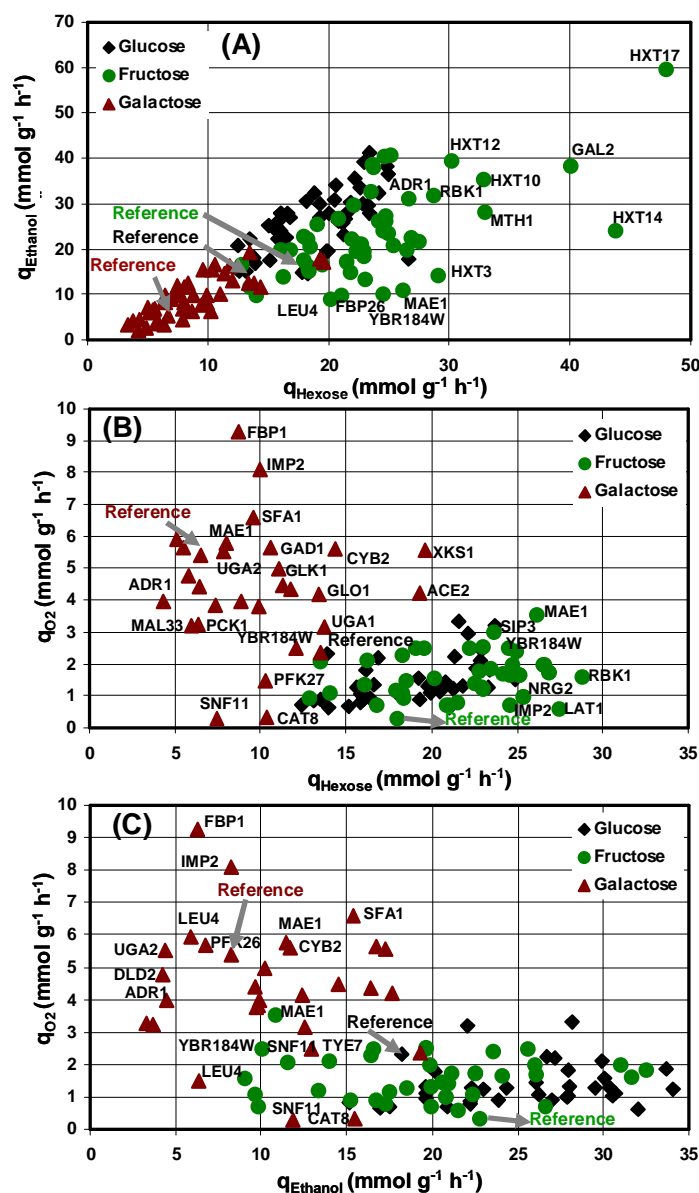


**Figure 5.5-6** Comparative profiling on glucose, galactose and fructose (A) Specific rate of ethanol production,  $q_{\text{ethanol}}$ , and (B) specific oxygen uptake rate,  $q_{\text{O}_2}$ , as a function of the specific hexose consumption rate,  $q_{\text{hexose}}$  (C) Specific oxygen uptake rate,  $q_{\text{O}_2}$ , as a function of the specific rate of ethanol production,  $q_{\text{ethanol}}$ . Arrows indicate the reference strain BY4742 *Mat $\alpha$  his3 $\Delta$ 1 leu2 $\Delta$ 0 lys2 $\Delta$ 0 ura3 $\Delta$ 0*.

Pair-wise comparison of specific rates on two different carbon sources allows identify the strains, which possess similar phenotypic profile on both the carbon sources. When specific growth rate,  $\mu_{\max}$ , was plotted on glucose against fructose (Figure 5.5-7A), few strains, *hxt1* $\Delta$ , *mth1* $\Delta$ , *gad1* $\Delta$ , *hxt12* $\Delta$  showed similar growth rates on both the sugars. Two strains, *xks1* $\Delta$  and *snf11* $\Delta$  had higher growth rates on glucose than on fructose. Mutant strains, *nrg1* $\Delta$ , *pfk26* $\Delta$  *hxt17* $\Delta$ , *imp2'* $\Delta$  and *gad1* $\Delta$  showed similar growth profiles on both glucose and galactose sugars (Figure 5.5-7B). Two strains, *xks1* $\Delta$  and *snf11* $\Delta$  had high growth rates on glucose and *mig2* $\Delta$  strain had high growth rate on galactose. Mutant strains, *snf3* $\Delta$ , *gad1* $\Delta$ , *fbp1* $\Delta$ , *mig2* $\Delta$ , and the reference strain had similar growth profiles on both galactose and fructose sugars (Figure 5.5-7C). Except *hxt4* $\Delta$  strain, none of the mutant strains had higher growth rates on galactose than on fructose.

When specific hexose uptake rate,  $q_{\text{Hexose}}$ , of glucose was plotted against  $q_{\text{Hexose}}$  of fructose (Figure 5.5-7D) two strains, *hxt1* $\Delta$  and *hxt4* $\Delta$  showed identical values on both the sugars. *hxt17* $\Delta$  strain had highest uptake rate on fructose and very high uptake rate on glucose. *hxt14* $\Delta$  strain, which had about an average value of  $q_{\text{Hexose}}$  of glucose had very high  $q_{\text{Hexose}}$  of fructose. *mig2* $\Delta$  strain had an identical values of  $q_{\text{Hexose}}$ , of glucose and galactose (Figure 5.5-7E). *xks1* $\Delta$  strain had highest uptake rate on galactose (Figure 5.5-7E) and similar uptake rates on glucose and fructose (Figure 5.5-7F) .

When specific ethanol production rate,  $q_{\text{Ethanol}}$ , on glucose was plotted against  $q_{\text{Ethanol}}$  on fructose (Figure 5.5-7G), two strains, *mig2* $\Delta$  and *hxt14* $\Delta$  showed identical values on both the sugars and two strains, *hxt1* $\Delta$  and *hxt4* $\Delta$  had about the similar profile. *hxt17* $\Delta$  strain, which had very high  $q_{\text{Ethanol}}$  on glucose had the highest  $q_{\text{Ethanol}}$  on fructose. *xks1* $\Delta$  and *snf11* $\Delta$ , which had very high  $q_{\text{Ethanol}}$  on glucose had low  $q_{\text{Ethanol}}$  on fructose. None of the strains had identical  $q_{\text{Ethanol}}$  profiles on glucose and galactose (Figure 5.5-7H). *mig2* $\Delta$  strain had highest  $q_{\text{Ethanol}}$  on galactose and about similar profile on glucose. *nrg1* $\Delta$  strain had lowest  $q_{\text{Ethanol}}$  on both the sugars. Mutant strains, *mig2* $\Delta$ , *xks1* $\Delta$ , *snf11* $\Delta$ , *mae2* $\Delta$  and *fbp26* $\Delta$  showed identical  $q_{\text{Ethanol}}$  profiles on galactose and fructose sugars (Figure 5.5-7I).

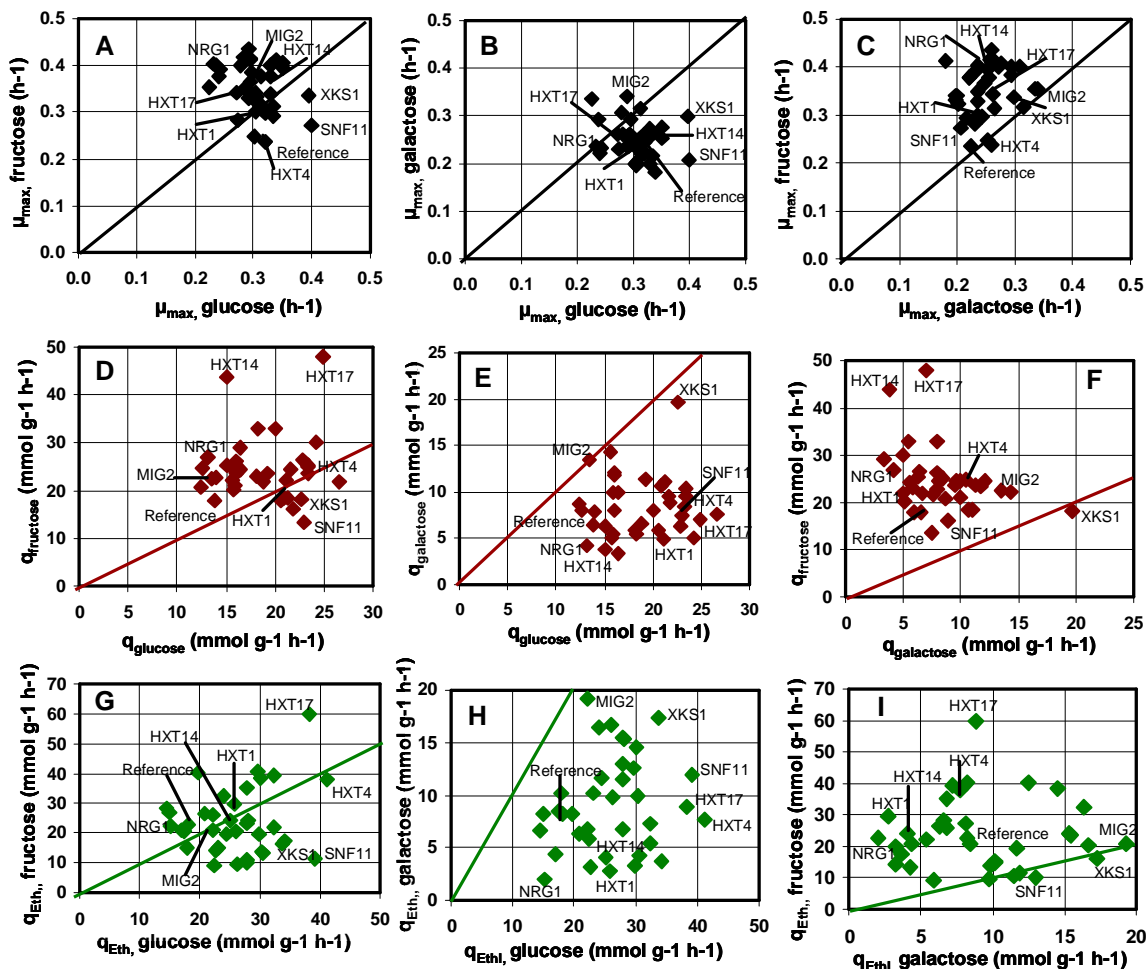


**Figure 5.5-7** Pair-wise comparison of specific rates (A) Specific growth rate,  $\mu_{\max}$ , on glucose vs.  $\mu_{\max}$  on fructose (B)  $\mu_{\max}$  on glucose vs.  $\mu_{\max}$  on galactose (C)  $\mu_{\max}$  on galactose vs.  $\mu_{\max}$  on fructose (D) specific hexose uptake rate,  $q_{\text{Hexose}}$ , of glucose vs.  $q_{\text{Hexose}}$  of fructose (E)  $q_{\text{Hexose}}$  of glucose vs.  $q_{\text{Hexose}}$  of galactose (F)  $q_{\text{Hexose}}$  of galactose vs.  $q_{\text{Hexose}}$  of fructose (G) specific ethanol production rate,  $q_{\text{Ethanol}}$ , on glucose vs.  $q_{\text{Ethanol}}$  on fructose (H)  $q_{\text{Ethanol}}$  on glucose vs.  $q_{\text{Ethanol}}$  on galactose (I)  $q_{\text{Ethanol}}$  on galactose vs.  $q_{\text{Ethanol}}$  on fructose. Solid line represents the identical values on both the axes.

### 5.5.3.2 Comparison of yields

Comparison of yields on different carbon sources indicates that the strains grown on galactose had very high biomass yields on substrate and very low biomass yields on oxygen, represents that the deletion strains grown on galactose are highly respiratory with high biomass yields when compared to glucose and fructose (Figure 5.5-8A). Strains grown on glucose had high ethanol yields representing that strains are more fermenting than on galactose and fructose grown strains (Figure 5.5-8B). Strains grown on fructose had higher biomass yields on oxygen indicating that some of the strains grown on fructose are almost respiratory deficient when compared to glucose and galactose grown strains (Figure 5.5-8C).

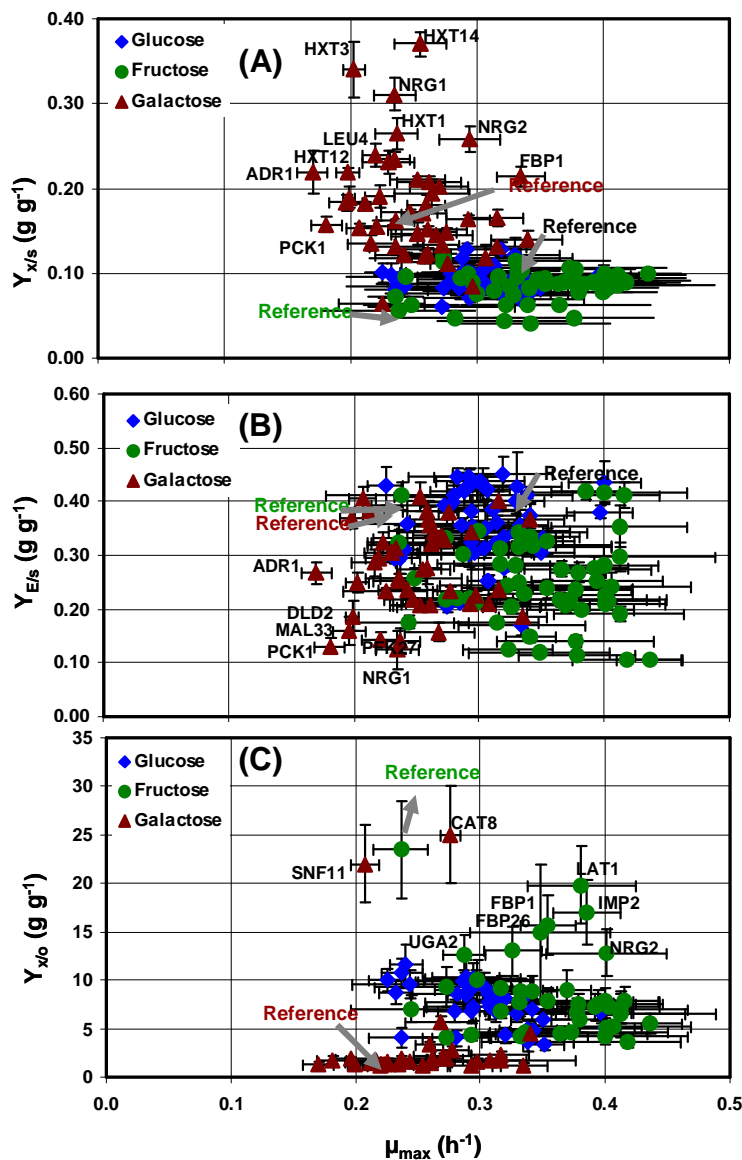


**Figure 5.5-8** Stoichiometric profiling of yeast deletion mutants on glucose, galactose and fructose. Correlation between specific growth rate,  $\mu_{\max}$ , and (A) biomass yield,  $Y_{X/S}$ , (B) ethanol yield,  $Y_{E/S}$ , as well as with (C) biomass yield on oxygen,  $Y_{X/O}$  (Table 5.5-2) Arrows indicate the reference strain BY4742 *Mat $\alpha$  his3 $\Delta$ 1 leu2 $\Delta$ 0 lys2 $\Delta$ 0 ura3 $\Delta$ 0*.

## 5.5.4 Physiologically interesting strains

Based on this comparative stoichiometric analysis on different carbon sources, yeast single knockout strains that revealed interesting phenotypes were selected and further discussed as follows.

### 5.5.4.1 *mae1* $\Delta$

This strain lacks *MAE1* gene, which encodes malic enzyme activity. It has been previously shown that on glucose substrate deletion of *MAE1* has no significant phenotype in *S. cerevisiae* (Boles et al., 1998) and in *C. glutamicum* (Petersen et al., 2000). Previous studies also reported that on fructose, flux through PPP is significantly lower (Kiefer et al., 2004) and the flux through TCA cycle and malic enzyme activity are higher (Dominguez, 1998). However, *mae1* $\Delta$  strain showed a clear phenotype of very high PPP flux when grown on galactose in order to maintain the NADPH levels (Velagapudi et al., 2007). As described in this chapter, when grown on fructose as sole carbon source, *mae1* $\Delta$  strain showed clear phenotype. *mae1* $\Delta$  strain had highest oxygen uptake rate (3.53 mmol/g/h) with very low ethanol yield (0.1 g/g). The biological interpretation of this phenotype on fructose could be due to lack of malic enzyme and reduced PPP flux on fructose; *mae1* $\Delta$  strain would have only 2 routes to maintain NADPH levels, one way via TCA cycle by activating NADPH specific isocitrate dehydrogenase activity forming alpha-keto glutarate from citrate, which is repressed during growth on glucose (Loftus et al., 1994; Haselbeck et al., 1993) and the other one via NADPH specific aldehyde dehydrogenase forming acetate from acetaldehyde (Kurita et al., 1999), which in turn produces acetyl-CoA, which could be transported back to mitochondrion and entering the TCA cycle. The missing carbon balance for this strain is 66.3% suggesting the formation of other by-products for e.g. glycerol and high CO<sub>2</sub> production.

### 5.5.4.2 *hxt1* $\Delta$ and *hxt3* $\Delta$

Low affinity transporters are highly expressed at very high levels of glucose or fructose and repressed at low sugar levels. There have been many studies that aim to characterise hexose transporters in yeast that usually used glucose as the substrate. On glucose, *hxt1* $\Delta$  and *hxt3* $\Delta$  strains showed similar phenotypic profiles (Please refer to chapter 5.4 for additional details) as these are single knockouts; the function is complemented by other Hxt. On fructose,

*hxt1Δ* and *hxt3Δ* strains showed different phenotypes. *hxt1Δ* strain grew with a growth rate of 0.3 h<sup>-1</sup> and fructose uptake rate ( $q_{\text{fru}} = 22.1$  mmol/g/h) and ethanol production rate ( $q_{\text{Eth}} = 29.8$  mmol/g/h) with high ethanol yield ( $Y_{\text{P/S}} = 0.344$  g/g). Whereas *hxt3Δ* strain had similar growth rate ( $\mu_{\text{max}} = 0.32$  h<sup>-1</sup>) and about similar fructose consumption rate ( $q_{\text{fru}} = 29.1$  mmol/g/h) but with low ethanol production rate ( $q_{\text{Eth}} = 14.1$  mmol/g/h). In addition, *hxt3Δ* strain had very low ethanol yield ( $Y_{\text{P/S}} = 0.12$  g/g) about three times less than *hxt1Δ* strain.

The possible explanation for this phenotype could be as follows. In a recent study by Luyten et al. (2002), it has been shown that Hxt3p has the highest capacity to support fermentation on fructose. That means, since *HXT3* is expressed in *hxt1Δ* strain, it consumed fructose at higher rates and produced very high ethanol when compared to *hxt3Δ* strain. It has also been shown that *HXT3* gene is responsible for the capacity for consuming fructose among certain yeasts and a mutation on allele of *HXT3* gene was responsible for improving the performance of wine yeasts by increased utilisation of fructose during fermentation that would be very desirable in cases of stuck fermentation (Guillaume et al, 2007). Analysis of hexose carrier expression and characterisation of transport kinetics during wine alcohol fermentation revealed that Hxt1p expression was predominant during growth phase and Hxt3p during fermentation phase (Perez et al., 2005). *hxt3Δ* strain is also sensitive to external ethanol perturbations and in a previous study it has been shown that *hxt3Δ* strain displayed growth defect when grown on 10% ethanol (Karpel et al., 2008).

#### 5.5.4.3 *hxt4Δ* and *hxt14Δ*

On fructose, *hxt4Δ* strain was growing slowly with  $\mu_{\text{max}} = 0.23$  h<sup>-1</sup> and produced at a relatively low biomass yield ( $Y_{\text{X/S}} = 0.05$  g/g) but had a very high ethanol yield ( $Y_{\text{P/S}} = 0.411$  g/g) when compared to other strains. On glucose *hxt4Δ* strain had  $\mu_{\text{max}} = 0.32$  h<sup>-1</sup>;  $Y_{\text{X/S}} = 0.076$  g/g and higher ethanol yield than other strains ( $Y_{\text{P/S}} = 0.451$  g/g) (please refer to section 5.4 for additional details).

On glucose, *hxt14Δ* strain had  $\mu_{\text{max}} = 0.33$  h<sup>-1</sup>, higher biomass yield  $Y_{\text{X/S}} = 0.121$  g/g and higher ethanol yield,  $Y_{\text{P/S}} = 0.426$  g/g. On galactose, it didn't show any specific phenotype. On fructose, *hxt14Δ* strain had  $\mu_{\text{max}} = 0.377$  h<sup>-1</sup> and had very high fructose uptake rate,  $q_{\text{fru}} = 43.8$  mmol/g/h but had very low biomass yield,  $Y_{\text{X/S}} = 0.048$  g/g and ethanol yield,  $Y_{\text{P/S}} = 0.141$  g/g, suggesting that a lot of carbon flux might be channelled through TCA cycle and

released as CO<sub>2</sub> or might be channelled to by-product formation e.g. acetate, glycerol or lactate etc.

These observations allowed to hypothesise that on fructose, Hxt4p might be interacting or interfering with the Hxt3p in *hxt1Δ* strain (please refer to section 5.5.4.2); since Hxt1p and Hxt3p have complementary functions on glucose, Hxt4p and Hxt14p might be interacting or interfering either with Hxt1p or Hxt3p and subsequently affecting the fermentation rates.

#### 5.5.4.4 *hxt8Δ*

On glucose and fructose, *hxt8Δ* strain was growing with similar growth rates ( $\mu_{\max} = 0.334 \text{ h}^{-1}$  and  $0.314 \text{ h}^{-1}$ , respectively), had similar biomass yields ( $Y_{X/S} = 0.07 \text{ g/g}$  and  $0.08 \text{ g/g}$ , respectively) and had similar but very low ethanol yields ( $Y_{P/S} = 0.171 \text{ g/g}$  and  $0.175 \text{ g/g}$ , respectively), whereas on galactose it had  $0.342 \text{ g/g}$  ethanol yield, which is similar to the reference, suggesting that on galactose deletion of *HXT8* had no role on fermentation but had severe effect on glucose and fructose fermentation.

Thus we can hypothesise that Hxt8p with limited known function so far might be involved in glucose and fructose fermentations but not in galactose fermentation. Another interesting phenotype of this strain is higher PPP and TCA fluxes on glucose than on galactose.

#### 5.5.4.5 *hxt17Δ*

On glucose and galactose, *hxt17Δ* strain was growing with similar growth rates ( $\mu_{\max} = 0.272 \text{ h}^{-1}$  and  $0.262 \text{ h}^{-1}$ , respectively) and on galactose it had about an average values of uptake rate and ethanol production rate. The strain had very high uptake rates and ethanol production rates on glucose and fructose sugars ( $q_{\text{glu}} = 24.85 \text{ mmol/g/h}$  and  $q_{\text{fru}} = 47.95 \text{ mmol/g/h}$ , respectively;  $q_{\text{Eth}} = 38.34 \text{ mmol/g/h}$  and  $q_{\text{Eth}} = 59.75 \text{ mmol/g/h}$ , respectively).

This observation suggests a possible role of this putative hexose transporter gene to be involved in glucose and fructose fermentation processes and also controlling the uptake rates.

#### 5.5.4.6 *xks1Δ*

On fructose and galactose, *xks1Δ* strain was growing with similar growth rates ( $\mu_{\max} = 0.336 \text{ h}^{-1}$  and  $0.297 \text{ h}^{-1}$ , respectively), had similar uptake rates ( $q_{\text{fru}} = 18.28 \text{ mmol/g/h}$  and  $q_{\text{gal}} = 19.62 \text{ mmol/g/h}$ , respectively) and similar ethanol production rates ( $q_{\text{Eth}} = 16.38 \text{ mmol/g/h}$

and  $q_{\text{Eth}} = 17.3$  mmol/g/h, respectively), whereas on glucose, it showed different profile, the strain was growing with a very high growth rate and also had higher rates than on galactose and fructose. Overall, *xks1Δ* strain had lower uptake rates and ethanol production rates on fructose followed by galactose and then glucose.

This observation suggests that *xks1Δ* strain (which had no xylulokinase activity, converting a ketopentose, xylulose to xylulose phosphate), showed a phenotype when grown on ketohexose, fructose rather than on aldohexoses, glucose and galactose.

### 5.5.4.7 *imp2'Δ*

Imp2'p is a sugar utilisation regulatory protein and a transcriptional activator involved in maintenance of ion homeostasis (Masson et al., 1998) and protects against DNA damage caused by bleomycin and other oxidants (Masson et al., 1996). *imp2'Δ* strain had no obvious phenotype when grown on glucose but on galactose it had the lowest  $\Phi_{\text{PPP,gal}}$  and showed highest oxygen uptake rate that was about ten times higher than on glucose (Velagapudi et al., 2007). That means most of the carbon flux was channelled to TCA cycle rather than PPP on galactose substrate. This is in agreement with previous findings, where Imp2'p was shown to have a positive effect on glucose derepression of Leloir pathway (*GAL* genes), raffinose and maltose utilisation pathways genes (Alberti et al., 2003) and in addition, *imp2Δ* strain is unable to grow on these sugars in the presence of inhibitors of mitochondrial protein synthesis or ethidium bromide (Donninni et al., 1992). That means higher mitochondrial activity is required in utilisation of galactose. On fructose, *imp2'Δ* strain had highest ethanol yield when compared to other strains and even higher when grown on glucose. This is industrially beneficial feature in wine industry with respect to higher fructose fermentation capacity.

## 5.5.5 Conclusions

In this chapter, a set of strains were selected and quantitative physiological profiling was done when the strains were grown on fructose as sole carbon source as described in previous chapters. The obtained data on fructose sugar was compared with glucose and galactose data. Comparative physiological profiling on three carbon sources clearly indicates that strains grown on galactose were growing slowly when compared to glucose and fructose. Strains grown on glucose had higher fermentation activity followed by fructose grown strains, whereas strains grown on galactose had higher respiratory capacity. On fructose, *mae1Δ*

strain had highest oxygen uptake rate with very low ethanol yield, which could be due to reduced PPP flux. *mae1* $\Delta$  strain would have only 2 routes to maintain NADPH levels, one way via TCA cycle by activating NADPH specific isocitrate dehydrogenase activity other one via NADPH specific aldehyde dehydrogenase. The obtained results suggested a positive effect of Hxt3p on fructose fermentation and Hxt8p on both glucose and fructose fermentations but not on galactose. Hxt4p on fructose and Hxt4p and Hxt14p on glucose might have negative effects on fermentation. Based on this analysis, physiologically and industrially beneficial strains could be identified.

## 5.6 FUNCTIONAL GENOMICS OF *S. CEREVISIAE* BY UTILISING PHENOTYPIC AND METABOLIC FLUX PROFILING DATA BY USING BIOINFORMATICS TOOLS

Velagapudi, V.R., Peddinti, G., Tang, J., Heinzle, E., 2009. Functional genomics of *S. cerevisiae* by utilising phenotypic and metabolic flux profiling data by using bioinformatics tools (in preparation)

### 5.6.1 Background

*S. cerevisiae* is an excellent eukaryotic model system and its genome was completely sequenced more than a decade ago. Even for this well studied microorganism, a major fraction of gene functions are uncharacterized. According to Saccharomyces Genome Database (as of May 2009) ([www.yeastgenome.org](http://www.yeastgenome.org)), there are only 72.82 % of protein coding genes with identified functions, whereas 14.91 % of genes are uncharacterized and the function of the 12.27 % of genes are still dubious. A powerful strategy to unravel the function of unknown genes is by studying the phenotypic effects of deletion mutants, with missing gene. Functional genomics represent a systematic approach to elucidating the function of the novel genes revealed by complete genome sequence.

Since the quantitative stoichiometric data and metabolic flux data is available on different carbon sources for a set of mutants that are known to be involved in central carbon metabolism, it is of great interest to check whether one can predict the function of uncharacterized genes based on this data. Hence, the first part of this chapter deals with an overview of all the mutants studied on different carbon sources and at the end functional predictions are made using bioinformatics tools.

### 5.6.2 Statistical analysis of the data

In this chapter, all the examined mutants were combined and analysed statistically applying hierarchical clustering algorithm using stoichiometric data i.e.,  $Y_{X/S}$ ,  $Y_{E/S}$  and  $\mu_{\max}$ , and metabolic flux data on different carbon sources using Euclidian distance as a distance metric to identify homogenous clusters of cases based on the measured data, which means mutants within each cluster are more closely related to one another than mutants assigned to other clusters. The relative Euclidian distances (d) were calculated between mutant pairs and also

between mutants and the reference strain. Finally the functions of hypothetical genes were predicted by combining all the available data.

### 5.6.2.1 Hierarchical clustering analysis

#### • Glucose

The top five most closely related mutant pairs on glucose were *pfk27Δ-hxt10Δ* ( $d = 0.032$ ); *gad1Δ-hxt1Δ* ( $d = 0.046$ ); *mae1Δ-ybr184wΔ* ( $d = 0.046$ ); *glo1Δ-sfa1Δ* ( $d = 0.048$ ); *dld2Δ-snf3Δ* ( $d = 0.051$ ). The measured Euclidean distances were visualised as dendrogram and the data revealed 4 clusters, highlighted with colours in Figure 5.6-1.

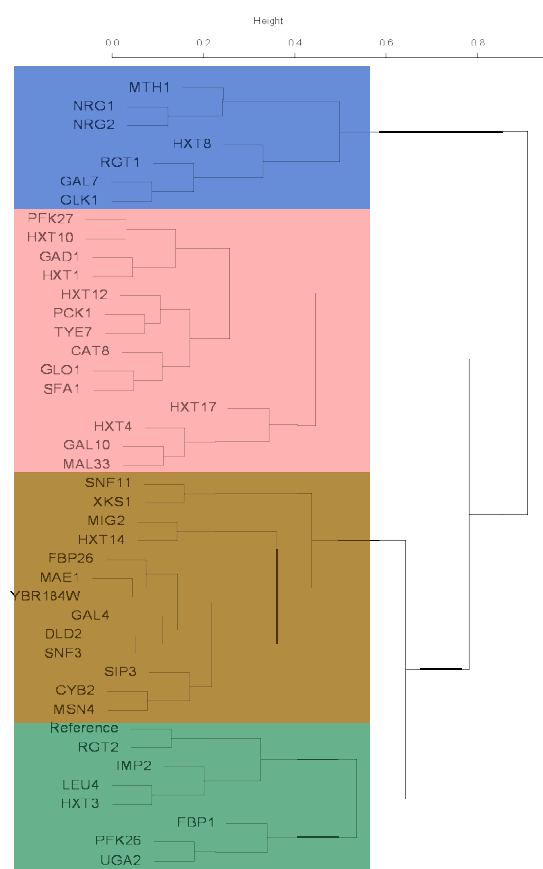


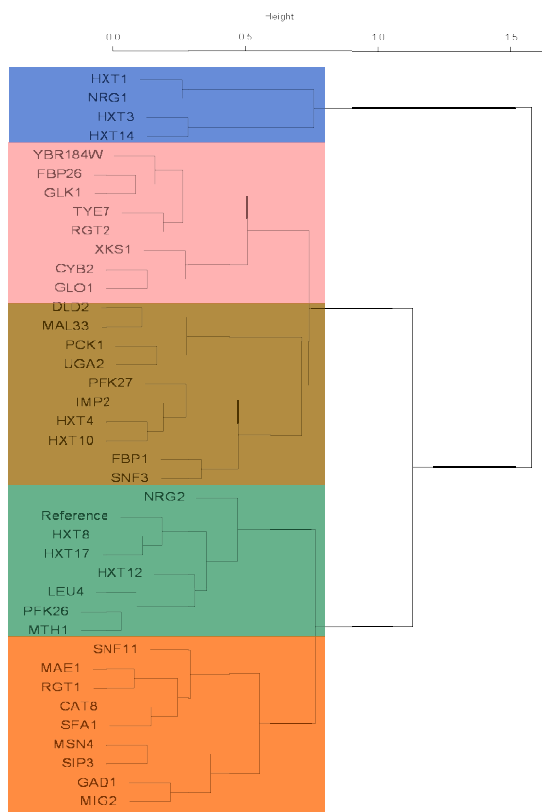
**Figure 5.6-1** Dendrogram on glucose. Hierarchical clustering was done using stoichiometric data by using Euclidean distances as a metric.

In the first cluster (bottom to top), few strains were clustered together with the reference strain for e.g., *rgt2Δ*, *leu4Δ* suggesting that these strains had no specific phenotype under the examined conditions. In the second cluster, genes that are related to pyruvate metabolism were clustered together. For instance, *cyb2Δ* (Cyb2p - lactate dehydrogenase) and *dld2Δ* (Dld2p - D-lactate dehydrogenase), *mae1Δ* (Mae1p - malic enzyme), *fbp26Δ* (Fbp26p - fruc-

tose 2, 6 bisphosphatase) and also *mig2Δ* and *msn4Δ* (Mig2p and Msn4p - transcription factors that are involved in glucose repression) were clustered together. The third cluster contains most of the hexose transporter knock out strains. In the fourth cluster, *mth1Δ*, *rgt1Δ* and *hxt8Δ* (Mth1p, Rgt1p and Hxt8p are involved in glucose signalling and transport), and *nrg1Δ* and *nrg2Δ* (Nrg1p and Nrg2p - transcription factors that are involved in glucose repression) were clustered together.

• **Galactose**

Similarly all the mutants grown on galactose were combined and analysed as above. The top five most closely related mutant pairs on galactose were *pfk26Δ-mth1Δ* (d = 0.032); *leu4Δ-mth1Δ* (d = 0.07); *mae1Δ-rgt1Δ* (d = 0.078); *fbp26Δ-glk1Δ* (d = 0.082); *leu4Δ-pfk26Δ* (d = 0.089).



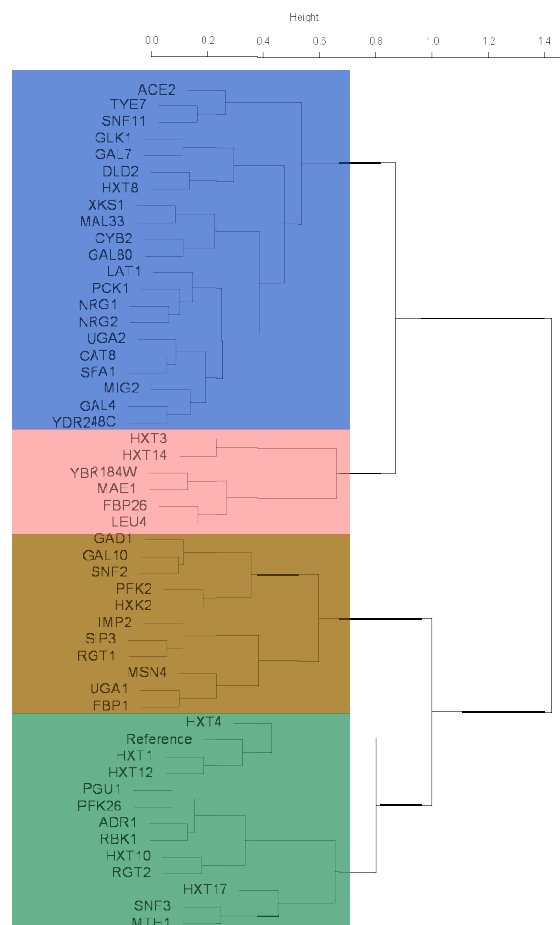
**Figure 5.6-2** Dendrogram on galactose. Hierarchical clustering was done using stoichiometric data by using Euclidean distances as a metric.

Figure 5.6-2 revealed five clusters on galactose. In the first cluster (bottom to top), strains with knockout genes that are involved in catabolite repression, for e.g., *cat8Δ*, *mig2Δ* were grouped. The second cluster contained hexose transporters and regulators knock out strains.

In the third cluster glucose and pyruvate metabolism and hexose transporters knock out strains were clustered. The fourth cluster comprises glucose, pyruvate, and glyoxalate metabolism knock out strains. The fifth cluster includes hexose transport knock out strains and *nrg1Δ* knock out strain (Nrg1p is a transcription repressor involved in glucose metabolism).

• **Fructose**

The top five most closely related mutant pairs were *cat8Δ-sfa1Δ* (d = 0.054); *gal4Δ-ydr248cΔ* (d = 0.055); *sip3Δ-rgt1Δ* (d = 0.055); *nrg1Δ-nrg2Δ* (d = 0.062); *pfk2Δ-hxk2Δ* (d = 0.072). The top three most closely related mutants with the reference strain were *hxt1Δ* (d = 0.204); *snf3Δ* (d = 0.288) and *rgt2Δ* (d = 0.313) and two mutants, *mae1Δ* (d = 1.02) and *ybr184wΔ* (d = 1.08) are distantly related to the reference strain with Euclidean distance, d above 1, indicating that these strains showed a clear phenotype when grown on fructose. The measured Euclidean distances were visualised as dendrogram and the data revealed 4 clusters, highlighted with colours in Figure 5.6-3.



**Figure 5.6-3** Dendrogram on fructose. Hierarchical clustering was done using stoichiometric data by using Euclidean distances as a metric.

In the first cluster (bottom to top), strains with silenced genes that are involved in hexose transportation, hexose sensing and regulation were clustered together for e.g., *hxt1Δ*, *hxt4Δ*, *hxt10Δ*, *hxt12Δ*, *hxt17Δ*, *snf3Δ*, *rgt2Δ* and *mth1Δ* suggesting that these strains had similar phenotype under the examined conditions. Interestingly the details of protein interactions and complexes using MIPS MPact Protein Interactions and Complex DB (Güldener et al., 2006) ([www.mips.gsf.de/genre/proj/impact](http://www.mips.gsf.de/genre/proj/impact)) revealed that Snf3p has direct interactions with Rgt2p (Yang and Bisson, 1996); Hxt4p (Ko et al., 1993); Hxt1p (Lewis and Bisson, 1991) and Mth1p (Irie et al., 1993). In the second cluster, *snf2Δ* and *sip3Δ* (Snf2p - which is a component of SNF1 protein complex, which in turn has direct interaction with Sip3p (Gavin et al., 2002; Lesage et al., 1994)) were clustered together. In addition, *pfk2Δ* (Pfk2p - phosphofructokinase activity) and *hck2Δ* (Hck2p - hexokinase activity) and *imp2'Δ* (Imp2'p - transcriptional activator involved in carbohydrate metabolic process) were clustered together. In the third cluster, genes that are related to pyruvate metabolism and glucose metabolic process, for instance, *mae1Δ* (Mae1p - Malic enzyme) and *fbp26Δ* (Fbp26p - Fructose 2, 6 bisphosphatase) were clustered together with the *ybr184wΔ* (YBR184W – hypothetical gene). In the fourth cluster, *glk1Δ* and *dld2Δ* (Glk1p and Dld2p are components of actin associated protein complex (Amberg et al., 1995)); *nrg1Δ* and *nrg2Δ* (Nrg1p and Nrg2p - transcriptional repressors) were clustered together; and *gal4Δ* and *gal80Δ* (Gal4p and Gal80p had direct physical interaction (Sil et al., 1999)) were clustered together. All these evidences provide a biological significance of clustering analysis.

### ● Combined analysis - Glucose, Galactose and Fructose

Another interesting analysis would be to combine all the strains on all the three carbon sources i.e., glucose, galactose and fructose and check for the most closely related strains. The top five most closely related mutant pairs were *cat8Δ-sfa1Δ* (d = 0.186); *fbp26Δ-ybr184wΔ* (d = 0.314); *msn4Δ-sip3Δ* (d = 0.319); *glk1Δ-tye7Δ* (d = 0.346); *cat8Δ-gad1Δ* (d = 0.395). Figure 5.6-4 revealed four main clusters. In the first cluster (bottom to top), mainly hexose transporters and regulators in glucose signalling knock out strains were clustered. Second cluster contained strains that had gene deletions in glucose metabolism. Third cluster contained hypothetical gene, *fbp26Δ*, *mae1Δ* and hexose transporters knock out strains. The last cluster contained strains that had gene deletions in glucose and pyruvate metabolism, gluconeogenesis and transcriptional repressors etc.

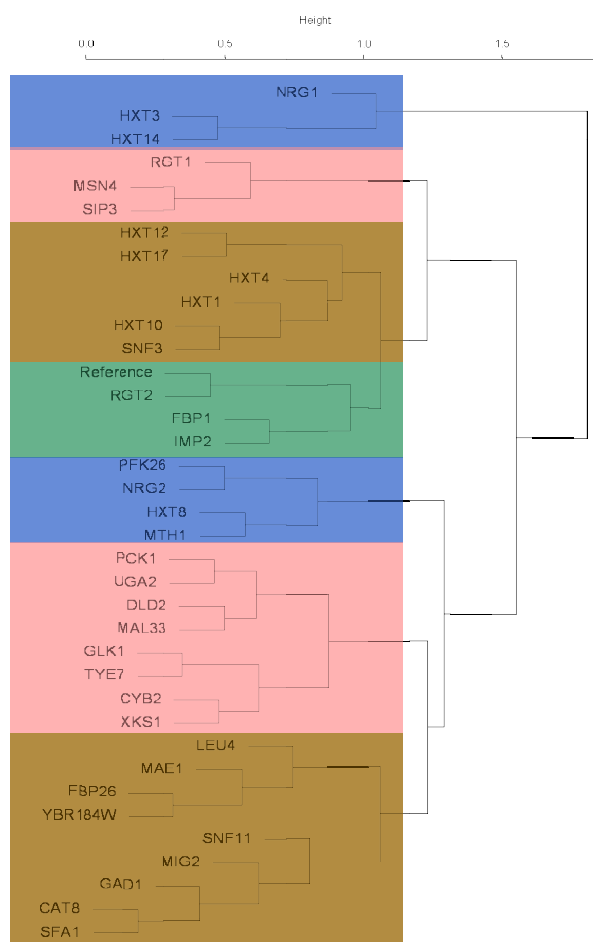


**Figure 5.6-4** Dendrogram of combined effects of glucose, galactose and fructose sugars

### 5.6.2.2 Data visualization as clustered heat maps

In order to obtain an overview of all the metabolic fluxes for all the strains, metabolic flux data of all the strains were combined and visualized as clustered heat maps using an algorithm written in 'R'. Flux data of mutants were normalized with respect to the reference strain flux data and the obtained fold change values were converted to log<sub>2</sub> values and then clustered using hierarchical method.

- Glucose:** All the strains with similar flux profiling were clustered together (Fig 5.6-5). In general, fermentation and PPP pathways were up regulated whereas anaplerotic and biosynthetic pathways were down regulated in mutants. In almost half of the strains, TCA cycle was down regulated and in another half upregulated. Glycolysis was almost unchanged in all the strains, which suggests that all the metabolic changes were occurred from lower glycolytic pathway. Knockout genes with similar function or acting in same pathway were clus-

tered together based on the flux data. For instance, in the lower half of the heat map, deletion strains involved in galactose utilisation pathway, *gal4Δ* and *gal10Δ*; gluconeogenic gene deletions, *fbp1Δ*, *fbp26Δ* and *mae1Δ*; hexose transporter knockouts, *hxt4Δ*, *hxt14Δ*; lactate metabolic process gene deletions, *cyb2Δ* and *dld2Δ*; and Snf1p interacting protein Sip3p knockouts, *sip3Δ* and *snf11Δ* were clustered together. In this cluster of strains, fermentation and PP pathways were highly up regulated, respiration and anaplerosis were significantly down regulated and glycolysis was unchanged (Fig 5.6-5). In the upper half of the heat map, strains showed up regulation of both PP pathway and TCA cycle, down regulation of anaplerosis and most of the strains showed unchanged glycolysis and fermentation (Fig 5.6-5).

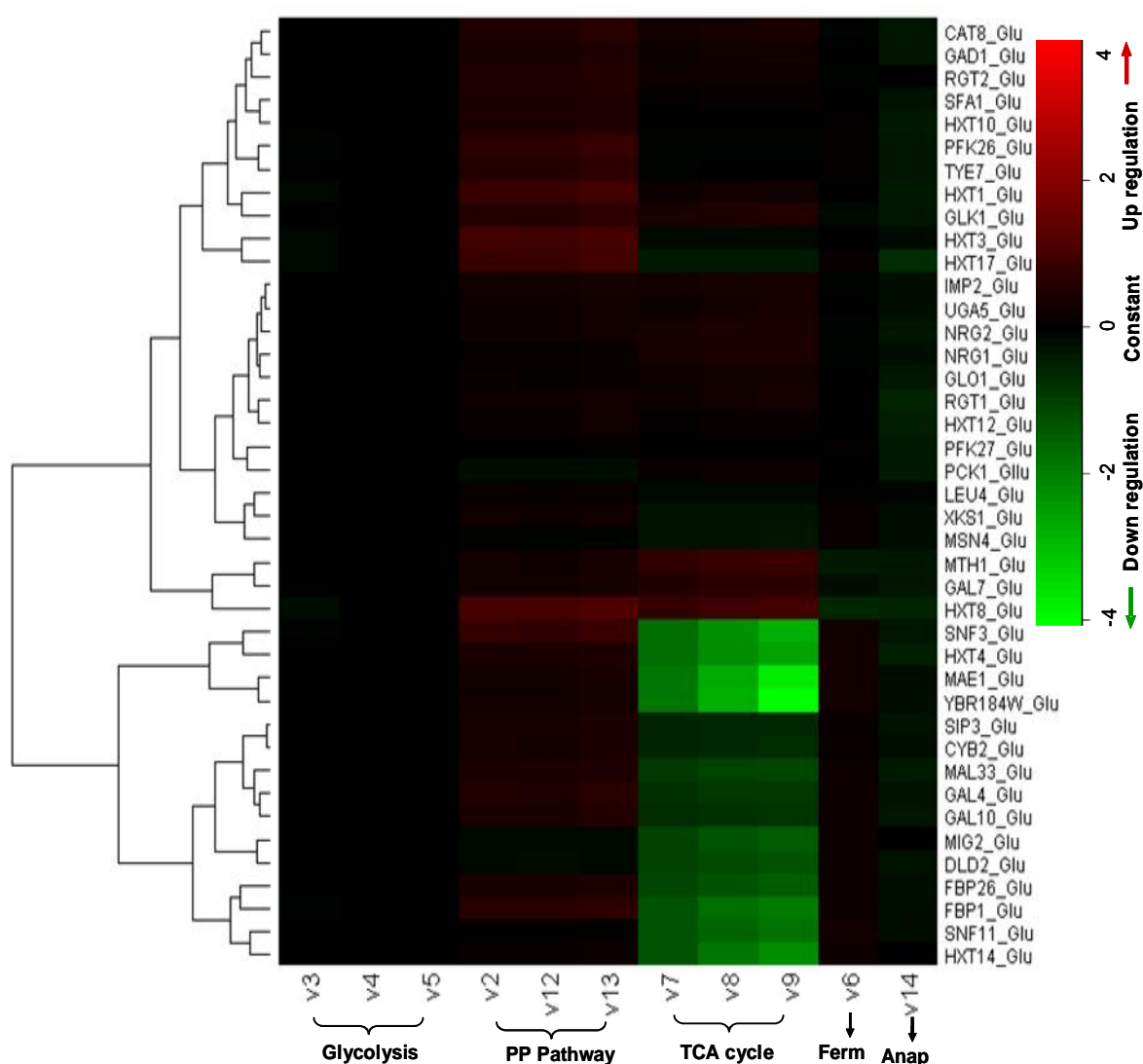


**Figure 5.6-5** Heat map with clustering representing the log<sub>2</sub> values of fold changes of flux values with respect to the reference strain on glucose. (Ferm – Fermentative pathway; Anap – Anaplerotic pathway)

- Galactose:** An overview of metabolic flux profiling of all the strains grown on galactose (Fig 5.6-6) revealed that the strains showed very high up regulation of respiration and down regulation of fermentation, anaplerosis and PP pathways and glycolysis was mostly unchanged (upper part of the heat map). However, there is a cluster of strains that showed significant down regulation of TCA cycle, which was complemented by moderate up regulation of fermentation (lower part of the heat map).

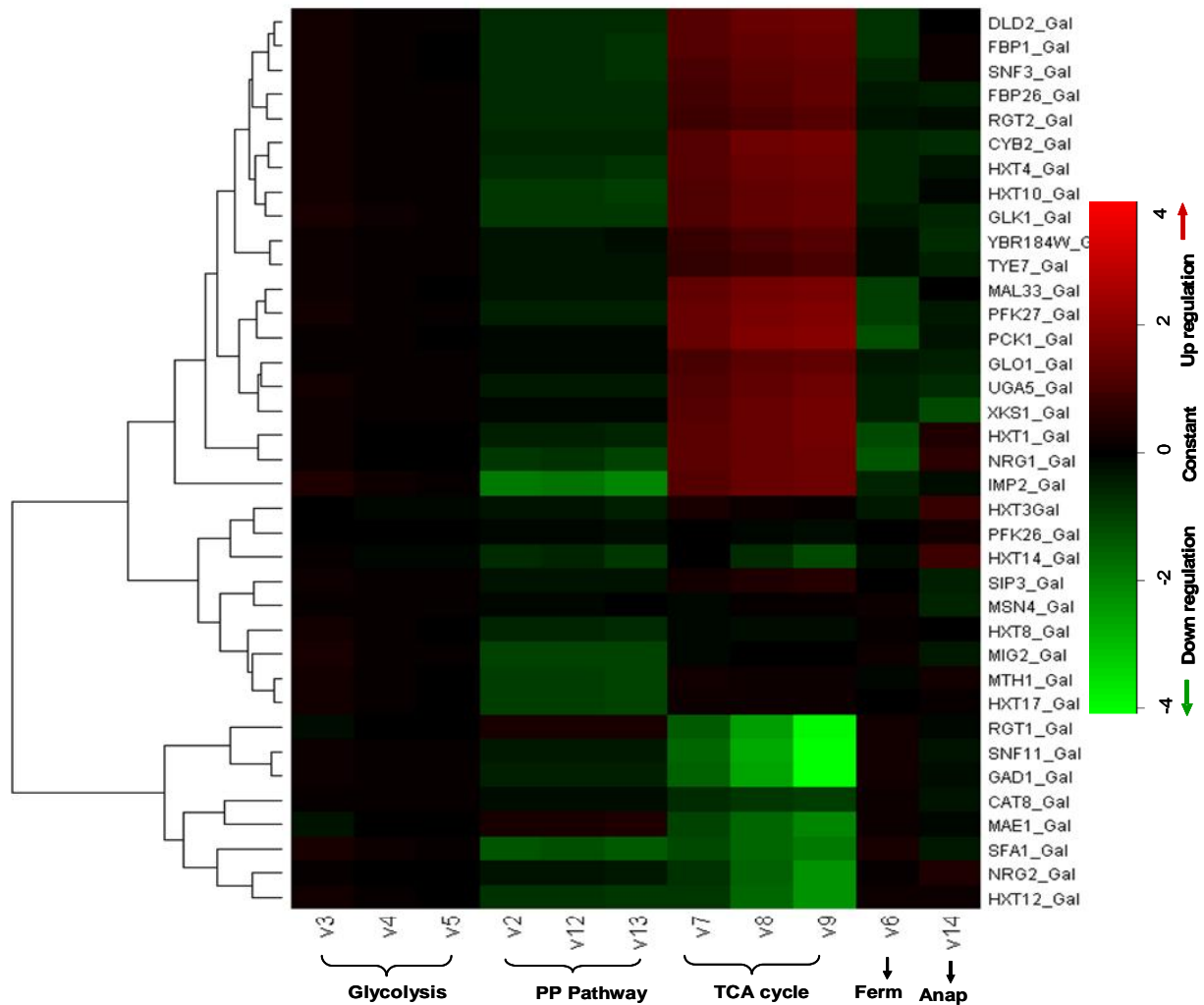


**Figure 5.6-6** Heat map with clustering representing the log<sub>2</sub> values of fold changes of flux values with respect to the reference strain on galactose. (Ferm – Fermentative pathway; Anap – Anaplerotic pathway)

### 5.6.2.3 Biological significance of mutant pairs

Hierarchical clustering on all the strains when combined the data of all the three carbon sources revealed most closely related clusters based on stoichiometric data (section 5.6.2.2) and the following explanation gives a possible biological link between the two mutant strains.

- ***cat8Δ-sfa1Δ* pair:** Cat8p encodes a zinc-finger cluster protein that is necessary for derepression of number of genes during non-fermentative growth conditions (Hedges et al., 1995). Genomic studies have shown that many of the genes encoding proteins involved in gluconeogenesis, ethanol utilization and glyoxylate cycle are regulated by Cat8p (Haurie et al., 2001; Tachibana et al., 2005). *SFA1* is a bifunctional enzyme encoding both alcohol dehydrogenase and glutathione-dependent formaldehyde dehydrogenase activities (Grey et al., 1996; Wehener et al., 1993). Clustering of these two strains was observed on all individual sugars and also in combined analysis. Even the metabolic flux profiling of these two strains on glucose (Fig 5.6-3) and galactose (Fig 5.6-4) revealed that these two strains had similar flux profiles and thus clustered together. Since both Cat8p and Sfa1p are somewhere involved in a common pathway, ethanol metabolism might be the reason for this clustering and it would be interesting to study this further.
- ***sip3Δ-msn4Δ* pair:** Clustering of this mutant pair was not only observed using combined stoichiometric data of all the sugars (Fig 5.6-2) but also using flux data on galactose (Fig 5.6-4). Msn4 is a transcriptional activator related to Msn2p and activated during several stress conditions (Martinez-Pastor et al., 1996; Gorner et al., 1998) and it is a Multicopy suppressor of SNF1 mutation (Estruch et al., 1993). Sip3p, a SNF1 Interacting Protein (Yang et al., 1992), which has transcription activity, has a direct physical interaction with Snf1p (Lesage et al., 1994).
- ***glk1Δ-tye7Δ* pair:** Both combined stoichiometric data of all the sugars (Fig 5.6-2) and flux data on glucose (Fig 5.6-3) and galactose (Fig 5.6-4) yielded the clustering of this mutant pair. Glk1p, glucokinase, catalyses phosphorylation of glucose (Herrero et al., 1995) in glycolysis pathway; Tye7p, TY-mediated expression, a serine-rich protein that contains a basic-helix-loop-helix DNA binding motif (Lohning et al., 1994). It binds to E-boxes of glycolytic genes and contributes to their expression (Sato et al., 1999). This could be a possible link between these two mutants.

### 5.6.3 Functional prediction of hypothetical genes

Since the quantitative stoichiometric data is available for all the selected deletion mutant strains on different carbon sources, it is of special interest to predict the role of unknown genes based on the phenotype and to see whether this study can already provide first indications for the hitherto unknown function of the gene product. It is obvious that studies of this type cannot always directly give conclusive functional information but allow to direct future research. Interesting phenotypes will, together with other established methods (Oliver et al., 1998) provide an important basis to the discovery of gene function in yeast. Among the selected mutant strains, one strain had a hypothetical gene deletion (*ybr184w* $\Delta$ ) and the other with pseudogene deletion (*yil170w* $\Delta$ ).

#### 5.6.3.1 Euclidean distance approach

One possibility is to compare these strains with all other strains and further investigate the most closely related ones by utilising the stoichiometric data on three different sugars,  $\mu_{\max}$ ,  $Y_{X/S}$  and  $Y_{E/S}$  (tables 5.1-3 and 5.1-4) and metabolic flux profiling data on glucose and galactose by calculating a relative Euclidian distance,  $d$  (detailed description is given in Materials and Methods section).

- **YBR184W (SGD ID: S000000388):** *YBR184W* alias *YBR1306*, located on chromosome II (Feldmann et al., 1994), is not an essential gene. The gene product of *YBR184W*, a putative protein of unknown function, has not been studied extensively (Kellis et al., 2003). However, the gene expression analysis revealed that this gene is induced during sporulation. Sequence analysis shows that it is similar to the gene *YSW1*, which encodes a spore-specific protein (Chu et al., 1998).

On glucose, the top five most closely related strains to *ybr184w* $\Delta$  and their distances are—*mae1* $\Delta$ -0.046; *fbp26* $\Delta$ -0.064; *dld2* $\Delta$ -0.103; *snf3* $\Delta$ -0.135; *cyb2* $\Delta$ -0.138 and the distance to reference is 0.435. All these strains also showed similar metabolic flux profiling and are part of a cluster where TCA cycle was down regulated (Fig 5.6-3). On galactose, the top five most closely related strains are—*fbp26* $\Delta$ -0.145; *glk1* $\Delta$ -0.158; *tye7* $\Delta$ -0.198; *sip3* $\Delta$ -0.218; *rgt2* $\Delta$ -0.259 and the distance to reference is 0.451. All these strains except *sip3* $\Delta$  also showed similar metabolic flux profiling and are part of a cluster where TCA cycle was up regulated (Fig

5.6-4). On fructose, the top five most closely related strains are—*mae1Δ*-0.127; *leu4Δ*-0.181; *fbp26Δ*-0.271; *dld2Δ*-0.377; *pck1Δ*-0.378; and the distance to reference is 1.08. Therefore, *fbp26Δ* is a common strain present among the top five most closely related strains in all three sugars followed by *mae1Δ* and *dld2Δ* present in two sugars, glucose and fructose. For all strains the distances to *ybr184wΔ* are less on glucose than on galactose and fructose. This is very pronounced for *fbp26Δ* with distances of 0.064 (Glucose), 0.145 (Galactose) and 0.271 (Fructose), and *mae1Δ* with distances of 0.046 (Glucose) and 0.127 (Fructose). In addition, *ybr184wΔ* strain is most distantly related to reference strain on fructose with distance of 1.08 when compared to glucose and galactose (0.435 and 0.451, respectively). One possible explanation is that *ybr184wΔ* has more specific effects during growth on fructose and galactose than on glucose.

On glucose *ybr184wΔ* has identical specific growth rate with *fbp26Δ*, identical biomass yield with *fbp26Δ*, *mae1Δ* and *cyb2Δ*, and identical ethanol yield with *mae1Δ* and *snf3Δ*. On fructose, *ybr184wΔ* is the fastest grower and had lowest ethanol yield and *mae1Δ* is closely related to  $\mu_{\max}$  and  $Y_{E/S}$  and there is no identity with respect to biomass yield among the top five closely related strains. On galactose *ybr184wΔ* has identical biomass yield with *glk1Δ* and ethanol yield with *tye7Δ* and there is no identity with respect to specific growth rate among the top five closely related strains.

Since *fbp26Δ* is one among the top five most closely related strains to *ybr184wΔ* in all the three carbon sources, it seems therefore likely that the effects of *ybr184wΔ* deletion are somewhat similar as *fbp26Δ* deletion. Fbp26p hydrolyzes fructose-2, 6-bisphosphate, which is activating phosphofructokinase, Pfk1p, and inhibiting fructose-1, 6-bisphosphatase, Fbp1p that is involved in gluconeogenesis pathway (Paravicini et al., 1992; Kretschmer et al., 1987). The next closely related strains are *mae1Δ* and *dld2Δ*. Mae1p, mitochondrial malic enzyme catalyses the oxidative decarboxylation of malate to pyruvate (Boles et al., 1998) has a strong similarity to other malate dehydrogenases and is involved in gluconeogenesis and pyruvate metabolic processes. Dld2p, D-lactate dehydrogenase activity, located in mitochondrial matrix (Chelstowska, et al., 1999) is involved in lactate metabolic process and pyruvate metabolism. Details of protein interactions and complexes using MIPS MPact Protein Interactions and Complex DB (Güldener et al., 2006) ([www.mips.gsf.de/genre/proj/impact](http://www.mips.gsf.de/genre/proj/impact)) revealed that

Ybr184wp has 2 direct physical interactions and one protein complex in which Mdh1p, malate dehydrogenase precursor is involved which in turn had protein complex with lactate/malate dehydrogenase (Ho et al., 2002). Based on these observations, one could predict that in a broader sense, Ybr184wp might be involved in glucose metabolic process or pyruvate metabolic pathways.

- **YIL170W (SGD ID: S 000001432):** YIL170W, a pseudogene *HXT12*, located on chromosome IX is a non-functional member of the hexose transporter family (Nelissen et al., 1995; Kruckeberg et al., 1996). This gene has high similarity to other 18-20 members of hexose transporter family (Wieczorke et al., 1999; Diederich et al., 1999).

On glucose, the top five most closely related strains to *yil170wΔ* and their distances are—*pck1Δ*-0.076; *tye7Δ*-0.105; *gad1Δ*-0.115; *hxt1Δ*-0.126; *hxt10Δ*-0.133 and the distance to reference is 0.566. All these strains also showed similar metabolic flux profiling and are part of a cluster where TCA cycle was up regulated (Fig 5.6-3). On galactose, the top five most closely related strains are—*pfk26Δ*-0.268; *mth1Δ*-0.274; *leu4Δ*-0.31; *hxt17Δ*-0.313; *hxt8Δ*-0.313 and the distance to reference is 0.247. All these strains also showed similar metabolic flux profiling and are part of a cluster where TCA cycle was either down regulated or constant (Fig 5.6-4). On fructose, the top five most closely related strains are—*hxt1Δ*-0.185; *rgt2Δ*-0.244; *hxt10Δ*-0.245; *hxt17Δ*-0.275; *rbk1Δ*-0.316 and the distance to reference is 0.323. Therefore, common strains present at least in two sugars among the top five most closely related strains are *hxt1Δ*, *hxt10Δ* and *hxt17Δ*. In general, for all the strains the distances to *yil170wΔ* are less on glucose than on fructose and galactose. This is very pronounced for *hxt10Δ* with distances of 0.133 (Glucose); 0.245 (Fructose), and *hxt1Δ* with distances of 0.126 (Glucose); 0.185 (Fructose). Even though the distances are relatively smaller on glucose than other two sugars, *yil170wΔ* strain is most distantly related to reference strain on glucose followed by fructose and galactose, which indicates substrate specific phenotypes of *yil170wΔ* strain. The deletion of *YIL170W* is somewhat similar to the deletion effects of low affinity transporter, *hxt1Δ*, and hexose transporters with limited known function, *hxt10Δ* and *hxt17Δ* as these are among the top five most closely related strains to *yil170wΔ* at least in two sugars.



- **Galactose**

Similar analysis was done using quantitative data on galactose (Figure 5.6-8). The network looks less connected when compared to glucose data suggesting that the mutant strains are quite independent when grown on galactose and had their own phenotype. Mutant strain *ybr184wΔ* showed a strong and significant direct dependency with *tye7Δ* strain with partial correlation,  $\rho = 0.97$ ;  $p$ -value = 0.0004, which is in accordance with the Euclidean distance approach results. Whereas mutant strain *yil170wΔ* showed a strong and significant direct dependency with *snf11Δ* strain with partial correlation,  $\rho = 0.1$ ;  $p$ -value = 0.0007.

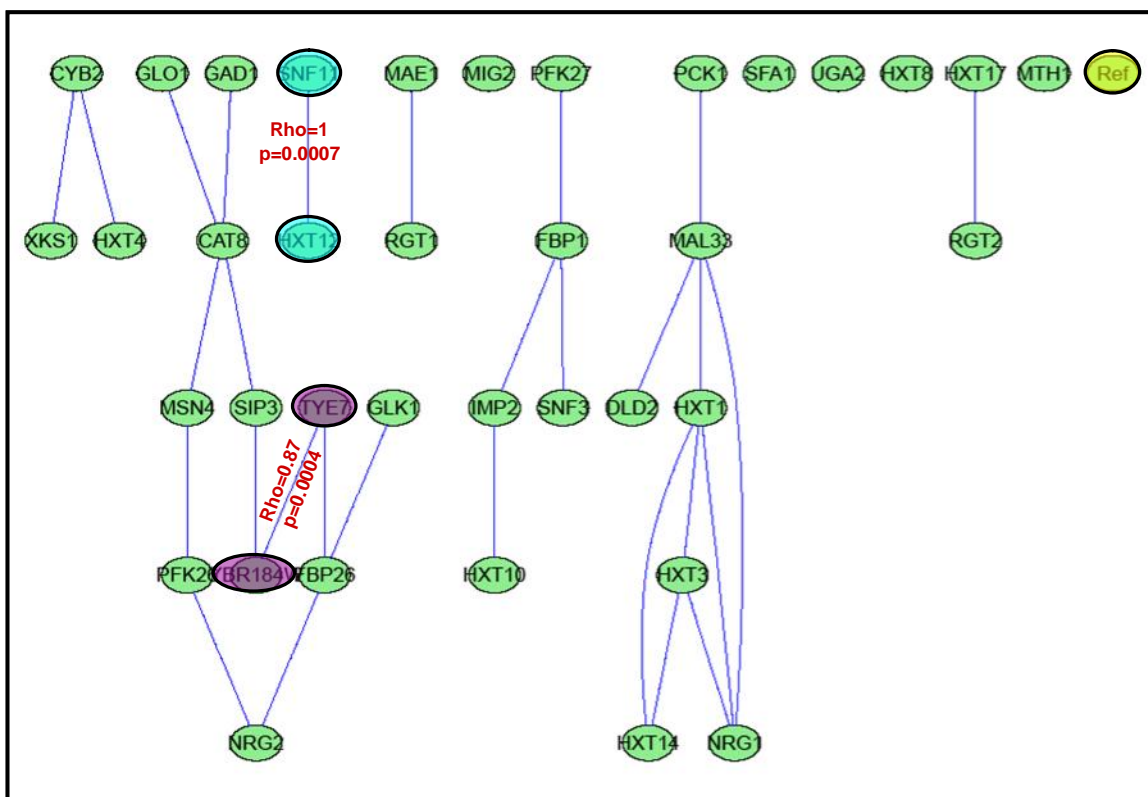


**Figure 5.6-8** q-order partial correlation graph (qp-graph) for galactose data.

- **Fructose**

Qp-graph on fructose data showed that several mutant strains had no dependencies on other mutant strains (Figure 5.6-9) and mutant strain *yil170wΔ* is one among them. Mutant strain *ybr184wΔ* showed a strong and significant direct dependency with *mae1Δ* strain with partial correlation,  $\rho = 0.99$ ; p-value = 0.01, which is in accordance with the Euclidean distance approach results.

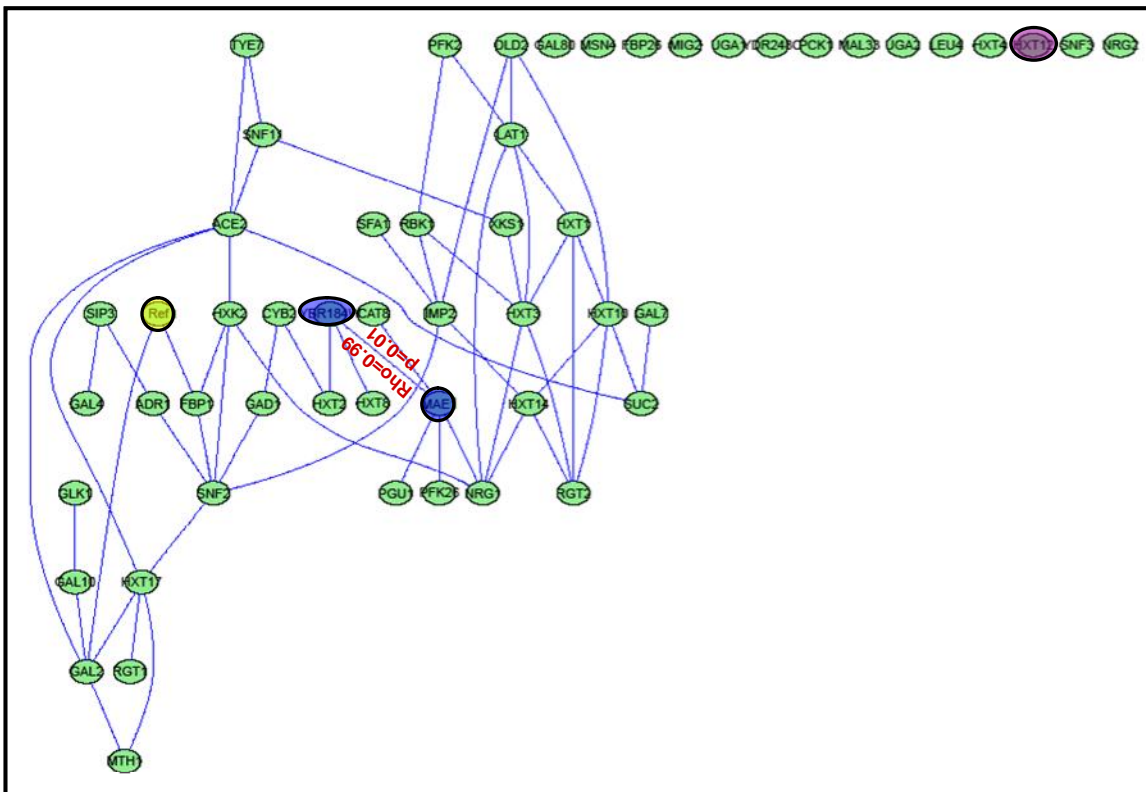


**Figure 5.6-9** q-order partial correlation graph (qp-graph) for fructose data.

### 5.6.4 Conclusions

In this overview chapter, all the strains studied on different carbon sources were combined and analysed either individually on each sugar or together. The following statistical analyses were employed for the computational analysis of the data (i) hierarchical clustering analysis, and (ii) metabolic flux data visualization using clustered heat maps, relation between mutant pairs using Euclidean distance measure and finally functional prediction of hypothetical genes by combining all the above analyses and also by graphical Gaussian model approach.

Hierarchical clustering analysis of the stoichiometric data on each sugar revealed most closely related mutant pairs. Combined clustering analysis revealed that *cat8Δ-sfa1Δ*; *fbp26Δ-ybr184wΔ*; *msn4Δ-sip3Δ*; *glk1Δ-tye7Δ*; *cat8Δ-gad1Δ* as most closely related mutant pairs, which is also consistent with the metabolic flux profiling data. The functional prediction of hypothetical gene *YBR184W* based on this quantitative data suggested a possible role in glucose metabolic process or pyruvate metabolic pathways as the most closely related strains in all the sugars were *fbp26Δ*, *mae1Δ* and *dld2Δ*. The functional prediction of a pseudogene, *YIL170W (HXT12)*, which is close to other hexose transporters suggested a possible close association with the low affinity transporter knockout, *hxt1Δ* and with other hexose transporters with limited known function knockouts, *hxt10Δ* and *hxt17Δ*.

## 6 SUMMARY AND CONCLUSIONS

The baker's yeast, *S. cerevisiae* is a versatile eukaryotic model organism, whose genome was first sequenced (Goffeau et al. 1996, 1997), and thoroughly investigated in several aspects, which is used for understanding and engineering eukaryotic cell function (Ostergaard et al., 2000). However, the function of a major fraction of genes coding for proteins has not yet been determined. A powerful approach to determine gene function is the phenotypic analysis of mutants missing the gene of interest (Winzeler et al., 1999; Que et al., 2002). The availability of the complete set of deletion mutants of *S. cerevisiae* provides a unique resource for systematic analysis of the functional role of individual genes (Giaever et al., 2002; Brachmann et al., 1998). To exploit this unique resource of complete set, high-throughput assays are needed to provide a quantitative phenotypic and metabolic profiles of the functional role of individual genes besides already existing large-scale screenings to find gene-environment interactions during several stress responses based on fitness (Giaever et al., 2002; Gasch et al., 2002; Weiss et al., 2004; Warringer et al., 2003; Mollapur et al., 2004).

The determination of basic physiological parameters of deletion mutants on different carbon sources would provide more detailed picture of metabolic activities of such mutants. Thus this sort of research motivated to select and investigate the quantitative physiological characterisation of a set of knockout strains involved in central carbon metabolism and hexose transporters on different carbon sources. In order to screen a large number of deletion mutants simultaneously, 96-well microtiter plates with immobilized oxygen sensors were used and metabolic flux profiling was studied by using labeled substrates and simplified fluxes were calculated using stoichiometric mass balances.

**The first chapter (5.1)** of the thesis dealt with the development and optimisation of high-throughput kinetic and stoichiometric analysis of yeast mutant libraries in 96 well microtiter plates with on-line sensing of dissolved oxygen at miniaturized scale and obtained reliable quantitative data of physiological parameters on glucose and galactose. Twenty-seven deletion mutants of *S. cerevisiae* were investigated using a novel method for high-content stoichiometric and kinetic metabolic profiling. We can detect, whether oxygen limitation is occurring during cultivation using the oxygen sensing microtiter plate. Secondly, dissolved oxygen profiles indicate most substrate limitations and diauxic behaviour. The application of

a simple balanced growth model allowed correction for ethanol and water evaporation during cultivation. From this new method, reliable data for specific growth rate, biomass and ethanol yields on carbon substrate and biomass yield on oxygen were calculated on both the sugars and allowed statistically significant discrimination of all mutants studied (Velagapudi et al., 2006).

**In the second chapter (5.2)**, a new method was developed for throughput quantification of isotope-labeled ethanol originating from 1-<sup>13</sup>C-labeling experiments using MALDI-ToF-MS, which permits the calculation of the flux split ratio between glycolysis and the pentose-phosphate pathway (PPP). This new application of the hydrazone reaction of 2,4-dinitrophenylhydrazine with acetaldehyde, formed by an enzymatic reaction, is a sufficiently sensitive method for the quantification of ethanol formed by fermentation. Ethanol quantification using this method was compared with enzymatic analysis and exhibited differences of less than 3.3 % on average. Comparison of flux partitioning ratios based on MALDI-TOFMS and gas chromatography GC/MS methods showed good agreement, with differences for ethanol and alanine labeling of only 4.3 % (Hollemeier et al., 2007).

**The third chapter (5.3)** of the thesis dealt with the comparative metabolic flux profiling on the selected mutants on glucose and galactose by utilizing the above developed methods. On glucose, the growth was predominantly fermentative with high yield of ethanol, low yield of biomass and low oxygen consumption rate. On galactose respiration was more active with correspondingly lower ethanol yields, higher biomass yields and higher rates of oxygen consumption. Some strains showed unexpectedly high or low growth rates and rates of ethanol production and respiration providing very informative data about the function of the corresponding gene. Deletion of malic enzyme gene, *MAE1*, did not show any significant phenotype when grown on glucose but a drastically increased branching from glucose 6-phosphate into the pentose phosphate pathway on galactose. This allows the conclusion that Mae1p is important for the supply of NADPH during aerobic growth on galactose (Velagapudi et al., 2007).

**The fourth chapter (5.4)** of the thesis dealt with the hexose transporter deletion mutant strains and each selected deletion mutant strain was grown on glucose and galactose to obtain quantitative stoichiometric and metabolic flux data. Since these are single knockouts and have complementary functions, these strains had no growth defects, except for *gal2Δ* on galactose but revealed substrate specific phenotypic profiles. On glucose, *hxt4Δ* strain was highly fermentative (had as low TCA fluxes as anaerobic fluxes), in contrast, on galactose,

it had higher respiratory flux. On glucose, *hxt8Δ* was the fastest grower with lowest fermentative capacity. However, the strain had highest specific glucose uptake rate, PPP and TCA cycle fluxes. On galactose, *rgt1Δ* strain had extremely high PPP flux and also high fermentative capacity with lower respiratory and anaplerotic fluxes. The mutant strain *hxt14Δ* had similar anaplerotic and TCA fluxes on both the sugars; and had similar TCA, PPP fluxes as well as ethanol yields on both the sugars.

**The fifth chapter (5.5)** of the thesis dealt with the comparative physiological profiling on three carbon sources, which clearly indicates that strains grown on galactose were growing slowly when compared to glucose and fructose. Strains grown on glucose had higher fermentative activity followed by fructose grown strains, whereas strains grown on galactose had higher TCA and therefore higher respiratory activity. *mae1Δ* strain had highest oxygen uptake rate with very low ethanol yield, which could be due to reduced PPP flux on fructose. *mae1Δ* strain would have only 2 routes to maintain NADPH levels, one way via TCA cycle by activating NADPH specific isocitrate dehydrogenase activity other one via NADPH specific aldehyde dehydrogenase. The obtained results suggested a positive effect of Hxt3p on fructose fermentation and Hxt8p on both glucose and fructose fermentations but not on galactose. Hxt4p on fructose and Hxt4p and Hxt14p on glucose might have negative effects on fermentation. Based on this analysis, physiologically and industrially potentially beneficial strains could be identified.

**The sixth chapter (5.6)** of the thesis dealt with the functional prediction of hypothetical genes by utilising the quantitative stoichiometric and metabolic flux data on different carbon sources. All the strains studied on different carbon sources were combined and analysed statistically. Combined hierarchical clustering analysis revealed that *cat8Δ-sfa1Δ*; *fbp26Δ-ybr184wΔ*; *msn4Δ-sip3Δ*; *glk1Δ-tye7Δ*; *cat8Δ-gad1Δ* as most closely related mutant pairs, which is also consistent with the metabolic flux profiling data. Moreover, these mutant pairs also have biological significance. Based on Euclidean distance approach, it seems that the hypothetical gene *YBR184W* might play a role in pyruvate metabolism as *ybr184wΔ* is close to *mae1Δ*, *dld2Δ* and *fbp26*. Pseudogene, *YIL170W (HXT12)*, might play a role as low affinity transporter as *yil170wΔ* is close to *hxt1Δ* and also with other hexose transporters with limited known functions, *hxt10Δ* and *hxt17Δ*. These results were also confirmed by Graphical Gaussian modelling approach.

## 7. OUTLOOK

- **Impact of the thesis work**

This thesis presents the high-throughput phenotypic and metabolic flux profiling of yeast single gene knockouts on different carbon sources. From the complete yeast knockout library, which contains over 6,000 gene-disruption mutants, a sub-set of over 60 deletion mutants whose gene functions are supposed to be involved in central carbon metabolism, hexose transportation, transcriptional factors and few uncharacterised genes were selected, i.e., about 1 % of the complete collection. Since the effects of most of the gene deletions are silent (silent phenotype due to complementary functions) or robust (due to tight integration of yeast metabolic network), three different sugars, glucose, galactose and fructose were selected as the sole carbon source. For parallel handling of deletion strains, 96-well microtiter plates with immobilised oxygen sensors were used for miniaturised cultivation purpose, which is both time and cost-effective approach.

Quantitative stoichiometric data and metabolic flux profiling data were obtained by implementing the developed novel methodology. This high-content metabolic screening of yeast mutants revealed unexpected metabolic mobilisation of metabolic potential and in addition metabolic flux screening of mutants on different carbon sources supported the elucidation of gene function. Furthermore, combined quantitative data analysis by using computational approaches enabled to predict the function of hypothetical genes. The work described in this thesis contributes significantly to the yeast community where the main goals of the yeast deletion project consortium are physiological profiling of each deletion knockout where the ultimate aim is to unravel the function of uncharacterised genes i.e., functional analysis of the yeast genome.

- **Directions for future research**

1. Metabolic flux results of *mae1Δ* strain revealed a very high PP pathway on galactose and very high oxygen uptake rate on fructose to maintain NADPH demand; it would be interesting to do in-depth analysis of this strain.
2. More in depth analysis of mutants on fructose sugar by measuring all possible extracellular products and subsequent metabolic flux analysis.
3. In order to confirm the early functional predictions of uncharacterised gene *YBR184W* further investigation of this strain and its closely related strains, *mae1Δ*, *fbp26Δ* and *dld2Δ* is necessary. For instance, similar analysis on non-fermentable carbon sources.
4. In order to obtain more insights on hexose transport, it would be interesting to carry out similar research on strains carrying only one *HXT* gene.

## 8. REFERENCES

1. Alfenore, S., Molina-Jouve, C., Guillouet, S.E., Uribelarrea, J.L., Goma, G., Benbadis, L., 2002. Improving ethanol production and viability of *Saccharomyces cerevisiae* by a vitamin feeding strategy during fed-batch process. *Appl Microbiol Biotechnol.* 60, 67-72.
2. Allen, J., Davey, H.M., Broadhurst, D., Heald, J.K., Rowland, J.J., Oliver, S.G., Kell, D.B., 2003. High-throughput classification of yeast mutants for functional genomics using metabolic footprinting. *Nat Biotechnol.* 21, 692-696.
3. Amberg, D.C., Basart, E., Botstein, D., 1995. Defining protein interactions with yeast actin in vivo. *Nature Struct. Biol.* 2, 28-35.
4. Andre, B., 1995. Overview of membrane transport proteins in *Saccharomyces cerevisiae*. *Yeast.* 16, 1575-611.
5. Baer, E., Stanacev, N.Z., 1964. Convenient Deuterium Labeling for Mass Spectrometry via Exchange of Enolizable Hydrogen on a Gas-Liquid Chromatography Column. *J. Amer. Chem. Soc.* 87, 3.
6. Barr, M.M., 2003. Super models. *Physiol Genomics.* 13, 15-24.
7. Barredo, J.L., Alvarez, E., Cantoral, J.M., Diez, B., Martin, J.F., 1988. Glucokinase-deficient mutant of *Penicillium chrysogenum* is derepressed in glucose catabolite regulation of both beta-galactosidase and penicillin biosynthesis. *Antimicrob Agents Chemother.* 32, 1061-1067.
8. Barwald, G., Fischer, A., 1996. Crabtree effect in aerobic fermentations using grape juice for the production of alcohol reduced wine. *Biotechnol Letters.* 18, 1187-1192.
9. Baudin, A., Ozier-Kalogeropoulos, O., Denouel, A., Lacroute, F., Cullin, C.A., 1993. Simple and efficient method for direct gene deletion in *Saccharomyces cerevisiae*. *Nucleic Acids Res.* 21, 3329-3330.
10. Berkey, C.D., Vyas, V.K., Carlson, M., 2004. Nrg1 and Nrg2 Transcriptional Repressors Are Differently Regulated in Response to Carbon Source. *Eukaryot Cell.* 3, 311-317.
11. Blank, L.M., Lehmbeck, F., Sauer, U., 2005a. Metabolic-flux and network analysis in fourteen hemiascomycetous yeasts. *FEMS Yeast Res.* 5, 545-548.
12. Blank, L.M., Kuepfer, L., Sauer, U., 2005b. Large-scale <sup>13</sup>C-flux analysis reveals mechanistic principles of metabolic network robustness to null mutations in yeast. *Genome Biology.* 6, R49.
13. Blank, L.M., Sauer, U., 2004. TCA cycle activity in *S. cerevisiae* is a function of the environmentally determined growth and glucose uptake rate. *Microbiology.* 150, 1085-1093.
14. Boles, E., de Jong-Gubbels, P., Pronk, J.T., 1998. Identification and characterization of MAE1, the *Saccharomyces cerevisiae* structural gene encoding mitochondrial malic enzyme. *J Bacteriol.* 180, 2875-2882.
15. Brachmann, C.B., Davies, A., Cost, G.J., Caputo, E., Li, J., Hieter, P., Boeke, J.D., 1998. Designer deletion strains derived from *Saccharomyces cerevisiae* S288C: A useful set of strains and plasmids for PCR mediated gene disruption and other applications. *Yeast.* 14, 115-138.
16. Carlson, M., 1999. Glucose repression in yeast. *Curr. Opin. Microbiol.* 2, 202-207.
17. Carpenter, A.E., Sabatini, D.M., 2004. Systematic genome-wide screens of gene function. *Nat Rev Genet.* 5, 11-22.
18. Celenza, J.L., Carlson, M., 1986. A yeast gene that is essential for release from glucose repression encodes a protein kinase. *Science.* 233, 1175-1180.

## References

---

19. Chelstowska, A., 1999. Signalling between mitochondria and the nucleus regulates the expression of a new D-lactate dehydrogenase activity in yeast. *Yeast*. 13, 1377-91.
20. Christensen, B., Nielsen, J., 2000. Metabolic network analysis of *Penicillium chrysogenum* using <sup>13</sup>C-labeled glucose. *Biotechnol. Bioeng.* 68, 652-659.
21. Chu, S., 1998. The transcriptional program of sporulation in budding yeast. *Science*. 282, 699–705.
22. Conde, R., Pablo, G., Cueva, R., Larriba, G., 2003. Screening for new yeast mutants affected in mannosylphosphorylation of cell wall mannoproteins. *Yeast*. 20,1189-211.
23. Diderich, J.A., Schepper, M., Hoek, P.V., Luttk, M.A.H., Johannes, P., van Dijken, Pronk, J.T., Klaassen, P., Boelens, H.F., de Mattos, M.J., van Dam, K., Kruckeberg, A.L., 1999. Glucose Uptake Kinetics and Transcription of *HXT* Genes in Chemostat Cultures of *Saccharomyces cerevisiae*. *J Biol Chem* 274, 15350–15359.
24. Doizaki, W.M., Lewitt, M.D., 1983. Gas chromatographic method for the determination of lower volatile alcohols in rat blood and in human stool specimens on a fused silica capillary column. *J Chromatogr.* 276, 11-18.
25. Dominguez, H., Rollin, C., Guyonvarch, A., Guerquin-Kern, J.L., Coccagn-Bousquet, M., Lindley, N.D., 1998. Carbon-flux distribution in the central metabolic pathways of *Corynebacterium glutamicum* during growth on fructose. *Eur. J. Biochem.* 254, 96–102.
26. Dong, J.Z., Moldoveanu, S.C., 2004. Gas chromatography-mass spectrometry of carbonyl compounds in cigarette mainstream smoke after derivatization with 2,4-dinitrophenylhydrazine. *J Chromatogr. A.* 1027, 25-35.
27. Dunn, I.J., Heinzle, E., Ingham, J., Prenosil, J.E. 2003. *Biological Reaction Engineering. Dynamic Modelling Fundamentals with Simulation Exercises.* 2<sup>nd</sup> Edition. Wiley-VCH, Weinheim.
28. Eberhardt, I., Cederberg, H., Li, H., König, S., Jordan, F., Hohmann, S., 1999. Autoregulation of yeast pyruvate decarboxylase gene expression requires the enzyme but not its catalytic activity. *Eur J Biochem.* 262, 191-201.
29. Estruch, F., Carlson, M., 1993. Two homologous zinc finger genes identified by multicopy suppression in a SNF1 protein kinase mutant of *Saccharomyces cerevisiae*. *Mol Cell Biol.* 7, 3872-3881.
30. Feldmann, H., Aigle, M., Aljinovic, G., André, B., Baclet, M.C., Barthe, C., Baur, A., Bécarn, A.M., Biteau, N., Boles, E., 1994. Complete DNA sequence of yeast chromosome II. *EMBO J.* 24, 5795-5809.
31. Fischer, E., Sauer, U., 2003. Metabolic flux profiling of *Escherichia coli* mutants in central carbon metabolism by GC-MS. *Eur J Biochem.* .270, 880-891.
32. Fischer, E., Zamboni, N., and Sauer, U. 2004. High-throughput metabolic flux analysis based on GC-MS-derived <sup>13</sup>C- constraints. *Anal Biochem.* 325, 308-321.
33. Flick, K.M., Spielewoy, N., Kalashnikova, T.I., Guaderrama, M., Zhu, Q., Chang, H.C., Wittenberg, C., 2003. Grr1-dependent inactivation of Mth1 mediates glucose-induced dissociation of Rgt1 from HXT gene promoters. *Mol. Biol. Cell.* 14, 3230–3241.
34. Frick, O., Wittmann, C., 2005. Characterization of the metabolic shift between oxidative and fermentative growth in *Saccharomyces cerevisiae* by comparative <sup>13</sup>C flux analysis. *Microb. Cell. Factories.* 4, 30-46.
35. Furukawa, K., Heinzle, E., and Dunn, I.J. 1983. Influence of oxygen on the growth of *Saccharomyces cerevisiae* in continuous culture. *Biotechnol. Bioeng.* 25, 2293-2317.

## References

---

36. Gafner, J., Schütz, M., 1996. Impact of glucose-fructose-ratio on stuck fermentations: practical experience to restart stuck fermentations. *Vitic Enol Sci.* 51, 214 - 218.
37. Gancedo, J.M., 1998. Yeast carbon catabolite repression. *Microbiol Mol Biol Rev.* 62, 334-361.
38. Gasch, A.P., Washburne, M.W., 2002. The genomics of yeast responses to environmental stress and starvation. *Funct Integr genomics.* 2, 181-192.
39. Gavin, A.C., Bösche, M., Krause, R., Grandi, P., Marzioch, M., Bauer, A., Schultz, J., Rick, J.M., Michon, A.M., Cruciat, C.M., Remor, M., Höfert, C., Schelder, M., Brajenovic, M., Ruffner, H., Merino, A., Klein, K., Hudak, M., Dickson, D., Rudi, T., Gnau, V., Bauch, A., Bastuck, S., Huhse, B., Leutwein, C., Heurtier, M.A., Copley, R.R., Edelmann, A., Querfurth, E., Rybin, V., Drewes, G., Raida, M., Bouwmeester, T., Bork, P., Seraphin, B., Kuster, B., Neubauer, G., Superti-Furga, G., 2002. Functional organization of the yeast proteome by systematic analysis of protein complexes. *Nature.* 10, 141-147.
40. Goffeau, A., Barrell, B.G., Bussey, H., Davis, R.W., Dujon, B., Feldmann, H., Galibert, F., Hoheisel, J.D., Jacq, C., Johnston, M., Louis, E.J., Mewes, H.W., Murakami, Y., Philippsen, P., Tettelin, H., Oliver, S.G., 1996. Life with 6000 genes. *Science.* 274, 563-567.
41. Gombert, A.K., Moreira, M., Christensen, B., Nielsen, J., 2001. Network identification and flux quantification in the central metabolism of *Saccharomyces cerevisiae* under different conditions of glucose repression. *J Bacteriol.* 183, 1441-1451.
42. Giaever, G., Chu, A.M., Ni, L., Connelly, C., Riles, L., Veronneau, S., Dow, S., Lucau-Danila, A., Anderson, K., Andre, B., Arkin, A.P., Astromoff, A., El-Bakkoury, M., Bangham, R., Benito, R., Brachat, S., Campanaro, S., Curtiss, M., Davis, K., Deutschbauer, A., Entian, K.D., Flaherty, P., Foury, F., Garfinkel, D.J., Gerstein, M., Gotte, D., Guldener, U., Hegemann, J.H., Hempel, S., Herman, Z., Jaramillo, D.F., Kelly, D.E., Kelly, S.L., Kotter, P., LaBonte, D., Lamb, D.C., Lan, N., Liang, H., Liao, H., Liu, L., Luo, C., Lussier, M., Mao, R., Menard, P., Ooi, S.L., Revuelta, J.L., Roberts, C.J., Rose, M., Ross-Macdonald, P., Scherens, B., Schimmack, G., Shafer, B., Shoemaker, D.D., Sookhai-Mahadeo, S., Storms, R.K., Strathern, J.N., Valle, G., Voet, M., Volckaert, G., Wang, C.Y., Ward, T.R., Wilhelmy, J., Winzeler, E.A., Yang, Y., Yen, G., Youngman, E., Yu, K., Bussey, H., Boeke, J.D., Snyder, M., Philippsen, P., Davis, R.W., Johnston, M., 2002. Functional profiling of the *Saccharomyces cerevisiae* genome. *Nature.* 418, 387-391.
43. Gorner, W., 1998. Nuclear localization of the C2H2 zinc finger protein Msn2p is regulated by stress and protein kinase A activity. *Genes Dev.* 12, 586-597.
44. Guillaume, C., Delobel, P., Sablayrolles, J.M., Blondin, B., 2007. Molecular basis of fructose utilization by the wine yeast *Saccharomyces cerevisiae*: a mutated HXT3 allele enhances fructose fermentation. *Appl Environ Microbiol.* 73, 2432 – 2439.
45. Guldener, U., Münsterkötter, M., Oesterheld, M., Pagel, P., Ruepp, A., Mewes, H.W., Stümpflen, V., 2006. MPact: the MIPS protein interaction resource on yeast. *Nucl. Acids Res.* 34, D436-D441.
46. Greatrix, B.W., Hennie, E., van Vuuren, J.J., 2006. Expression of the HXT13, HXT15 and HXT17 genes in *Saccharomyces cerevisiae* and stabilization of the HXT1 gene transcript by sugar-induced osmotic stress. *Curr Genet.* 49, 205–217.
47. Grey, M., 1996. Overexpression of ADH1 confers hyper-resistance to formaldehyde in *Saccharomyces cerevisiae*. *Curr Genet.* 29, 437-440.
48. Gross, C., Kelleher, M., Iyer, V.R., Brown, P.O., Winge, D.R., 2000. Identification of the copper regulon in *Saccharomyces cerevisiae* by DNA microarrays. *J Biol Chem.* 275, 32310-32316.

## References

---

49. Hammerle, M., Bauer, J., Rose, M., Szallies, A., Thumm, M., Dusterhus, S., Mecke, D., Entian, K.D., Wolf, D.H., 1998. Proteins of newly isolated mutants and the amino-terminal proline are essential for ubiquitin-proteasome-catalyzed catabolite degradation of fructose-1,6-bisphosphatase of *Saccharomyces cerevisiae*. *J Biol Chem.* 273, 25000-25005.
50. Haselbeck, R.J., McAlister-Henn, L., 1993. Function and expression of yeast mitochondrial NAD- and NADP-specific isocitrate dehydrogenases. *J Biol Chem.* 16, 12116-12122.
51. Haurie, V., 2001. The transcriptional activator Cat8p provides a major contribution to the reprogramming of carbon metabolism during the diauxic shift in *Saccharomyces cerevisiae*. *J Biol Chem.* 276, 76-85.
52. Hedges, D., 1995. CAT8, a new zinc cluster-encoding gene necessary for derepression of gluconeogenic enzymes in the yeast *Saccharomyces cerevisiae*. *Mol Cell Biol.* 15, 1915-1922.
53. Herrero, P., 1995. Transcriptional regulation of the *Saccharomyces cerevisiae* HXK1, HXK2 and GLK1 genes. *Yeast*, 11, 137-144.
54. Ho, Y., Gruhler, A., Heilbut, A., Bader, G.D., Moore, L., Adams, S.L., Millar, A., Taylor, P., Bennett, K., Boutilier, K., Yang, L., Wolting, C., Donaldson, I., Schandorff, S., Shewnarane, J., Vo, M., Taggart, J., Goudreault, M., Muskat, B., Alfarano, C., Dewar, D., Lin, Z., Michalickova, K., Willems, A.R., Sassi, H., Nielsen, P.A., Rasmussen, K.J., Andersen, J.R., Johansen, L.E., Hansen, L.H., Jespersen, H., Podtelejnikov, A., Nielsen, E., Crawford, J., Poulsen, V., Sørensen, B.D., Matthiesen, J., Hendrickson, R.C., Gleeson, F., Pawson, T., Moran, M.F., Durocher, D., Mann, M., Hogue, C.W., Figeys, D., Tyers, M., 2002. Systematic identification of protein complexes in *Saccharomyces cerevisiae* by mass spectrometry. *Nature.* 415, 180-183.
55. Hollemeyer, K., Velagapudi, V.R., Wittmann, C., Heinzle, E., 2007. Matrix-assisted laser desorption/ionization time-of-flight mass spectrometry for metabolic flux analyses using isotope-labeled ethanol. *Rapid Commun.Mass Spectrom.* 21, 336-342.
56. Irie, K., Takase, M., Lee, K.S., Levin, D.E., Araki, H., Matsumoto, K., Oshima, Y., 1993. MKK1 and MKK2, which encode *Saccharomyces cerevisiae* mitogen-activated protein kinase-kinase homologs, function in the pathway mediated by protein kinase C. *Mol Cell Biol.* 13, 3076-3083.
57. John, G.T., Klimant, I., Wittmann, C., Heinzle, E., 2003. Integrated optical sensing of dissolved oxygen in microtiter plates – A novel tool for microbial cultivation. *Biotechnol Bioeng.* 81, 829-836.
58. Johnston, M., 1999. Feasting, fasting and fermenting. Glucose sensing in yeast and other cells. *Trends Genet.* 15, 29–33.
59. Jungmann, J., Reins, H.A., Lee, J., Romeo, A., Hassett, R., Kosman, D., Jentsch, S., 1993. MAC1, a nuclear regulatory protein related to Cu-dependent transcription factors is involved in Cu/Fe utilization and stress resistance in yeast. *EMBO J.* 12, 5051-5056.
60. Kaniak, A., Xue, Z., Macool, D., Kim, J.H., Johnston, M., 2004. Regulatory network connecting two glucose signal transduction pathways in *Saccharomyces cerevisiae*. *Eukaryot Cell.* 3, 221-231.
61. Karpel, J.E., Place, W.R., Bisson, L.F., 2008. Analysis of the Major Hexose Transporter Genes in Wine Strains of *Saccharomyces cerevisiae*. *Am. J. Enol. Vitic.* 3, 265-275.
62. Kellis, M., Patterson, N., Endrizzi, M., Birren, B., Lander, E.S., 2003. Sequencing and comparison of yeast species to identify genes and regulatory elements. *Nature.* 423, 241-254.
63. Kiefer, P., Heinzle, E., Wittmann, C., 2002. Influence of glucose, fructose and sucrose as carbon sources on kinetics and stoichiometry of lysine production by *Corynebacterium glutamicum*. *J Ind Microbiol Biotechnol.* 28, 338-343.

## References

---

64. Kiefer, P., Heinzle, E., Zelder, O., Wittmann, C., 2004. Comparative Metabolic Flux Analysis of Lysine-Producing *Corynebacterium glutamicum* Cultured on Glucose or Fructose. *Appl. Env. Microbiol.* 70, 229-239.
65. Kleijn, R.J., van Winden, W.A., Ras, C., van Gulik, W.M., Schipper, D., Heijnen, J.J., 2006. <sup>13</sup>C-Labeled Gluconate Tracing as a Direct and Accurate Method for Determining the Pentose Phosphate Pathway Split Ratio in *Penicillium chrysogenum*. *Appl. Environ. Microbiol.* 72, 4743-4754.
66. Klockow, C., Stahl, F., Scheper, T., Hitzmann, B., 2008. In vivo regulation of glucose transporter genes at glucose concentrations between 0 and 500 mg/L in a wild type of *Saccharomyces cerevisiae*. *Journal of Biotechnology.* 135, 161–167.
67. Knapp, D.R., 1979. In *Handbook of Analytical Derivatization Reactions*, Ed.: John Wiley & Sons: New York. 26-63.
68. Ko, C.H., Liang H., Gaber, R.F., 1993. Roles of Multiple Glucose Transporters in *Saccharomyces cerevisiae*. *Mol.Cell. Biol.* 13, 638-648.
69. Kretschmer, M., Schellenberger, W., Otto, A., Kessler, R., Hofmann, E., 1987. Fructose-2,6-bisphosphatase and 6-phosphofructo-2-kinase are separable in yeast. *Biochem J.* 246, 755–759.
70. Kruckeberg, A.L., 1996. The hexose transporter family of *Saccharomyces cerevisiae*, *Arch. Microbid.* 166, 283-292.
71. Kuchin, S., Treich, I., Carlson, M., 2000. A regulatory shortcut between the Snf1 protein kinase and RNA polymerase II holoenzyme. *Proc. Natl.Acad. Sci. USA* 97, 7916–7920.
72. Kuchin, S., Vyas, V.K., Carlson, M., 2002. Snf1 protein kinase and the repressors Nrg1 and Nrg2 regulate *FLO11*, haploid invasive growth, and diploid pseudohyphal differentiation. *Mol. Cell. Biol.* 22, 3994–4000.
73. Kumar, S., Wittmann, C., Heinzle, E., 2004. Minibioreactors. *Biotechnol Lett.* 26, 1-10.
74. Kurita, O., Nishida, Y., 1999. Involvement of mitochondrial aldehyde dehydrogenase ALD5 in maintenance of the mitochondrial electron transport chain in *Saccharomyces cerevisiae*. *FEMS Microbiol Lett.* 2, 281-287.
75. Lafuente, M.J., Gancedo, C., Jauniaux, J.C., Gancedo, J.M., 2000. Mth1 receives the signal given by the glucose sensors Snf3 and Rgt2 in *Saccharomyces cerevisiae*. *Mol. Microbiol.* 35, 161–172.
76. Lesage, P., Yang, X., Carlson, M., 1994. Analysis of the SIP3 protein identified in a two-hybrid screen for interaction with the SNF1 protein kinase. *Nucleic Acids Res.* 22, 597-603.
77. Lewis, D.A., Bisson, L.F., 1991. The HXT1 gene product of *Saccharomyces cerevisiae* is a new member of the family of hexose transporters. *Mol Cell Biol.* 11, 3804–3813.
78. Li, F.N., Johnston, M., 1997. Grr1 of *Saccharomyces cerevisiae* is connected to the ubiquitin proteolysis machinery through Skp1: coupling glucose sensing to gene expression and the cell cycle. *EMBO J.* 16, 5629–5638.
79. Liang, H., Gaber, R.F., 1996. A Novel Signal Transduction Pathway in *Saccharomyces cerevisiae* Defined by Snf3-regulated Expression of HXT6. *Mol Biol Cell.* 7, 1953-1966.
80. Loftus, T.M., Hall, L.V., Anderson, S.L., McAlister-Henn, L., 1994. Isolation, characterization, and disruption of the yeast gene encoding cytosolic NADP-specific isocitrate dehydrogenase. *Biochemistry.* 32, 9661-9667.
81. Lohning, C., Ciriacy, M., 1994. The TYE7 gene of *Saccharomyces cerevisiae* encodes a putative bHLH-LZ transcription factor required for Ty1-mediated gene expression. *Yeast.* 10, 1329-1339.

## References

---

82. Luyten, K., Riou, C., Blondin, B., 2002. The hexose transporters of *Saccharomyces cerevisiae* play different roles during enological fermentation. *Yeast*. 19, 713–726.
83. Martinez-Pastor, M.T., 1996. The *Saccharomyces cerevisiae* zinc finger proteins Msn2p and Msn4p are required for transcriptional induction through the stress response element (STRE). *EMBO J.* 15, 2227-2235.
84. Massart, D.L., Vandeginste, B.G.M., Buydens, L.M.C., De Jong, S., Lewi, P.J., Smeyers-Verbeke, J., 1997. *Handbook of Chemometrics and qualimetrics: Part A*, Elsevier, Amsterdam, 94.
85. Masson, J.Y., Ramotar, D., 1996. The *Saccharomyces cerevisiae* *IMP2* Gene Encodes a Transcriptional Activator That Mediates Protection against DNA Damage Caused by Bleomycin and Other Oxidants. *Mol Cell Biol* 16, 2091-2100.
86. Masson, J.Y., Ramotar, D., 1998. The Transcriptional Activator Imp2p Maintains Ion Homeostasis in *Saccharomyces cerevisiae*. *Genetics*. 149, 893-901.
87. Mollapour, M., Fong, D., Balakrishnan, K., Harris, N., Thompson, S., Schuller, C., Kuchler, K., Piper, P.W., 2004. Screening the yeast deletant mutant collection for hypersensitivity and hyper-resistance to sorbate, a weak organic acid food preservative. *Yeast*. 21, 927-946.
88. Moriya, H., Johnston, M., 2004. Glucose sensing and signaling in *Saccharomyces cerevisiae* through the Rgt2 glucose sensor and casein kinase I. 101, 1572-1577.
89. Muller, S., Zimmermann, F.K., Boles, E., 1997. Mutant studies of phosphofructo-2-kinases do not reveal an essential role of fructose-2, 6-bisphosphate in the regulation of carbon fluxes in yeast cells. *Microbiology*. 143, 3055-3061.
90. Neef, D.W., Kladde, M.P., 2003. Polyphosphate loss promotes SNF/SWI- and Gcn5-dependent mitotic induction of PHO5. *Mol Cell Biol*. 23, 3788-3797.
91. Nehlin, J.O., Carlberg, M., and Ronne, H. 1989. Yeast galactose permease is related to yeast and mammalian glucose transporters. *Gene*. 85, 313-319.
92. Nelissen, B., 1995. Phylogenetic classification of the major superfamily of membrane transport facilitators, as deduced from yeast genome sequencing. *FEBS Lett*. 377, 232-236.
93. Oeggerli, A., Heinzle, E., 1994. On-line Exhaust Gas Analysis of Volatiles in Fermentation Using Mass Spectrometry. *Biotechnol. Prog.* 10, 284-290.
94. Oliver, S.G., Winson, M.K., Kell, D.B., Baganz, F., 1998. Systematic functional analysis of the yeast genome. *Trends Biotechnol.* 16, 373–378.
95. Ostergaard, S., Olsson, L., Nielsen, J., 2000. Metabolic engineering of *Saccharomyces cerevisiae*. *Microbiol Mol Biol Rev.* 64, 34-50.
96. Ostergaard, S., Olsson, L., Nielsen, J., 2001. In vivo dynamics of galactose metabolism in *Saccharomyces cerevisiae*: metabolic fluxes and metabolite levels. *Biotechnol Bioeng.* 5, 412-425.
97. Özcan, S., Johnston, M., 1999. Function and regulation of yeast hexose transporters. *Microbiol Mol Biol Rev.* 63, 554-569.
98. Ozcan, S., Leong, T. and Johnston, M. 1996. Rgt1p of *Saccharomyces cerevisiae*, a key regulator of glucose-induced genes, is both an activator and a repressor of transcription. *Mol. Cell. Biol.* 16, 6419-6426.
99. Ozcan, S. and Johnston, M. 1995. Three different regulatory mechanisms enable yeast hexose transporter (HXT) genes to be induced by different levels of glucose. *Mol. Cell. Biol.* 15, 1564-1572.
100. Paravicini, G., Kretschmer, M., 1992. The yeast FBP26 gene codes for a fructose-2,6-bisphosphatase. *Biochemistry*. 31, 7126-7133.

## References

---

101. Park, S.H., Koh, S.S., Chun, J.H., Hwang, H.J., Kang, H.S., 1999. Nrg1 is a transcriptional repressor for glucose repression of *STAI* gene expression in *Saccharomyces cerevisiae*. *Mol. Cell. Biol.* 19, 2044–2050.
102. Park, H., Girdaukas, G.G., 2006. Northrop DB. Effect of pressure on a heavy-atom isotope effect of yeast alcohol dehydrogenase. *J. Am. Chem. Soc.* 128, 1868-1872.
103. Perez, M., Luyten, K., Michel, R., Riou, C., Blondin, B., 2004. Analysis of *Saccharomyces cerevisiae* hexose carrier expression during wine fermentation. Both low and high affinity Hxt transporters are expressed. *FEMS Yeast Res.* 5, 351–361.
104. Petersen, S., de Graaf, A.A., Eggeling, L., Mollney, M., Wiechert, W., Sahm, H., 2000. In vivo quantification of parallel and bidirectional fluxes in the anaplerosis of *Corynebacterium glutamicum*. *J. Biol. Chem.* 75, 35932–35941.
105. Platt, A., Reece, R.J., 1998. The yeast galactose genetic switch is mediated by the formation of a Gal4p-Gal80p-Gal3p complex. *EMBO J.* 17, 4086-4091.
106. Postma, E., Verduyn, C., Scheffers, W.A., Van Dijken, J.P., 1989. Enzymic analysis of the crabtree effect in glucose-limited chemostat cultures of *Saccharomyces cerevisiae*. *Appl Environ Microbiol.* 55, 468-477.
107. Que, Q.Q., Winzeler, E.A., 2002. Large-scale mutagenesis and functional genomics in yeast. *Funct Integr Genomics.* 2, 193-198.
108. Reifengerger, E., Boles, E., Ciriacy, M., 1997. Kinetic characterization of individual hexose transporters of *Saccharomyces cerevisiae* and their relation to the triggering mechanisms of glucose repression. *Eur J Biochem.* 15, 324–333.
109. Reifengerger, E., Freidel, K., Ciriacy, M., 1995. Identification of novel *HXT* genes in *Saccharomyces cerevisiae* reveals the impact of individual hexose transporters on glycolytic flux. *Mol. Microbiol.* 16, 157- 167.
110. Rintala, E., Wiebe, M.G., Tamminen, A., Ruohonen, L., Penttilä, M., 2008. Transcription of hexose transporters of *Saccharomyces cerevisiae* is affected by change in oxygen provision. *BMC Microbiology.* 8, 53.
111. Rodriguez-Pena, J.M., Cid, V.J., Arroyo, J., Nombela, C., 1998. The YGR194c (XKS1) gene encodes the xylulokinase from the budding yeast *Saccharomyces cerevisiae*. *FEMS Microbiol Lett.* 162, 155-160.
112. Rolland, F., Winderickx, J., Thevelein, J.M., Glucose-sensing and -signalling mechanisms in yeast. *FEMS Yeast Res.* 2, 183–201.
113. Sato, T., 1999. The E-box DNA binding protein Sgc1p suppresses the *gcr2* mutation, which is involved in transcriptional activation of glycolytic genes in *Saccharomyces cerevisiae*. *FEBS Lett.* 463, 307-311.
114. Sauer, U., 2004. High-throughput phenomics: experimental methods for mapping fluxomes. *Curr Opin Biotechnol.* 15, 58-63.
115. Schmidt, M.C., McCartney, R.R., Zhang, X., Tillman, T.S., Solimeo, H., Wolfl, S., Almonte, C., Watkins, S.C., 1999. Std1 and Mth1 proteins interact with the glucose sensors to control glucose-regulated gene expression in *Saccharomyces cerevisiae*. *Mol. Cell. Biol.* 19, 4561–4571.
116. Schulz, J.M., Watson, A.L., Sanders, R., Ross, K.L., Thoden, J.B., Holden, H.M., Fridovich-Keil, J.L.J., 2004. Determinants of function and substrate specificity in human UDP-galactose 4'-epimerase. *Biol Chem.* 30, 32796-32803.
117. Schutz, M., Gafner, J., 1995. Lower fructose uptake capacity of genetically characterized strains of *Saccharomyces bayanus* compared to strains of *Saccharomyces cerevisiae*: a likely cause of reduced alcoholic fermentation activity. *Am. J. Enol. Vitic.* 46, 175-180.

## References

---

118. Sellick, C.A., Campbell, R.N., Reece, R.J., 2008. Galactose metabolism in yeast-structure and regulation of the leloir pathway enzymes and the genes encoding them. *Int Rev Cell Mol Biol.* 269, 111-150.
119. Siebert, T.E., Smyth, H.E., Capone, D.L., Neuwohner, C., Pardon, K.H., Skouroumounis, G.K., Herderich, K.H., Sefton, M.A., Pollnitz, A.P. 2005 Stable isotope dilution analysis of wine fermentation products by HS-SPME-GC-MS. *Anal Bioanal. Chem.* 381, 937-947.
120. Sil, A.K., Alam, S., Xin, P., Ma, L., Morgan, M., Lebo, C.M., Woods, M.P., Hopper, J.E., 1999. The Gal3p-Gal80p-Gal4p Transcription Switch of Yeast: Gal3p Destabilizes the Gal80p-Gal4p Complex in Response to Galactose and ATP. *Mol Cell Biol.* 19, 7828-7840.
121. Stephanopoulos, G., Aristidou, A., Nielsen, J., 1998. *Metabolic Engineering.* Academic Press, San Diego.
122. Tachibana, C., 2005. Combined global localization analysis and transcriptome data identify genes that are directly coregulated by Adr1 and Cat8. *Mol Cell Biol.* 25, 2138-2146.
123. Tangerman, A., 1997. Highly sensitive gas chromatographic analysis of ethanol in whole blood, serum, urine, and fecal supernatants by the direct injection method. *Clin. Chem.* 43, 1003-1009.
124. Thevelein, J.M., de Winde, J.H., 1999. Novel sensing mechanisms and targets for the cAMP-protein kinase A pathway in the yeast *Saccharomyces cerevisiae*. *Mol Microbiol.* 33, 904-918.
125. Toh, H., Horimoto, K., 2002. Inference of a genetic network by a combined approach of cluster analysis and graphical Gaussian modelling. *Bioinformatics.* 18, 287-297.
126. Toivari, M.H., Aristidou, A., Ruohonen, L., Penttila, M., 2001. Conversion of xylose to ethanol by recombinant *Saccharomyces cerevisiae*: importance of xylulokinase (XKS1) and oxygen availability. *Metab. Eng.* 3, 236-249.
127. Tschopp, J.F., Emr, S.D., Field, C., and Schekman, R. 1986. GAL2 codes for a membrane-bound subunit of the galactose permease in *Saccharomyces cerevisiae*. *J. Bacteriol.* 166, 313-318.
128. Valdes-Hevia, M.D., de la Guerra, R., Gancedo, C., 1989. Isolation and characterization of the gene encoding phosphoenolpyruvate carboxykinase from *Saccharomyces cerevisiae*. *FEBS Lett.* 258, 313-316.
129. Van Maris, A.J., Abbott, D.A., Bellissimi, E., van den Brink, J., Kuyper, M., Luttik, M.A., Wisselink, H.W., Scheffers, W.A., van Dijken, J.P., Pronk, J.T., 2006. Alcoholic fermentation of carbon sources in biomass hydrolysates by *Saccharomyces cerevisiae*: current status. *Antonie Van Leeuwenhoek.* 90, 391-418.
130. Van Winden, W.A., van Dam, J.C., Ras, C., Kleijn, R.J., Vinke, J.L., van Gulik, W.M., Heijnen, J.J., 2005. Metabolic-flux analysis of *Saccharomyces cerevisiae* CEN.PK113-7D based on mass isotopomer measurements of <sup>13</sup>C-labeled primary metabolites, *FEMS Yeast Res.* 5, 559-568.
131. Velagapudi, V.R., Wittmann, C., Lengauer, T., Talwar, P., Heinzle, E., 2006. Metabolic screening of *Saccharomyces cerevisiae* single knockout strains reveals unexpected mobilization of metabolic potential. *Process Biochem.* 41, 2170-2179.
132. Velagapudi, V.R., Wittmann, C., Schneider, K., Heinzle, E., 2007. Metabolic Flux Screening of *Saccharomyces cerevisiae* Single Knockout Strains on Glucose and Galactose Supports Elucidation of Gene Function. *J Biotechnol.* 132, 395-404.
133. Von Meyenburg, K., 1969. Katabolit-Repression und der Sprossungszyklus von *Saccharomyces cerevisiae*. Dissertation No. 4279, ETH, Zurich.
134. Vyas, V.K., Kuchin, S., Carlson, M., 2001. Interaction of the repressors Nrg1 and Nrg2 with the Snf1 protein kinase in *Saccharomyces cerevisiae*. *Genetics.* 158, 563-572.

## References

---

135. Waddell, P.J., Kishino, H., 2000. Correspondence analysis of genes and tissue types and finding genetics links from microarray data. *Genome Informatics*. 11, 83-95.
136. Warringer, J., Ericson, E., Fernandez, L., Nerman, O., Blomberg, A., 2003. High-resolution yeast phenomics resolves different physiological features in the saline response. *Proc Natl Acad Sci USA*. 100, 15724-15729.
137. Watts, M.T., McDonnald, O.L., 1987. The effect of biological specimen type on the gas chromatographic headspace analysis of ethanol and other volatile compounds. *Am J. Clin. Pathol.* 87, 79-85.
138. Wehner, E.P., Rao, E., Brendel, M., 1993. Molecular structure and genetic regulation of SFA, a gene responsible for resistance to formaldehyde in *Saccharomyces cerevisiae* and characterization of its protein product. *Mol Gen Genet.* 237, 351-358.
139. Weiss, A., Delproposto, J., Giroux, N.C., 2004. High-throughput phenotypic profiling of gene-environment interactions by quantitative growth curve analysis in *Saccharomyces cerevisiae*. *Anal Biochem.* 327, 23-34.
140. Westergaard, S.L., Oliveira, A.P., Bro, C., Olsson, L., Nielsen, J., 2007. A systems biology approach to study glucose repression in the yeast *Saccharomyces cerevisiae*. *Biotechnol Bioeng.* 96, 134-45.
141. Wiechert, W., Mollney, M., Petersen, S., de Graaf, A.A., 2001. A universal framework for  $^{13}\text{C}$  metabolic flux analysis. *Metab. Eng.* 3, 265-283.
142. Wiczorke, R., Krampe, S., Weierstall, T., Freidel, K., Hollenberg, C.P., Boles, E., 1999. Concurrent knock-out of at least 20 transporter genes is required to block uptake of hexoses in *Saccharomyces cerevisiae*. *FEBS Lett.* 464, 123-128.
143. Winzeler, E.A., 1999. Functional characterization of the *S. cerevisiae* genome by gene deletion and parallel analysis. *Science.* 285, 901-905.
144. Wittmann, C., Kim, H.M., Heinzle, E., 2004. Metabolic flux analysis of lysine producing *Corynebacterium glutamicum* at miniaturized scale. *Biotechnol Bioeng.* 87, 1-6.
145. Wittmann, C., Heinzle, E., 1999. Mass Spectrometry for Metabolic Flux Analysis. *Biotechnol. Bioeng.* 62, 739-750.
146. Wittmann, C., Heinzle, E., 2001(a). Novel approach for metabolic flux analysis - application of MALDI-TOF MS to lysine-producing *Corynebacterium glutamicum*. *Eur. J. Biochem.* 268, 2441-2455.
147. Wittmann, C., Heinzle, E., 2001(b). MALDI TOF MS for quantification of substrates and products in cultivations of lysine producing *Corynebacterium glutamicum*. *Biotechnol. Bioeng.* 72, 642-647.
148. Wittmann, C., Heinzle, E., 2001(c). Modeling and experimental design for metabolic flux analysis of lysine-producing corynebacteria by mass spectrometry. *Metabol. Eng.* 3, 173-191.
149. Wittmann, C., Heinzle, E., 2002. Genealogy profiling through strain improvement using metabolic network analysis – metabolic flux genealogy of several generations of lysine producing corynebacteria. *Appl. Environ. Microbiol.* 68, 5843-5859.
150. Wittmann, C., 2002. Metabolic flux analysis using mass spectrometry. *Adv. Biochem. Eng. Biotechnol.* 74: 39-64.
151. Yang, T.H., 2006. In vivo respirometric  $^{13}\text{C}$  flux analysis. Design, Modeling, Optimisation and Application. PhD thesis, Saarland University, Germany.
152. Yang, T.H., Bolten, C.J., Coppi, M.V., Sun, J., Heinzle, E., 2009. Numerical Bias Estimation for MS Mass Isotopomer Analysis. *Anal Biochem.* 388, 192-203.

## References

---

153. Yang, X., 1992. A protein kinase substrate identified by the two-hybrid system. *Science*. 257, 680-682.
154. Yang, Z., Bisson, L.F., 1996. The SKS1 protein kinase is a multicopy suppressor of the *snf3* mutation of *Saccharomyces cerevisiae*. *Yeast*. 12, 1407-1419.
155. Zamboni, N., Sauer, U., 2004. Model-independent fluxome profiling from  $^2\text{H}$  and  $^{13}\text{C}$  experiments for metabolic variant discrimination. *Genome Biol.* 5, R99.
156. Zhou, H., Winston, F., 2001. *NRG1* is required for glucose repression of the *SUC2* and *GAL* genes of *Saccharomyces cerevisiae*. *BMC Genetics*. 2, 5.

## 9. APPENDICES

### 9.1 SYMBOLS AND ABBREVIATIONS

$\mu$	Specific growth rate
$q_{O_2}$	Specific oxygen uptake rate
$q_{\text{hexose}}$	Specific hexose uptake rate
$q_{\text{ethanol}}$	Specific ethanol production rate
AcCoA	Acetyl CoA
ADP	Adenosine diphosphate
AKG	$\alpha$ -Ketoglutarate
ALA	Alanine
ARG	Arginine
ASN	Asparagine
ASP	Aspartic acid
ATP	Adenosine triphosphate
CIT	Citrate
DNA	Deoxyribonucleic acid
E4P	Erythrose-4-phosphate
F6P	Fructose-6-phosphate
FAD	Flavin adenine dinucleotide oxidised
FADH	Flavin adenine dinucleotide reduced
FUM	Fumarate
G6P	Glucose-6-phosphate
GAP	Glyceraldehyde-3-phosphate
GLC	Glucose
GLU	Glutamic acid
GLY	Glycine
HIS	Histidine
ILE	Isoleucine
LAC	Lactate
LEU	Leucine
LYS	Lysine
$K_{L,a}$	Volumetric mass transfer coefficient
MTP	Microtiter plate
NAD	Nicotinamide adenine dinucleotide oxidised
NADH	Nicotinamide adenine dinucleotide reduced
NADP	Nicotinamide adenine dinucleotide phosphate oxidised
NADPH	Nicotinamide adenine dinucleotide phosphate reduced
OAA	Oxaloacetate
OUR	Oxygen uptake rate
P5P	Pentose-5-phosphate
PG	Phosphoglycerate
PHE	Phenylalanine
PPP	Pentose phosphate pathway
PYR	Pyruvate
RNA	Ribonucleic acid
S7P	Sedoheptulose-7-phosphate
SUC	Succinate
TCA	Tricarboxylic acid
$Y_{X/S}$	Biomass yield on substrate

$Y_{E/S}$  Ethanol yield on substrate  
 $Y_{X/O}$  Biomass yield on oxygen

## 9.2 BERKELEY MADONNA PROGRAM FOR $K_LA$ ESTIMATION

{Created by Prof.Elmar Heinzle. Berkeley Madonna program for calculation of  $k_La$  using microtiter plate with integrated oxygen sensor. Oxygen removed by addition of dithionite. After consumption of dithionite which reacts rapidly with oxygen, oxygen concentration rises again}

```
DT = 0.01
DTMAX = 0.1
DTOUT = 0.1
TOLERANCE = 0.001
 $K_LA$  = 0.001 ;volumetric liquid phase mass transfer coefficient ( $h^{-1}$ )
CLS = 100 ;Saturation concentration of Oxygen (%)
init CS = 0.5 ;Initial concentration of Dithionite (mM)
k = 200 ;Rate constant for dithionite reaction
init CL = 0 ;Initial concentration of oxygen
{Oxygen balance for dithionite oxidation}
DCLDT =  $K_LA*(CLS-CL)-k*CL*CS$ 
d/dt (CL) = DCLDT
{Rate equation for dithionite oxidation}
d/dt (CS) =  $-k*CL*CS$ 
Limit CL >= 0
```

## 9.3 BERKELEY MADONNA PROGRAM FOR $Y_{X/O}$ ESTIMATION

{Created by Prof.Elmar Heinzle Yeast growth and ethanol production assumptions: 1) constant specific growth rate; 2) constant biomass yield; 3) constant ethanol yield; 4) constant  $k_La$ ; X biomass g/L; G glucose g/L; E ethanol g/L; O oxygen g/L}

```
METHOD STIFF
STARTTIME = 0
STOPTIME = 15
DT = 0.02
Tolerance = 0.0001
muem = 0.3 ; $h^{-1}$ 
KSG = 0.1 ;g/L
KS2 = 0.1 ;g/L
KSO = 7e-5 ;g/L
YXG = 0.3 ;gX/gS
Osat = 7.53e-3 ;gO/100% saturation
YEX = 0.2 ;gE/gX
revap_H2O = 1e-3 ;g/h
YXO = 1 ;gX/gO
Vinit = 0.15e-3 ;L
rho = 1000 ;g/L
kevap_E = 5.2e-6 ; $L*h^{-1}$ 
Exp_evap = 2
 $k_La$  = 1.45 ; $h^{-1}$ 
Xinit = 0.024 ;g/L
Ginit = 22 ;g/L
Einit = 0 ;g/L
Oinit = 7e-3
```

```

INIT V = Vinit
INIT XV = Xinit*Vinit
INIT GV = Ginit*Vinit
INIT EV = Einit*Vinit
INIT OV = Oinit*Vinit
INIT ENV = Einit*Vinit
rEtOH_evap = kevap_E*E^Exp_evap
V' = (-revap_H2O - rEtOH_evap)/rho
Gkin = G/(KSG+G)
Okin = O/(KSO+O)
mue = muem*Gkin*Okin
rX = mue*X
rXtot = rX*V
XV' = rXtot
X = XV/V
GV' = -rXtot/YXG
G = GV/V
qGlc = mue/YXG
EV' = rXtot*YEX - rEtOH_evap
limit EV> = 1e-10
E = EV/V
OV' = kLa*(Osat-O)*V - rXtot/YXO
limit OV> = 0
O = OV/V
Oproz = O/Osat*Kproz
Kproz = 100
ENV' = rXtot*YEX
EN = ENV/V

```

## 9.4 PROGRAM FOR ETHANOL CORRECTION

{ Created by Prof.Elmar Heinzle Yeast growth and ethanol production assumptions:

```

1) constant specific growth rate
2) constant biomass yield
3) constant ethanol yield
4) constant kla
X biomass g/L; G glucose g/L; E ethanol g/L; O oxygen g/L}
METHOD STIFF
STARTTIME = 0
STOPTIME = 30
DT = 0.02
Tolerance = 0.0001
muem = 0.3 ;h-1
KSG = 0.1 ;g/L
KSO = 7e-5 ;g/L
YXG = 0.3 ;gX/gS
Osat = 7e-3 ;gO/100% saturation
YEX = 0.2 ;gE/gX
revap_H2O = 1e-3 ;g/h
YXO = 1 ;gX/gO
Vinit = 0.15e-3 ;L
rho = 1000 ;g/L
kevap_E = 0.052 ;L*h-1

```

```

kLa = 0.246           ;h-1
Xinit = 0.024         ;g/L
Ginit = 22           ;g/L
Einit = 0             ;g/L
Oinit = 7e-3
INIT V = Vinit
INIT XV = Xinit*Vinit
INIT GV = Ginit*Vinit
INIT EV = Einit*Vinit
INIT ENV = Einit*Vinit
rEtOH_evap = kevap_E*E
V' = (-revap_H2O - (rEtOH_evap*V))/rho
Gkin = G/(KSG+G)
Okin = 1 ;O/(KSO+O)
mue = muem*Gkin*Okin
rX = mue*X
rXtot = rX*V
XV' = rXtot
X = XV/V
GV' = -rXtot/YXG
G = GV/V
qGlc = mue/YXG
EV' = rXtot*YEX -(rEtOH_evap*V)
limit EV> = 1e-10
E = EV/V
ENV' = rXtot*YEX
EN = ENV/V

```

## 9.5 MATLAB PROGRAMS FOR SOLVING CARBON MASS ISOTOPOMER DISTRIBUTIONS AND CORRECTING NATURAL ISOTOPIIC EFFECTS FOR ETHANOL

```

% - High-Level Artificial Intelligence Technology (HiLAIT) by Dr.Tae hoon Yang
% << OHmasscorr.m >> Version 1.00 .....
% - solving carbon mass isotopomer distributions for ethanol
% - Multiple measurement of ethaol MALDI-derivatives (m; m+1; m+2)
% - nonlinear least squares minimization using fmincon
% - input mat-file
%   input.mat: << MSintmat >> measured mass isotopomer intensities
% - output mat-file
%   output.mat: << mdvcorr >> carbon mass isotopomer distributions.
% - DO NOT SUPPLY NORMALIZED DATA!
% .....
echo on; disp(' ')
echo off
warning off
% 3-times clear
clear; clear globals; clear all
% molecule structure and name of GCMS fragments
load input
% check size of matrices (multiple measurement of ETOH)

```

```

[rMDV, cMDV] = size(MSintmat);
% numerical calculation MDV of carbon mass isotopomers
% structure identification
CCHONSiS = [2, 6, 9, 4, 4, 0, 0];
global sumerrcounter sumerror
sumerrcounter = 1;
% normalization
for iteration = 1: cMDV
    clear global Matcorr MDVexp sumvec1 Weight
    clear MSnorm sumvector idvcar mdvcar mdv skeleton Mcorr MDVexp xmdv
    global Matcorr MDVexp sumvec1 Weight
        sumvector = ones(1,3);
        MSnorm = MSintmat(:,iteration)/(sumvector*MSintmat(:,iteration))
% size of positional carbon isotopomer distribution
    idvcar = zeros(2^CCHONSiS(1),1);
    mdvcar = zeros(CCHONSiS(1)+1,1);
% calculation of additional mass distribution except carbon skeleton of the metabolite
    [mdv,skeleton] = mdvresidue(idvcar, CCHONSiS);
% matrix composition
    Mcorr = zeros(skeleton+1, length(mdvcar));
        for k = 1:(skeleton+1)
            Mcorr(k:(k+length(mdv)-1),k) = mdv;
        end
% experimental MDV data
    Matcorr = Mcorr(1:3,:);
% optimization process to solve carbon mass isotopomer distribution
    MDVexp = MSnorm;
    xmdv = mdveqsolver(Matcorr, MDVexp, mdvcar);
    sumerrcounter = sumerrcounter+1;
    disp('>> Difference between measured and calculated Mass Isotopomer Distribution .....')
    Difference = MDVexp - (Matcorr*xmdv/sum(Matcorr*xmdv))
    disp('.....')
% resize of xmdv to horizontal concatenation (maximum allowed carbon = 12)
    mdvcorr(:,iteration) = xmdv
end
filename = input('Filename to save results e.g. 25-OCT-04 >> ','s');
save(['output_',filename], 'mdvcorr')
copyfile('input.mat',['input_',filename,'.mat'])
clear all
warning off MATLAB:mir_warning_variable_used_as_function
warndlg = warndlg('Created By TAE HOON YANG September 2004','HiLAIT Technology');
pause(1.5)
close(warndlg)

*****
function xmdv = mdveqsolver(Matcorr, MDVexp, mdvcar);

% << mdveqsolver.m >> Version 1.00 .....
% - solving equation system of carbon mass isotopomer distributions using
%   nonlinear least-square approach.
% - High-Level Artificial Intelligence Technology (HiLAIT) by Tae hoon Yang
% .....
% Optimization to solve carbon isotopomer distributions
global sumvec1 Weight sumerrcounter sumerror

```

```

sumvec1 = ones(1,length(mdvcar));
% initial guess
if length(MDVexp) ~= length(mdvcar)
    xmdv0 = zeros(length(mdvcar),1);
else
    xmdv0 = MDVexp;
end
% linear equality constraint
Aeq = sumvec1;
beq = 1;
% lower and upper bounds
lb = zeros(length(mdvcar),1);
ub = ones(length(mdvcar),1);
for optim = 1:1
    loopstop = 0; % loopstop deactivation
    exitflag = 1; % exitflag = 1 for starting iteration
    if optim == 1
        tolX = 1e-15;
        tolfun = 1e-30;
        Weight = eye(length(MDVexp),length(MDVexp));
    end
    if optim > 1
        xmdv0 = xmdv;
        if rcond(diag(residabs)) <= 2*eps
            Weight = pinv(diag(residabs));
        else
            Weight = diag(residabs)\eye(length(MDVexp),length(MDVexp));
        end
    end
    tolerror = 1;
    flagone = 1;
    flagzero = 1;
    displaying = 'iter';
% logical loop operation (Yang et al. 2004. Met. Eng.)
while loopstop ~= 1
    % Optimization setting and function designation
    options = optim-
set('Display',displaying,'LargeScale','off','GradObj','on','TolX',tolX,'TolFun',tolfun,'TolCon',1e-100, ...
'DiffMaxChange',0.1,'DiffMinChange',1e-10,...
'MaxFunEvals',50,'MaxIter',50,...
'LevenbergMarquardt','on');
    [xmdv,fval,exitflag,output,lambda,grad] = fmin-
con(@getmdv,xmdv0,[],[],Aeq,beq,lb,ub,[],options);
    % Successful Optimization: Overwriting results
    if exitflag > 0
        % sum of mdv check
        errmdv = 0;
        sumxmdv = sum(xmdv);
        minusmdv = any(xmdv < 0);
        % Finalizing conditions
        if sumxmdv >= 1+(1e-14) | sumxmdv <= 1-(1e-14) | minusmdv ~= 0 % > 0.01 % Error of
Sum of mdv or Negativ Frequency
            errmdv = 1;
        else

```

```

    errmdv = 0;
end
if errmdv == 1
    if flagone == 1
        disp(' ')
        disp('... Please wait.. HiLAIIT is trying to isolate the system root...')
        disp(' ')
        flagzero = 1;
        flagone = 0;
        displaying = 'off';
    end
    xmdvcheck = abs(xmdv);           % no negative distribution allowed
    sumxmdv = sum(xmdvcheck);
    while abs(1-sumxmdv) >= 1e-14    % no significant digits error
        xmdvcheck = xmdvcheck/sum(xmdvcheck);
        sumxmdv = sum(xmdvcheck);
    end
    counter = 0;
    while sumxmdv ~= 1 & counter ~= 20
        xmdvcheck(1) = xmdvcheck(1) + (1-sumxmdv);
        sumxmdv = sum(xmdvcheck);
        counter = counter + 1;
    end
    disp(' ')
    disp('>>>> TOLERANCE dereased')
    tolx = tolx*0.1;
    tolfun = tolfun*0.1;
    xmdv0 = xmdvcheck;
    loopstop = 0;
    clear xmdvcheck sumxmdv
    elseif errmdv == 0
        xmdvfin = xmdv;
        disp(' ')
        disp('... System root found by HiLAIIT technology ...')
        disp(' ')
        xmdvcheck = abs(xmdv);           % no negative distribution allowed
        sumxmdv = sum(xmdvcheck);
        while abs(1-sumxmdv) >= 1e-14    % no significant digits error
            xmdvcheck = xmdvcheck/sum(xmdvcheck);
            sumxmdv = sum(xmdvcheck);
        end
        counter = 0;
        while sumxmdv ~= 1 & counter ~= 20
            xmdvcheck(1) = xmdvcheck(1) + (1-sumxmdv);
            sumxmdv = sum(xmdvcheck);
            counter = counter + 1;
        end
        xmdv = xmdvcheck;
        loopstop = 1;
        clear xmdvcheck sumxmdv
    end
elseif exitflag ~= 1
    if flagzero == 1
        disp(' ')

```

```

disp('... Lost in the space.. HiLAIIT activated...')
disp(' ')
flagone = 1;
flagzero = 0;
displaying = 'off';
end
xmdvcheck = abs(xmdv);           % no negative distribution allowed
sumxmdv = sum(xmdvcheck);
while abs(1-sumxmdv) >= 1e-14    % no significant digits error
    xmdvcheck = xmdvcheck/sum(xmdvcheck);
    sumxmdv = sum(xmdvcheck);
end
counter = 0;
while sumxmdv ~= 1 & counter ~= 20
    xmdvcheck(1) = xmdvcheck(1) + (1-sumxmdv);
    sumxmdv = sum(xmdvcheck);
    counter = counter + 1;
end
xmdv0 = xmdvcheck;
loopstop = 0;
tolerror = tolerror+1;
if tolerror > 5
    tolx = tolx*10;
    tolfun = tolfun*10;
    tolerror = 1;
end
end
end
end
residabs = abs(MDVexp -(Matcorr*xmdv/sum(Matcorr*xmdv)));
sumerror(sumerrcounter,1) = sum(residabs)
end

*****
function [mdv,skeleton] = mdvresidue(idvcar, CCHONSiS);
% << mdvresidue.m >> Version 1.0.....
% - idvcar: zero vector
% - CCHONSiS: molecular formular C[a,molecule]C[b,TBDMS]H[c]O[d]N[e]Si[f]S[g] as an array [a
b c d e f g]
% - since
% - see Rosman and Taylor (1998) Isotopic Compositions of the Elements 1997
%   Representative isotopic composition
% .....
mCarbon   = [1.2e+1;1.3003355e+1];
fCarbon   = [9.893e-1;1.07e-2]; fCarbon = fCarbon/sum(fCarbon);
mHydrogen = [1.0078250; 2.0141020];
fHydrogen = [9.99885e-1;1.15e-4]; fHydrogen = fHydrogen/sum(fHydrogen);
mNitrogen = [1.4003074e+1;1.5000109e+1];
fNitrogen = [9.9632e-1; 3.68e-3]; fNitrogen = fNitrogen/sum(fNitrogen);
mOxygen   = [1.5994915e+1;1.6999131e+1;1.7999159e+1];
fOxygen   = [9.9757e-1;3.8e-4;2.05e-3]; fOxygen = fOxygen/sum(fOxygen);
mSilicon  = [2.7976928e+1;2.8976496e+1;2.9973772e+1];
fSilicon  = [9.22297e-1;4.6832e-2;3.0872e-2]; fSilicon = fSilicon/sum(fSilicon);
mSulfur   = [32;33;34;36];
fSulfur   = [9.493e-1;7.6e-3;4.29e-2;2e-5]; fSulfur = fSulfur/sum(fSulfur);

```

```

if CCHONSiS(1) ~= 0
    for k = 1:length(idvcar)
        binind = dec2bin(k-1);
        clear mass
        for j = 1:length(binind); mass(j) = str2num(binind(j)); end
        massind(k,1) = sum(mass)+1;
    end
end
skeleton = CCHONSiS(1);
CHONSiS = CCHONSiS(2:7);
atoms = {'Carbon','Hydrogen','Oxygen','Nitrogen','Silicon','Sulfur'};
[CHONSiS, indexist] = sort(CHONSiS);
atoms = atoms(indexist);
nonzero = find(CHONSiS ~= 0);
molstructure = CHONSiS(nonzero);
isotopes = atoms(nonzero);
clear CHONSiS atoms indexist nonzero
for atomloop = 1:length(molstructure)
    if atomloop == 1
        if molstructure(atomloop) == 1
            eval(['mdv_temp = f,char(isotopes(atomloop)),',';]);
        else
            for subloop_01 = 1:molstructure(atomloop)
                if subloop_01 == 1
                    eval(['mdv_temp = f,char(isotopes(atomloop)),',';]);
                else
                    clear mdmtemp
                    eval(['mdm_temp = mdv_temp*f,char(isotopes(atomloop)),',';]);
                    clear mdv_temp
                    mdm_temp = fliplr(mdm_temp);
                    [row,col] = size(mdm_temp);
                    diagmax = col-1;
                    diagmin = 1-row;
                    diagind = fliplr([diagmin:1:diagmax]);
                    for subloop_02 = 1:length(diagind);
                        mdv_temp(subloop_02,1) = sum(diag(mdm_temp,diagind(subloop_02)));
                    end
                end
            end
        end
    end
else
    for subloop_01 = 1:molstructure(atomloop)
        clear mdm_temp
        eval(['mdm_temp = mdv_temp*f,char(isotopes(atomloop)),',';]);
        clear mdv_temp
        mdm_temp = fliplr(mdm_temp);
        [row,col] = size(mdm_temp);
        diagmax = col-1;
        diagmin = 1-row;
        diagind = fliplr([diagmin:1:diagmax]);
        for subloop_02 = 1:length(diagind);
            mdv_temp(subloop_02,1) = sum(diag(mdm_temp,diagind(subloop_02)));
        end
    end
end
end
end

```

```

end
end
mdv = mdv_temp;
clear mdv_temp;

*****
function [f,g] = getmdv(xmdv);
% << getmdv.m >> Version 1.00 .....
% - solving equation system of carbon mass isotopomer distributions using
% nonlinear least-square approach.
% - High-Level Artificial Intelligence Technology (HiLAIT) by Tae hoon Yang
% .....
global sumvec1 Matcorr MDVexp Weight
% objective function
f = (MDVexp-(Matcorr*xmdv/(sumvec1*Matcorr*xmdv)))'*Weight*(MDVexp-
(Matcorr*xmdv/(sumvec1*Matcorr*xmdv)));
% output function's derivative
Jacsys = ((Matcorr-
(Matcorr*xmdv)*(sumvec1*Matcorr)/(sumvec1*Matcorr*xmdv))/(sumvec1*Matcorr*xmdv));
if nargin > 1
% analytical gradient
g = ((Matcorr*xmdv/(sumvec1*Matcorr*xmdv))-MDVexp)'*(Weight'+
Weight)*eye(length(MDVexp),length(MDVexp))*Jacsys;
end
*****

```

## 9.6 MATLAB PROGRAM FOR FLUX CALCULATIONS

```

% Created by Dr.Tae hoon Yang
global Ndata StMat StMatex k
load inputs % save inputs StMat StMatex
% StMat: Stoichiometric matrix for intracellular fluxes
% StMatex: Stoichiometric matrix for effluxes and anabolic fluxes
disp(' ')
Ndata = input('The Number of Data Sets ? >> '); % 1
for k = 1:Ndata % putmatrix MeasMat (input qs, qp, μ, Φppp)
eval(['load meas',int2str(k)]); % save meas1 MeasMat

% MeasMat : measurement matrix
[row, col] = size(MeasMat);
% MeasVec: particular measurement vector
for kk = 1:col
MeasVec = MeasMat(:,kk);
StMat(1,1) = -1/MeasVec(4,1);
StMat(3,1) = (1-MeasVec(4,1))/MeasVec(4,1);
intflux = inv(StMat)*StMatex*MeasVec(1:3);
FluxMat(:,kk) = intflux;
clear intflux
end
FluxMat
savename = ['save result',int2str(k),' FluxMat'];
eval(savename)
clear

```

```

    global Ndata StMat StMatex k
end

```

## 9.7 PROGRAM FOR QP-GRAPH ANALYSIS

```

# Created by Dr. Jing Tang
# function for qpgraph analysis
# Input:
# data:
# The column is the one defining the random variables
# The row defines samples(conditions)
# variable_name:
# dim(variable_name) = [1 colnum]
# sample_name:
# dim(sample_name) = [1 rownum]
#source("http://bioconductor.org/biocLite.R")
#biocLite("Rgraphviz")
#library(Rgraphviz)
#setwd("d:/Obesity/data")
#data<-read.table("discordant_preprocessed.txt",header=F,sep=" ",quote="");
#data<-t(data)
#variable_name<-read.table("variable_name.txt",header=F,sep="\t",quote="");
#sample_name<-read.table("sample_name.txt",header=F,sep="\t",quote="")
#variable_name<-t(variable_name)
#sample_name<-t(sample_name)

qpgraph<-function(data, variable_name, sample_name, t)
{

  colnames(data)<-variable_name
  rownames(data)<-sample_name

  # averageNrr
  avgnrr.estimates<-qpAvgNrr(data,long.dim.are.variables=FALSE)

  g<-qpGraph(avgnrr.estimates, threshold=t, return.type="graphNEL")
  gSymbols<-g
  nodes(gSymbols)<-as.character(variable_name)

  # chech the clique number
  # browser()

  cliquenumber<-qpCliqueNumber(g)
  if(cliquenumber > dim(data)[1])
    stop("clique number larger than the sample size, pac estiamtion unreliable, try smaller
threshold")

  else {
    # browser()
    pac.estimates<-qpPAC(data,g,return.K=FALSE,long.dim.are.variable=FALSE, verbose=FALSE)
    #nrrs<-avgnrr.estimates
    #pacs.rho<-pac.estimates$R
    #pacs.pva<-pac.estimates$P
  }
}

```

```

pcc.estimates<-qpPCC(data,long.dim.are.variable=FALSE)
#pccs.rho<-pcc.estimates$R
#pccs.pva<-pcc.estimates$P

      edL<-edges(g)[names(edges(g))[unlist(lapply(edges(g),length))>0]]
edM<-matrix(unlist(sapply(names(edL),function(x)
t(cbind(x,edL[[x]])),USE.NAMES=FALSE)),ncol=2,byrow=TRUE)
edM <- matrix(as.numeric(edM), nrow=nrow(edM), ncol=ncol(edM))

idx1<-edM[,1]
idx2<-edM[,2]

nrns<-avgnrr.estimates[cbind(idx1,idx2)]
pacs.rho<-pac.estimates$R[cbind(idx1,idx2)]
pacs.pva<-pac.estimates$P[cbind(idx1,idx2)]
      pccs.rho<-pcc.estimates$R[cbind(idx1,idx2)]
      pccs.pva<-pcc.estimates$P[cbind(idx1,idx2)]

network<-
data.frame(AvgNRR=round(nrns,digits=2),PCC.rho=round(pccs.rho,digits=2),PCC.pva=format(pccs.
pva,scientific=TRUE,digit=3),PAC.rho=round(pacs.rho,digits=2),PAC.pva=format(pacs.pva,scientific=TRUE,digits=3))
networkSymbols<-network

rownames(network)<-paste(edM[,1],edM[,2],sep=" -> ")

networkSymbols[sort(networkSymbols[["AvgNRR"]],index.return=TRUE)$ix,]
summary<-network[sort(network[["AvgNRR"]],index.return=TRUE)$ix,]

edM1<-matrix(unlist(sapply(names(edL),function(x)
t(cbind(x,edL[[x]])),USE.NAMES=FALSE)),ncol=2,byrow=TRUE)
edSymbols<-
cbind(as.character(variable_name[1,edM[,1]]),as.character(variable_name[1,edM[,2]]))
rownames(networkSymbols)<-paste(edSymbols[,1],edSymbols[,2],sep=" -> ")
summary<-network[sort(network[["AvgNRR"]],index.return=TRUE)$ix,]
summarySymbols<-networkSymbols[sort(network[["AvgNRR"]],index.return=TRUE)$ix,]

write.csv(summarySymbols,"summarySymbols1.csv")
write.csv(summary,"summary1.csv")

x11()
g<-layoutGraph(g)
gSymbols<-layoutGraph(gSymbols)
graph.par(list(edges=list(col="purple")))
nodeRenderInfo(g)<-list(shape="ellipse",fill="lightgray", textCol="black", fontsize=10,lwd=1)
rownames(network)<-paste(edM[,1],edM[,2],sep="~")
edgeweight<-matrix()
for(i in 1:numEdges(g)){edgeweight[i]<-
network$AvgNRR[ which(rownames(network)==as.character(edgeNames(g)[i]))]}
names(edgeweight)<-as.character(edgeNames(g))
edgeRenderInfo(g)<-list(lwd=round(t*10-edgeweight*10))
renderGraph(g)

x11()

```

```

graph.par(list(edges=list(col="purple")))
nodeRenderInfo(gSymbols)<-list(shape="ellipse", textCol="black", fontsize=26,lwd=2)
rownames(networkSymbols)<-paste(edSymbols[,1],edSymbols[,2],sep="~")
edgeweightSymbols<-matrix()
for(i in 1:numEdges(g)){ edgeweightSymbols[i]<-
networkSym-
bols$AvgNRR[which(rownames(networkSymbols)==as.character(edgeNames(gSymbols)[i]))]}
names(edgeweightSymbols)<-as.character(edgeNames(gSymbols))
edgeRenderInfo(gSymbols)<-list(lwd=round(t*10-edgeweightSymbols*10))
renderGraph(gSymbols)

# adjacency matrix
g_adj<-as(g,"matrix")
colnames(g_adj)<-variable_name
rownames(g_adj)<-variable_name
}
}

```

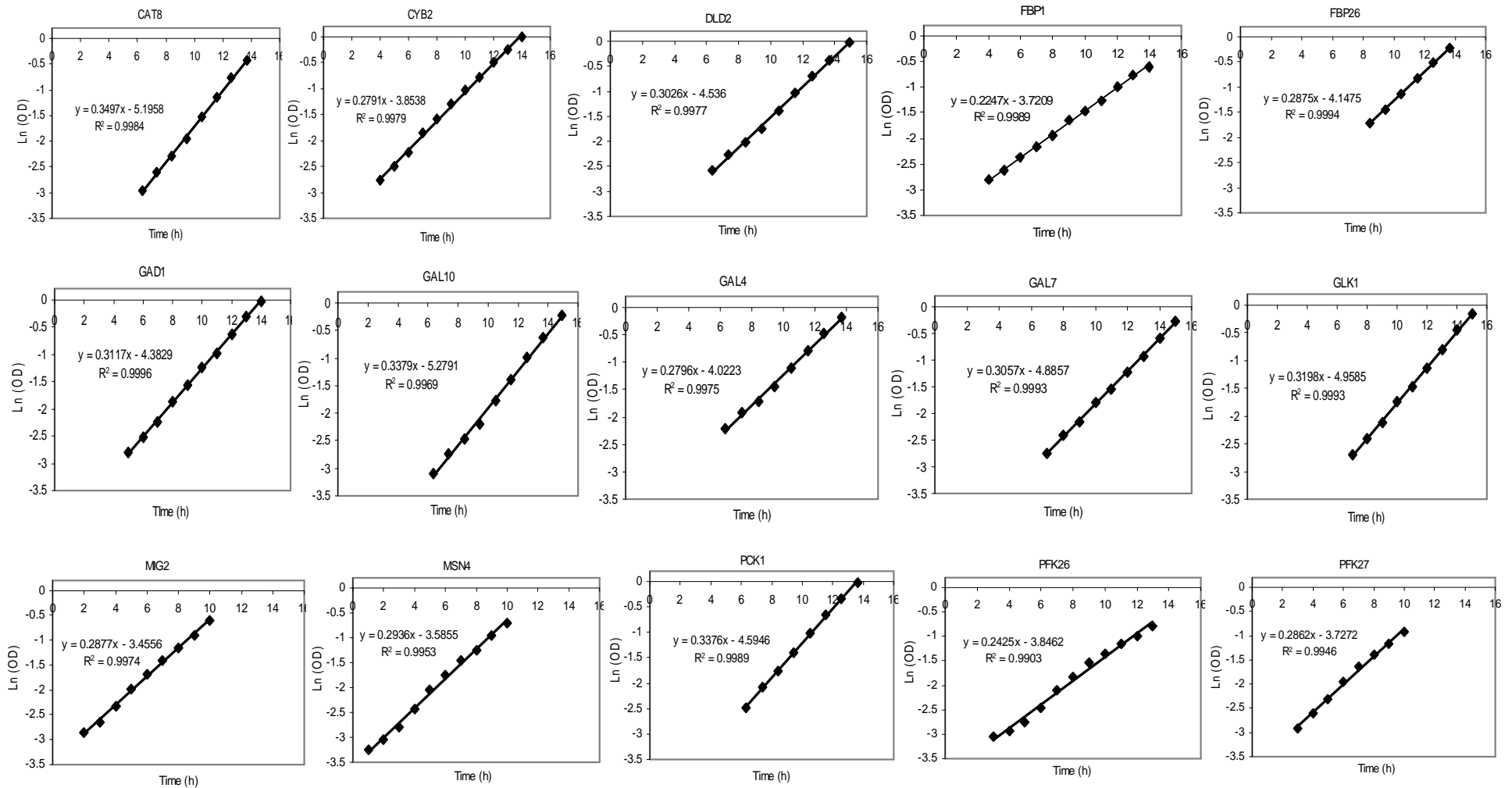
## 9.8 STOICHIOMETRIC MATRICES USED FOR METABOLIC FLUX CALCULATIONS

$$S = \begin{bmatrix} G6P \\ P5P \\ F6P \\ GAP \\ PYR \\ AcCoA \\ AKG \\ SUC \\ OAA \\ E4P \\ S7P \end{bmatrix} = \begin{bmatrix} -1 & 0 & 0 & 0 & 0 & 0 & 0 & 0 & 0 & 0 & 0 \\ 1 & 0 & 0 & 0 & 0 & 0 & 0 & -2 & 0 & -1 & 0 \\ 0 & -1 & 0 & 0 & 0 & 0 & 0 & 0 & 1 & 1 & 0 \\ 0 & 2 & -1 & 0 & 0 & 0 & 0 & 1 & -1 & 1 & 0 \\ 0 & 0 & 1 & -1 & 0 & 0 & 0 & 0 & 0 & 0 & -1 \\ 0 & 0 & 0 & 1 & -1 & 0 & 0 & 0 & 0 & 0 & 0 \\ 0 & 0 & 0 & 0 & 1 & -1 & 0 & 0 & 0 & 0 & 0 \\ 0 & 0 & 0 & 0 & 0 & 1 & -1 & 0 & 0 & 0 & 0 \\ 0 & 0 & 0 & 0 & -1 & 0 & 1 & 0 & 0 & 0 & 1 \\ 0 & 0 & 0 & 0 & 0 & 0 & 0 & 0 & 1 & -1 & 0 \\ 0 & 0 & 0 & 0 & 0 & 0 & 0 & 1 & -1 & 0 & 0 \end{bmatrix} b = \begin{bmatrix} G6P \\ P5P \\ F6P \\ GAP \\ PYR \\ AcCoA \\ AKG \\ SUC \\ OAA \\ E4P \\ S7P \end{bmatrix} = \begin{bmatrix} v_1 & v_6 & vb \end{bmatrix} \begin{bmatrix} -1 & 0 & 2.24 \\ 0 & 0 & 0.11 \\ 0 & 0 & 0 \\ 0 & 0 & 0.08 \\ 0 & 1 & 1.22 \\ 0 & 0 & 2.57 \\ 0 & 0 & 0.96 \\ 0 & 0 & 0 \\ 0 & 0 & 0.65 \\ 0 & 0 & 0.23 \\ 0 & 0 & 0 \end{bmatrix}$$

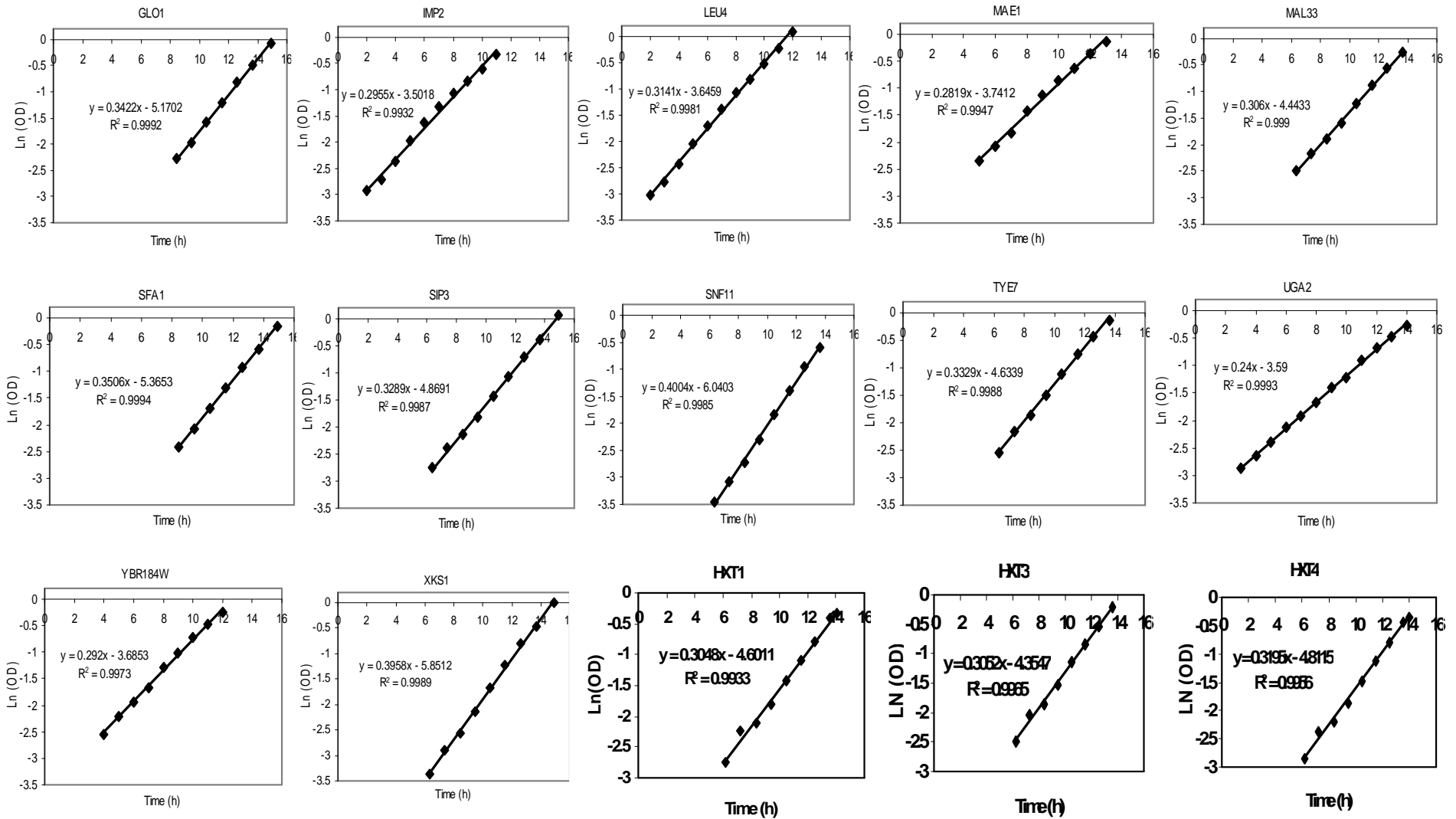
$$v = \begin{bmatrix} v_2 \\ v_4 \\ v_5 \\ v_7 \\ v_8 \\ v_9 \\ v_{10} \\ v_{11} \\ v_{12} \\ v_{13} \\ v_{14} \end{bmatrix} \text{ Vector of fluxes } - v \qquad \text{Net specific excretion rate vector } - b \text{ (Signs are changed)}$$

## 9.8 GROWTH PROFILES ON GLUCOSE

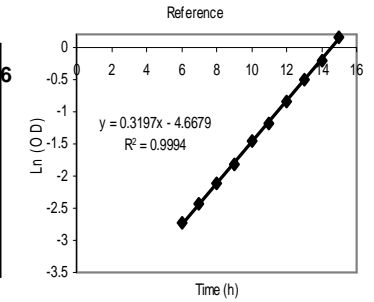
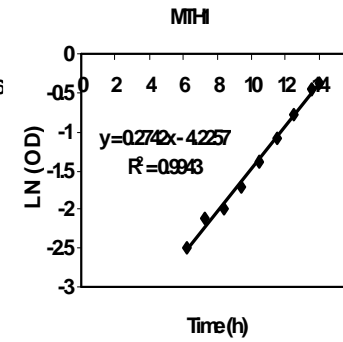
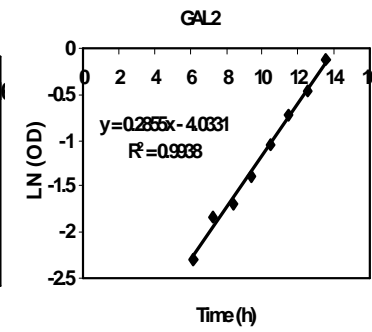
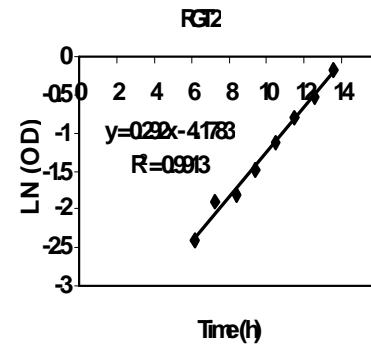
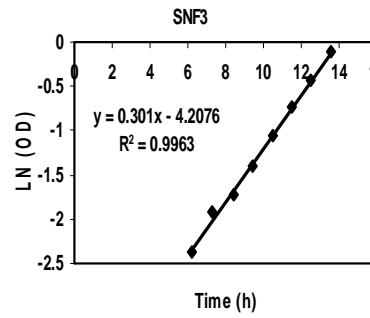
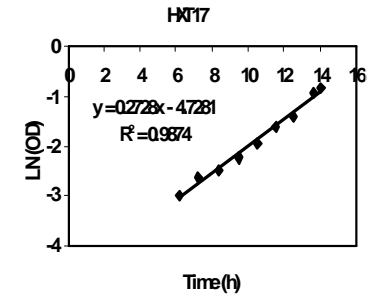
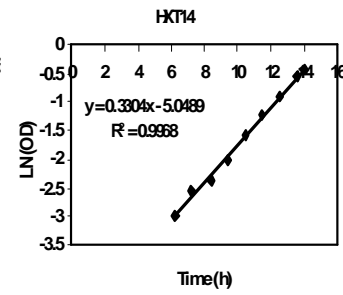
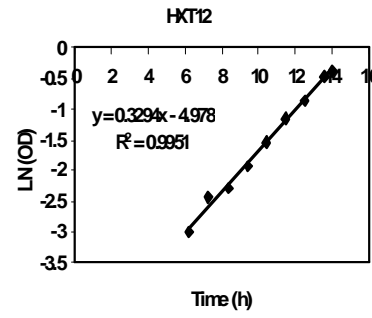
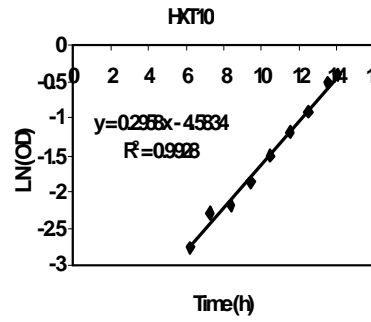
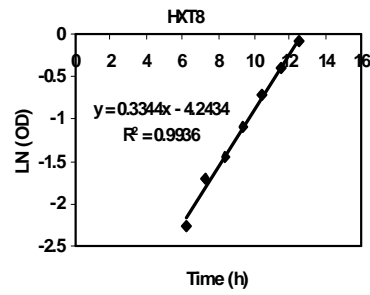
Growth profiles of *S.cerevisiae* single knockout strains grown on glucose. Mutants were cultivated in a 96-well microtiter plates with immobilized oxygen sensors. Natural log of optical density [Ln (OD)] was plotted against time [t]. Only regions with clear exponential growth are shown.



# Appendicies

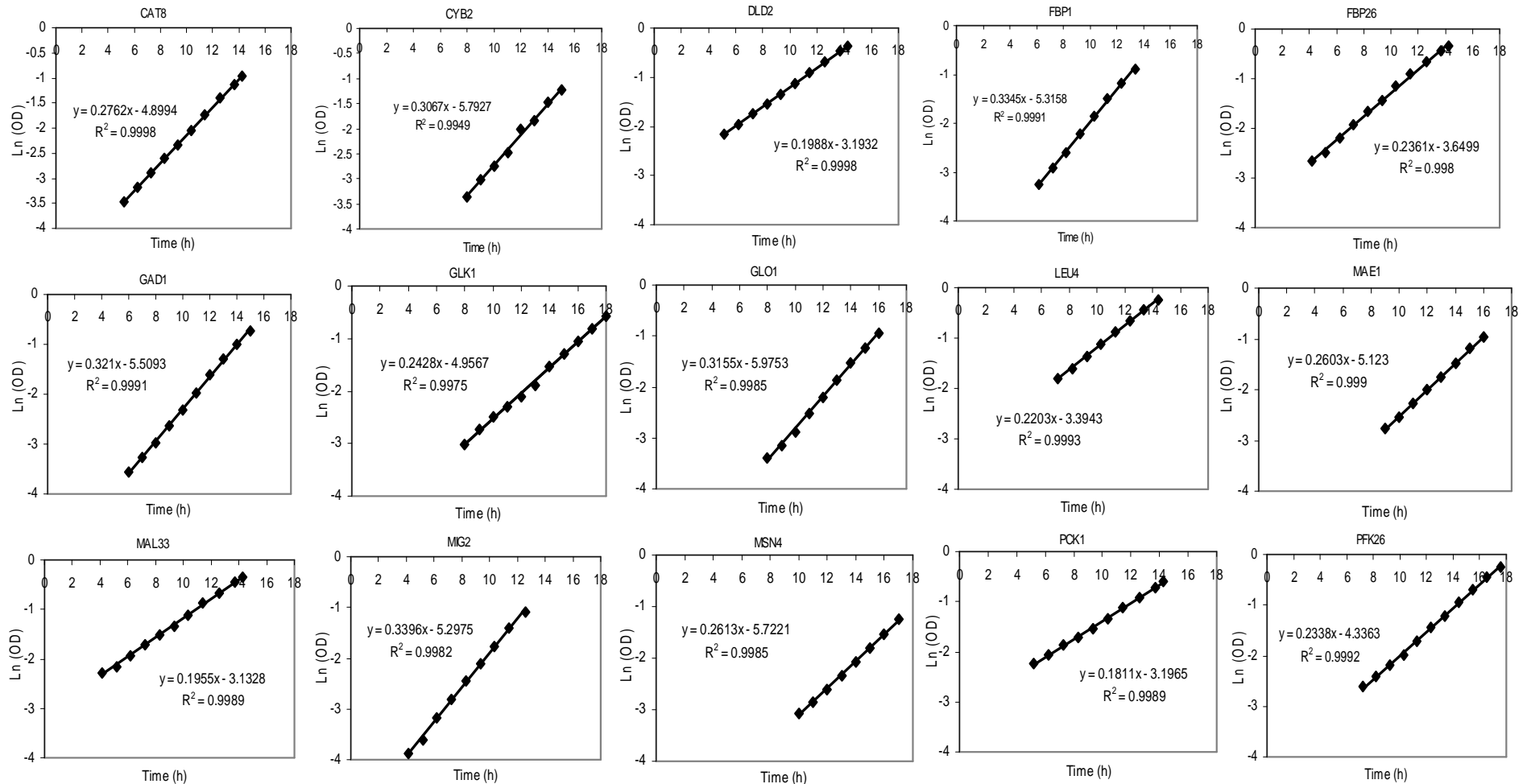


# Appendicies

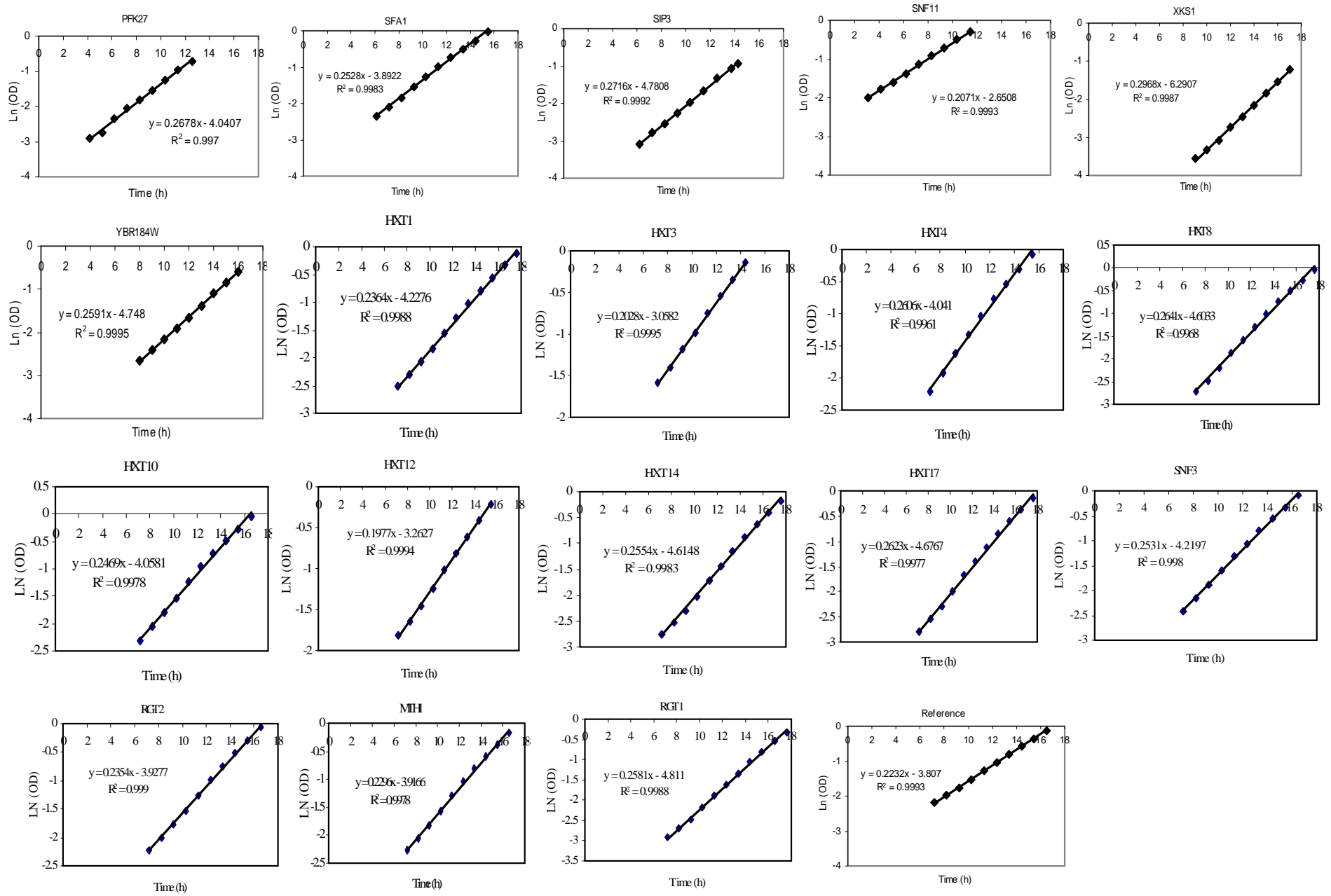


## 9.9 GROWTH PROFILES ON GALACTOSE

Growth profiles of *S.cerevisiae* single knockout strains grown on galactose. Mutants were cultivated in a 96-well microtiter plates with immobilized oxygen sensors. Natural log of optical density [Ln (OD)] was plotted against time [t]. Only regions with clear exponential growth are shown.

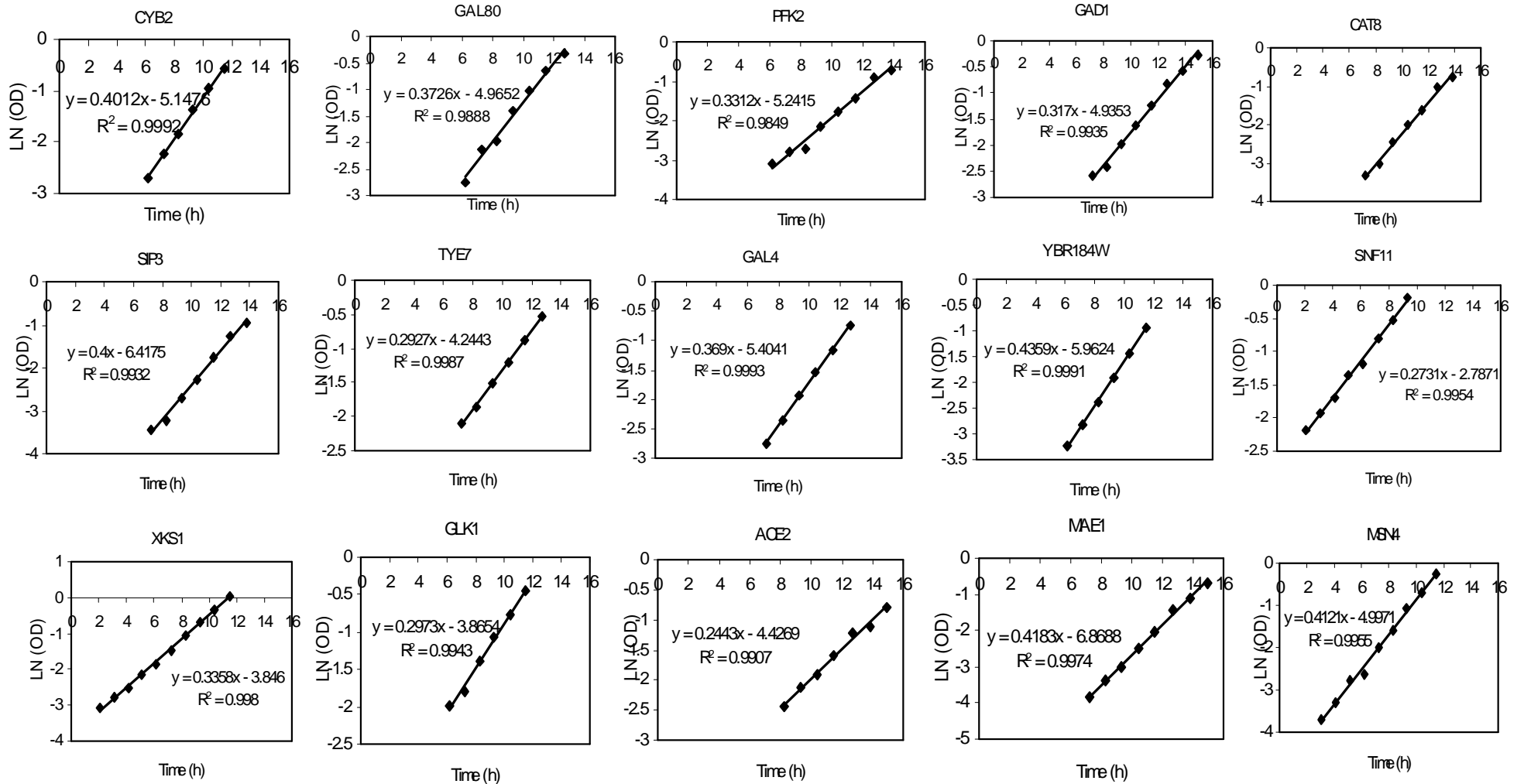


# Appendices

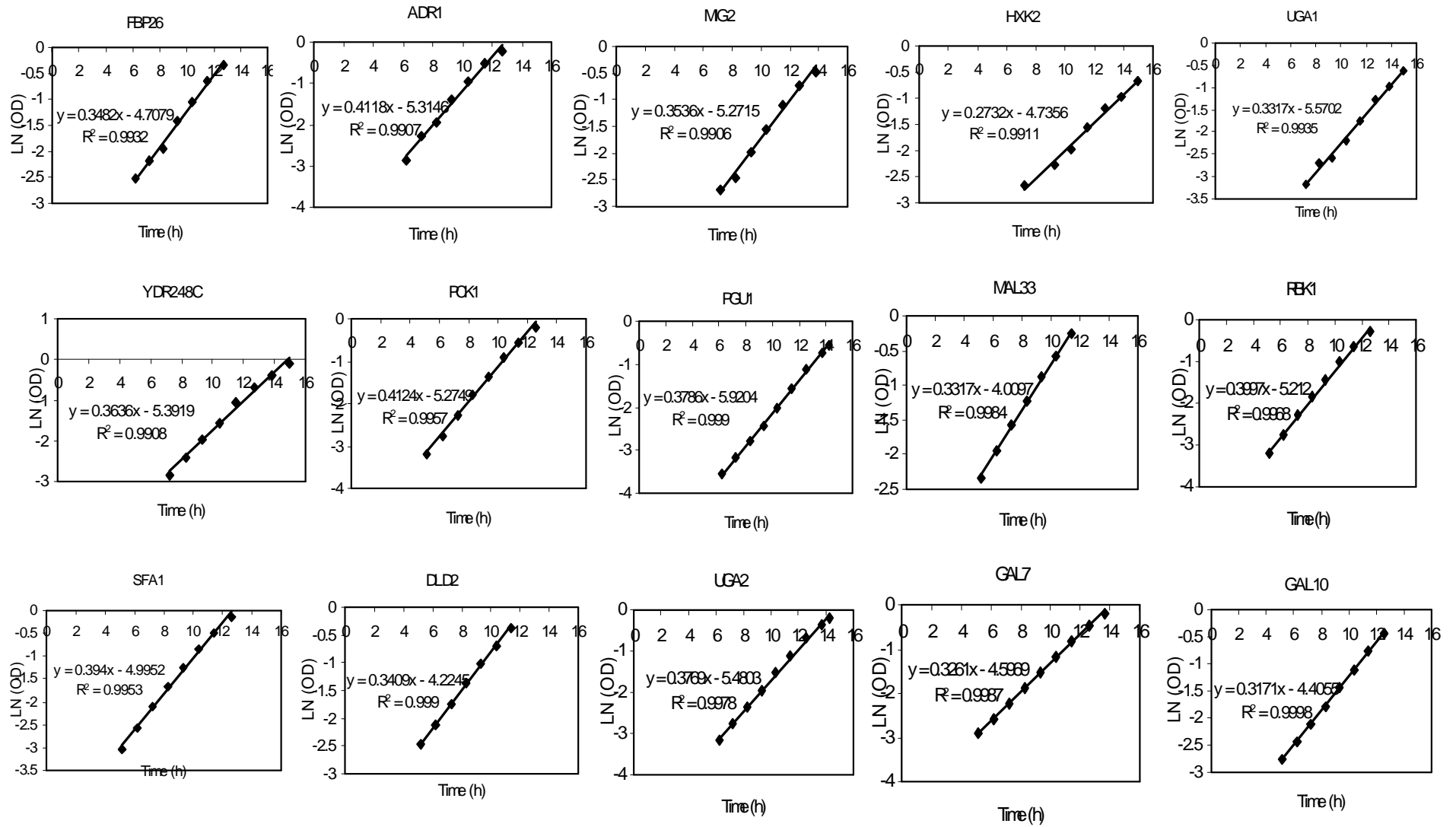


## 9.10 GROWTH PROFILES ON FRUCTOSE

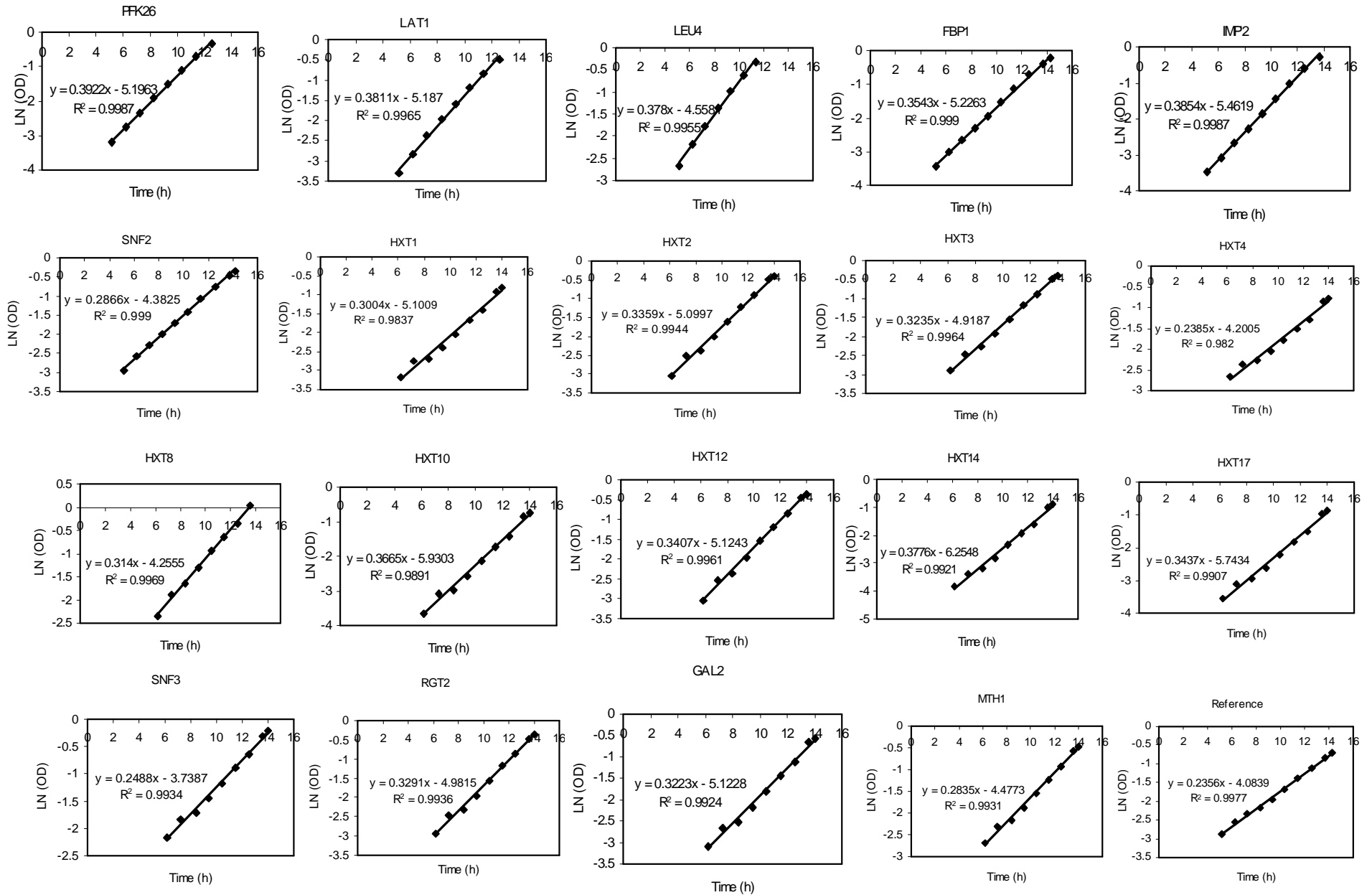
Growth profiles of *S.cerevisiae* single knockout strains grown on fructose. Mutants were cultivated in a 96-well microtiter plates with immobilized oxygen sensors. Natural log of optical density [Ln (OD)] was plotted against time [t]. Only regions with clear exponential growth are shown.



# Appendices

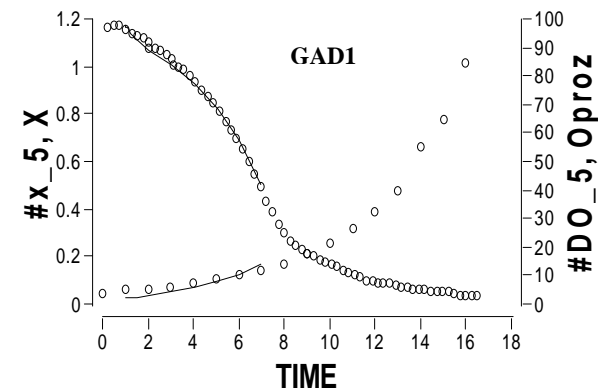
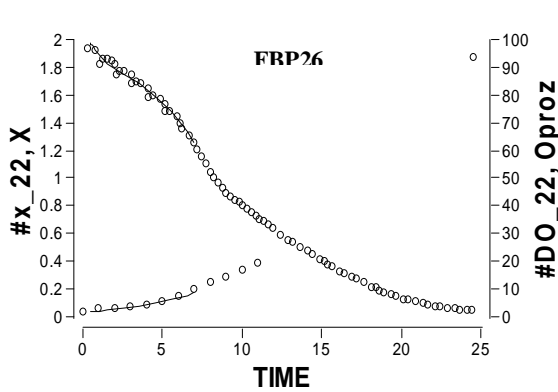
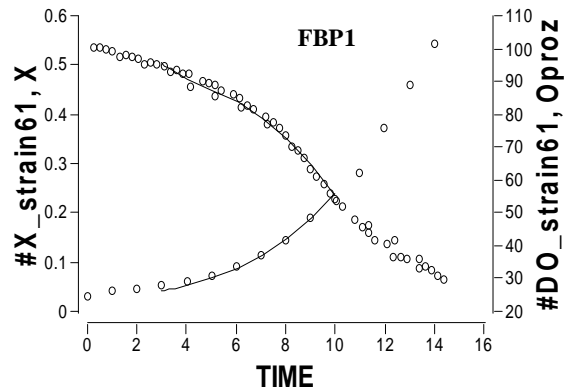
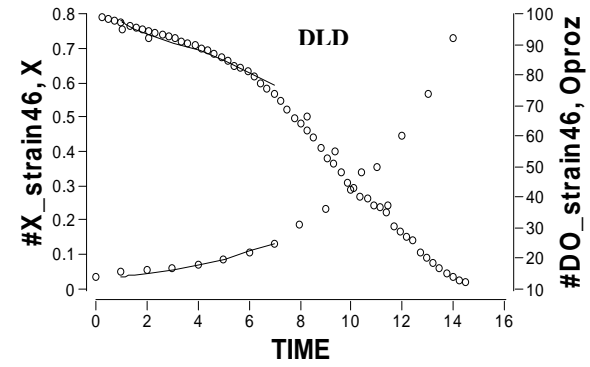
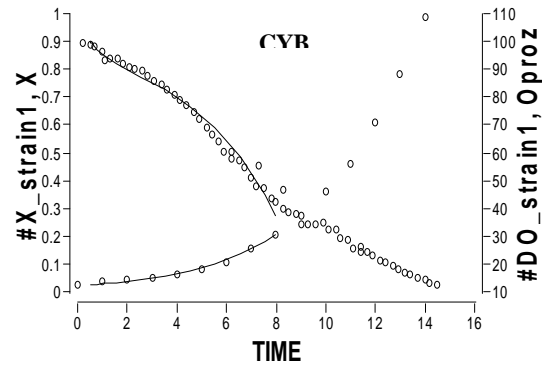
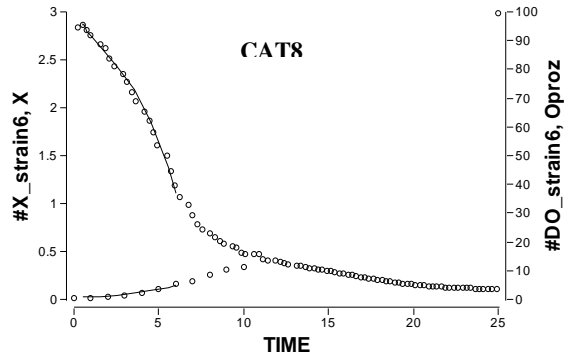


# Appendices

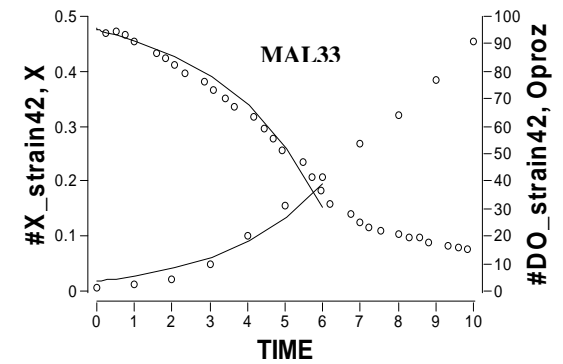
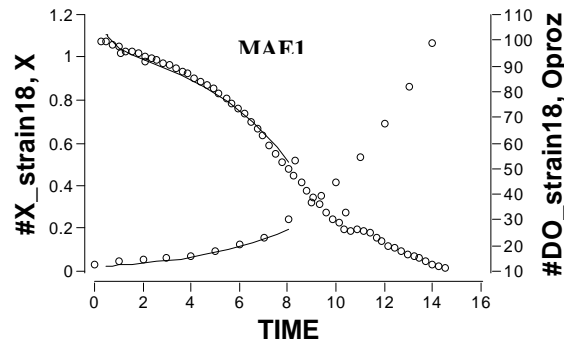
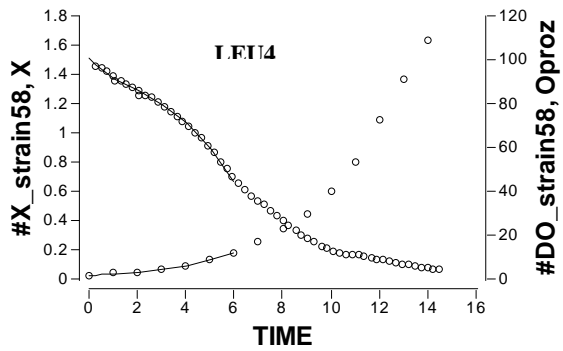
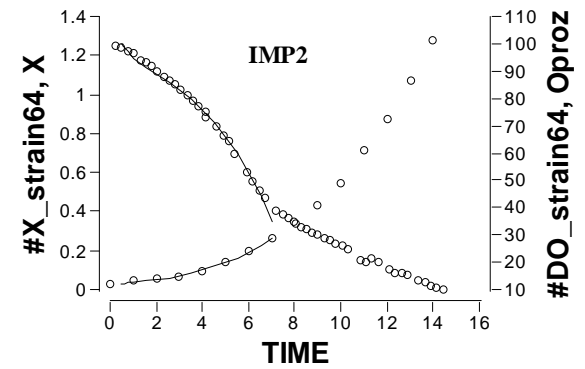
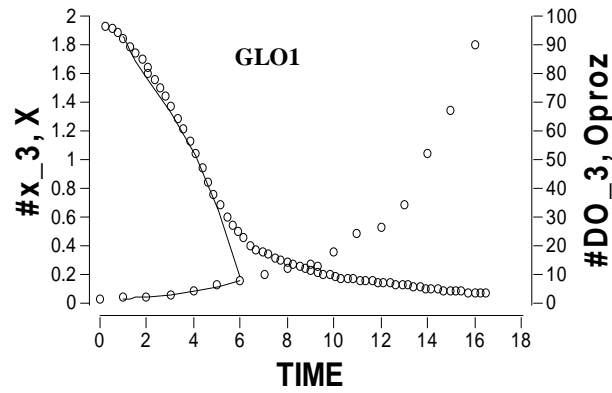
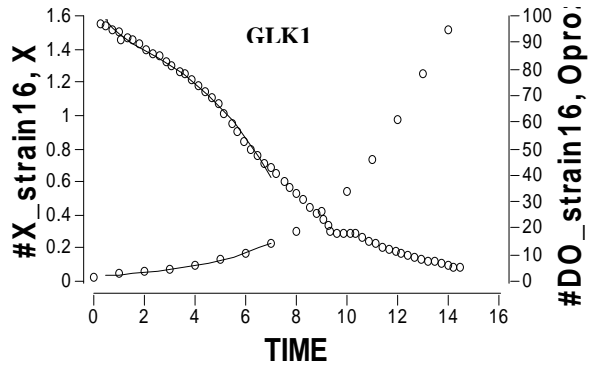
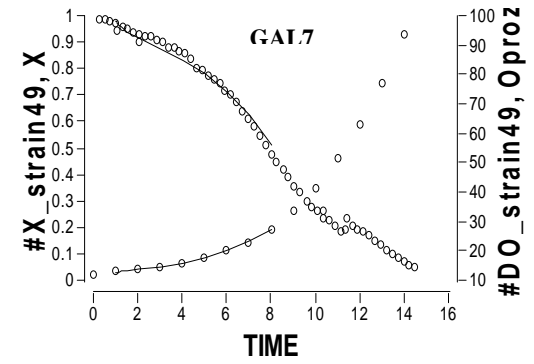
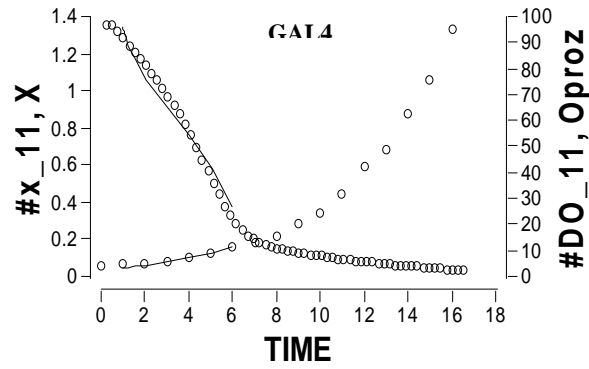
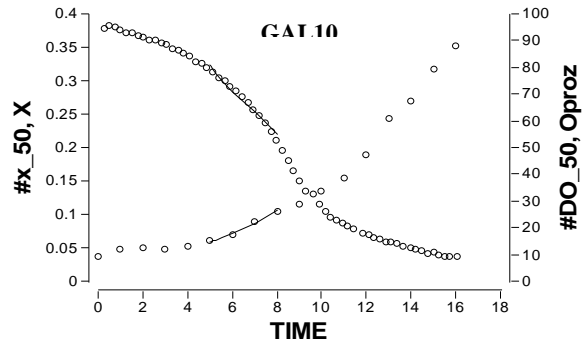


## 9.11 DISSOLVED OXYGEN PROFILES ON GLUCOSE

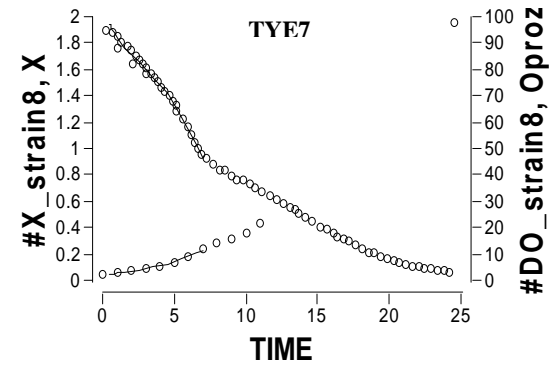
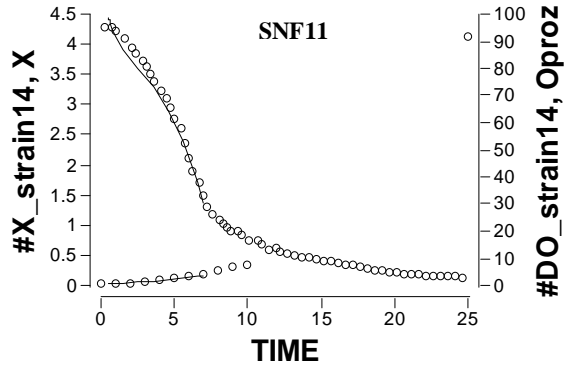
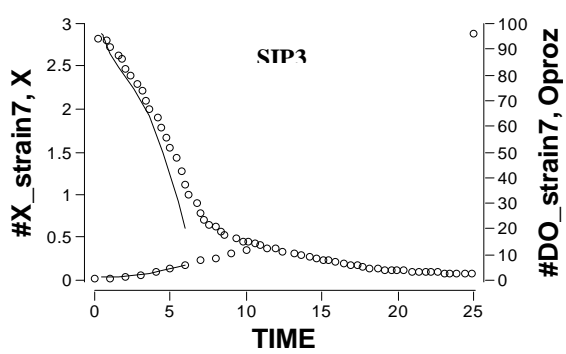
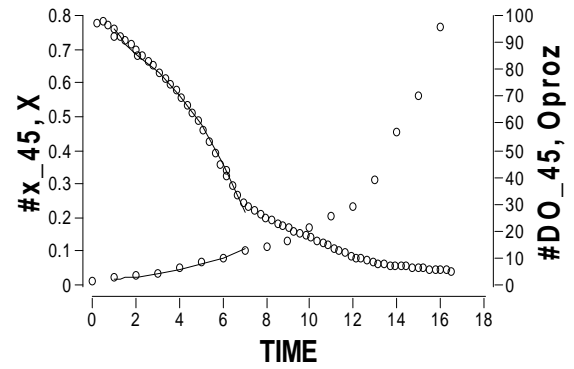
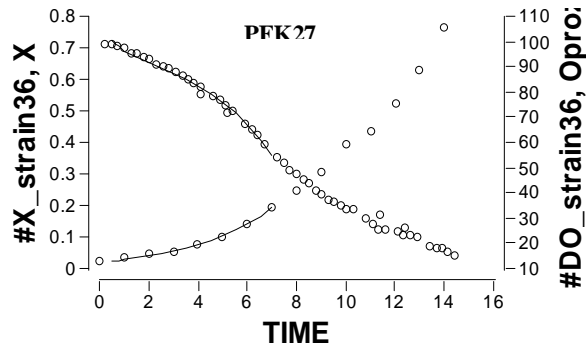
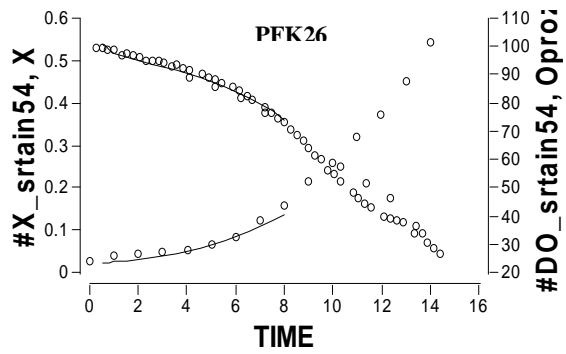
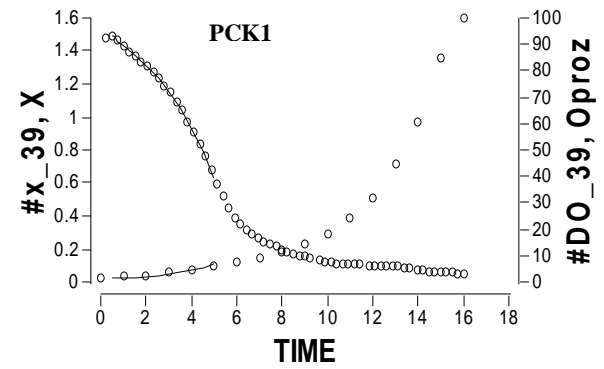
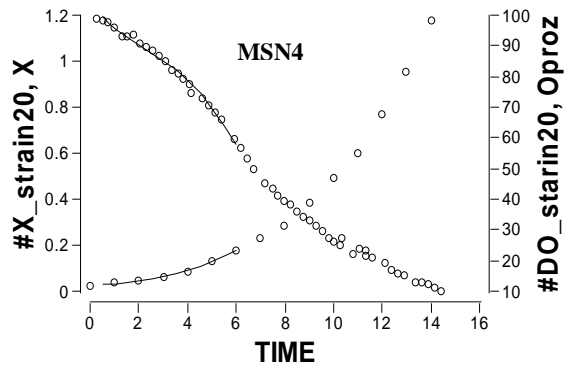
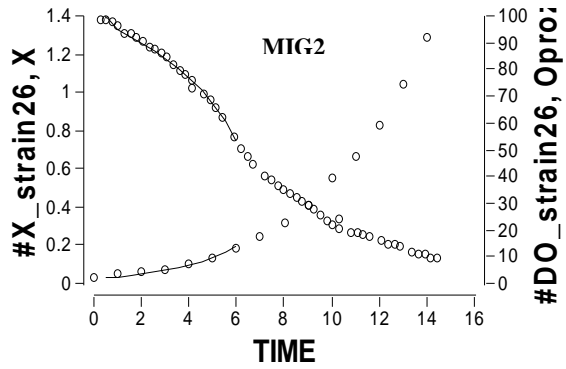
Dissolved oxygen (%) and biomass (g/L) profiles for the strains grown on glucose.

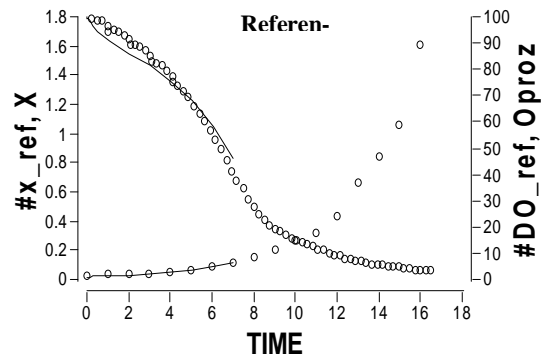
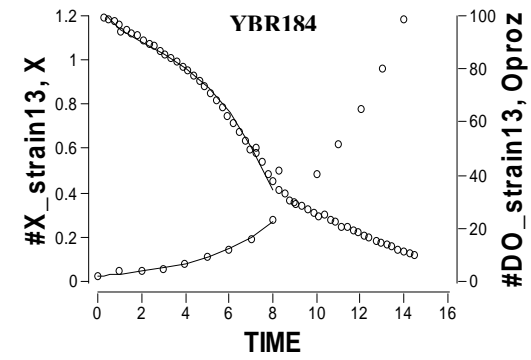
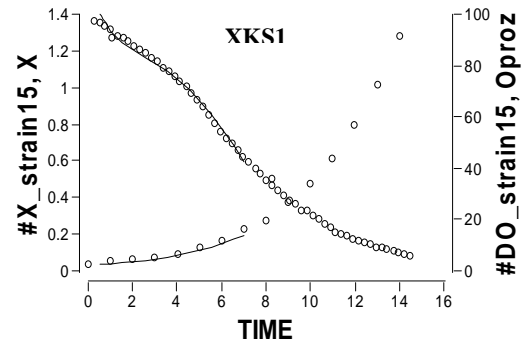
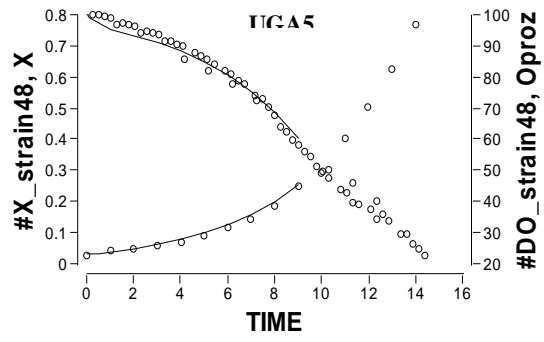


# Appendices



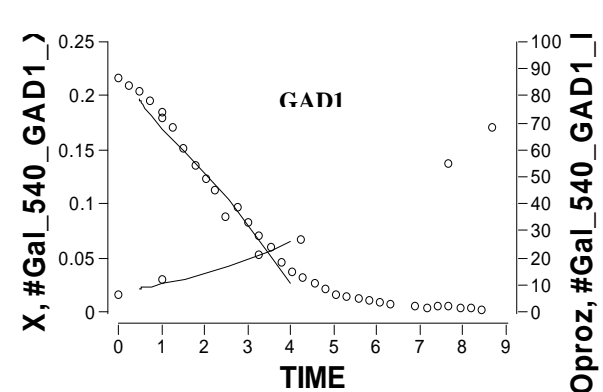
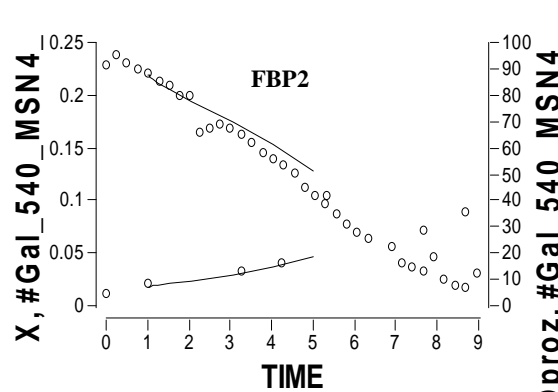
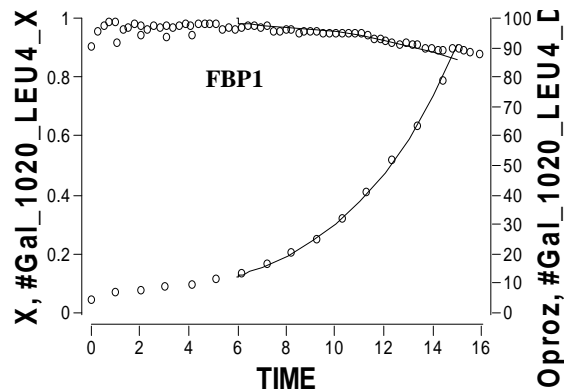
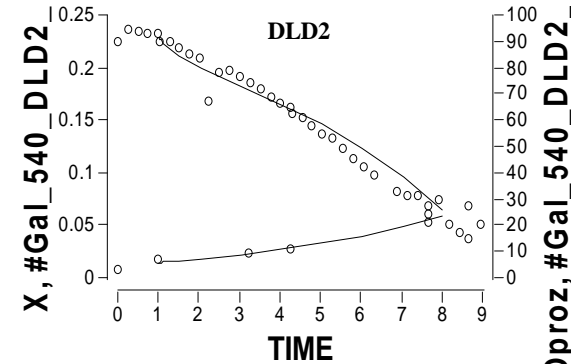
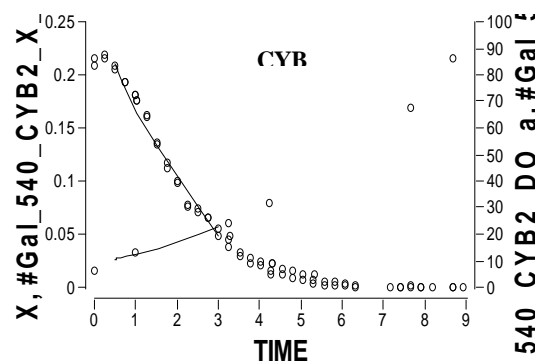
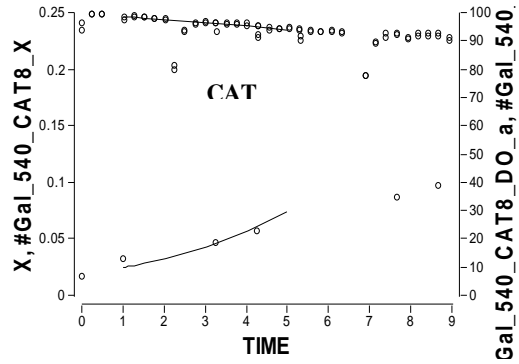
# Appendices



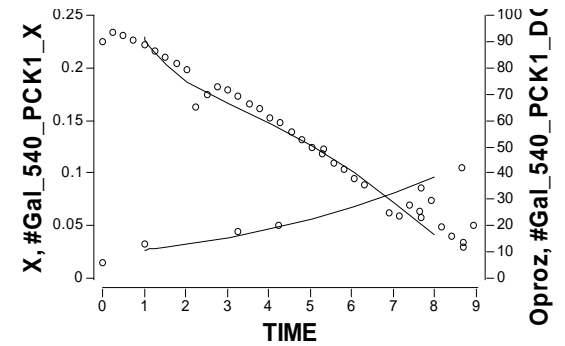
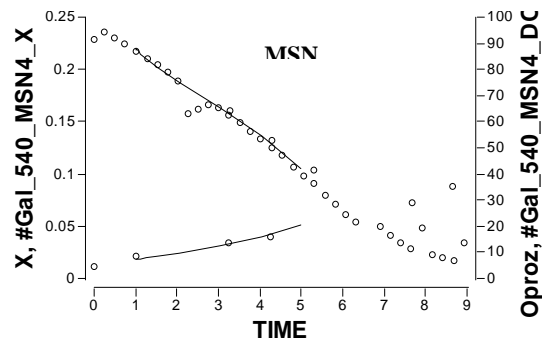
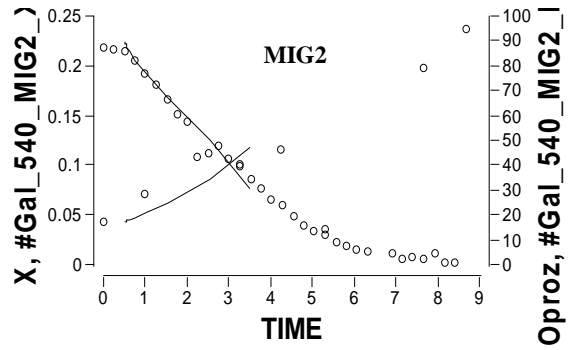
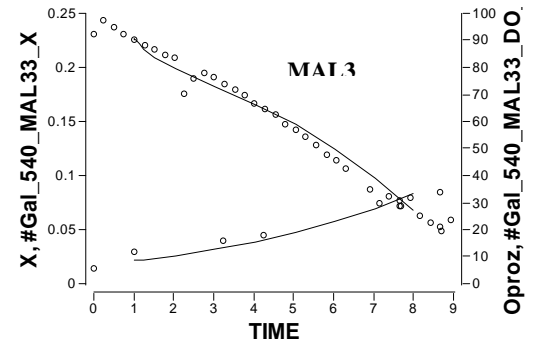
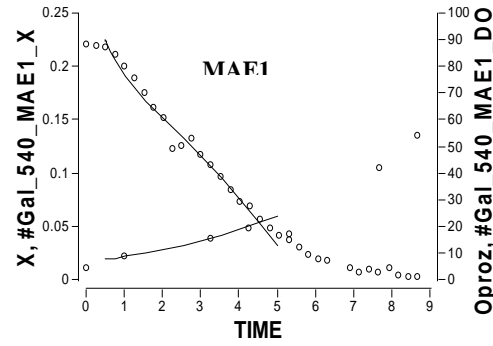
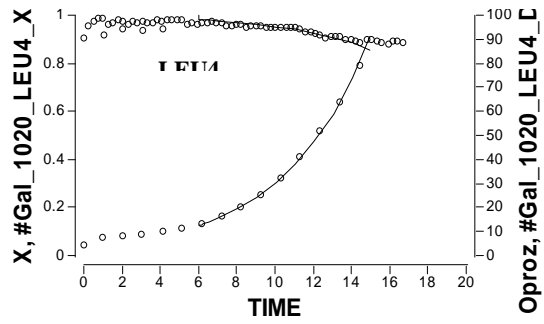
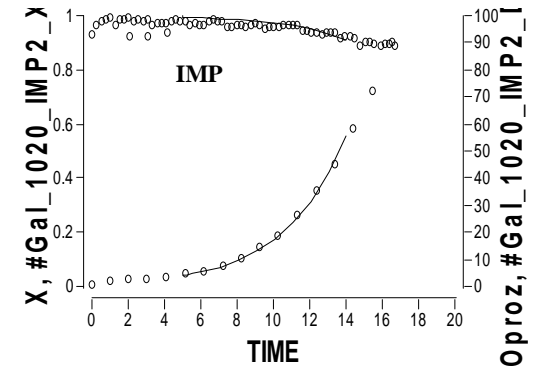
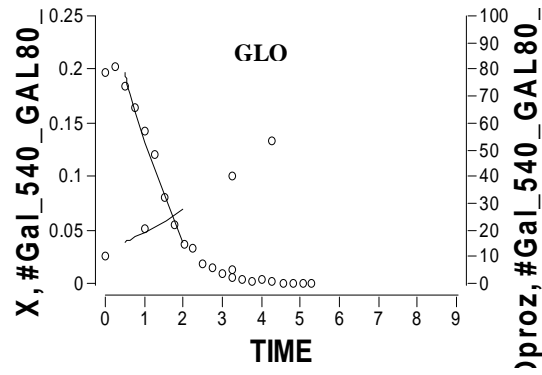
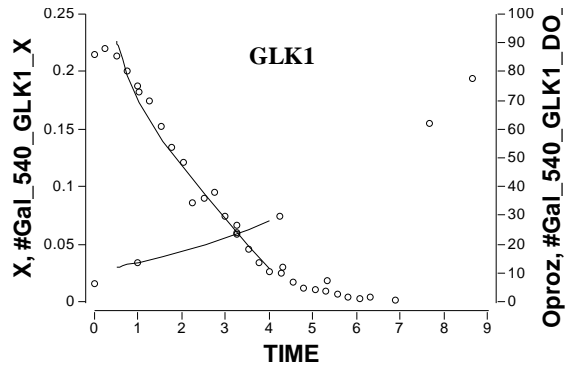


## 9.12 DISSOLVED OXYGEN PROFILES ON GALACTOSE

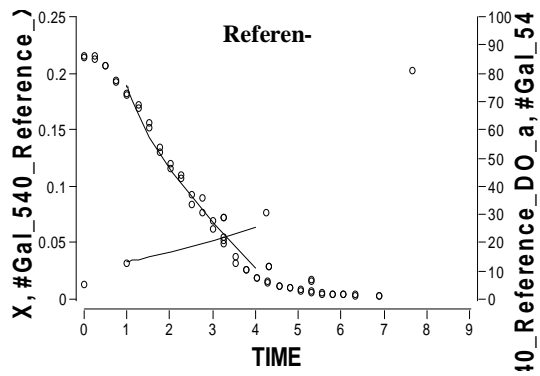
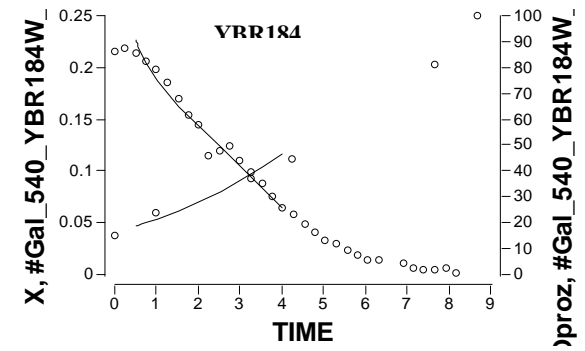
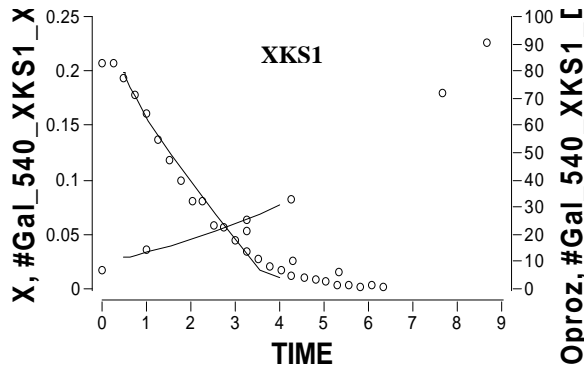
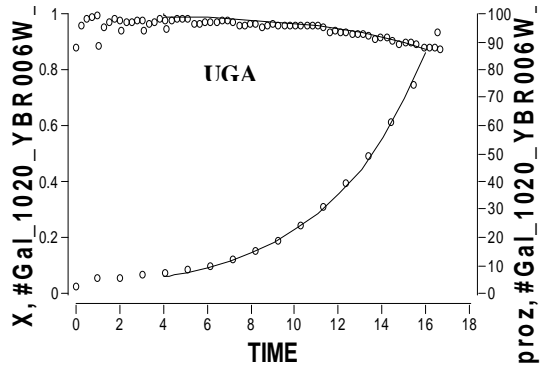
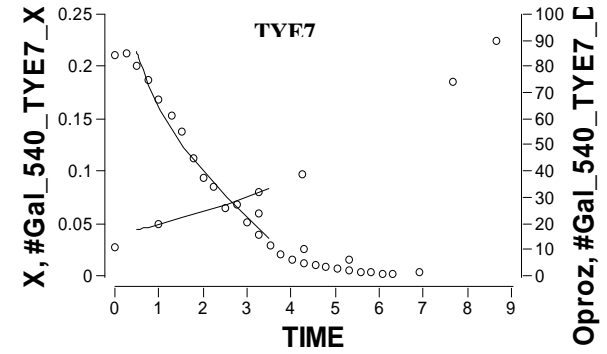
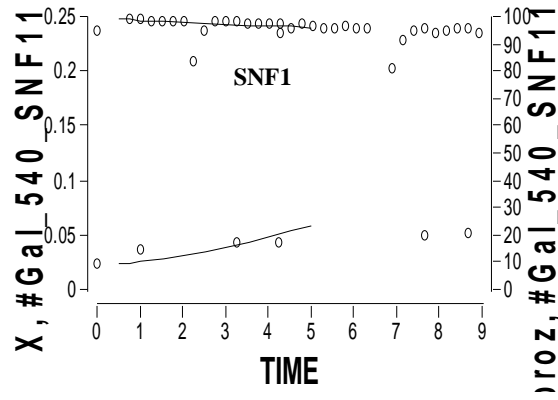
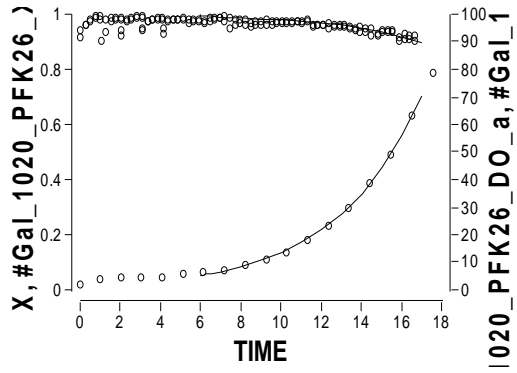
Dissolved oxygen (%) and biomass (g/L) profiles for the strains grown on galactose.



# Appendices



# Appendices



### Vidya R.Velagapudi, Ph.D

#### Contact Information

Kalakontintie – 1B-37,  
Espoo-02230, Finland  
E-mail: vidya.velagapudi@vtt.fi  
Website: <http://sysbio.vtt.fi>

#### Personal Details

Nationality: Indian  
Age: 29 yrs  
Gender: Female  
Phone: +358-40-5825754

Date: September 2009  
Status: Married (Dec, 2003)  
Children: One Girl (2 yrs)  
Fax: +358-20-7227071

#### Academic background

- 2006-2006 *PDF* at Systems Biology, QBIX group, VTT Technical Research Center of Finland (Jan – Dec) in collaboration with University of Cambridge, UK and Helsinki medical school
- 2003-2005 *Ph.D* at Applied Biochemistry, University of Saarland & Max-Planck Institute for Informatics, Saarbrücken, Germany with “*Magna cum laude*” (~ Very Good) grade
- 2001-2002 *PGDiploma* Bioinformatics from JNU, New Delhi, India with 6.5/9 CGPA ~ 71.5%
- 1999-2001 *M.Sc* Biotechnology from University of Hyderabad, Hyderabad, India with 72%
- 1996-1999 *B.Sc* Biosciences from Sri Venkateswara University, Tirupathi, India with 80%

#### Certificate courses and short-term training

- 2009 (Nov) Course on detection & characterisation of T-cells in Type 1 diabetes, Paris, France
- 2009 (Feb) Advanced course on Mass spectrometric metabolomics, Copenhagen, Denmark
- 2009 (Jan) Advanced course on Multivariate data modeling for Systems Biology, Oslo, Norway
- 2008 (July) Training course on Project Management, VTT Management/Finance team, Finland
- 2007 (Mar) Microarray data analysis using R package/Bioconductor, CSC, Espoo, Finland
- 2005 (Mar) Advanced lecture course on Systems Biology, FEBS, Gosau, Austria.

#### Professional Experience (3.5 yrs)

- 2007 - Research Scientist *cum* Project Manager at Quantitative Biology and Bioinformatics (QBIX) group, VTT Technical Research Center of Finland, Espoo, Finland (Jan – )
- 2002 - 2002 Research Associate in Proteomics group, Bioinformatics division, Zenovus Biotech Limited, Dr. Reddy's Laboratories, Hyderabad, India (June – Dec)

#### Academic Research Experience (5.5 yrs)

- *PDF project* (Jan 2006 - Dec 2006)  
Comprehensive metabolomic characterization of lipoproteins in insulin resistance and normal subjects
- *Ph.D thesis* (Jan 2003 - Dec 2005)  
Physiological and metabolic flux screening of *S. cerevisiae* mutants on different carbon sources
- *PGDiploma thesis* (Jan - May 2002)  
Statistical characterization of complete microbial genomes
- *Masters thesis* (July 2000 - Apr 2001)  
Screening for phosphate solubilising activity of Rhizobacteria and cloning one Rhizobacterial isolate
- *Summer project* (May - July 2000)  
Sugar transport defective mutants of *S. pombe*: Analysis of genomic and cDNA clones

#### Teaching Experience (6 months)

- 2003-2005 Supervisor to under-graduate and post-graduate students in a Biochemistry practical course at Biochemical Engineering Institute, University of Saarland, Germany.

#### Fellowships

- 2006- Post Doctoral Fellowships from EU FP6 and FP7 and Human Frontier Science organization (HFSO) through VTT Technical Research Center of Finland, Espoo.
- 2003-2005 Doctoral Fellowship from Center for Bioinformatics under BioSapiens project FP6 programme and Deutsche Forschungsgemeinschaft

- 2000-2000 Visiting Student Research Program Fellowship (VSRP-2000) from Tata Institute of Fundamental Research (TIFR), Mumbai, India during summer internship
- 1999-2002 Merit Fellowships from Department of Biotechnology, India during both Masters degree and Advanced Postgraduate Diploma in Bioinformatics (PGDiploma)

### Awards, Grants and Academic Achievements

- Award for Merit - 2008 (Cash prize & Certificate) for excellent collaborative work in establishment of Systems Biology platform at VTT Technical Research Centre of Finland, Finland
- Award for Merit - 2007 (Hike in salary & Certificate) for exceptionally well performed project work at VTT Technical Research Centre of Finland, Finland.
- Young post-doctoral scientist grant to attend first focused “FutureSysBio” workshop, Nov 19<sup>th</sup> - 21<sup>st</sup>, 2008 Gothenburg, Sweden.
- Young scientist bursary scheme award to attend “Genomes to systems” conference, Mar 22<sup>nd</sup> - 24<sup>th</sup>, 2006 Manchester, UK.
- Graduate Student grants to attend 5<sup>th</sup> European Symposium on Biochemical Engineering Science (ESBES), Sep 8<sup>th</sup> -11<sup>th</sup>, 2004 Stuttgart, Germany.
- Selected in All India National level entrance for 2 months summer internship in Tata Institute of Fundamental Research (TIFR), Center for DNA fingerprinting and diagnosis (CDFD) and International Crops Research Institute for the Semi-Arid Tropics (ICRISAT), India (2000).

### Professional Activities

- Visiting Scientist in Metabolic Research Laboratories, University of Cambridge, UK - Nov 2009.
- Coordinator for Metabolomics for clinical research training course at VTT, Finland, Oct 2009
- Member in Metabolomics Society, MA, USA.
- Member in “The Biobio Society”, Helsinki, Finland.
- Member in international research organizations- FEBS, FEMS, IUBMB, IUMS, IUPAB, EBSA

### Technical Expertise

<i>Analytical</i>	Mass spectrometry (UPLC-MS/MS [QToF]; LC-MS, GC-MS; GC-FID; GCxGC-ToF-MS, MALDI-TOF-MS; HPLC), Spectrophotometry; Fluorescence and Absorbance Readers; Chromatography (Affinity, Paper, TLC and Gel Filtration);
<i>Fermentation</i>	Microtiter plate and Shake flask cultivation techniques
<i>Proteomics</i>	Protein extraction and quantification; 2-D-, SDS-, native- PAGE; IEF
<i>Molecular Biology</i>	Plasmid and Genomic DNA isolation; Cloning; PCR; Transformation of Bacteria, Transfection, Agarose Gel Electrophoresis; Western blotting
<i>Tissue Culture</i>	Basic animal tissue culture techniques; Maintenance of Cell Lines; Plant tissue culture techniques- Callus production, Artificial seed synthesis

### Computational Skills

<i>Bioinformatics:</i>	Multivariate & Univariate analyses, Clustering & Regression analyses
<i>Softwares:</i>	MATLAB, PERL, C, R/Bioconductor, MySQL RDBMS,
<i>Platforms:</i>	MS Windows, XP, MS Office and Linux

### Publications (\* Joint Authors)

#### Research Articles

10. López, M., Varela, L.,\* **Velagapudi, V.R.**,\* Lage, R., Vázquez, M.J., Tovar, S., Rodríguez-Cuenca, S., Gonzalez, C.R., Martinez de Morentin, P.B., Nogueiras, R., Carling, D., Lelliott, C.J., Saha, A.K., Orešič, M., Diéguez C., Vidal-Puig, A., 2009. Dysregulation of hypothalamic AMPK and fatty acid metabolism mediates hyperthyroidism-induced alterations in energy balance. *Nature Medicine*. (Submitted)

9. **Velagapudi, V.R.**, Hezaveh, R., Reigstad, C., Peddinti, G.V., Felin, J., Yetukuri, L., Mattila, I., Borén, J., Orešič, M., Bäckhed, F., 2009. The gut microbiota as a global modulator of host metabolism. *Molecular Systems Biology*. (Submitted)
8. Medina-Gomez, G., Yetukuri, L., **Velagapudi, V.R.**, Campbell, M., Jimenez-Linan, M., Blount, M., Ros, M., Orešič, M., Vidal-Puig, A., 2009. Early mechanisms of beta cell adaptation and failure in the insulin resistant ob/ob and POKO mice. *Disease Models and Mechanisms*. (In Press)
7. Kotronen, A.,\* **Velagapudi, V.R.**,\* Yetukuri, L., Westerbacka, J., Bergholm, R., Ekroos, K., Makkonen, J., Taskinen, M.R., Orešič, M., Yki-Järvinen, H., 2009. Saturated fatty acids containing triglycerides are better markers of insulin resistance than total serum triglyceride concentrations. *Diabetologia*. 52, 684-690.
6. Peddinti, G.V.,\* **Velagapudi, V.R.**,\* Lindfors, E., Halperin, E., Oresic, M., 2009. Dynamic network topology changes in functional modules predict responses to oxidative stress in yeast. *Molecular BioSystems*. 5, 276-287.
7. **Velagapudi, V.R.**, Wittmann, C., Schniden, K., Heinzle, E., 2007. Metabolic Flux Screening of *Saccharomyces cerevisiae* Single Knock-out Strains on Glucose and Galactose Supports Elucidation of Gene Function. *Journal of Biotechnology*. 132, 395-404.
4. Sysi-Aho, M., Vehtari, A., **Velagapudi, V.R.**, Westerbacka, J., Yetukuri, L., Bergholm, R., Taskinen, M.R., Yki-Järvinen, H., Orešič, M., 2007. Predicting the lipoprotein composition using Bayesian regression on serum lipidomic profiles. *Bioinformatics*. 23, i519 – i528.
3. Kolak, M\*., Westerbacka, J\*., **Velagapudi, V.R.**, Wågsäter, D., Yetukuri, L., Makkonen, J., Rissanen, A., Häkkinen, A.M., Lindell, M., Hamsten, A., Eriksson, P., Fisher, R.M., Orešič, M., Yki-Järvinen, H., 2007. Adipose Tissue Inflammation And Increased Ceramide Content Characterize Subjects with High Liver Fat Content Independent of Obesity. *Diabetes*. 56, 1960.
2. Hollemeyer, K., **Velagapudi, V.R.**, Wittmann, C., Heinzle, E., 2007. Matrix-assisted laser desorption/ionization time-of-flight mass spectrometry for metabolic flux analyses using isotope-labeled ethanol. *Rapid Communications in Mass Spectrometry*. 21, 336-342.
1. **Velagapudi, V.R.**, Wittmann, C., Lengauer, T., Talwar, P., Heinzle, E., 2006. Metabolic Screening of *Saccharomyces cerevisiae* Single Knock-out Strains Reveals Unexpected Mobilization of Metabolic Potential. *Process Biochemistry*. 41, 2170-2179.

### Conference Talks

5. **Velagapudi, V.R.**, (2009) Microbial regulation of host physiology. In: Academy of Finland's Annual seminar in Research Programme on Nutrition, Food and Health, Mar 19<sup>th</sup>, Finland.
6. **Velagapudi, V.R.**, (2009) Systems biology approach to examine gut microbial effects on host metabolism in mice. In: Mass spectrometric metabolomics workshop, Feb 27<sup>th</sup>, Denmark.
3. **Velagapudi, V.R.**, (2009) Multivariate analysis of lipidomics data. In: Multivariate data modeling for Systems Biology (Sysdiet) workshop, Jan 16<sup>th</sup>, Oslo, Norway
2. **Velagapudi, V.R.**, (2008) Microbial regulation of host metabolism - A metabolomics strategy. In: The Second Finnish Gut day, Nov 7<sup>th</sup>, Helsinki, Finland.
1. **Velagapudi, V.R.**, (2008) Lipidomic profiling of animal models. In: EU Consortium meeting of Hepatic & Adipose tissue and functions in the metabolic syndrome (HEPADIP), Oct 23<sup>rd</sup>, France.

### Refereed Conference talk Abstracts

8. **Velagapudi, V.R.**, Hezaveh, R., Reigstad, C., Peddinti, G.V., Felin, J., Yetukuri, L., Mattila, I., Borén, J., Orešič, M., Bäckhed, F., 2009. The gut microbiota regulates energy and lipid metabolism. In: *Frontier lipidology: Lipidomics in health and diseases*. May 10-13, Sweden
7. Sysi-Aho, M., Vehtari, A., **Velagapudi, V.R.**, Westerbacka, J., Yetukuri, L., Bergholm, R., Taskinen, M.R., Yki-Järvinen, H., Orešič, M., 2007. Predicting the lipoprotein composition using Bayesian regression on serum lipidomic profiles. In: 15<sup>th</sup> ISMB/ECCB, July 21-25, Austria
6. **Velagapudi, V.R.**, Yetukuri, L., Westerbacka, J., Sysi-Aho, M., Bergholm, R., Vehtari, A., Taskinen, M.R., Yki-Järvinen, H., Orešič, M., 2007. Characterisation of Lipoprotein Fractions using Comprehensive UPLC/MS and GCxGC ToF/MS Analyses in patients with metabolic syndrome. In: *Metabolomics 3<sup>rd</sup> Scientific Meeting*. June 11-14, Manchester, UK.

5. Heinzle, E., Wittmann, C., **Velagapudi, V.R.**, Kim, H.M., John, G.T., 2006. Miniaturization and mini-bioreactors In: Engineering conferences international (ECI) - Natural products discovery and production: New challenges, new opportunities. June 4-8, New Mexico, USA
4. C. Wittmann., Kim, H.M., **Velagapudi, V.R.**, Heinzle, E., 2005. Metabolic network analysis at miniaturized scale - A novel tool in strain and process development. In: Industrial Microbiology & Biotechnology Conference SIM Annual Meeting, August 21-25, Chicago, IL, USA.
3. Heinzle, E., **Velagapudi, V.R.**, Wittmann, C., Hollemeyer, K., Talwar, P., Lengauer, T., 2005. Metabolische Hochdurchsatz-Charakterisierung von Deletionsmutanten von *Saccharomyces cerevisiae*. In: Systembiologie für industrielle Prozesse, May 1-4, Braunschweig, Germany.
2. Heinzle, E., John, G., **Velagapudi, V.R.**, Desphande, R., Wittmann, C., 2004. Biocatalyst screening using novel microtiter plates. In: Bioperspectives, May 4-6, Wiesbaden, Germany.
1. Wittmann, C., Kim, H.M., **Velagapudi, V.R.**, Heinzle, E., 2004. Cultivation and metabolic profiling at miniaturized scale. In: Bioperspectives, May 4-6, Wiesbaden, Germany.

### Refereed Conference Poster Abstracts

16. **Velagapudi, V.R.**, Bäckhed, F., Orešič, M., 2009. A systems biology approach to examine gut microbial effects on host metabolism in mice. In: The fifth International Conference of the Metabolomics Society, Aug 30 – Sep 2, Edmonton, Alberta, Canada.
15. Peddinti, G.V.,\* **Velagapudi, V.R.**,\* Lindfors, E., Halperin, E., Oresic, M., 2008. Dynamic network topology changes in functional modules predict responses to oxidative stress in yeast. In: 9<sup>th</sup> International Conference on Systems Biology (ICSB-9), Aug 22 – 28, Gothenburg, Sweden.
14. Peddinti, G.V., **Velagapudi, V.R.**,\* Lindfors, E., Halperin, E., Oresic, M., 2007. Dynamic network topology changes as result of cellular stress. In: 15<sup>th</sup> ISMB/ECCB, July 21-25, Austria.
13. **Velagapudi, V.R.**, Yetukuri, L., Westerbacka, J., Sysi-Aho, M., Bergholm, R., Vehtari, A., Taskinen, M.R., Yki-Järvinen, H., Orešič, M., 2007. Comprehensive metabolomic characterisation of lipoprotein fractions reveals differential lipoprotein-specific regulation of xenobiotic and pro-inflammatory metabolites in patients with metabolic syndrome. In: 76<sup>th</sup> EAS, June, Finland.
12. Talwar, P., Lengauer, T., Wittmann, C., **Velagapudi, V.R.**, Heinzle, E., 2006. Development of Computational Methods for Analysis of Metabolic Profiling Data. In: 7<sup>th</sup> ICSB, Japan.
11. Peddinti, G.V.,\* **Velagapudi, V.R.**,\* Lindfors, E., Halperin, E., Oresic, M., 2007. Dynamic network topology changes as result of cellular stress. In: ISSY-25, June 18-21, Espoo, Finland.
10. **Velagapudi, V.R.**, Wittmann, C., Hollemeyer, K., Lengauer, T., Talwar, P., Heinzle, E., 2006. Metabolic high-throughput characterization of yeast deletion mutants. In: ISSY-25. Finland.
9. **Velagapudi, V.R.**, Wittmann, C., Lengauer, T., Talwar, P., Heinzle, E., 2006. Functional Genomics of Yeast by Phenotypic and Metabolic Flux Profiling. In: Genomes to Systems Conference, 3<sup>rd</sup> Consortium for Post-genome science, Mar 22-24, Manchester, UK.
8. Talwar, P., Lengauer, T., Rahnenführer, J., Heinzle, E., **Velagapudi, V.R.**, Wittmann, C., 2005. Computational methods for protein functional prediction using metabolomics and transcript co-response data. In: 6<sup>th</sup> ICSB, Oct 19 – 23, Boston, USA.
7. Talwar, P., Lengauer, T., Rahnenführer, J., Wittmann, C., **Velagapudi, V.R.**, Heinzle, E., 2005. Computational methods for protein functional prediction using metabolomics data. In: International workshop on systems biology, May 12-13, Milan, Italy.
6. **Velagapudi, V.R.**, Wittmann, C., Lengauer, T., Talwar, P., Heinzle, E., 2005. High-throughput screening of *Saccharomyces cerevisiae* Knockout Library: Method Development and Stoichiometric Profiling. In: FEBS Advanced Course on Systems Biology, March 12-18, Austria.
5. Talwar, P., Lengauer, T., Rahnenführer, J., Wittmann, C., **Velagapudi, V.R.**, Heinzle, E., 2004. Computational Methods for Metabolite Screening. In: 12<sup>th</sup> ISMB/ECCB, July 31-Aug 4, UK.
4. Talwar, P., Lengauer, T., Rahnenführer, J., **Velagapudi, V.R.**, Wittmann, C., Heinzle, E., 2004. Computational Methods for Metabolite Screening. In: 5<sup>th</sup> ICSB, Oct 9 – 13, Heidelberg, Germany.
3. **Velagapudi, V.R.**, Wittmann, C., Talwar, P., Lengauer, T., Heinzle, E., 2004. Functional Genomics of Yeast by Metabolic Flux Profiling. In: 5<sup>th</sup> ICSB, Oct 9-13, Heidelberg, Germany.
2. **Velagapudi, V.R.**, Wittmann, C., Lengauer, T., Talwar, P., Heinzle, E., 2004. Metabolic Flux Profiling of *Saccharomyces cerevisiae* Mutants with Deletion of Genes in Central Metabolism at Miniaturized Scale. In: 5<sup>th</sup> ESBES, Sep 8-11, Stuttgart, Germany.
1. Talwar, P., Lengauer, T., Wittmann, C., **Velagapudi, V.R.**, Heinzle, E., 2003. Towards cellular function through metabolite screening. In: Metabolic Profiling-Pathways in Discovery, Cambridge Healthtech Institute Conference, Dec 8-9, New Jersey, USA